UNIVERSITÉ DU QUÉBEC À CHICOUTIMI

THÈSE

PRÉSENTÉ À

L'UNIVERSITÉ DU QUÉBEC À CHICOUTIMI

COMME EXIGENCE PARTIELLE

DU DOCTORAT EN INGÉNIERIE

PAR

MOHAMED FAWZY IBRAHIM

LES EFFETS DES INTERACTIONS DE Be, Sr, Fe ET DU Mg SUR LA MICROSTRUCTURE ET LES PROPRIÉTÉS MÉCANIQUES DES ALLIAGES AÉRONAUTIQUES À BASE D'ALUMINIUM

FÉVRIER 2015

UNIVERSITY OF QUEBEC AT CHICOUTIMI

THESIS PRESENTED TO THE

UNIVERSITY OF QUEBEC AT CHICOUTIMI

IN PARTIAL FULFILLMENT OF

THE REQUIREMENTS FOR THE DEGREE OF

DOCTOR OF PHILOSOPHY IN ENGINEERING

BY

MOHAMED FAWZY IBRAHIM

EFFECTS OF Be, Sr, Fe AND Mg INTERACTIONS ON THE MICROSTRUCTURE AND MECHANICAL PROPERTIES OF ALUMINUM BASED AERONAUTICAL ALLOYS

FEBRUARY 2015

This thesis is dedicated
to the memory of my father,
and to my mother, my wife, and my son.

Résumé

Le présent travail porte sur une série d'alliages d'aluminium traitable thermiquement de qualité aéronautique contenant différentes teneurs en magnésium (Mg), fer (Fe), strontium (Sr) et béryllium (Be). La conception aéronautique nécessite l'utilisation de ces alliages particuliers pour leur résistance et leur ductilité. Ces propriétés peuvent à leur tour être améliorées en contrôlant l'ajout d'éléments d'alliage aussi bien que par les paramètres du traitement thermique. Les objectifs de cette étude étaient de déterminer l'effet que l'interaction entre les éléments d'additions et le traitement thermique avait sur la microstructure et les propriétés mécaniques de l'alliage.

Des éprouvettes d'essai de traction (distance interdendritique ~ 24µm) ont été mises en solution pour des périodes de 5 et 12 heures à 540 °C, suivi d'une trempe à l'eau chaude (60°C). Par la suite, ces échantillons trempés ont été vieillis à 160°C pour une période allant jusqu'à 12 heures. Une analyse microstructurale a été menée en utilisant l'analyse thermique, l'analyse d'images et le microscope électronique à balayage à émission de champs. Toutes les éprouvettes de traction ont été fracturées à la température ambiante en utilisant une machine servohydraulique d'essai de traction.

Les résultats montrent que le Be cause une modification partielle des particules de silicium (Si) eutectique similaire à celle observée lors de l'ajout de Mg. L'addition de 0,8% en poids de Mg a réduit la température eutectique d'environ 10°C. Pendant la solidification des alliages contenant des hautes teneurs en Fe et en Mg, sans Sr, un pic correspondant à la formation des particules de la phase Be-Fe (Al_8Fe_2BeSi) a été détecté à une température de 611°C, laquelle est près de la température de formation de l'α-Al. Le précipité de la phase Be-Fe se présente sous la forme de script.

Une nouvelle réaction eutectique quinaire se produisant vers la fin de la solidification des alliages contenant du Be ainsi que des hautes teneurs en Mg et en Fe a été observée. Cette nouvelle réaction eutectique implique de fines particules avec des phases de Si, Mg_2Si, π-$Al_8Mg_3FeSi_6$ et de (Be-Fe). La fraction volumique de cette réaction a diminué avec l'ajout de Sr. L'ajout de Be a eu un effet notable sur la diminution de la longueur des particules de la phase β, ou sur la fraction volumique, cet effet pourrait être limité par l'ajout de Sr. L'addition de béryllium provoque également la précipitation de la phase β sous la forme nodulaire, laquelle réduit les effets néfastes de ces intermétalliques sur les propriétés mécaniques de l'alliage. L'augmentation de la teneur en Mg et en Fe mène à une hausse de la quantité des particules de la phase π; l'augmentation de la teneur en Fe mène à un accroissement de la fraction volumique des phases partiellement solubles β et π. Un changement de morphologie des plaquettes de la phase β a été observé causé par la dissolution, l'amincissement, la striction et la fragmentation de ces plaquettes au fur et à

mesure que le temps de mise en solution augmente. La phase π se dissout ou transforme en groupement de très fines plaquettes de la phase β. À l'état telle que coulée, l'augmentation de la teneur en Mg mène à une transformation accrue des plaquettes de la phase β en script chinois de la phase π peu importe la teneur en Fe. Ceci réduit, à son tour, l'effet néfaste de la phase β.

L'augmentation du temps de mise en solution conduit à une décomposition de la phase π vers la phase β, une fragmentation de la phase β et une sphéroïdisation du silicium eutectique et des particules de la phase π, améliorant ainsi les propriétés de traction de l'alliage. Deux mécanismes de croissance du précipité Mg_2Si ont été observés: (1) la maturation d'Ostwald pour les échantillons traités thermiquement et (2) le regroupement. La croissance augmente avec le temps croissant de mise en solution, de vieillissement et aussi bien qu'avec la teneur en Mg haussant. Une teneur en Fe accrue diminue les valeurs d'indice de la qualité (Q), alors que l'ajout de Mg les augmente. L'ajout de Be, bien qu'il soit un produit toxique, de Sr ou les deux à la fois, améliore les valeurs de l'indice de qualité de l'alliage, indépendamment du temps de mise en solution ou du niveau de Fe et de Mg.

Les valeurs de l'index de qualité augmentent avec le temps de mise en solution de 5 à 12 heures. Des teneurs plus élevées en Mg aboutissent à une augmentation de la ductilité, de la résistance à la traction (UTS) et de la limite d'élasticité (YS), tandis que des niveaux plus élevés en Fe peuvent diminuer considérablement ces propriétés. Pour les mêmes teneurs en Fe ou en Mg, le Be et le Sr améliorent considérablement les propriétés mécaniques de l'alliage; ces effets peuvent être facilement observés pour des faibles teneurs en Fe et des teneurs élevées en Mg. L'ajout de Be est bénéfique lorsque la teneur en Fe est élevée car il réduit les effets néfastes de la phase Fe pour les alliages Al-Si. Lorsque la teneur en Fe est élevée, l'addition de 500 ppm de Be semble ne pas être suffisante compte tenu de toutes les interactions avec les autres éléments d'alliage. Pendant le processus de fusion la formation de la phase Be-Sr (probablement le composé $SrBe_3O_4$) diminue le Be efficace ainsi que les propriétés mécaniques de l'alliage. Le rôle du Be qui est de prévenir l'oxydation du Mg et en changeant la composition chimique et la morphologie des composés intermétalliques Fe est observable par l'amélioration des propriétés mécaniques des alliages contenant du Be. La modification partielle causée par le Mg et le Be semble améliorer les propriétés mécaniques de traction de l'alliage.

Les temps de mise en solution et de vieillissement sont des paramètres importants affectant les propriétés mécaniques de traction. Les précipités Mg_2Si sont les principaux composés responsables du durcissement des alliages 356 et 357. La limite d'élasticité augmente avec des teneurs en Mg plus élevées, des teneurs en Fe réduites, l'ajout de Be, la modification par le Sr, le temps de mise en solution et le temps de vieillissement. Dans l'industrie aéronautique, la conception est influencée par la limite d'élasticité. Ainsi, une augmentation de la limite d'élasticité est d'une importance.

Une étude de l’alliage d’aluminium expérimental 7075 a été ajoutée au présent travail. Les résultats montrent qu'une mise en solution de 48 heures à 460 °C et 470 °C conduit à la dissolution des particules des phases riche en Mg et en Cu, alors que les particules des phases riches en Fe sont restées dans la matrice. L’augmentation de la température de mise en solution à 485°C a provoqué la fonte hâtive des particules des phases riche en Cu. L'utilisation d'additifs appropriés, de déformation à chaud et à froid, l'homogénéisation et le vieillissement, tel qu'ils sont appliqués dans cette étude, montre que l’alliage 7075 a le potentiel d’atteindre un niveau de résistance à la traction aussi élevé que 980 MPa. La ductilité de l’alliage pourrait être améliorée en utilisant une technologie de moulage appropriée. Les résultats de cette étude indiquent également qu’une modification de la composition des alliages et de la technique de coulée permettrait d’augmenter la ductilité. La spectroscopie de dispersion d’énergie appliquée aux surfaces de rupture des échantillons traités thermiquement démonte une dissolution du Zn, Mg et Cu dans la matrice d'aluminium. En revanche, la présence de fragments de particules intermétalliques de Fe a également été observée sur les surfaces de rupture, en raison de leur faible solubilité dans la matrice. Les surfaces de rupture des échantillons vieillis ont montré une rupture par clivage causée par une faible ductilité de l'alliage. D’ultra-fines fossettes, causées par la précipitation d'un mélange de fines particules, à savoir Al_2Cu, Mg_2Si et $MgZn_2$, ont également été observées.

L’augmentation marquée de la résistance à la traction de l’alliage provenant de l’ajustement de la chimie et des paramètres de traitement thermique peut être attribuée à la distribution uniforme de la précipitation des particules denses ultra-fines de la phase Al_2Cu à travers la matrice. En ajustant la composition chimique de l’alliage 7075 jumelé à des techniques de coulée et de traitement thermique appropriées, l’alliage pourrait atteindre 1 GPa avec 5-8% de déformation.

Abstract

The present work was carried out on a series of heat-treatable aluminum-based aeronautical alloys containing various amounts of magnesium (Mg), iron (Fe), strontium (Sr) and beryllium (Be). The design of aeronautical alloys requires the use of these particular alloys for their strength and ductility. These properties can be further enhanced by controlling the added alloying elements as well as the heat treatment parameters. The objective of the present work was to determine the effect of the interactions between element additions and heat treatment on the alloy microstructure and mechanical properties.

Tensile test bars (dendrite arm spacing ~ 24µm) were solutionized for either 5 or 12 hours at 540°C, followed by quenching in warm water (60°C). Subsequently, these quenched samples were aged at 160°C for times up to 12 hours. Microstructural assessment was performed using a thermal analysis technique, image analysis and field emission scanning electron microscopy. All heat-treated samples were pulled to fracture at room temperature using a servo-hydraulic tensile testing machine.

The results show that Be causes partial modification of the eutectic silicon (Si) particles similar to that reported for Mg addition. Addition of 0.8 wt.% Mg reduced the eutectic temperature by ~10°C. During solidification of alloys containing high levels of Fe and Mg, without Sr, a peak corresponding to the formation of a Be-Fe phase (Al_8Fe_2BeSi) was detected at 611°C, which is close to the formation temperature of α-Al. The Be-Fe phase precipitates in a script-like morphology.

A new quinary eutectic-like reaction was observed to take place near the end of solidification of high Mg, high Fe, Be-containing alloys. This new reaction is composed mainly of fine particles of Si, Mg_2Si, π-$Al_8Mg_3FeSi_6$ and (Be-Fe) phases. The volume fraction of this reaction decreased with the addition of Sr. The addition of Be has a noticeable effect on decreasing the β-phase length, or volume fraction, this effect may be limited by adding Sr. Beryllium addition also results in the precipitation of the β-phase in a nodular form, which reduces the harmful effects of these intermetallics on the alloy mechanical properties. Increasing both Mg and Fe levels led to an increase in the amount of the π-phase; increasing the iron content led to an increase in the volume fraction of the partially soluble β- and π-phases, while Mg_2Si particles were completely dissolved. The β-phase platelets were observed to undergo changes in their morphology due to the dissolution, thinning, necking and fragmentation of these platelets upon increasing the solutionizing time. The π-phase was observed to dissolve and/or transform into a cluster of very fine β-phase platelets. In the as-cast conditions, increasing the Mg content leads to increased transformation of β-phase platelets into Chinese-script π-phase, regardless of the Fe content. This, in turn, decreases the harmful effect of the β-phase.

Increasing the solutionizing time leads to a decomposition of the π-phase to the β-phase, fragmentation of the β-phase and spheroidization of both the eutectic Si and the π-phase particles, thus improving alloy tensile properties. Two mechanisms of Mg_2Si precipitate coarsening were observed to occur: (1) Ostwald ripening in the solution heat-treated samples and (2) clustering. Coarsening increases with increased solution heat treatment time, increased aging time, as well as with greater Mg contents. Increased Fe levels decrease the alloy quality index (Q) values, whereas adding Mg increases them. Introducing Be, in spite of it being a toxic material, Sr, or both, simultaneously improves the alloy quality index values, regardless of solutionizing time or Fe and Mg levels.

Quality index values increase with solution heat treatment time from 5 to 12 hours. Higher Mg contents lead to an increase in alloy ductility, ultimate tensile strength (UTS) and yield strength (YS), while higher Fe levels can drastically decrease these properties. For the same levels of Fe and/or Mg, Be and Sr have significant effects in improving alloy mechanical properties; these effects can be readily observed in low levels of Fe and high Mg contents. Beryllium addition is beneficial in the case of high Fe contents as it lowers the harmful effects of Fe-phases in Al-Si alloys. In the case of high Fe contents, it seems that the addition of 500 ppm of Be is not sufficient for all interactions with other alloying elements. During the melting process the formation of Be-Sr phase (probably $SrBe_3O_4$ compound) decreases the free Be content and hence the alloy mechanical properties. The role of Be in preventing the oxidation of Mg and in changing the chemistry and morphology of the Fe-intermetallics is observed through improved mechanical properties of Be-containing alloys. The partial modification effect of both Mg and Be appears to improve the alloy tensile properties.

Solutionizing and aging times are important parameters affecting the alloy tensile properties. The Mg_2Si precipitates were confirmed to be the main hardening components of the 356 and 357 alloys investigated. The yield strength increases with greater Mg levels, reduced Fe levels, addition of Be, Sr-modification, solution heat treatment time and aging time. In the aeronautical industry, design considerations are influenced by the YS. Therefore, an increase in the YS is of significance.

The present work was extended to include an investigation of the experimental 7073 aluminum alloy. The results show that a solution heat treatment of 48 hours at 460°C and 470°C resulted in dissolution of the Mg- and Cu-rich phases, whereas the Fe-rich phases remained in the matrix. Increasing the solution temperature to 485°C resulted in incipient melting of the Cu-rich phases. The use of proper additives, cold/hot deformation, homogenization and aging, as applied in this study, shows that 7075 alloys have the potential to reach UTS levels as high as 980 MPa. Alloy ductility could be improved by using proper casting technology. The results of this study also indicate that modification of both alloy composition and casting technique would provide the means to achieve greater percentage elongation values. Energy dispersive spectroscopy spectra taken from the fracture surfaces of solution heat-treated samples pointed towards the dissolution of Zn, Mg and Cu in the aluminum matrix. In contrast, the presence of fragments of Fe-based

intermetallic particles were also observed on the fracture surfaces, due to their low solubility in the matrix. The fracture surfaces of aged samples exhibited cleavage fracture due to poor alloy ductility. Ultra-fine dimples, caused by the precipitation of a mixture of fine particles, namely Al_2Cu, Mg_2Si and $MgZn_2$, were also observed.

The marked increase in the alloy strength from adjusting the alloy chemistry and heat treatment parameters may be attributed to uniformly distributed precipitation of a dense ultrafine particles of the Al_2Cu phase throughout the matrix. By adjusting the chemical composition of the 7075 alloy with proper casting and heat treatment techniques, the alloy could reach up to 1 GPa with 5-8% elongation.

ACKNOWLEDGMENTS

I would like to express my sincere gratitude to my supervisor, Prof. Fawzy H. Samuel for motivating me to complete my Ph.D. degree; without his continuous guidance and support it would have been impossible to do so. I am much indebted to him for helping me so generously over the last two years. I feel privileged to have been able to work with someone whose dedication and contribution to the field of science will be a constant inspiration to me throughout my life.

I would also like to express my sincere thanks to my co-supervisors; Prof. Agnes M. Samuel and Prof. Abdulrahman M.A. Al-Ahmari, Center of Excellence for Research in. Engineering Materials (CEREM), Advanced Manufacturing Institute, King Saud University, Riyadh, Saudi Arabia, for their supervision, guidance, and support during different stages of this research work.

Financial support in the form of scholarships received from the Natural Sciences and Engineering Research Council of Canada (NSERC) and from Alcoa Technology Center, PA, U.S.A. who has suggested the topic of this research, is gratefully acknowledged.

I would like to extend my appreciation to Prof. Raynald Gauvin, Department of Mining and Materials Engineering, McGill University, Montreal, QC, Canada, for helping with the FESEM work, as well as to Prof. Hany Ammar, Department of Metallurgical & Materials Engineering, Faculty of Petroleum & Mining Engineering, Suez University, Suez, Egypt, for helping with the presentation of the Q-charts.

Thanks are also due to Ms Amal Samuel, for enhancing the quality of micrographs.

Credit goes to the members of my family, especially to my mother, my wife, and my son, as well as to all my brothers and sisters for their sound advice and unfailing encouragement during the time it took to write my thesis.

PUBLICATIONS

Seven publications in the form of journal articles, conference papers and posters were prepared, published or are in press, from the current Ph.D. study. Three other publications regarding precipitation hardening, quality index and mechanical properties assessment of Al-Si-Mg casting alloys will be submitted shortly for publication.

Journal Papers

1- M.F. Ibrahim, A.M. Samuel and F.H. Samuel, "A preliminary Study on Optimizing the Heat Treatment of High Strength Al–Cu–Mg–Zn Alloys," *Materials & Design*, Vol. 57, May 2014, pp. 342-350.

2- M.F. Ibrahim, A.M. Samuel and F.H. Samuel, "Microstructural Analysis of Be-Containing Al-Si-Mg Alloys," *Metallography, Microstructure, and Analysis*, Accepted with minor corrections, 2015.

3- M.F. Ibrahim, A.M. Samuel and F.H. Samuel, "Formation of New Eutectic Reaction in Be Treated Al-Si-Mg Alloy," *International Journal of Materials Research*, in Revision, 2015.

Conference Presentations and Proceedings

4- M.F. Ibrahim, A.M. Samuel, S.A. Alkahtani and F.H. Samuel, "A Novel Solution Heat Treatment of 7075-Type alloy," *Light Metals*, DOI: 10.1002/9781118663189.ch67, *TMS 142nd*, 2013, San Antonio, Texas, USA.

5- M.F. Ibrahim, G.H. Garza-Elizondo, A.M. Samuel, S.A. and F.H. Samuel, "Optimizing the Heat Treatment of High Strength 7075-Type Wrought Alloys: A Metallographic Study," *119th Metalcasting Congress*, April 21-23, 2015, Columbus, OH, USA.

Scientific Posters

6- M.F. Ibrahim, A.M. Samuel and F.H. Samuel, "Production of Super Strong Aluminum Based Alloys," Poster presented at "Journee des Etudiants du REGAL" (REGAL Students Day), October 22, 2013, Montreal, QC, Canada, Published in *The Encyclopaedia of Research on Aluminium in Quebec*.

7- M.F. Ibrahim, A.M. Samuel, S.A. Alkahtani and F.H. Samuel, "Production of Super Strong Aluminum Alloys for Aeronautical Applications," Poster presented at "Journee des Etudiants du REGAL" (REGAL Students Day), November 15, 2012, Trois-Rivières, QC, Canada, Published in *The Encyclopaedia of Research on Aluminium in Quebec*.

TABLE OF CONTENTS

LIST OF FIGURES

CHAPTER 2

CHAPTER 5

LIST OF TABLES

CHAPTER 5

CHAPTER 1

DEFINING THE PROBLEM

CHAPTER 1

DEFINING THE PROBLEM

1.1 INTRODUCTION

Aluminum (Al) alloys are used in a wide variety of applications in the automobile, marine and aerospace industries, thanks to their low specific gravity, high strength-to-weight ratio, high wear resistance, high reflectivity, excellent heat and electrical conductivity, low melting point, negligible gas solubility (with the exception of hydrogen), excellent castability and good corrosion resistance.

Aluminum alloys can generally be classified as wrought alloys and casting alloys. Aluminum casting alloys constitute a group of cast materials that, in tonnage terms, is second only to ferrous castings. [1] This is largely because aluminum casting alloys are among the most versatile of foundry alloys. Moreover, many aluminum alloys are relatively free of hot short cracking and tearing tendencies, while at the same time yielding a good as-cast surface finish with few or no blemishes at all. [2]

Aluminum-silicon (Al-Si) base alloys belong to the 3xx and 4xx series. The three major heat-treatable alloy systems in the 3xx series are Al-Si-Mg, Al-Si-Cu and Al-Si-Cu-Mg, where magnesium (Mg) and copper (Cu) represent two significant alloying elements that serve as strengtheners. [2] The most well-known of the Al-Si-Mg alloys are the 356 and 357 alloys. While Mg is added to increase the strength, iron (Fe), manganese (Mn), nickel

(Ni) and chromium (Cr) are usually present as impurity elements. [3]

When combined with strontium (Sr), Mg negates the effect of Sr modification to such an extent, that a higher level of Sr is required to achieve full modification of the eutectic Si structure. In the Sr-modified Mg-free alloy, the Al-Si eutectic is better modified than the in the case of a Mg-containing alloy modified with the same amount of Sr. [3, 4] The volume fraction of the Fe-rich intermetallics in 357 alloys is larger than it is in 356 alloys as a result of the formation of larger amounts of the π-AlFeMgSi iron-intermetallic phase due to the higher Mg content of the former. [5, 6]

Aluminum-copper-magnesium-zinc (Al-Cu-Mg-Zn) heat-treatable alloys belong to the 7xxx series of aluminum wrought alloys, where Mg and Cu are added to act as strengtheners. [2] Zinc is known to increase hot-cracking tendency in aluminum casting alloys and for its sensitivity to stress-corrosion cracking with respect to aluminum wrought alloys; such effects limit its use. When added with other elements, however, zinc offers the highest combination of tensile properties in wrought aluminum alloys. The addition of copper, for example, to aluminum, magnesium and zinc, together with small amounts of chromium and manganese, results in some very high strength aluminum wrought alloys.

In the Al-Cu-Mg-Zn alloying system, zinc and magnesium control the aging process. The effect of copper is to increase the aging rate via the nucleation of the $CuMgAl_2$ phase. Copper also increases the quench sensitivity upon heat treatment of these alloys as well as the resistance to stress corrosion. Minor alloy additions, such as Cr and Zr, have a marked effect on mechanical properties and corrosion resistance of 7xxx series wrought alloys. [2, 7] Beside its tendency to form very coarse constituents with other

impurities or additions such as Mn, Fe and Ti, Cr is used to control grain structure, to prevent grain growth in Al-Mg alloys, and to prevent recrystallization in Al-Si-Mg or Al-Mg-Zn alloys during hot working or heat treatment whereas Zr is used to increase the recrystallization temperature and to control the grain structure in Al-Mg-Zn wrought products. Two well-known examples of Al-Cu-Mg-Zn alloys include the 7075 and 7475 alloys.

In both the Al-Si-Mg casting and Al-Cu-Mg-Zn wrought alloy systems, beryllium (Be) is added to prevent oxidation of magnesium as well as to improve the alloy strength and ductility by influencing the morphology and chemistry of Fe-containing intermetallics.[8] The mechanical behavior of a given alloy, i.e. the alloy strength and quality, is usually affected by the alloy chemical composition and any heat treatment conditions that may have been applied.

The aeronautical industry is the main field using such heat-treatable alloying systems, where engine parts can be made from Al-Si-Mg casting alloys, while other structural applications are produced from Al-Cu-Mg-Zn wrought alloys. Such critical applications are designed for high strength and ductility, both of which can be improved by adjusting the alloy chemical composition or through the use of a specific heat treatment. The importance of these applications forms the primary motivation behind the current study.

1.2 OBJECTIVES

The main purpose of this study is to investigate the effects of alloying elements and heat treatment conditions on the microstructure and mechanical behaviour of non-modified and Sr-modified 356- and 357-type alloys, as well as to adjust and develop both the alloy composition and heat treatment(s) for 7075- and 7475-type alloys, in order to obtain an ultimate tensile strength value of ~1 GPa. In order to accomplish these objectives, the following factors and aspects were examined:

(i) The influence of alloying elements on the aging behaviour of alloy castings with respect to Fe content, Sr modification, grain refining, addition of Mg and Be, as well as solution heat treatment and aging parameters.

(ii) Microstructural analysis of the precipitated phases during solidification.

(iii) Correlating the results obtained from tensile tests along with the microstructural analysis to determine the effects of alloying elements, intermetallic phases, changes in the morphology, solutionizing parameters and aging conditions on a given alloy's mechanical properties.

(iv) Improving both the alloy tensile properties and quality.

(v) Technology transfer.

CHAPTER 2

REVIEW OF THE LITERATURE

CHAPTER 2

REVIEW OF THE LITERATURE

2.1 ALUMINUM ALLOYS

The properties and quality of aluminum alloys are influenced by the alloying elements and impurities usually present in aluminum. The main alloying elements are silicon (Si), copper (Cu), magnesium (Mg), manganese (Mn) and zinc (Zn), whereas the main impurities and additions include iron (Fe), chromium (Cr), titanium (Ti), nickel (Ni), cobalt (Co), silver (Ag), lithium (Li), vanadium (V), zirconium (Zr), tin (Sn), lead (Pb), and bismuth (Bi). Some elements found or added as trace elements are strontium (Sr), beryllium (Be), boron (B), sodium (Na) and/or antimony (Sb).

2.1.1 Classification of Aluminum Alloys

As Figure 2.1 shows, aluminum alloys can be classified into four groups, mainly, casting alloys, wrought alloys, work-hardenable alloys, and age-hardenable alloys. This classification depends mainly on the alloying content and on whether or not an alloy can be hardened by the addition of alloying elements, as in the case of the precipitation-hardened alloys which can be strengthened by aging. The work-hardenable alloys are those that cannot be hardened by aging, and are hardened by working the alloy. [9]

2.1.1.1 Aluminum-Silicon Casting Alloys

Worldwide, Al-Si base casting alloys are widely used in high strength industrial applications on account of their low density and capacity for being cast in complex shapes. Nowadays, such alloys are used extensively in the automotive industry for engine components including blocks, cylinder heads, pistons, intake manifolds, and brackets, where these alloys have replaced cast iron components in many cases. [9]

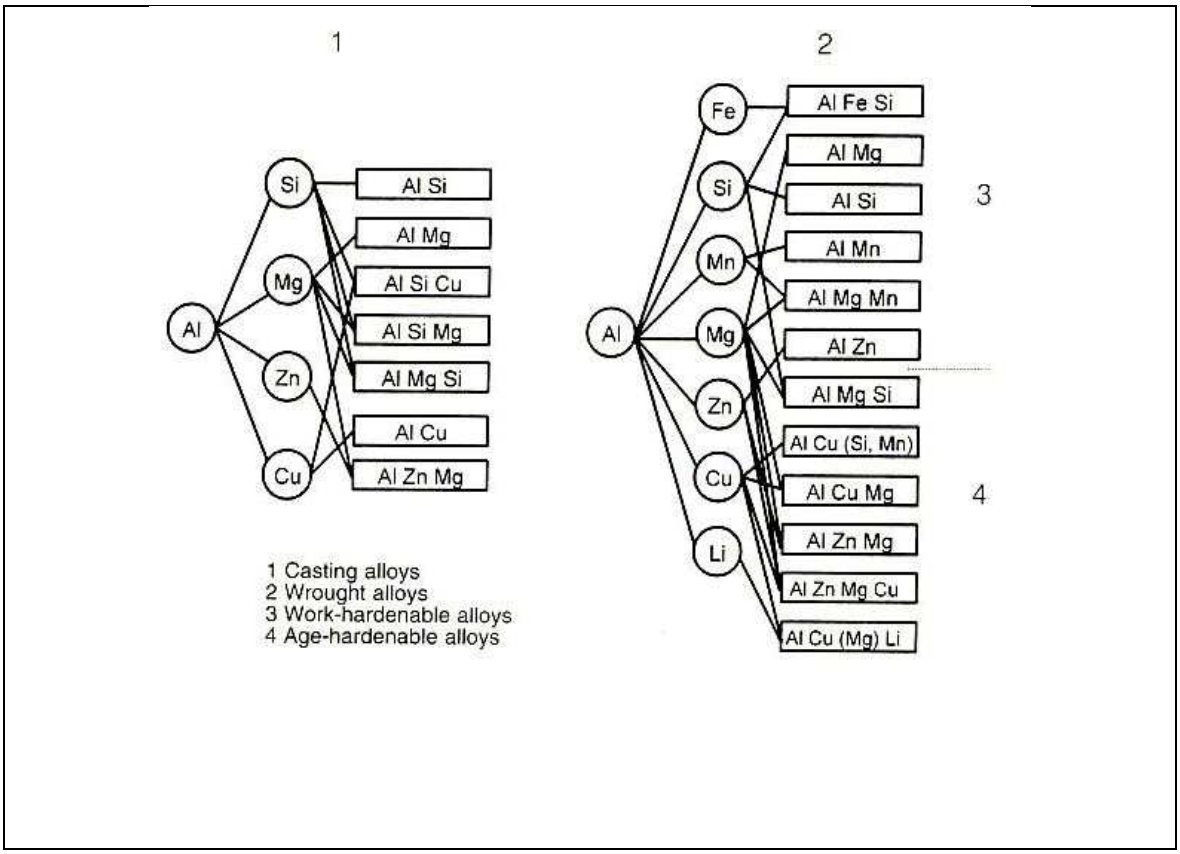

Figure 2.1 Schematic diagram showing cast and wrought aluminum alloys: (1) Casting alloys, (2) Wrought alloys, (3) Work-hardenable alloys and (4) Age-hardenable alloys. [9]

Silicon has a lower density compared to aluminum, and is one of the few elements which may be added to it without the loss of a weight advantage. Alloys with silicon as a major alloying element are of significance in the industry and are widely used because of their superior casting characteristics. The Al-Si base alloys constitute 85% to 90% of all aluminum castings. Their other outstanding features include high corrosion resistance, a low thermal expansion coefficient, weldability, and high mechanical properties. [2, 10]

Depending on the silicon content, Al-Si alloys are divided into three groups: hypoeutectic alloys with a Si content of between 5 and 10%, eutectic alloys with 11-13% Si, and hypereutectic alloys, commonly having a Si content of between 14 and 20%.

The excellent castability and mechanical properties of Al–Si–Mg cast alloys make them popular foundry alloys for aerospace applications. These alloys are usually heat-treated in order to obtain an optimum combination of strength and ductility. The relevant heat treatment consists of solution treatment and quenching, followed by artificial aging. Magnesium is often added as an alloying element to increase strength and hardenability values, whereas Fe, Mn, Ni, and Cr are usually present as impurity elements.

The mechanical properties may also be enhanced by changing the morphology of the eutectic silicon particles from their normally acicular brittle form to a more fibrous and rounded form. The desired modification may be obtained through the addition of a chemical modifier such as sodium (Na) or Sr to the alloy, or else by means of solution heat treatment during which the Si particles are fragmented and become spheroidized. Long solution treatment times can lead to particle coarsening. [2, 11]

The percentage of Si in Al-Si alloys together with the shape and distribution of this element all play an important role in determining mechanical properties**;** under normal conditions, eutectic silicon displays an acicular or lamellar morphology**.** Strontium is commonly used in Al-Si casting alloys to modify the morphology of eutectic silicon from a coarse, flake-like form to a fine fibrous one so as to improve the mechanical properties of the alloy, particularly ductility.

With the addition of Sr, the eutectic temperature of the Al-Si eutectic reaction is depressed**;** subsequently this depression is often used to estimate the degree of modification which has taken place in the Al-Si alloy. Other alloying elements such as Mg and Be, together with varying amounts of iron, manganese**,** and zinc as impurity elements, go into solid solution in the matrix and form intermetallic particles during solidification.

When combined with Sr, Mg negates the effect of Sr modification to such an extent, that a much higher level of Sr is required to achieve full modification of the eutectic Si structure. In the Sr-modified Mg-free alloy, the Al-Si eutectic is better modified than the one in the Mg-containing alloy modified with the same amount of Sr. The volume fraction of the iron-rich intermetallics in 357 alloys is larger than it is in 356 alloys containing same level of Mg as a result of the formation of larger amounts of the π-AlFeMgSi iron-intermetallic phase. [5, 6]

The tensile properties can be correlated to the microstructure and to the formation of intermetallic phases and porosity. In general, with an increase in the volume fraction and size of intermetallics and porosity, the tensile properties tend to decrease.

Heat-treatable aluminum alloys are those whose mechanical properties may be improved by using a specified heat treatment or temper. Heat treatment is an elevated temperature process designed to allow soluble elements such as Mg to become supersaturated in solid solution, followed by cooling which is rapid enough to prevent the excess solute from precipitating. The T6 heat treatment process involves three stages, namely, solution heat treatment, quenching, and aging. The purpose of the solution heat treatment is to put the maximum amount of hardening solutes such as Mg into solid solution in the aluminum matrix.

The recommended solution temperature for 356 and 357 alloys is 540 ± 5^{o}C; this temperature was selected to obtain maximum concentrations of Mg and Si in solid solution.[5, 12] Quenching is the step which follows upon solution heat treatment; it is usually conducted in water, making it possible to freeze the structure for a brief period of time. The purpose of this process is to preserve the solid solution formed at the solution heat treating temperature by means of rapid cooling to some lower temperature usually close to room temperature.

Aging treatment is the controlled process of allowing the hardening constituents to re-precipitate either at room temperature (natural aging) or at an elevated temperature (artificial aging), thereby producing a hardening effect. The highest strength values may thus be obtained by the proper combination of solution heat treatment, quenching, and artificial aging**.**

2.2 Al-Si-Mg ALLOY SYSTEM

An important group of alloys, used for critical aerospace applications, in the Al-Si system are Al-Si-Mg alloys, which are hardened by Mg_2Si, such as the 356 and 357 alloys. Magnesium is the basis for strength and hardness development in heat-treated Al-Si alloys. In the heat-treated condition, the hardening phase Mg_2Si has a solubility limit corresponding to approximately 0.7% Mg. [13] Beyond this limit, no further strengthening occurs nor does matrix softening take place. At room temperature, quantities of magnesium exceeding 0.3% Mg will be present as Mg_2Si. An increase of magnesium, within the alloy range, results in increased strength at the expense of ductility. Magnesium also has a beneficial effect on corrosion resistance. By including additional elements, it is possible to improve the mechanical properties of Al-Si-Mg alloys.

With regard to these alloys, iron is considered an impurity originating in the process of mining aluminum from the ore. It often appears in the form of AlFeSi intermetallics at the grain boundaries, causing a severe loss of ductility in the alloy; strength may also be noticeably affected. As a result, the iron-content is kept significantly low in premium quality alloys which are used for aircraft and aerospace castings requiring high-grade quality properties. Copper is present primarily as an impurity in Al-Si-Mg alloys and decreases the sensitivity of the alloy to quench rates. It also increases the stress-hardening effect as well as the strength in the T6 temper. Higher copper-content decreases ductility and resistance to corrosion, while additions of manganese, chromium, and zirconium inhibit recrystallization during solution treatment. Manganese additions increase creep and fatigue resistance and, to some extent, counteract copper in neutralizing the corrosion

susceptibility of the alloy. Manganese converts the crystallization of needle-like intermetallic phases to cubic or globular forms, such as Chinese script morphology, which have less harmful characteristics. This type of morphology improves tensile strength, elongation and ductility. [14-16] Furthermore, it should be noticed that small amounts of manganese (usually Mn:Fe is 1:2) play a positive role by breaking up the iron needles. [16] When added in a higher ratio or in the presence of chromium, depending on the melt temperature, manganese produces a hard multi-component intermetallic compound, commonly referred to as sludge, which affects the mechanical properties of the casting. Lead and bismuth may be deemed useful additions for improving the machining characteristics of the alloy. [17, 18]

The most well-known alloys belonging to the Al-Si-Mg alloy system are the 356 and 357 alloys. The chemical compositions for various 356 and 357-type alloys are presented in Table 2.1. [19]

Table 2.1 Chemical composition of 356 and 357 alloys (wt%) [19]

AA Alloy No.*	**Chemical Composition (wt%)****					
	Si	**Fe**	**Cu**	**Mg**	**Zn**	**Other**
356	7.0	<0.6	<0.25	0.35	<0.35	…
A356	7.0	<0.2	<0.2	0.35	<0.1	…
B356	7.0	<0.09	<0.05	0.35	<0.05	…
357	7.0	<0.15	<0.05	0.55	<0.05	…
A357	7.0	<0.20	<0.2	0.55	<0.10	0.05 Be
B357	7.0	<0.09	<0.05	0.50	<0.05	…

* AA: Aluminum Association
** Unlisted Aluminum or impurities

2.3 INTERMETALLIC PHASES IN Al-Si-Mg ALLOYS

Both of 356 and A357 alloys contain 7 wt% Si but have different Mg levels of approximately 0.45 wt% and 0.7 wt% Mg, respectively. Alloys 356 and 357 have been widely used for automotive and aerospace applications requiring the highest strength with reasonable ductility. A357 alloys also contain a small amount of beryllium which is added in order to improve strength and ductility through its effect on the morphology and chemistry of the π-phase iron-containing intermetallic. [20]

The solid solubility of iron in molten aluminum is about 0.03-0.05 wt% at the eutectic temperature of 577^{o}C. Thus, most of the iron present above this level appears in the form of iron intermetallic phases. When iron combines with Al and Si, it forms a β-Al_5FeSi intermetallic phase displaying a platelet-like shape. In the case where Mg is present, another intermetallic tends to form and is called the π-phase whereby $Al_9FeMg_3Si_5$ may be produced. Experimental studies have demonstrated that the formation of iron intermetallic compounds is influenced by alloy composition as well as by the cooling rate. Iron intermetallic phases have a crystal structure which differs from that of aluminum; normally they have high hardness values, with low plasticity compared to the Al-matrix. Thus, iron intermetallic phases appear to have a significant effect on Al-Si-Mg alloys by reducing their strength and ductility. [21-23]

Bäckerud *et al.* [24] reported that the main reactions to be observed in the Al-7Si-0.56Mg alloy containing 0.14wt% Fe are (i) the formation of primary α-Al dendrites, (ii) the formation of the Al-Si eutectic along with the β-phase iron-intermetallic phase, and (iii) the formation of secondary eutectic phases, as may be seen in Table 2.2. The cooling curve

and its first derivative are shown in Figure 2.2. It will be observed that there are two possible reactions required for the formation of the π-phase: the first is a result of the transformation of the β-Al_5FeSi phase into the π-phase through a peritectic reaction, as will be found listed under reaction 4 in Table 2.2; the second, on the other hand, forms as a result of the quaternary eutectic reaction occurring at the end of the solidification sequence, as listed under reaction 5. The general microstructure of Al-7%Si-Mg alloys consists of (i) primary α-Al; (ii) Mg_2Si displaying Chinese script morphology; (iii) β-phase (Al_5FeSi) with its plate-like morphology; and (iv) the script-like π-phase ($Al_8FeMg_3Si_6$), as shown in Figure 2.3.

Table 2.2 Expected reactions to occur in A357 alloys [24]

Reaction No.	Reaction	Temperature ºC
1	Dendritic network	611
2	$L \rightarrow Al + Si$	577
3	$L \rightarrow Al + Si + Al_5FeSi$	575
4	$L + Al_5FeSi \rightarrow Al + Si + Al_8FeMg_3Si_6$	567
5	$L \rightarrow Al + Si + Mg_2Si$	555
6	$L \rightarrow Al + Si + Mg_2Si + Al_8FeMg_3Si_6$	550

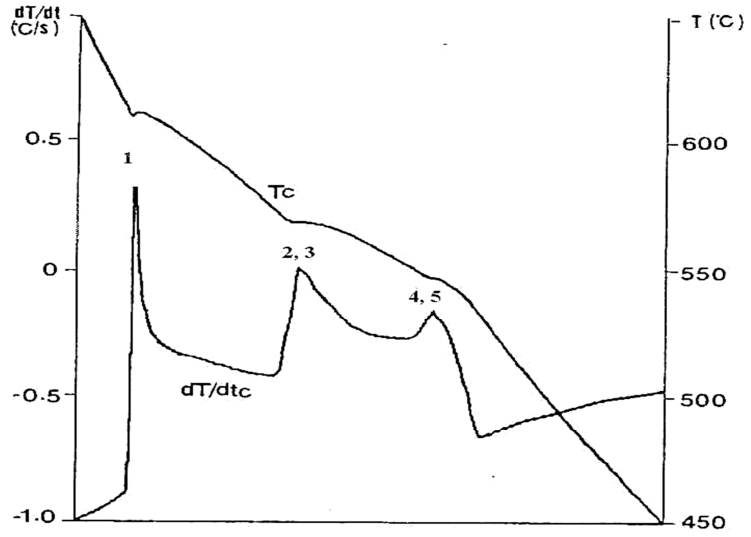

Figure 2.2 Cooling curve and its derivative for alloy A357. [24]

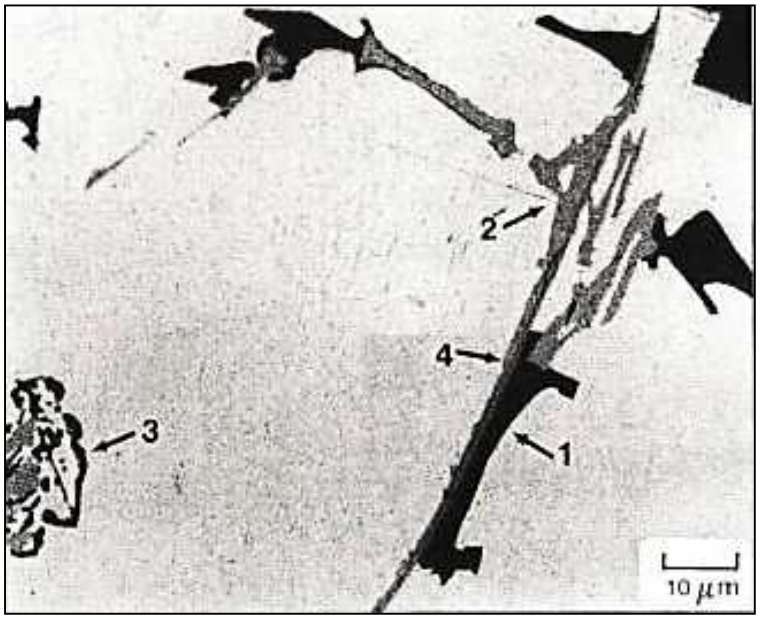

Figure 2.3 Optical micrograph of non-modified 357 alloy showing: (1) eutectic silicon, (2) $Al_8FeMg_3Si_6$ Chinese script, (3) Mg_2Si Chinese script, (4) Al_5FeSi needles. [24]

Phragmén [25] reported that the composition of the β-Al_5FeSi phase is 27% Fe and 13.5% Si with a density of 3.30-3.35 g/cm^3, appearing in the form of thin platelets or needles in the microstructure. The β-Al_5FeSi phase grows in a lateral or faceted mode and contains multiple (001) growth twins parallel to the growth direction. [26] The possible morphology of β-Al_5FeSi is shown in Figure 2.3. The first suggestion of the stoichiometry of the π-phase by Foss *et al.* [27] was $Al_9FeMg_3Si_5$; this stoichiometry deviates from the $Al_8FeMg_3Si_6$ suggested by others. The π-phase is a quaternary phase having a script-like morphology, often linked with β-Al_5FeSi. [28] The chemical composition of this π-phase is 10.9% Fe, 32.9% Si, and 14.1% Mg, with a density of 2.82 g/cm^3. Figure 2.4 shows the only two possible morphologies observed for the π-phase. [28-30]

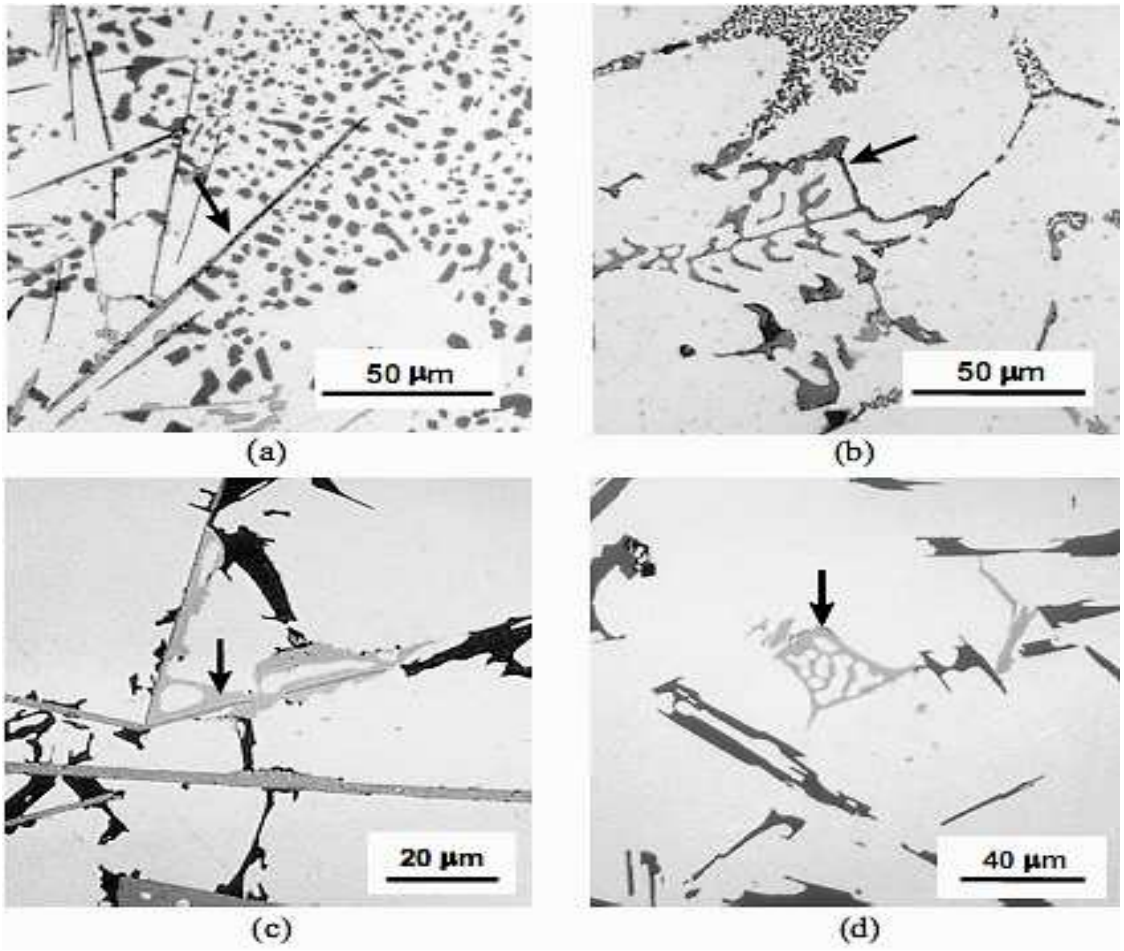

Figure 2.4 Optical micrographs showing various iron-containing intermetallics (arrowed) and their typical morphologies in Al-5%Si-1%Cu-0.5%Mg-(Fe) alloys: (a) β-Al_5FeSi platelets, (b) script-like α-Al_8Fe_2Si, (c) π-$Al_8FeMg_3Si_6$ phase growing from and connected with β and (d) script-like π-phase. [30]

2.4 ROLE OF ALLOYING ELEMENTS AND IMPURITIES

Casting alloys are defined by their chemical composition and according to the major alloying elements present in the alloy. The alloying elements and impurities present in an alloy together with the cooling rate, determine which constituents will precipitate. These major alloying elements are added to increase the strength and other properties of aluminum casting alloys.

2.4.1 Role of Strontium Modification

The improvement in mechanical properties has generally been attributed to variations in the morphology and size of the eutectic silicon particles. Silicon content and its morphology in the structure have a significant influence on the mechanical properties of the alloys. Chemical modifiers are elements which are used mainly for transforming the morphology of the coarse acicular silicon in the eutectic structure of Al-Si alloys into a finer or more fibrous form in order to improve the mechanical properties. The most common modifying elements used are sodium and strontium, [31] although nowadays Sr is mostly employed for modification purposes, in the form of Al-Sr master alloys. The modification mechanism of the Si particles and changes in their morphology has been described by Mondolfo. [29] Although the presence of strontium can change the morphology of the silicon particles, when the Al-Si alloy contains more than 0.05 wt% Sr, the formation of undesirable Sr-compounds such as Al_2SrSi_2 contributes to a decrease in mechanical properties. [32] The addition of Sr is associated with an increase in the amount of porosity and inclusions.

It has been reported that the iron intermetallic volume fraction is lower in the Sr-modified alloys compared to non-modified alloys. The lower volume fraction of the iron intermetallics in the Sr-modified alloys may be attributed to the effects of Sr modification on the fragmentation of iron intermetallics in the as-cast Al-Si alloys. [33] Peyman *et al.* [34] studied the influence of Sr addition on intermetallic compound morphologies in an Al-Si-Cu-Fe cast alloy; they observed that the length and volume fraction of the β-phase decreases and that the number density of particles increases upon adding 0.015 % Sr,

indicating that Sr proves to be an effective element in the modification and shortening of the β-intermetallic phase particles.

It has been observed that the addition of strontium acts as an obstacle for the nucleation of the β-needles, by reducing the number of sites ultimately available for nucleation. As a result, the β-iron phase precipitates at a smaller number of sites, leading to the precipitation of needles which are larger compared to those in the non-modified alloy.[35] These studies [34, 35] contradict each other. It has been found that for 319 alloy containing 0.46% Fe and which solidified at a slow cooling rate, the optimum Sr levels lie closer to the limit of 400 ppm. As the iron level increases, the optimum Sr level will be observed to shift towards the higher limit. [36]

Silicon content and its morphology in the structure have a significant influence on the mechanical properties of the alloys as shown by the curves in Figure 2.5. As the silicon content increases, the tensile strength of the alloy is enhanced; however, at the same time, the brittle nature and flake morphology of the unmodified silicon phase will affect the alloy ductility adversely. After modification, both tensile strength and elongation are improved, with the greatest improvement being observed in the elongation. [37]

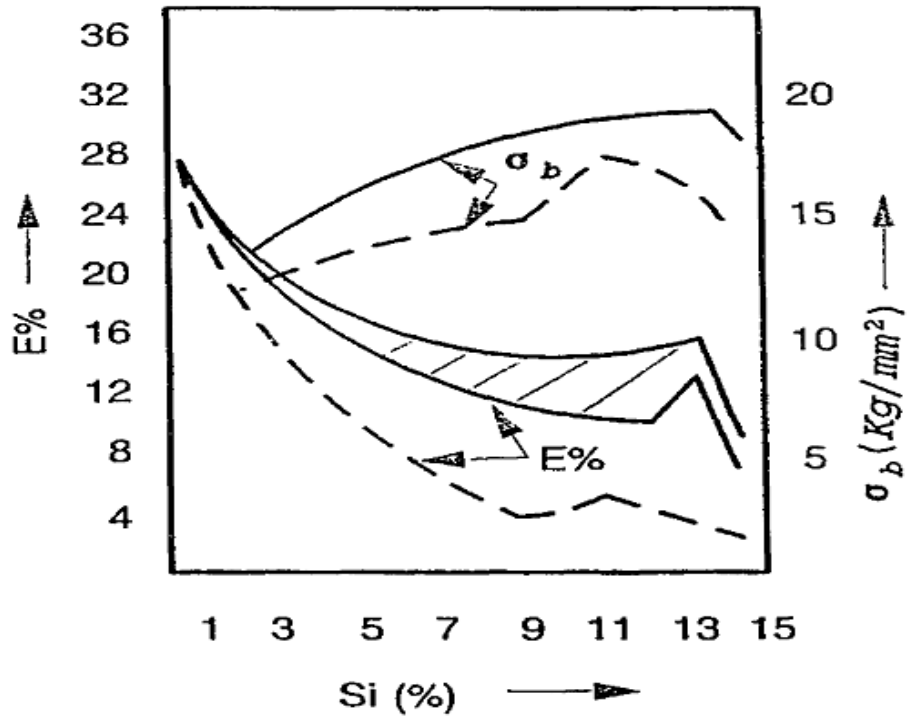

Figure 2.5 Influence of Si-content on the mechanical properties of Al-Si alloys; full lines: modified alloys; dashed lines: unmodified alloys. [37]

Figure 2.6 shows the variation in the elongation with differing strontium levels for three different cooling rates in a 356 alloy. At all cooling rates, the elongation due to strontium modification was observed to have been improved. The detrimental effect due to over modification at higher Sr levels is also evident from the figure. [38] A comparison of the mechanical properties for modified and unmodified alloys is given in Table 2.3 for some commonly used T6-heat treated 356 alloys. [39]

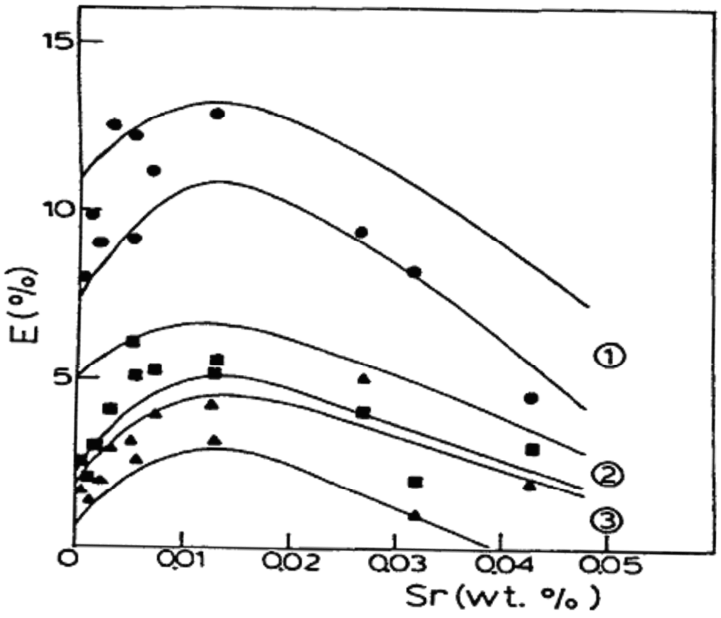

Figure 2.6 Variation of the elongation with Sr level for three different cooling rates, Band 1**:** cooling rate 1.5°C/s. Band 2**:** cooling rate 0.5°C/s. Band 3**:** cooling rate 0.08°C/s. [38]

Table 2.3 Typical mechanical properties of as-cast and modified 356 alloys [39]

Alloy and temper	Modification	UTS (MPa)	Elongation (%)
356.0-T6	None	288.9	2.0
	0.07% Sr	293.0	3.0
A356.0-T6	None	275.8	4.8
	0.07% Sr	296.5	8

Figure 2.7 shows the mechanical properties of A356.0 alloy modified with strontium. [1] Impact properties are much more sensitive to modification than tensile properties, where the impact strength of the modified alloy is seen to increase to three times its value, the elongation value is doubled, although both yield and strength remain virtually unaffected.

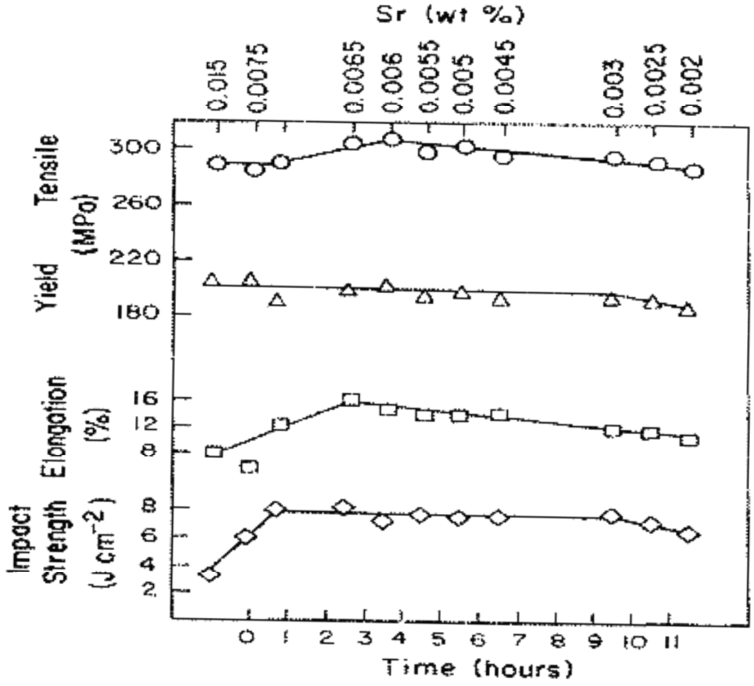

Figure 2.7 Mechanical properties of A356.0 alloy modified with strontium. [1]

The relationship between the Quality Index and the changes occurring in the microstructure of A356 alloys as a result of heat treatment and the addition of different levels of pure Sr was investigated by Closset *et al*. [38, 40] They plotted the Q values as a function of different cooling rates and Sr content, as shown in Figure 2.8. This figure reveals an increase in the Q value with increases in Sr content, but at certain values of the Sr content, the Q value starts to decrease for all the cooling rates studied (Band 1**:** cooling rate 1.5^{o}C/s. Band 2**:** cooling rate 0.5^{o}C/s. Band 3**:** cooling rate 0.08^{o}C/s). [38] The increase in the Q values observed with Sr additions of up to 0.03 wt% is a result of changes in the acicular morphology of the Si particles to a fibrous form, leading to a decrease in the number of crack initiation sites and thus also to an increase in the elongation to fracture.

The apparent reason for the drop in quality values, as the Sr content grew greater than 0.03 wt%, was the over-modification of the Si particles and the formation of the Al_3SrSi intermetallic phase, which is brittle and also not affected by heat treatment. The optimum mechanical properties were also obtained in the Sr range of 0.005 to 0.015%. [10, 31]

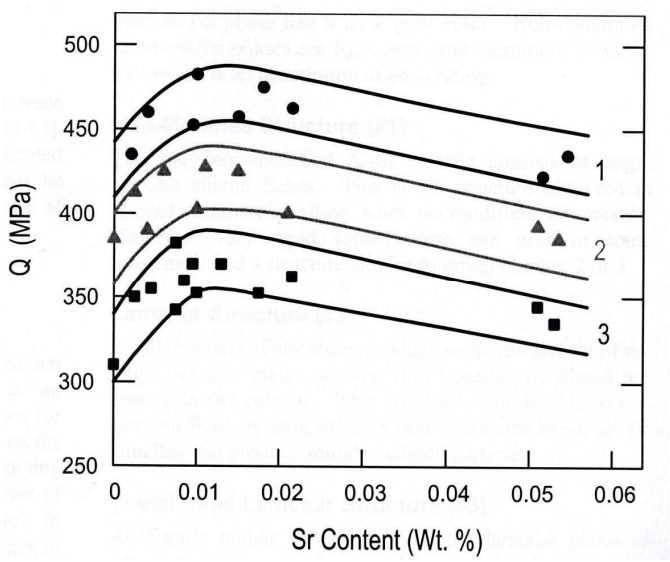

Figure 2.8 Variation of the Quality Index (Q) in relation to Sr content for different cooling rates.[38]

2.4.2 Role of Magnesium

The Al-Si-Mg system is represented by the pseudo-binary Al-Mg_2Si diagram shown in Figure 2.9. The structure of Al-Si-Mg alloys is controlled through eutectic modification and heat treatment resulting in enhancing the alloy properties compared to the non-modified and/or as-cast case. Alloy 357 can be distinguished from 356 alloys by its higher Mg level; consequently, heat-treated 357 alloys have higher tensile strength than 356 alloys. A356.0 and A357.0 alloys are higher purity versions of 356.0 and 357.0 alloys, and hence

have higher mechanical properties.

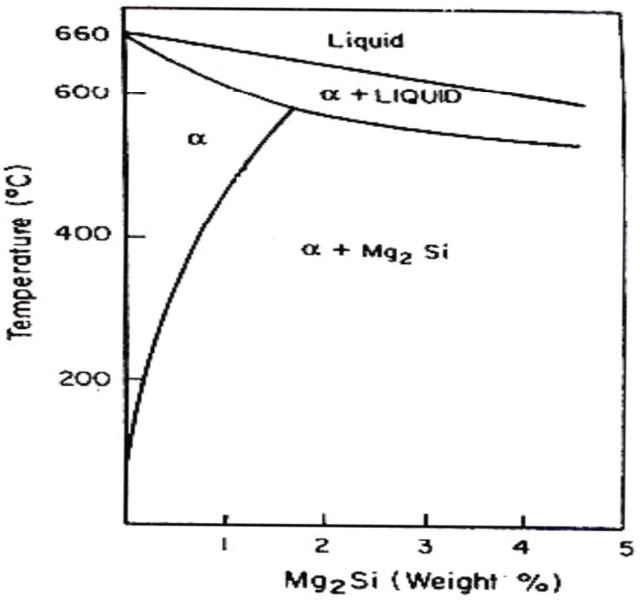

Figure 2.9 Pseudo-binary Al-Mg_2Si phase diagram. [1]

For Al-Si-Fe-Mg cast alloys, the results reveal that the π-phase and β-phase volume fractions remain constant regardless of the Mg content, whereas the amount of Mg_2Si appears to increase generally, as shown in Figure 2.10. [41] Cáceres *et al.* [42] studied the microstructures of two Al-Si-Mg casting alloys, respectively containing 0.4 wt% and 0.7wt% Mg. They observed that the iron intermetallic phases in high Mg-content alloys are larger than they are in alloys containing low levels of magnesium, and that the iron-rich intermetallic phases in low-Mg alloys were exclusively small β-phase plates, while large π-phase ($Al_9FeMg_3Si_5$) particles were dominant in high-Mg alloys together with a small proportion of the β-phase. It has been observed that the addition of Mg to Al-Si-Mg casting

alloys, at three different cooling rates, changes the solidification sequence and the type of iron intermetallic phase formed. [24] At Mg additions of more than 1%to molten 319 type alloys, the volume fraction of the β-phase is reduced as a result of the transformation of the β-phase into the π-phase. [33] It has been reported that increasing the Mg content from 0.4 to 0.7wt% in 357 alloys significantly increases the potential for the formation of the Mg-containing $Al_8FeMg_3Si_6$ iron intermetallic phase. [43]

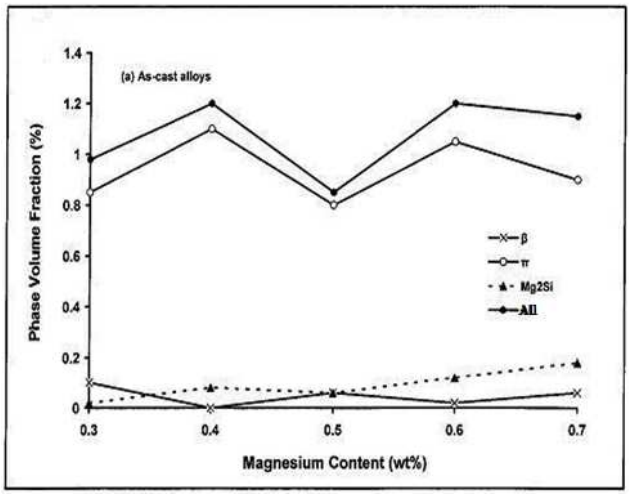

Figure 2.10 Volume fractions of Mg_2Si, β-Fe, and π-Fe intermetallic phases in as-cast Al-7Si-0.12Fe-xMg alloys as a function of Mg content. [41]

Adding magnesium allows the casting to be heat-treated, whereby Mg_2Si precipitates upon aging, hardening the alloy and providing a specific combination of strength and ductility. High Mg levels increase the amount of Mg_2Si precipitates formed during aging, thereby increasing the yield strength (YS) and the ultimate tensile strength (UTS) of the alloy. Increasing Mg even in small amounts will result in an increase in the

yield strength of Be-free Al-Si-Mg alloys, as shown in Figure 2.11. [44, 45] The low YS for the high-Mg alloys results from the presence of the π-phase iron intermetallic, which in itself consumes large amounts of magnesium from the solid solution, thereby reducing the amount of Mg available to form Mg_2Si precipitates after ageing. [6, 46]

Möller *et al.* [47] reported that increasing the Mg content from 0.25 to 0.45 wt% greatly increases the UTS and YS, although increasing this content beyond 0.45wt% causes an increase in YS and UTS to less than expected values. The expected values were obtained, however, by a linear extrapolation of the strength of lower Mg content in A356 alloys to actual F357 Mg concentrations (same as A357 except no Be), as shown in Figure 2.12. A number of authors [42, 43] have reported that an increase in the YS and UTS is usually accompanied by a decrease in the ductility, especially in the presence of high levels of Mg as in 357 alloys. This reduction results from the presence of π-phase particles which are much larger than the silicon particles in Sr-modified 357 alloys, [42] or from the fracture of π-phase particles which plays an important role in the reduction of ductility, especially in the modified alloy, where these particles are more easily fractured than in the non-modified alloy. [43]

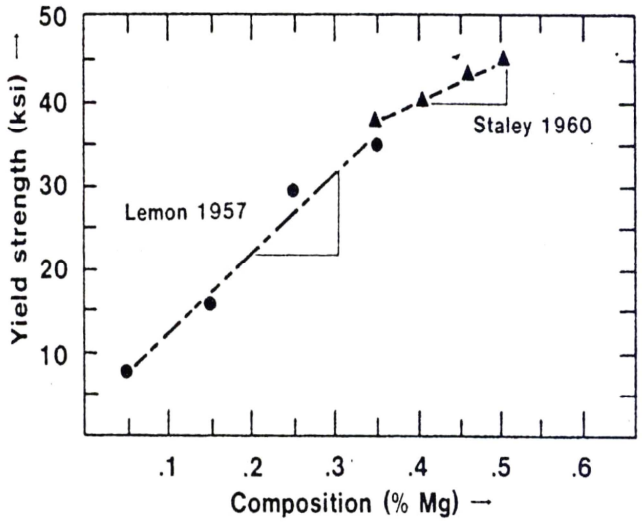

Figure 2.11 Effect of Mg on T6 yield strength in hypoeutectic Al-Si alloys. [44]

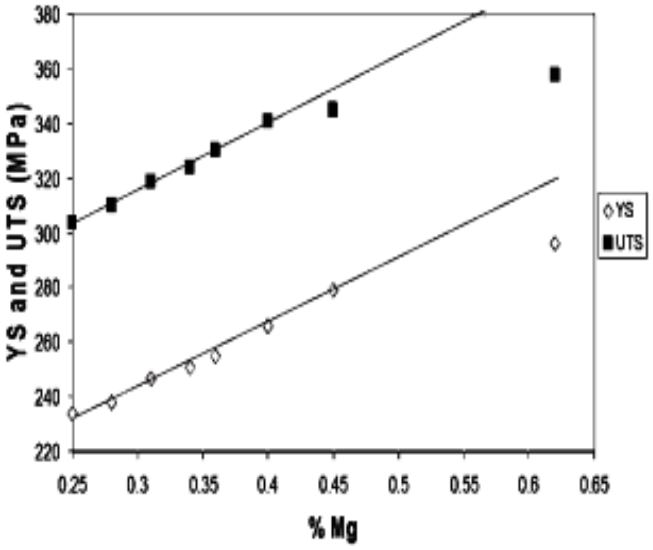

Figure 2.12 Yield strength and ultimate tensile strength of T6-A356 alloy as a function of the bulk Mg concentration of the alloys. [47]

2.4.3 Role of Iron

Any element which is not classified as an alloying component is termed an impurity, and as such it is deemed to have a negative effect on the castability, mechanical properties and heat treatment of aluminum alloys. Among such elements, iron is a common impurity in aluminum alloys arising from a number of sources. It is usually considered detrimental for Al-Si based casting alloys.[33,48] Iron can enter the melt during further downstream melt activity through two basic mechanisms: (i) liquid aluminum is capable of dissolving iron from unprotected steel tools and furnace equipment, or (ii) iron may also enter an aluminum melt via the addition of low-purity alloying materials such as Si, or via the addition of scrap that contains higher background iron than the primary metal.

Manganese is a common alloying element used as an addition to neutralize the effect of iron and to modify the morphology and type of the intermetallic phases formed. Manganese is added to many of the alloys for two main purposes: (i) to increase high-temperature strength and creep resistance through the formation of the high melting point compounds; $Cu_2Mn_3Al_{20}$, $MnCrAl_{12}$, $Al_{15}(Fe,Mn)_3Si_2$ and more complex compounds containing chromium and nickel; and (ii) to correct the embrittling effect of Fe. [33, 48]

Figure 2.13 shows the binary Al-Fe equilibrium phase diagram. [48] With long holding times, Fe levels can reach 2 wt% at a normal melt temperature of ~700^{o}C and an Al-Fe eutectic exists at 1.7 wt% Fe, 655^{o}C. For a melt held at 800^{o}C, the Fe level may reach up to 5%.

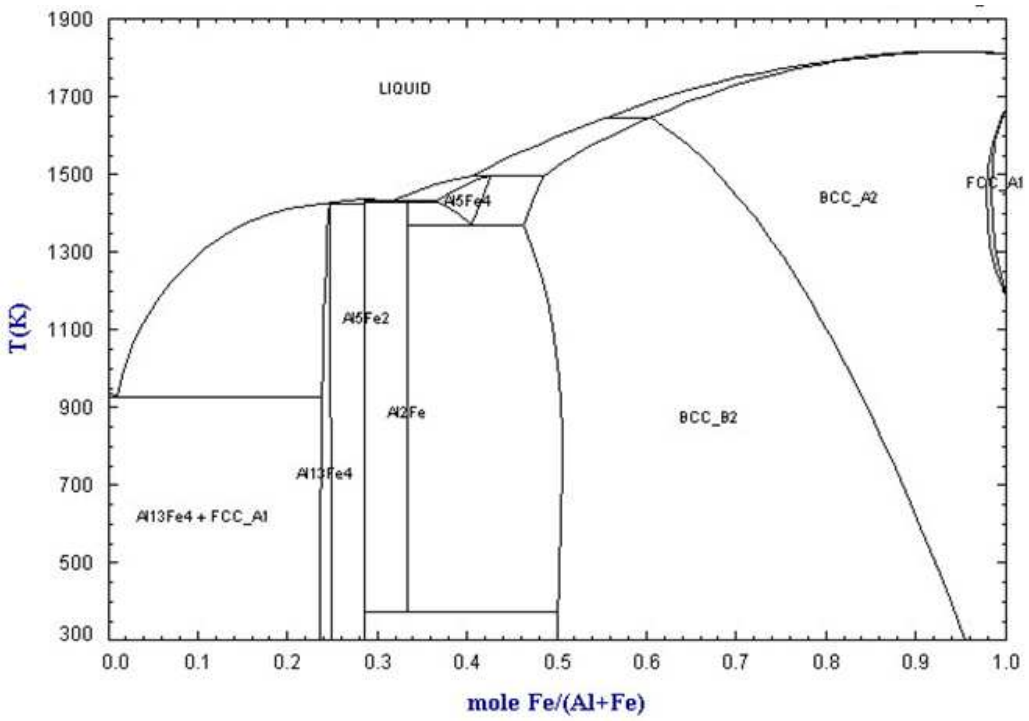

Figure 2.13 Binary Al-Fe equilibrium phase diagram. [48]

The detrimental effect of iron begins at a somewhat low primary Fe-level but becomes far more serious once a critical Fe-level, dependent on the alloy composition, is exceeded. The critical iron level is directly related to the concentration of both Si and Mg in the alloy; this concentration controls the formation of Fe phases, mainly β-Al_5FeSi, α-$Al_{15}(Fe,Mn)_3Si_2$ and π-$Al_8FeMg_3Si_6$. Increasing Fe leads to a gradual reduction in the elongation, impact strength, and tensile strength of Al-Si alloys, while the Brinell hardness and yield strength are reported to increase gradually. Iron contents of up to 0.2% improve the tensile strength, while higher levels reduce the tensile strength and elongation, and increase hardness. [49] It has been reported that the percentage of the β-phase rapidly

increases with the iron concentration for a given concentration of Mn, as shown in Figure 2.14. [50]

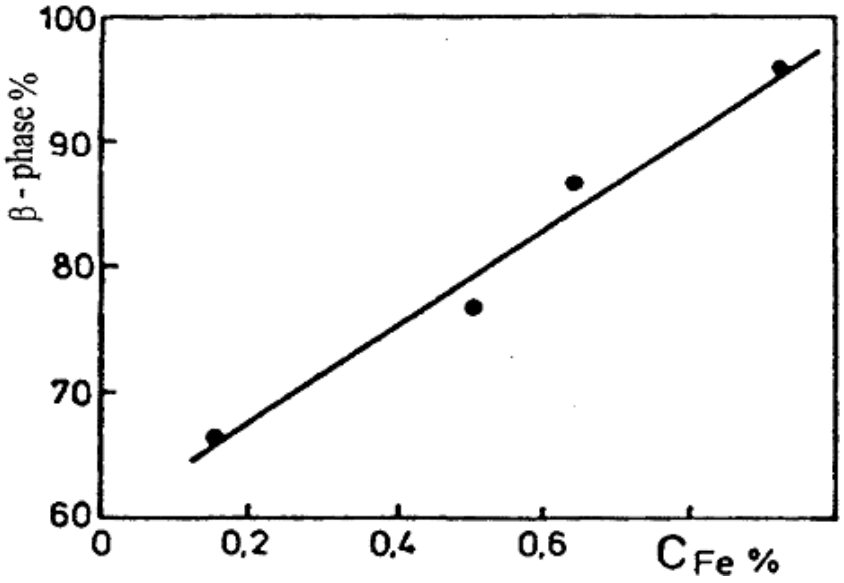

Figure 2.14 Dependence of the percentage of *β*-phase *vs*. iron content in Al-Si cast alloys. [50]

The effects of Fe on the Quality Index, Q, in A356 alloys are shown in Figure 2.15, and indicate that Q decreases upon increasing the Fe content from 0.16 to 0.4% wt. [40] Figure 2.16 reveals that a significant decrease in the yield strength is observed for A357 alloys at Fe contents higher than 0.06 wt% Fe, [44] whereas in 356 alloys, the UTS and YS decrease significantly, by 20 and 18%, respectively, as the Fe level increases from 0.2 to 0.8 wt%, as shown in Figure 2.17. [51]

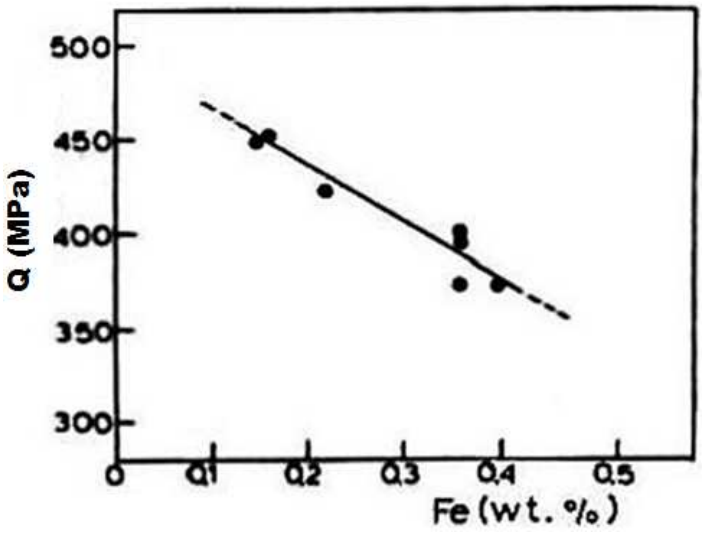

Figure 2.15 Variation of the quality index with Fe content. [40]

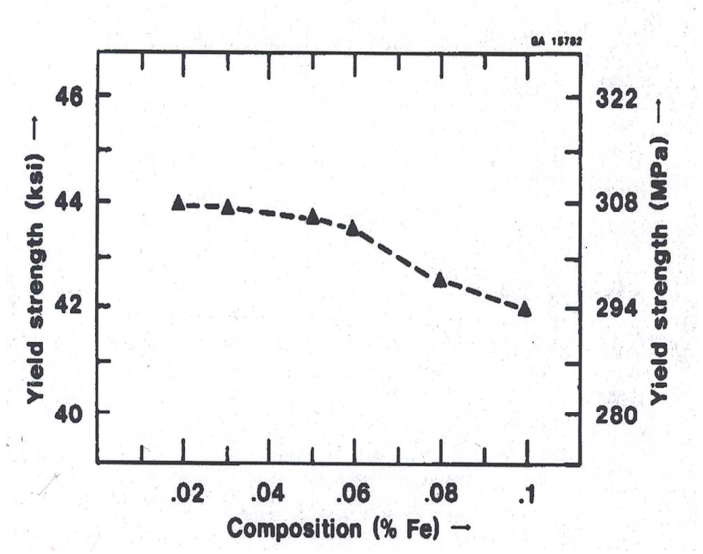

Figure 2.16 Effect of Fe on the yield strength in an A357 alloy. [44]

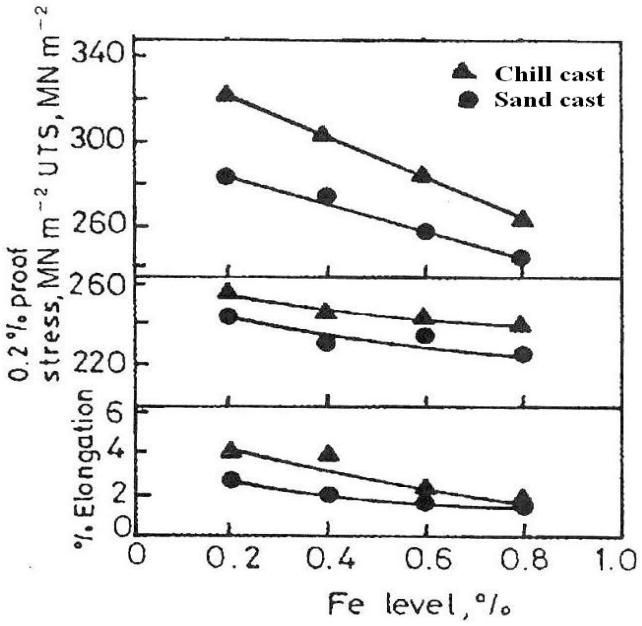

Figure 2.17 Effects of Fe impurity on the mechanical properties of 356 alloys. [50]

Taylor *et al.* [41] studied the effects of Fe content on the volume fraction of the three intermetallic phases, Mg_2Si, β-Fe, and π-Fe in as-cast Al-7Si-0.4Mg alloy; they found that all the intermetallic phases appear to increase with the Fe content, as shown in Figure 2.18, where it may be observed that the dominant phase in all the as-cast alloys studied is the π-iron intermetallic phase.

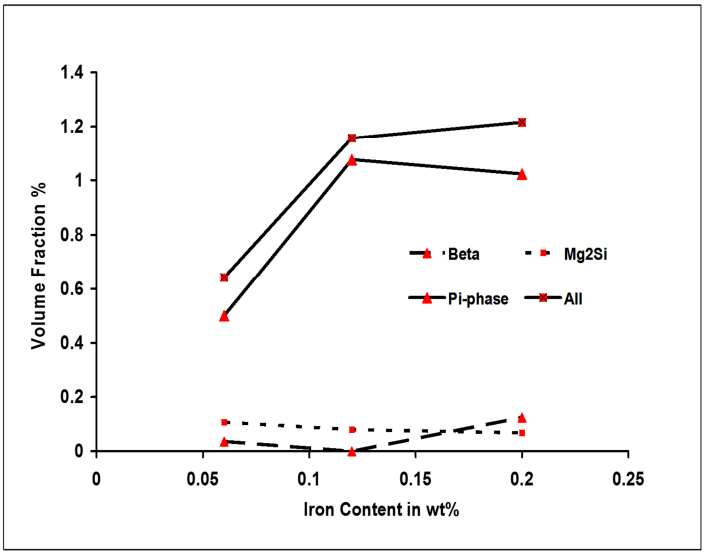

Figure 2.18 Volume fractions of the Mg_2Si, β-Fe and π-Fe phases present in as-cast Al-7Si-xMg-0.12Fe alloy. [41]

2.4.4 Role of Beryllium

Reducing the detrimental effects of iron intermetallics by adding certain elements in trace amounts to the melt has been reported to act as an effective neutralizer of the effects of iron in forming iron intermetallic phases. There are several trace elements which are liable to neutralize the embrittlement effect of iron intermetallics; these include chromium, beryllium, cobalt, manganese, and molybdenum. Beryllium is found or added as a trace element to Al alloys. Figure 2.19 shows the binary Al-Be equilibrium phase diagram. [52] An Al-Be eutectic composition exists at 0.5-1.4 wt% Be with the eutectic temperature at 644-647^{o}C.

The presence of Be in Al-Si casting alloys reduces the oxidation of the molten metal. The diffusion of the small beryllium ions into the oxide film causes a contraction of the oxide which establishes a denser, more protective film on the melt surface thereby impeding attack from the oxygen present in the atmosphere. [53] Adding Be in premium quality aluminum alloys leads to the production of a clean melt and to the formation of an oxidation layer which also prevents Mg from oxidizing, consequently increasing the amount of Mg available to form Mg_2Si for the strengthening of the Al-Si-Mg alloys. [53]

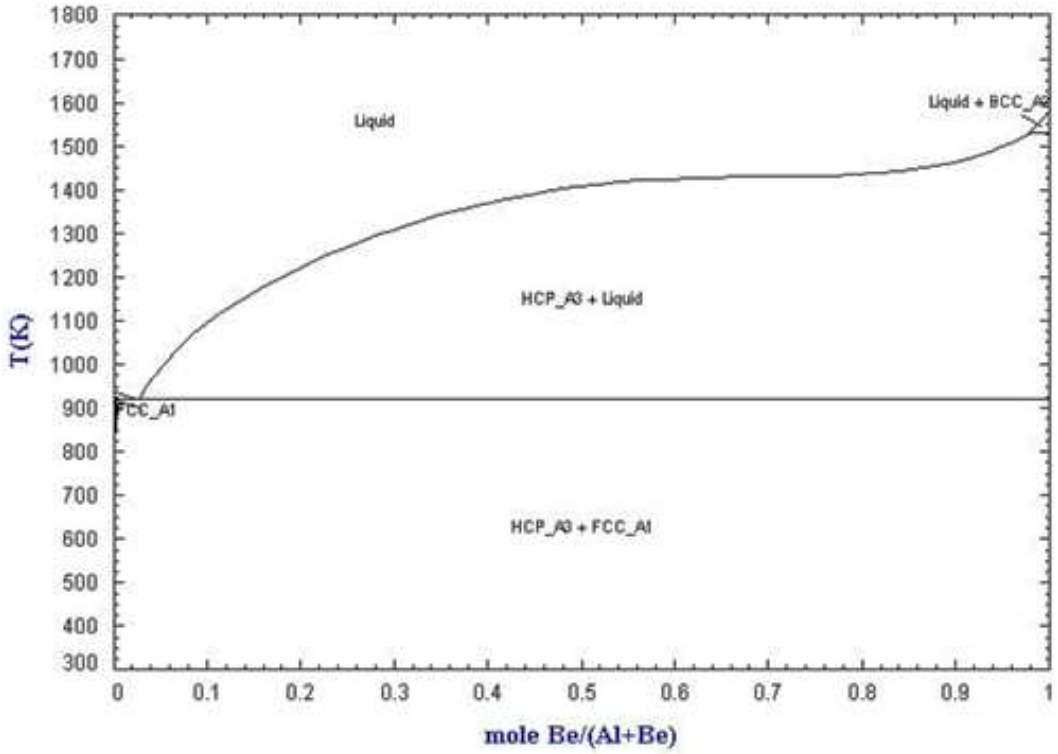

Figure 2.19 Binary Al-Be equilibrium phase diagram. [41]

The amount of π-phase intermetallic in the Be-free 357 alloy is higher than it is in a Be-containing alloy, particularly in the presence of high Mg levels. Also, in Be-containing 357 alloys, the β-Al_5FeSi phase is replaced by the Chinese-script Al_8Fe_2Si phase, which reduces the embrittlement effect of the former. [54] An improvement in the mechanical properties of 356 alloys observed as a result of adding small amounts of Be was attributed to the change in solidification behavior as well as to alterations in the morphology of the β-phase when changing into the Be-Fe (Al_8Fe_2BeSi) Chinese-script phase. [55-57] It has been concluded that the addition of 500 ppm Be reduces the amount of the π-phase formed in Al-7Si-xMg-0.1Fe alloys, such additions also facilitate the decomposition of the π-phase into the β-phase, particularly at higher levels of Mg content, that is to say, 1.0 wt%. [56]

The addition of 500 ppm Be to Al-7Si-xMg-0.1Fe alloys containing 0.4, 0.6, and 1.0wt% Mg has the potential for decreasing the volume fraction of the π-phase intermetallic in both non-modified and Sr-modified alloys, as shown in Figures 2.20 (a) and (b), respectively. Figure 2.21 shows the formation of Be-Fe phases with script morphology in Be-containing Al-7Si-0.6Mg alloys. [56] It has been found that the addition of 0.2% Be to Al-7Si-0.3Mg-0.8Fe results in the replacement of the β-phase by the α-Be-Fe phase; this phase tends to precipitate at temperatures which are higher than the formation temperature of the β-phase, consequently, reducing the iron available to form the β-phase. [57]

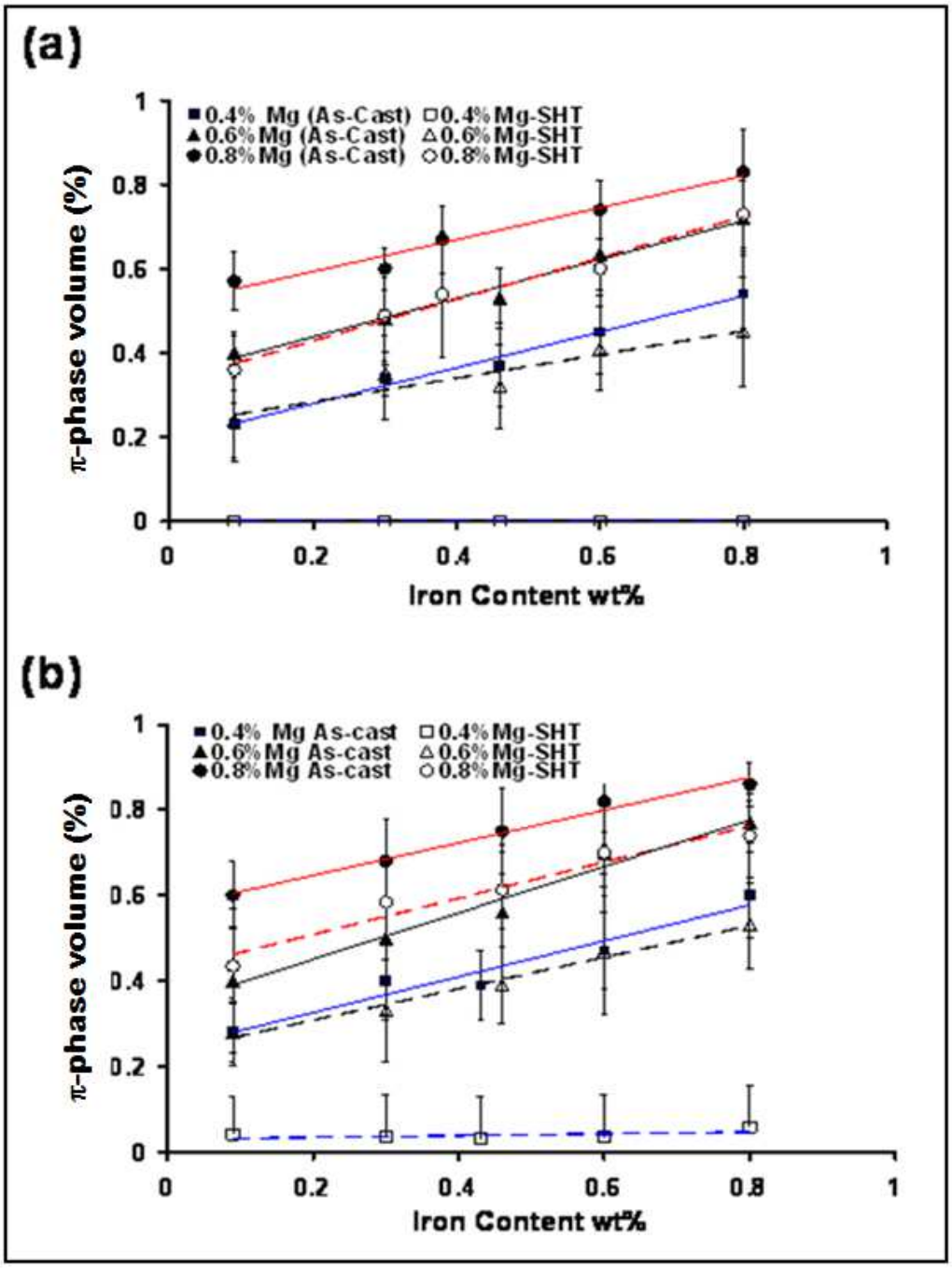

Figure 2.20 Effects of Fe and Mg contents on the volume fraction of π-phase in Al-7Si-xMg-0.1Fe-0.05Be alloys: (a) non-modified alloys; (b) Sr-modified alloys.[56]

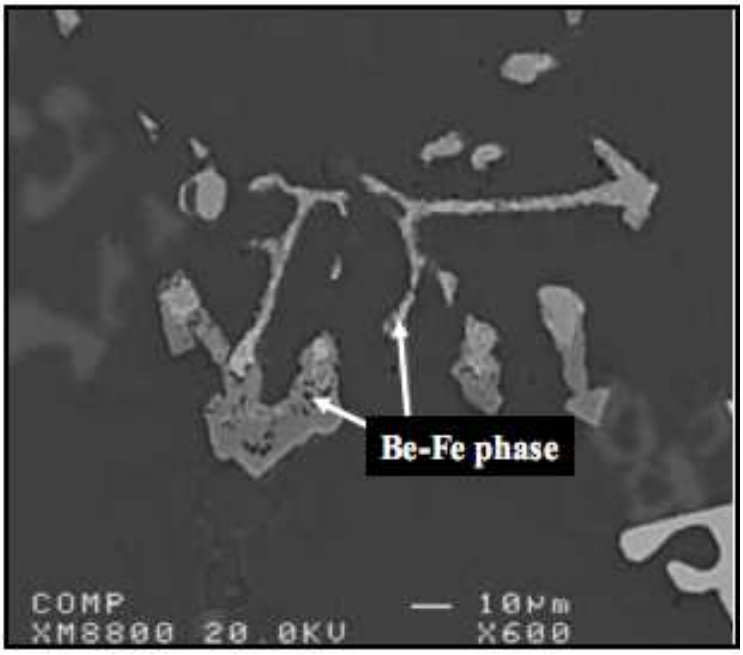

Figure 2.21 Backscattered electron image of Be-containing Sr-modified 357 alloy in the as-cast condition, showing the Be-Fe phase. [56]

Beryllium has a positive effect on enhancing the mechanical properties of Al-Si-Mg alloys. It has been observed that the Be-containing alloys exhibit higher values of tensile strength at all levels of iron content, as shown in Figure 2.22, it is also observed that while the ductility of the Be-containing alloys initially decreases, it still remains higher than the ductility values for the other alloys. [51]

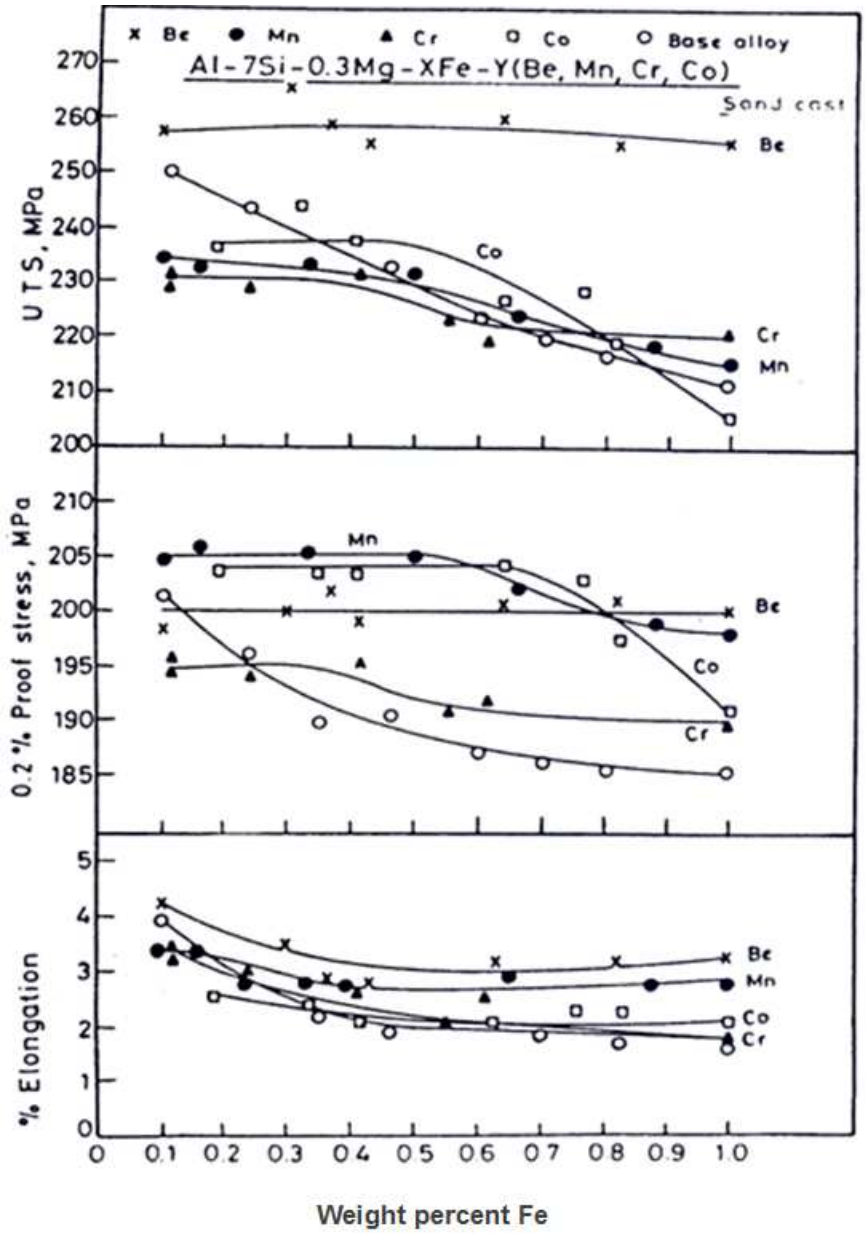

Figure 2.22 Effects of trace additions on the tensile properties of Al-Si-Mg-xFe alloys as a function of Fe content. [51]

2.4.5 Role of Titanium

The quality of Al-Si alloy castings may be improved by grain refinement which reduces the size of the primary α-Al grains in the microstructure, which would otherwise solidify into a coarse columnar grain structure. Chemical grain refinement involves the addition of special substrates to act as nucleants or to react with other elements in the melt to form solid nucleant particles. A fine grain size is promoted by the presence of an enhanced number of nuclei, with solidification proceeding at minimal undercooling. Furthermore, chemical grain refinement is beneficial to mechanical properties, particularly those which are sensitive to hot tearing and porosity. Chemical grain refiners are added to the melt as master alloys, mainly aluminides ($TiAl_3$) and borides (TiB_2), acting as heterogeneous nuclei for the formation of α-Al grains or crystals. According to the Al-Ti phase diagram shown in Figure 2.23, [58] the corresponding peritectic reaction occurs at 1.2 wt% titanium and 665^{o}C, with the limit of the peritectic horizontal placed at 0.15% Ti.

With the addition of Ti as a grain refiner, which introduces large amounts of nucleants into the melt, a number of equiaxed grains are formed, resulting in an improvement in the properties of cast solid solution type alloys. This improvement includes improved soundness, finer distribution of gas porosity, better mechanical deformation characteristics, and improved mechanical properties, such as yield strength, toughness and fatigue life. Grain refinement also improves machinability, the deep drawing ability of products, and surface finishing.

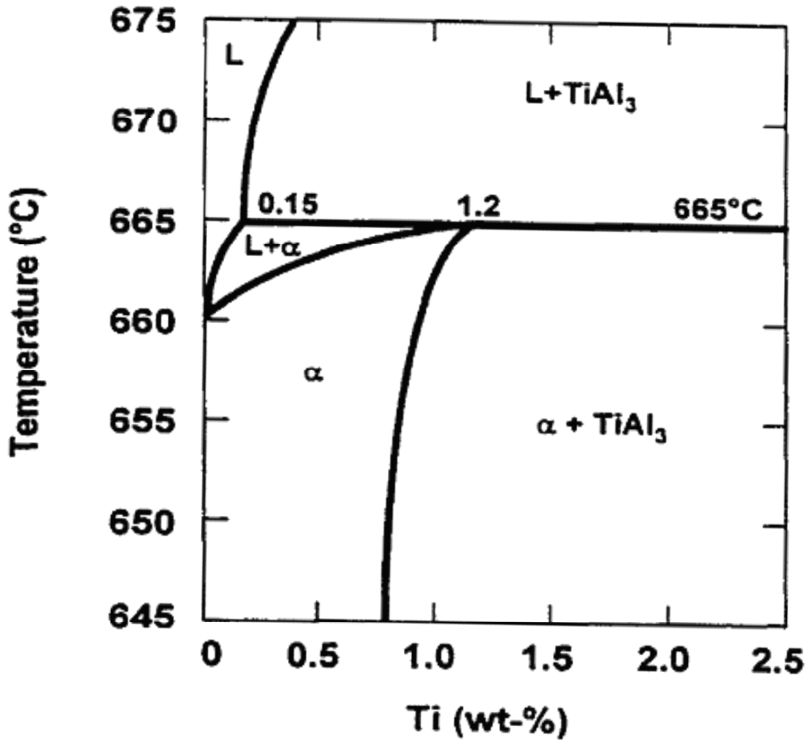

Figure 2.23 Aluminum-titanium phase diagram. [58]

2.4.6 Combination Effect of Beryllium with the Other Alloying Elements

Beryllium, in the presence of iron, changes the *β*-phase platelets into the Be-Fe (Al_8Fe_2BeSi) Chinese-script phase [55-57, 59-62] which confirms its effect on the morphology and chemistry of iron-rich phases and may be increase mechanical performance values of Al-Si iron-containing alloys.

Adding beryllium changes the morphology of iron-rich compounds to Chinese scripts and polygons. The aggregative Be–Fe phases are found in high Fe containing alloys. Be–Fe phases are located inside the *α*-Al. The fracture always takes place on iron-rich compounds. In the Be-containing alloy with iron, the crack propagation on Fe-phase was

delayed during fracture, and this is considered to be beneficial to the fracture toughness of the alloy. The mechanical properties of Be-containing alloys improve significantly. This is attributed to the alteration of Fe phase shape. [59]

It was reported that the mechanical behavior of Al-11%Si casting alloys is dominated by the morphologies of the iron-rich phase and eutectic silicon. The morphology of iron-rich phase is changed from needle-shape into the Chinese-script and the eutectic silicon is refined when beryllium is added. The effect of the addition of Sr on the strength and ductility is superior to that of the addition of Be. The ductility and strength are increased as both the Be and Sr contents are increased. [60] In their study to investigate the mechanism for linear and nonlinear optical effects in $SrBe_3O_4$ crystal, Lin *et al*. [61] have reported that both calculated and experimental birefringence of the $SeBe_3O_4$ crystal are small. Thus it is expected that the crystal would have difficulty fulfilling the phase matching conditions. They confirm the Sr-Be interaction by means of electronic and band structure calculations, but did not assess whether this reaction will affect the alloy mechanical performance leading us to conclude this phase has a relatively negligible effect on the alloy performance.

In Be-containing A357 alloys, both the plate-like β-Al_5FeSi and the script-type π-$Al_8FeMg_3Si_6$ increase with increasing iron content. The iron-bearing phase is mostly transformed from the plate-like β-Al_5FeSi to the script-type π-$Al_8FeMg_3Si_6$ with the addition of Be. The hardness increases with increasing the iron level and with the addition of Be. [62]

The effects of Be and Fe additions on the microstructure and mechanical properties of A357.0 alloys were investigated by Yen-Hung and co-workers. [63] They concluded that a large amount of plate-like shape and Chinese-script shape of Mg-containing structure of iron-bearing phases were found in Be-free alloys. These structures are replaced by nodular shape and script morphology Mg-free structures of iron-bearing constituents when Be is added. The addition of Be could (i) enhance the precipitation kinetics and increase the amounts of Mg_2Si, (ii) reduce the amount and modify the morphology of iron-rich compounds, (iii) lower the ternary and binary eutectic melting point, and (iv) improve the tensile properties. In Be-containing alloys, the silicon particles are smaller, their aspect ratio is closer to 1, and the small nodular iron-bearing compounds can improve the tensile properties. The effect on decreasing mechanical properties damage is more apparent in the higher Fe level than in the lower Fe content when Be is added. [63]

In the case of Al-Si-Mg alloys, where magnesium is one of the main alloying elements, the $MgBe_{13}$ phase precipitates during solidification. The equilibrium phase diagram of the Mg-Be system has not been determined as well as the effect of $MgBe_{13}$ phase formation on the microstructure and mechanical properties has not been evaluated. [64-66] Recently, the Fact Sagedatabase documentation [67] has presented this equilibrium phase diagram, Figure 2.24, from which the $MgBe_{13}$ phase starts solidification at temperature less than 650^oC (925K). In their study of sintered Mg-Be alloys, Ivanov *et al.* [66] have reported that the addition of finely dispersed magnesium oxide and an excess beryllium phase to the magnesium matrix secures an excellent combination of long-time

oxidation and heat resistance at temperatures substantially above the permissible operating temperatures of the usual magnesium-base alloys.

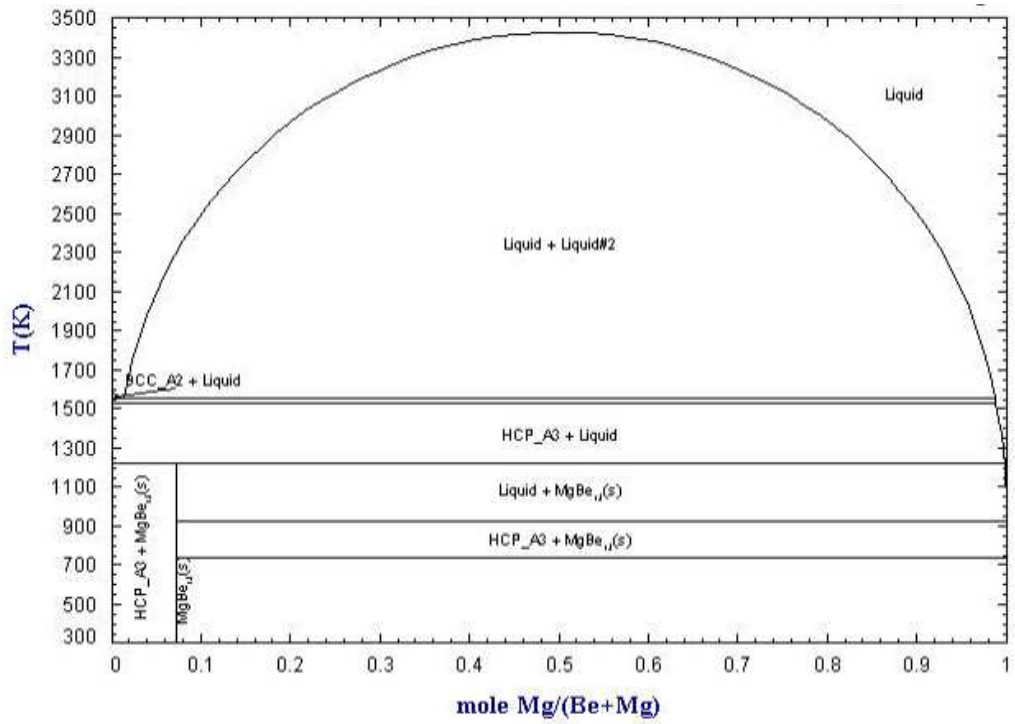

Figure 2.24 Magnesium-beryllium phase diagram. [67]

The addition of magnesium increases strength values during aging as a result of the precipitation of submicroscopic and metastable phases containing Mg and Si which provide distinct obstacles to dislocation movement. [68] In their investigation of the influence of alloying elements in the thermal analysis of Al-Si cast alloys, Heusler and Schneider [69] observed that any Sr-modified microstructure is clearly affected when magnesium is present. Microstructural parameters as obtained from image analysis, such as silicon particle size and aspect ratio, were found to increase with an increasing Mg content, subsequently becoming increasingly inhomogeneous. The reason for the deterioration in

modification is believed to be the formation of intermetallic phases of the type $Mg_2SrAl_4Si_3$, where the addition of Mg also lowers the eutectic temperature; as may be seen in Figure 2.25, the eutectic temperature decreases with increasing Mg content. It was also reported, however, that a magnesium content of ~1 wt% itself acts as a refiner for the eutectic silicon in unmodified Al–Si alloys. [70]

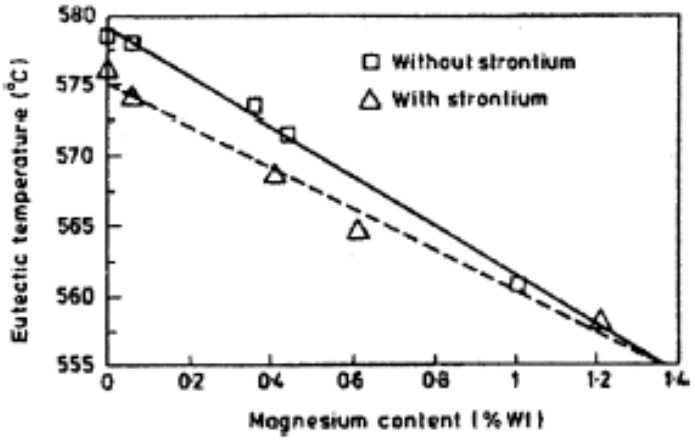

Figure 2.25 Depression of the eutectic temperature as a function of magnesium level for unmodified and strontium-modified Al-Si alloys. [69]

2.5 HEAT TREATMENT OF AL-SI-MG ALLOYS

The main objectives of heat treating cast Al-Si-Mg alloys include homogenization, stress relief, improved dimensional stability, and optimization of the strength and ductility parameters. The T6 heat-treated Al-Si-Mg alloys have an optimum combination of strength and ductility. The typical heat treatment specification of a T6 temper consists of solid solution treatment and quenching, followed by aging. The main effects of solution heat treatment are the dissolution of Mg_2Si particles, the homogenization of the casting, and

modification the morphology of eutectic silicon through fragmentation and spheroidization at critical temperatures. The recommended solution temperature for 356 and 357 alloys is 540±5^{o}C. [5, 12]

The purpose of quenching is to preserve the solid solution formed at the solution heat treatment temperature by rapid cooling to room temperature. The quenching medium and rate are the parameters which control the mechanical properties. The highest strength can be ensured when the material is subjected to a rapid quenching rate. Aging is the final stage of heat treatment in cast Al-Si-Mg alloys. The aging can be natural or artificial. Alloy mechanical properties depend on both aging temperature and time. The main objective of artificial aging is to heat the as-quenched castings to an intermediate temperature between 150^{o}C and 200^{o}C for 4 to 8hrs in order to precipitate the excess solutes which were supersaturated in α-Al during the solution heat treatment process. The improvement achieved in the mechanical properties during artificial aging is due to the precipitation of metastable phases from the supersaturated solution. Al-Si-Mg alloys fulfill the following precipitation sequences: [5, 71]

SS → needle-shaped GP zones → rod-like β' precipitates → platelets of Mg_2Si

For Al-Si-Mg alloys, the solubility of Mg and Si in the Al matrix decreases with temperature, as shown in Figure 2.26. In order to obtain a maximum concentration of Mg and Si particles in solid solution, the solution temperature should be close to the eutectic temperature. For the 356 and 357 alloys, the solution temperature is 540 ± 5^{o}C. At this temperature, about 0.6% Mg can be place in solid solution. The dissolution of Mg_2Si into Mg and Si occurs in the two alloys at 475^{o}C and 540^{o}C, respectively. [12]

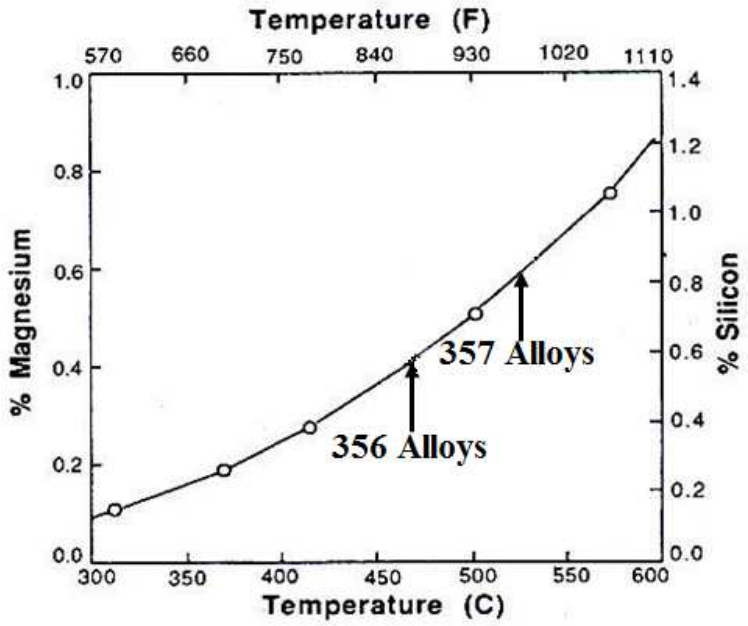

Figure 2.26 Equilibrium solubility of Mg and Si in solid aluminum when both Mg_2Si and Si are present. [12]

Solution heat treatment may also be employed as a useful technique for the dissolution or transformation of iron-rich intermetallic phases. It has been found that, in 357 alloys, there is a reduction in the amount of π-phase at different levels of Mg after heat treatment. Closset and Gruzleski, [38] who studied the effects of solution heat treatment in 356 alloy, observed that the dissolution of the π-phase depends on the levels of iron and magnesium present; thus, at levels of 0.16 wt% Fe and 0.45 wt% Mg the π-phase dissolves, whereas it is only partially dissolved at Mg levels of 0.65%. Gustafsson *et al.* [28] studied the effects of T6 temper on the microstructure of the same alloy as that used by Closset and Gruzleski; [38] they found that no changes were observed in the β-phase, although the π-phase was seen to dissolve after solution heat treatment.

An investigation [72] was carried on the effects of T6 and T4 tempers on the tensile properties of non-modified and Sr-modified A356 alloys obtained from permanent mold and sand mold castings. The results showed that the yield strength is not appreciably influenced by the change in Si-particle characteristics. The UTS and %El increases significantly with increases in the solution treatment time at 540^{o}C, as shown in Figures 2.27 (a), (b), and (c). Also it observed that upon modification with Sr the fracture mode changes from brittle to ductile especially in sand castings. Both non-modified and Sr-modified alloys obtained from permanent mold casting, however, showed ductile fracture mode. All the improvements in the tensile properties reported upon were related mainly to the changes which occurred in the Si particle aspect ratio and particle size during solution treatment.

Yoshida and Arrowood [73] investigated the effects of variations from T6 standard treatment on the hardness, ductility, and UTS of aluminum alloy A356 cast in a permanent mold with and without strontium modification. The main variables considered in the experiments were solutionizing time and temperature. The as-cast samples were solutionized for various periods of time (2, 4, 8, 16, and 32 hrs) at 520^{o}C/540^{o}C and aged at 160^{o}C for 6.5 hours. The highest hardness was obtained at the shortest solutionizing time of 2 hrs for both the unmodified and modified A356 alloy, while the highest ductility was not reached until the samples were solutionized for 8 hrs at the same temperature. A slight change in solutionizing temperature did not cause much variation in hardness, ductility, or UTS. It may also be concluded that the Sr-modified samples exhibit higher elongation than the unmodified ones under all the heat treatment conditions reported in this study.

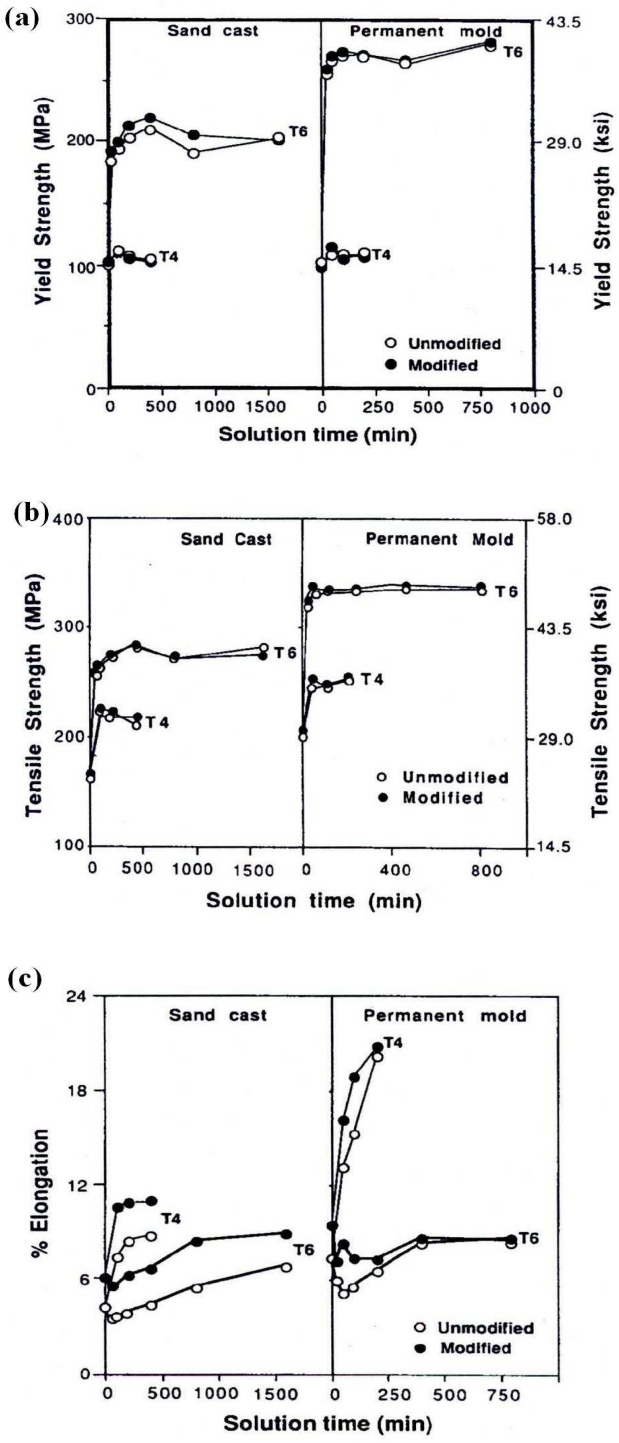

Figure 2.27 Effects of solutionizing time on: (a) Yield Strength, (b) Ultimate Tensile Strength and (c) % Elongation. [72]

A valuable study was carried out by Moustafa *et al.* [74] They concluded that the addition of Sr decreases the hardness and strength (YS, UTS) of the Mg-containing alloys, which could probably arise from a retardation of the precipitation of Mg_2Si during the aging process (i.e., increasing the incubation period prior to the commencement of precipitation), regardless of the solution time. Also, alloying element additions of Mg and Be result in improving the hardness and strength of the base alloy, especially in the T6 condition, where adding small amount of Be (~0.02%) prevents Mg oxidation (i.e., formation of MgO and $MgAl_2O_4$ (spinel)) during melting, the hardness increased slightly. Figure 2.28 (a) and (b) shows the effects of alloying elements additions and the T5 conditions presented in this study; where M1 is Sr-modified, high Mg-containing alloy; M2 is Sr-modified, low Mg-containing alloy; M2B is the alloy M2 after adding Be; M3 is Sr-modified, high Mg-containing alloy; M4 is Sr-modified, low Mg-containing alloy, respectively. [74]

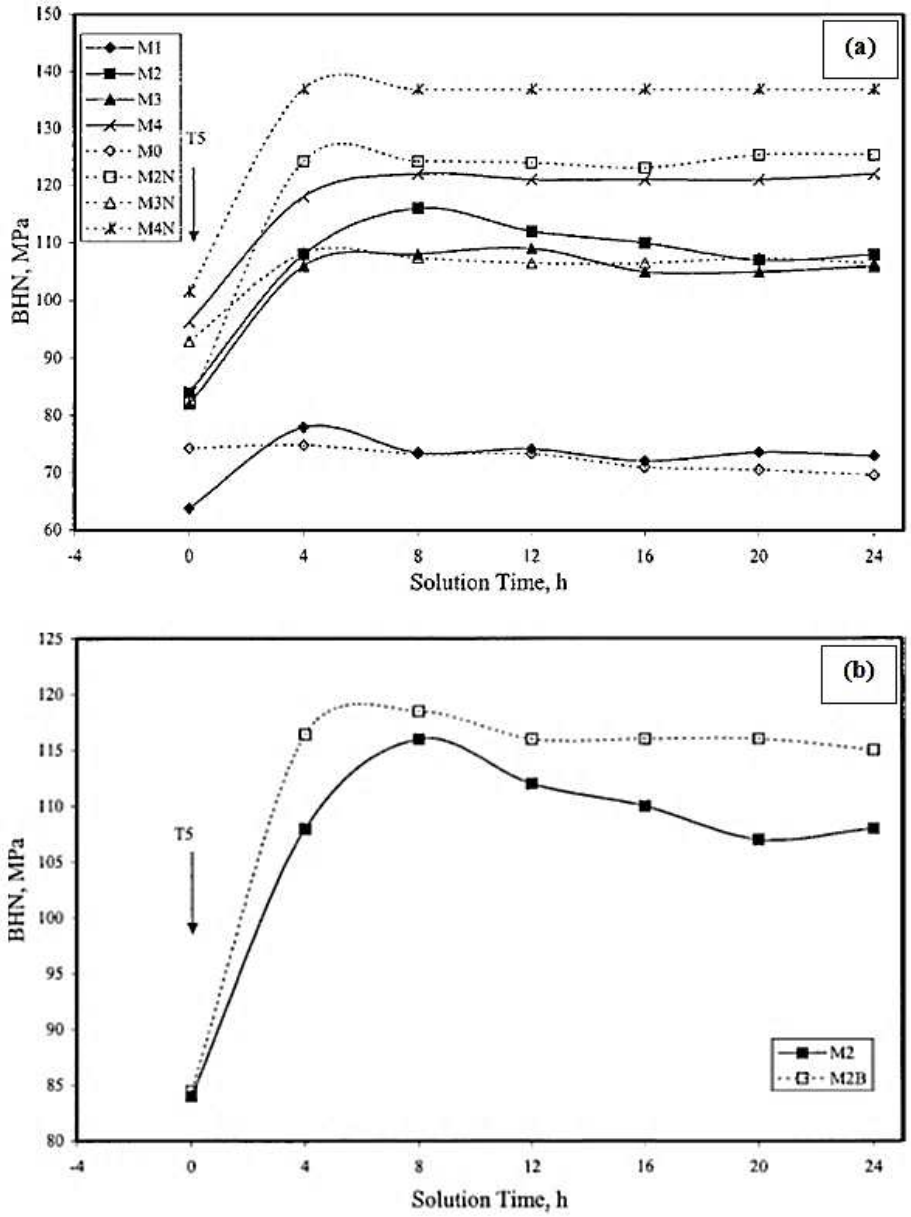

Figure 2.28 (a) Effect of Mg and Cu additions on the hardness of unmodified and Sr-modified A413.1 alloys treated at different solution times and (b) Effect of Be addition on the hardness of M2 alloy as a function of solution time. [74]

2.6 MECHANICAL PROPERTIES OF Al-Si-Mg ALLOYS

Strength, hardness, toughness, elasticity, brittleness, and ductility are all mechanical properties used to determine how metals behave under an applied load. Any improvement in mechanical properties is commonly evaluated through the tensile and impact properties of the material. The following may be considered among the most important of the many variables which affect the mechanical properties of the Al-Si-Mg alloy castings investigated in this study. [1, 2]

(i) Alloy type and the variations in the chemical composition within the specified limits for that alloy; [75-79]

(ii) Metal soundness, which may be affected by gas porosity, shrinkage porosity and non-metallic inclusions; [80, 81]

(iii) Metallurgical characteristics, examples of which are macro-grain size and micro-constituent distribution; [82]

(iv) Solidification rate, which may be related directly to the secondary dendrite arm spacing; [83-85] and

(v) Heat-treatment, which brings about phase transformation of the alloy in the solid state. [86, 87]

2.6.1 Tensile Testing

Tension tests provide information on the strength and ductility of materials under a uniaxial applied load. There are some basic assumptions which must be considered when analyzing the data obtained from such a test: firstly, that the loading must be entirely axial,

and secondly, that the deformation should take place uniformly along the length and through the cross-section of the test specimen. The data recorded from load and elongation may be normalized by either the original specimen length or the instantaneous specimen length to produce engineering stress-strain plots or true stress-true strain plots, respectively. The American Society for Testing and Materials (ASTM) has produced standard test specimen geometries and guidelines for tension testing. [88]

A stress-strain curve has two distinct regions: elastic deformation and plastic deformation. The curve shown in Figure 2.29 is typical of metallic behavior. Elastic deformation is temporary deformation, and displays full recovery when the load is removed. The elastic region of the stress-strain curve is the initial linear portion. Plastic deformation is permanent deformation. It does not recover when the load is removed, although a small elastic component may do so. The plastic region is the nonlinear portion generated once the load-strain exceeds its elastic limit. There is some difficulty in specifying precisely the point at which the stress-strain curve deviates from linearity and enters the plastic region. The convention defines yield strength as the intersection of the deformation curve with a straight-line parallel to the elastic portion and offset 0.2% on the strain axis. The yield strength represents the stress necessary to generate this small amount of permanent deformation. The slope of the stress-strain curve in the elastic region is the modulus of elasticity.

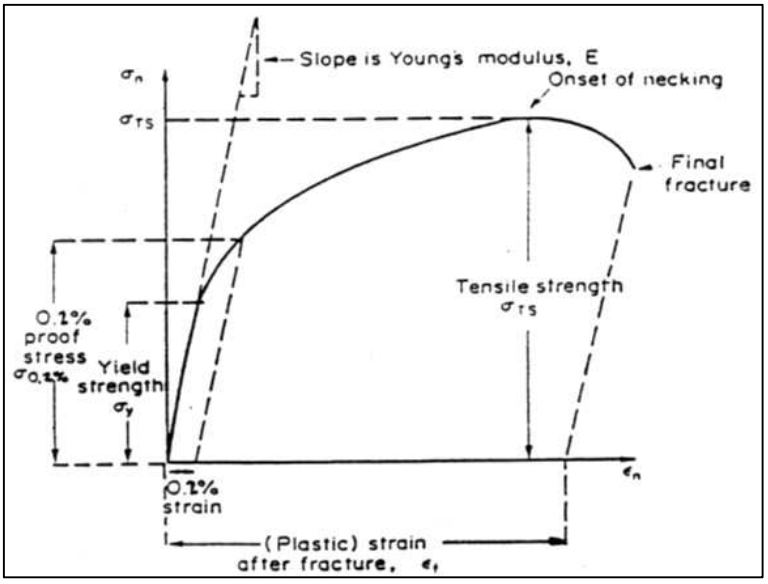

Figure 2.29 Effects Characteristics of the engineering stress-strain curve. [88]

2.7 QUALITY INDEX CHARTS FOR ALUMINUM FOUNDRY ALLOYS

Quality index chart is an applicable evaluation tool used for selecting the optimum conditions to be applied in practice in order to develop superior tensile properties and optimum quality in Al-Si casting alloys. The optimum alloy quality in engineering applications is the great result of applying the maximum performance combined with cost efficiency. Alloy composition, solidification rate, heat treatment procedures, casting defects, and such microstructural features as grain size and intermetallic phases, are all parameters which closely affect alloy quality since they also influence the mechanical properties of the casting. The quality of aluminum alloy castings may be defined using numerical values which correlate to their mechanical properties. [89] The concept of quality

indices and quality charts as well as their progress since 1980 will be reviewed in the following subsections.

For aluminum foundry alloys, the quality of castings may be defined using numerical values which correlate to their mechanical properties. Drouzy *et al.* [90] first proposed these numerical values in 1980 and termed them quality indices; these may be represented by the following equation:

$$Q = UTS + d * \log (El) \quad (1)$$

where Q is the quality index in MPa, UTS refers to the ultimate tensile strength in MPa, El refers to the percentage elongation to fracture and d is a material constant equal to 150 MPa for Al-7Si-Mg alloys. The probable yield strength (YS) for the same alloy may be proposed as:

$$YS = a * UTS - b * \log (El) + c \quad (2)$$

where the coefficients a, b and c for Al-7Si-Mg were determined as 1, 60, and -13 respectively, while the constants b and c are expressed in units of MPa.

Equation (1) is used to generate the iso-Q lines in the quality charts proposed by Drouzy *et al.* [90, 91] whereas Equation (2) is used to generate the iso-probable yield strength lines. The quality chart generated using Equations (1) and (2) is shown in Figure 2.30. These quality charts are generated for use as a simple method of evaluating, selecting, and also predicting the most appropriate metallurgical conditions which may be applied to the castings so as to obtain the best possible compromise between tensile properties and casting quality. The quality index value, Q, is intrinsically related to the level of the quality of the castings which are susceptible to improvement through adequate control of the impurity

elements, casting defects, modification, solution heat treatment and solidification conditions. The probable yield strength, YS, depends mainly on the hardening elements such as magnesium and copper and also on the age-hardening conditions applied to the castings. [89-92] The right selection of the factors mentioned earlier may increase both quality index values and the probable yield strength in the directions shown in Figure 2.30.

The quality chart shown in this figure provides sufficient information for each point located on this type of plot. This information supports the use of these charts in the evaluation of the appropriate metallurgical conditions to be applied to Al-Si casting alloys in order to obtain the specific prerequisite properties. [89] As may be seen in Figure 2.30, the properties which are known for each point located in the chart are the tensile strength, UTS, elongation to fracture, El, yield strength, YS, and the quality index value ,Q.

After plotting the experimentally-determined tensile strength and tensile ductility for a particular alloy, the material of the best quality will be located near the upper right-hand corner. Different alloys or processing conditions may thus be assessed on the basis of their locus on the chart. This is the logic behind the development of quality index charts.[93] The quality index chart proposed by Drouzy *et al*. [90] is the most form applicable for Al-7Si-Mg 356 and 357 alloys as illustrated later.

Din *et al.* [94] observed that the aging results obtained from Al-Cu alloys display curvilinear behavior upon plotting tensile strength versus the logarithm of elongation to fracture. According to these findings, Din *et al.* [94] concluded that the concept described in Equations (1) and (2) is not transferable to Al-Cu alloys. Thus, they proposed an alternative

definition of the quality concept. This new definition of quality index, can be applied also for Al-Si-Mg alloys, has the form of:

$$Q_N = S_{0.2} + k * \log (El) \quad (3)$$

where $S_{0.2}$ is the 0.2% proof strength and k is a material constant expressed in MPa which has a value of 50 for the under-aged and over-aged properties of A356 and A357 alloys. Figure 2.31 shows the quality chart generated using Equation (3) and also illustrates the properties which may be obtained for each point located in this particular type of chart.

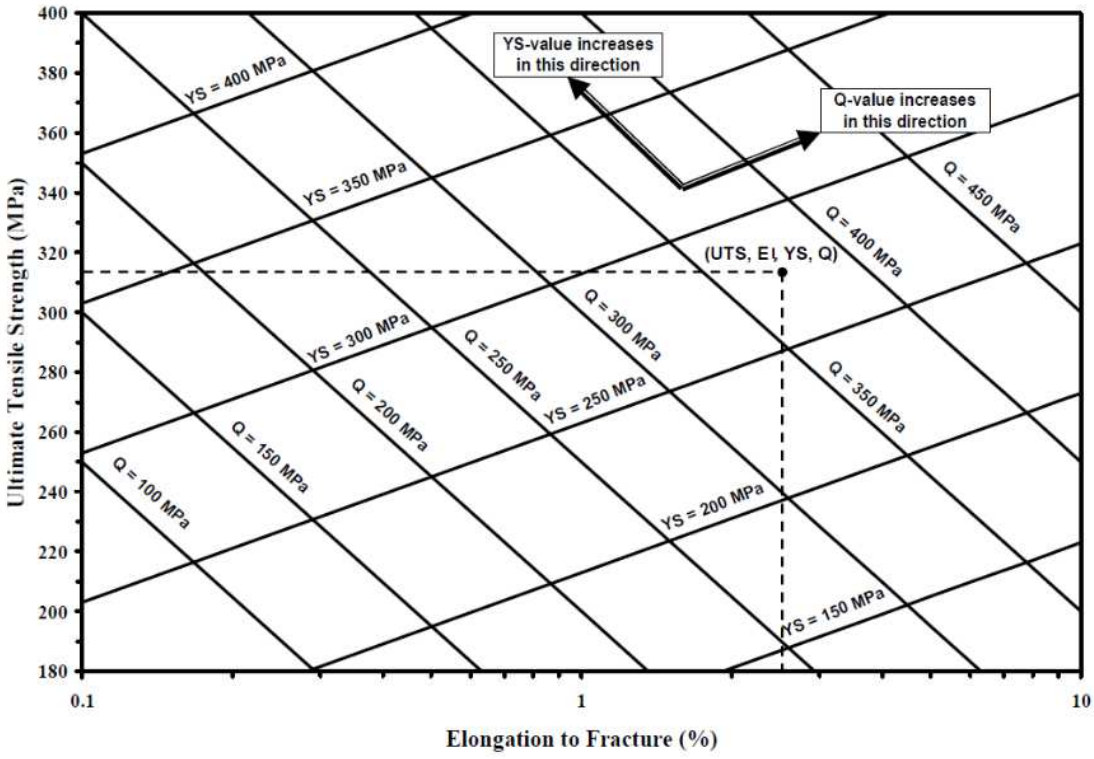

Figure 2.30 Example of the quality chart proposed by Drouzy *et al.* [90] generated using Equations (1) and (2).

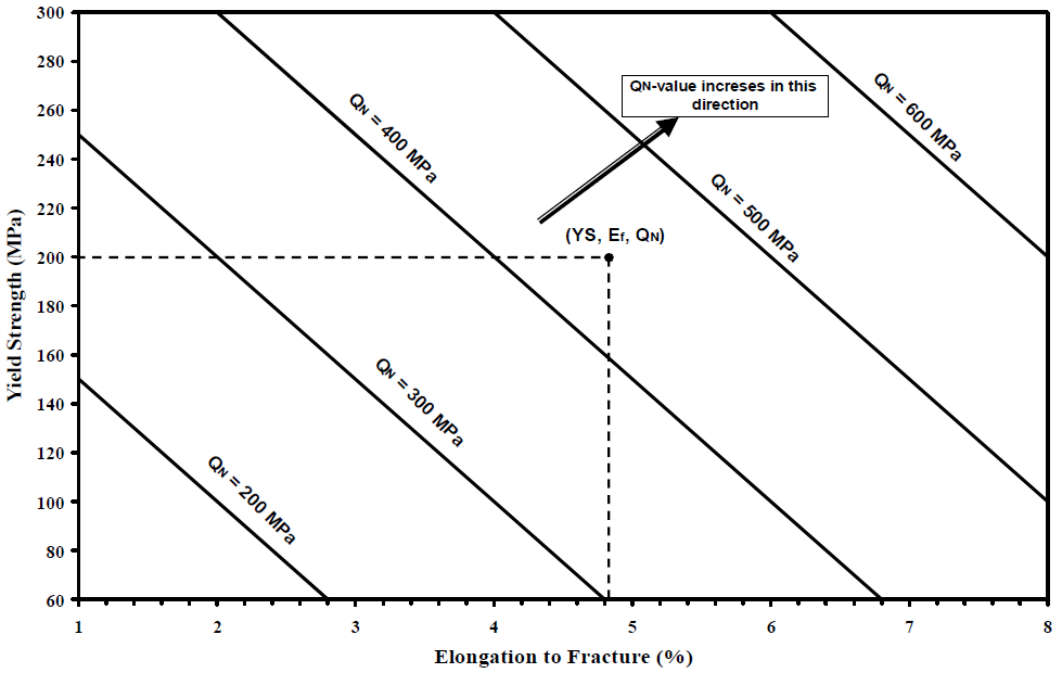

Figure 2.31 Example of the quality chart proposed by Din *et al.* [94] generated using Equation (3) for Al-Si-Mg casting alloys with k = 50 MPa.

Several authors [95-102] have developed some other definitions and forms for the quality index. The form suggested by Cáceres [95, 96] has developed as a theoretical model that depends on both the true stress and the true strain in the plastic deformation region through tensile testing. This form is similar to that presented by Din *et al.* [94] for Al-Cu alloys with more parameters each of them represent a factor affecting alloy quality. The Q index charts proposed by Alexopoulos and Pantelakis [97-101] as well as by Tiryakioğlu *et al.*[102] used for evaluating aluminum casting alloys for aircraft applications. These charts based on strain energy which is an indicator for the ductility and fracture toughness of the aluminum castings i.e. the amount of the absorbed energy up to fracture.

2.8 Al-Cu-Mg-Zn WROUGHT ALLOYS

The 7075 alloy demonstrates a high response to age hardening. [103-109] It was reported that the T73 (180-280°C/8h) treatment with aging at a higher temperature reduces tensile strength by 15%. Using a combination of T6 (120°C/24h) and T73 tempers was recommended to resist stress corrosion cracking; also, increasing the Cu content compensates for the overaging effect in strength reduction. [108-112] Thermomechanical treatments, *i.e.* combinations of aging and deformation, and retrogression and re-aging (RRA) are other procedures used to optimize the 7000 alloy series tensile properties. The RRA sequence after solution heat treatment and quenching in cold water is: (i) T6 aging, 120°C/24h, (ii) short time heating, 200-250°C/5-10 min, followed by cold water quenching and (iii) T6 re-aging, 120°C/24h. [112-114]

At room temperature, high strength age hardenable 7xxx alloys are difficult to process by plastic deformation processes. The 7075 alloy develops an ultrafine structure and higher strength when it has been processed at cryorolling (CR) temperatures compared to room temperature rolling (RTR). The higher strain (more than 3.4) sample produced an ultrafine grained structure in case of RTR, but the yield stress was still low due to the effective suppression of dynamic recovery and accumulation of the high dislocation density during low temperature rolling. In the case of CR samples, the hardness, yield strength and tensile strength were increased from 107 to 194 MPa, 155 to 559 MPa and 368 to 602 MPa, respectively. It was concluded that cryorolling is an ideal process to deform the 7075 alloys up to a high rolling strain (3.4), while the RTR limits the deformability of these alloys due to deformation of GP zones. [115]

Many studies [116-122] focused on the effect of heat treatment on the strength of 7075 alloys. The solutionizing and aging temperatures are the main factors controlling the relative alloying elements which precipitate in the grain boundaries; the solutionizing temperature is the main influence on grain boundary segregation. The precipitates on the grain boundaries consisted of large amounts of Mg, Si and Al along with a lesser amount of Zn and Cu. The Zn-rich precipitates were predominant in heat treatments during low solution annealing (394°C) while the Fe-rich precipitates were predominant in the case of high solution temperature (482-527°C). [116] Precipitates with high interfacial energies tend to precipitate at grain boundaries, resulting in embrittlement. Low interfacial energy means easy nucleation, a uniform precipitate distribution and resistance to coarsening at elevated temperatures. [117]

The microstructure of commercial 7075 alloy in the peak-aged T651 temper (stress-relieved by stretching and 100°C/8h-24h) contains predominantly the ή transition phase (the primarily plate-shaped ή particles have diameters ranging from 3 to 10 nm) before formation of the stable η-$MgZn_2$ phase take place. Some of these transition phase particles are heterogeneously nucleated on dislocation lines. In the T7 microstructure, the overall particle concentration is high, consisting mainly of coarse transition plate-shaped phase particles η_1, η_2 (in a bimodal size distribution where η_2 particles ranging from 12.5 to 30 nm in diameter and finer η1 particles 5 to 10 nm in diameter) and the lath-type morphology η_4 beside small amount of fine particles of the last three phases (η1, $\eta_{2 \text{ and }} \eta_4$). Increase in the hardness of the 7075 alloy is believed to arise mainly from of the fine dispersion of

small ή particles. [118] Retrogression aging treatments for 7075 alloy sheets at various temperatures (180, 200 and 220°C) and times (2-80 min) showed that an increase in treatment temperature decreased both the hardness and strength, while increasing the impact toughness. This can be explained by the dissolution of phases in the matrix during RRA and enlargement of segregation during subsequent aging. The decrease in the hardness in the first stage of RRA is explained by the partial dissolution of the GP zones while the subsequent increase in hardness refers to the formation and growth of the ή-phase to a specific size of stable η particles. [119]

The structure of the grain boundary particles which depends on the aging process is the main parameter controlling the 7075 alloy mechanical properties. The high strength of this alloy in the RRA temper is considered to arise from both the presence of many fine ή particles, which are probably coherent, and of the high overall concentration of particles in this structure. [120] The double aging (DA) of 7075 alloy has a positive effect on hardness, and yield and ultimate tensile strengths. Moreover, double aging to peak hardness results in a significantly reduced processing time from 48 to 2 hours, which can lead to reduced energy and cost. Thermomechanical double aging causes further acceleration of precipitation, reducing the total heat treatment time to 80 minutes, with an increase in both hardness and strength, but a decrease in the ductility relative to single aging. [121] During study of secondary aging, it was concluded that the T614 temper produces tensile properties close to or greater than those for the T6 condition. [122] According to Lumley *et al*. [122] the T614 consists of Solution treat, quenched, aged at 130°C, quenched then aged at 65°C.

Several authors have studied the effects of alloying elements and heat treatment conditions on the tensile properties of 7xxx alloys. [123-132] Their investigations showed that Ag-free T6-tempered (121°C/24h) 7075 alloys exhibit low strengths, attributed to a relatively coarse dispersion of the hardening precipitates, while Ag-containing alloys display higher strengths. When Cr and Mn were added to the Ag-containing alloys, they resulted in low strengths as with the Ag-free alloys, due to quench sensitivity of particles containing either Cr or Mn. On the other hand, adding the latter two elements to Ag-free alloys resulted in higher strengths. Adding 0.3 to 0.4% Ag did not increase the strength of single and double-aging tempered alloys in both T6 and T7 treatments (121, 157, 162 and 177°C), whereas the stress corrosion cracking (SCC) resistance was improved. Alloys containing Cr, in particular those also containing Zr and Mn, were more resistant and increased in strength, as a result of the reduced sensitivity to quenching rate. Higher strengths were obtained by increasing Cu content in alloys containing Mn and Zr in the case of double aging treatments. Zinc levels in Cr-containing alloys increased both the SCC resistance and quench sensitivity with little strength advantage. [123, 124]

Investigation on direct chill (DC) cast 7xxx series, modified with Zr and Sc, revealed that: (i) Sc additions produced a grain-refined microstructure with equiaxed grain morphology, where an addition of 0.18%Sc reduced the grain size to 120 µm and inhibited the formation of twinned columnar grains and solidification cracks, (ii) higher Sc levels such as 0.38% and 0.48% formed the brittle primary Al_3(Sc,Zr) phase, which led to a deterioration of mechanical properties, (iii) homogenization and T6 treatments developed both the strength and ductility of alloys containing Sc, where the room temperature yield

strength and elongation were 490-590 MPa and 15%, respectively; at liquid nitrogen temperatures (-196°C to -210°C), however, the values obtained were 610 MPa and 10%, respectively, with a UTS of 720 MPa. [125] The Sc-modified 7075 alloy presented the highest strength (640 MPa) and significantly increased the SCC resistance. Addition of 0.2% Sc resulted in the formation of $Al_3(Sc_{1-x}Zr_x)$ phase which refined the microstructure. The addition of Ce had little strengthening effect. [126] The presence of 2% of Al-5Ti-1B master alloy to Al-12 Zn-3Mg-2.5Cu alloy reduced its grain size from 480 µm to 40 µm; the hardness of Ti-refined and T6-tempered alloys was significantly increased.[127] The results obtained by researchers [123-127] are similarly close to those reported by others. [128-134]

CHAPTER 3

EXPERIMENTAL PROCEDURES

CHAPTER 3

EXPERIMENTAL PROCEDURES

3.1 INTRODUCTION

This chapter will provide all the relevant details concerning the alloys and additives used in the current research, together with a description of the general melting and casting procedures applied; this will include a characterization of the microstructure and a discussion of the tensile testing method used to determine the mechanical properties of the alloys investigated. It is worthwhile mentioning here that the number of samples which were cast for the study was considerable, in the order of 3000 test bars, giving an idea of the quantity of molten metal which was processed in the preparation of the castings. Three kinds of test samples were produced: (i) thermal analysis specimens; (ii) tensile test bars; and (iii) samples for chemical analysis.

3.2 ALLOY PREPARATION AND MELTING PROCEDURES

The B356 and B357 alloys used in the present study were received in the form of 12.5-kg ingots, the chemical composition of which is shown in Table 2.1 (section 2.2). The Mg level of the alloy was increased by adding pure Mg to the alloy melts to obtain Mg levels of 0.4 wt%, 0.6 wt% and 0.8 wt%. The Fe and Be were added in the form of Al-

25%Fe and Al-5%Be master alloys, respectively, to the alloy melt to obtain Fe levels of 0.09 wt%, 0.2 wt% and 0.6 wt%, and a Be level of 0.05 wt%. For Sr-modification and grain refining purposes, Sr and Ti were respectively added in the form of Al-10% Sr and Al-5% Ti master alloys to the alloy melts, to obtain levels of 0.02 wt% Sr and 0.15 wt% Ti.

Experimental 7075 alloy (coded alloy A) was prepared through the addition of measured amounts of Mg, Zn, Si, Cu and Fe to a commercially pure aluminum melt. Alloying elements were added in the form of master alloys or pure metals to obtain the predetermined level/levels of each. Table 3.2 shows the average chemical composition of the aluminum base metal and the alloy A. In addition, a variation of the experimental 7075 alloy (termed “B alloy” hereafter) was also used in this study, the composition of which is proprietary to TAMLA research group, UQAC. In order to avoid hot tearing, small amounts of TiB_2 and Zr were added in the form of Al-5%Ti-1%B and Al-25% Zr master alloys, respectively. Beryllium was added in the form of Al-5%Be master alloy as mentioned before.

3.3 MELTING AND CASTING PROCEDURES

The alloys were prepared using an electrical resistance furnace having a large 40-kg crucible capacity. About 35 kg of each alloy was prepared. The melting temperature was maintained at 750˚C ± 5˚C. At this temperature, measured additions of Mg, Fe, Be, Sr, Zr and Ti were made to the melt by means of a perforated graphite bell. Prior to casting, the molten metal was degassed for 15 minutes using pure, dry argon, to remove the hydrogen and inclusions. In addition to the required number of tensile test bar castings prepared from

each melt, one sampling for thermal analysis purposes and two samplings for chemical analysis - one before the start of casting and one at the end of casting - were also taken from each melt. The chemical analysis was carried out using arc spark spectroscopy at General Motors facilities in Milford, NH. The actual chemical composition of each of the alloys prepared is shown in Tables 3.1 and 3.2, representing average values taken over three spark measurements made for each chemical analysis sample. The alloys A1 through C3B shown in the table represent the eighteen non-modified alloys, whereas alloys A1S to C3BS correspond to their Sr-modified counterparts. The Sr level ranged from 0 to 0.02 wt% in these alloys.

In Table 3.1, prefixes A, B and C correspond to Fe levels of 0.09, 0.2 and 0.6, respectively, while codes 1, 2 and 3 correspond to Mg levels of 0.4, 0.6 and 0.8, respectively, and suffixes B and S represent Be addition and Sr modification, respectively.

Table 3.1 Average chemical composition (wt%) of the 356 and 357 alloys studied

Alloy Code	Element Concentration (wt%)								
	Si	**Fe**	**Mg**	**Cu**	**Mn**	**Ti**	**Sr**	**Be**	**Al**
A1	7.02	0.101	0.376	0.050	0.010	0.143	0.001	-	Bal.
B1	7.00	0.203	0.383	0.008	<0.001	0.151	0.001	-	Bal.
C1	6.97	0.630	0.372	0.011	0.002	0.174	0.001	-	Bal.
A2	6.99	0.113	0.590	0.042	0.008	0.164	0.001	-	Bal.
B2	7.03	0.210	0.570	0.009	0.002	0.179	0.001	-	Bal.
C2	6.88	0620	0.540	0.010	0.002	0.172	0.001	-	Bal.
A3	7.08	0.123	0.760	0.034	0.007	0.192	0.002	-	Bal.
B3	7.35	0.226	0.750	0.009	0.002	0.197	0.001	-	Bal.
C3	7.07	0.630	0.750	0.010	0.003	0.183	0.002	-	Bal.
A1B	7.33	0.093	0.368	0.052	0.006	0.180	0.001	**0.034**	Bal.
B1B	6.61	0.197	0.474	0.011	<0.001	0.180	0.001	**>0.036**	Bal.
C1B	6.89	0.670	0.510	0.011	0.002	0.186	0.003	**>0.036**	Bal.
A2B	7.26	0.081	0.530	0.006	<0.001	0.173	0.001	**>0.036**	Bal.
B2B	6.60	0.184	0.710	0.007	<0.001	0.177	0.001	**>0.036**	Bal.
C2B	6.22	0.680	0.700	0.007	0.002	0.183	0.001	**>0.036**	Bal.
A3B	6.50	0.127	0.980	0.034	0.006	0.203	0.001	**0.026**	Bal.
B3B	6.38	0.196	0.960	0.009	0.001	0.210	0.001	**>0.036**	Bal.
C3B	5.96	0.560	0.920	0.009	0.003	0.221	0.002	**>0.036**	Bal.
A1S	7.06	0.103	0.338	0.046	0.010	0.139	**0.016**	-	Bal.
B1S	7.18	0.217	0.354	0.014	0.002	0.165	**0.019**	-	Bal.
C1S	7.18	0.660	0.349	0.007	0.002	0.172	**0.017**	-	Bal.
A2S	7.07	0.105	0.520	0.033	0.002	0.156	**0.018**	-	Bal.
B2S	7.26	0.217	0.530	0.009	0.001	0.169	**0.015**	-	Bal.
C2S	7.17	0.640	0.530	0.008	0.002	0.154	**0.017**	-	Bal.
A3S	7.98	0.101	0.820	0.035	0.002	0.152	**0.013**	-	Bal.
B3S	7.26	0.185	0.730	0.030	0.002	0.171	**0.009**	-	Bal.
C3S	6.84	0.710	0.860	0.034	0.005	0.169	**0.006**	-	Bal.
A1BS	6.54	0.122	0.640	0.041	0.007	0.227	**0.048**	**>0.036**	Bal.
B1BS	6.12	0.190	0.491	0.009	<0.001	0.217	**0.027**	**>0.036**	Bal.
C1BS	7.78	0.810	0.530	0.084	0.012	0.210	**0.016**	**>0.036**	Bal.
A2BS	7.64	0.123	1.030	0.010	0.002	0.243	**0.024**	**>0.036**	Bal.
B2BS	5.93	0.194	0.730	0.007	<0.001	0.227	**0.023**	**>0.036**	Bal.
C2BS	7.06	0.670	0.710	0.007	0.002	0.222	**0.022**	**>0.036**	Bal.
A3BS	7.26	0.105	0.950	0.020	0.002	0.188	**0.023**	**>0.036**	Bal.
B3BS	6.33	0.194	0.950	0.021	0.002	0.189	**0.017**	**>0.036**	Bal.
C3BS	6.21	0.690	0.850	0.033	0.005	0.207	**0.014**	**>0.036**	Bal.

Table 3.2 Average chemical composition (wt %) of the base metal and the 7075 alloys studied

Alloy Code / Alloying Elements	**Si**	**Fe**	**Cu**	**Mn**	**Cr**	**Ni**	**Zn**	**Mg**	**Ti**	**Zr**	**Al**
Base Metal (Pure aluminum)	0.050	0.090	<0.001	<0.001	<0.001	0.006	0.002	<0.001	0.005	<0.001	99.83
A (Base Alloy)	0.172	0.384	1.980	0.330	0.303	0.022	6.420	2.260	0.016	0.021	Bal.
B	0.1 - 0.4	0.12 - 0.50	1.2 - 2.0	0.06 - 0.30	0.2 - 0.4	0.05 - 0.40	5.2 - 6.5	1.5 - 3.0	0.06 - 0.20	0.10 - 0.35	Bal.

3.3.1 Thermal Analysis

In order to obtain the cooling curves and to identify the main reactions and corresponding temperatures occurring during the solidification of Al-Si-Mg alloys, thermal analysis was carried out for all of the compositions prepared. The molten metal for each composition was poured into a cylindrical graphite mold of 80 mm height and 60 mm diameter which had been preheated to 600°C so as to create a slow cooling rate resembling equilibrium conditions in order to facilitate identifying the phases formed. A high sensitivity Type-K (chromel-alumel) thermocouple, which had been insulated using a double-walled ceramic tube, was attached to the centre of the graphite mold, as shown in Figure 3.1(a). The temperature-time data was collected using a high speed data acquisition system linked to a computer. From this data, the cooling curves and the corresponding first derivative curves for the different alloys were plotted so as to identify the main reactions occurring during solidification with the corresponding temperatures. Cylindrical specimens, 15 mm deep, were sectioned off at the centre of each graphite mold casting close to the thermocouple tip. Samples, 2.5 x 2.5 cm in cross-section, were machined from these

specimens, mounted in bakelite and polished following standard procedures, for qualitative and quantitative microstructural analysis.

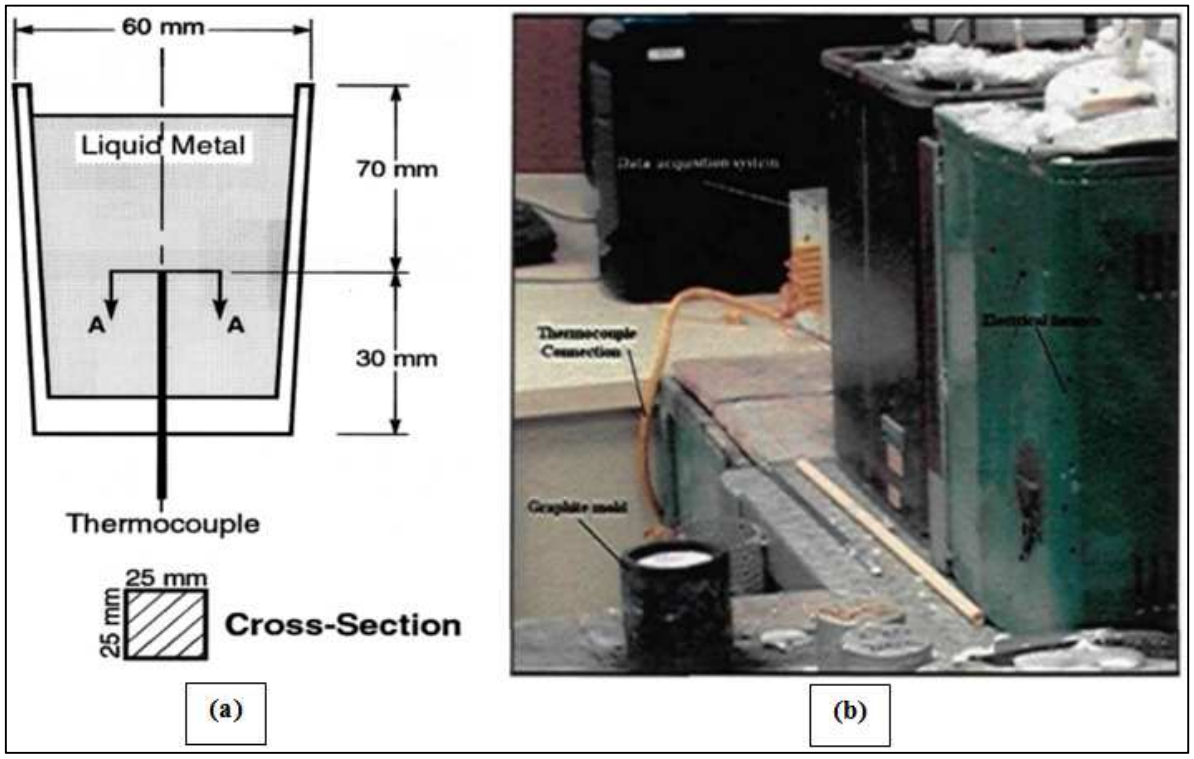

Figure 3.1 (a) Schematic drawing showing the graphite mold and (b) set-up used for thermal analysis.

3.3.2 Preparation of Tensile Bars

The various 356, 357 and 7075 alloys were used to prepare castings from which test bars were obtained for tensile testing purposes. With this aim in mind, the degassed molten metal was carefully poured into an ASTM B-108 permanent mold preheated to 450°C, to obtain castings for tensile testing. At the bottom of the pouring cup a ceramic foam filter (10 ppi) was placed to prevent inclusions and oxide films from entering the mold. This mold and casting set-up used are shown in Figure 3.2(a) while Figure 3.2(b) shows the actual casting obtained. As may be seen from Figure 3.2(c), each casting provided two test bars, each with a gauge length of 50 mm and a cross-sectional diameter of 12.8 mm.

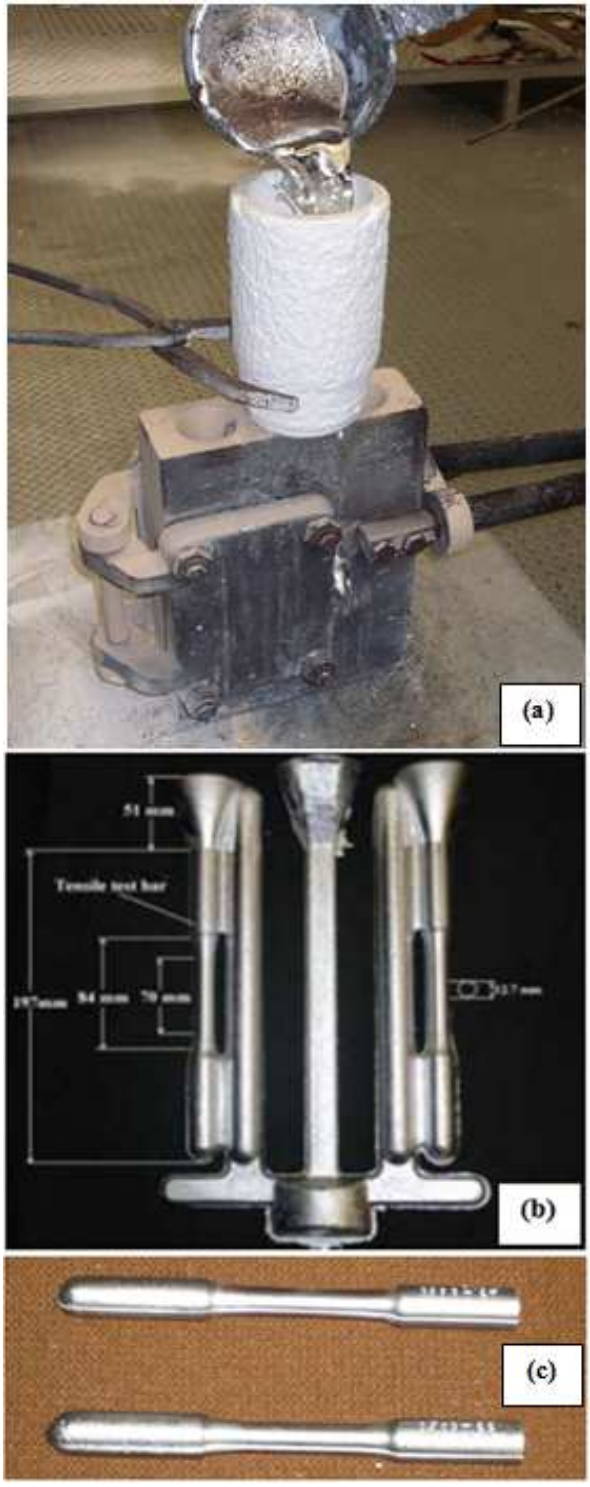

Figure 3.2 (a) Standard ASTM B-108 permanent mold and casting set-up used, (b) actual tensile test casting, and (c) actual test bars sectioned from the casting.

3.4 HEAT TREATMENT PROCEDURES

The bars of 356 and 357 alloys prepared for each alloy composition were divided into thirteen sets; one set was kept in the as-cast condition; one set was solution heat-treated at 540ºC for 5 hours, then quenched in warm water at 65ºC and maintained in the solution heat-treated condition; one set was solution heat-treated at 540ºC for 12 hours, then quenched in warm water at 65ºC and maintained in the solution heat-treated condition; five sets were solution heat-treated at 540ºC for 5 hours, then quenched in warm water at 65ºC followed by artificial aging at 160ºC for 2, 4, 6, 8, and 12 hours, respectively; the remaining five sets were solution heat-treated at 540ºC for 12 hours, then quenched in warm water at 65ºC followed by artificial aging at 160ºC for 2, 4, 6, 8, and 12 hours, respectively. Prior to Aging treatments, samples were stabilized at room temperature (25ºC) for 24 hours. The solution and aging heat-treatments were carried out in a forced-air Blue M electric furnace equipped with a programmable temperature controller, accurate to ± 2ºC. The quench delay was less than 10 s. For each individual heat treatment, five test bars were used.

For the 7075 alloys, the test bars were prepared for each alloy composition and divided into different sets according to both the recommended traditional heat treatment and the proposed new heat treatment conditions. Six sets of five bars of the base alloy A were conventionally heat-treated, i.e., solution heat-treated at 470ºC/8h, then quenched in 65°C warm water. One set was kept in the solution heat-treated condition, while the other five sets were aged subsequently, using different aging conditions; the first set was subjected to single aging at 120ºC/24h, the second set to single aging at 280ºC/8h, the third

set to double aging at 120ºC/24h, followed by 180ºC/8h, the fourth set to retrogression and re-aging at 180ºC/8h, followed by 120ºC/24h, and, finally, the last set was subjected to retrogression and re-aging at 280ºC/8h, followed by 120ºC/24h, respectively. Two sets of the B alloy were heat-treated by means of homogenization and the proposed new aging process (also proprietary to TAMLA research group, Université du Québec à Chicoutimi). For each heat treatment, ten tensile bars were tested.

3.5 TENSILE TESTING

Test bars corresponding to each alloy composition/heat treatment condition were pulled to fracture at room temperature at a strain rate of 4×10^{-4}/s using a Servohydraulic MTS Mechanical Testing machine, as shown in Figure 3.3. The same machine was also used for stretching the 7075 alloy samples as a deformation process. This cold/hot deformation was varied in the range between 1 and 10% for alloy bars deformed. A strain gauge extensometer was attached to the test bar to measure percentage elongation as the load was applied. The yield strength (YS) was calculated according to the standard 0.2% offset strain, and the elongation to fracture was calculated as the percent elongation (%El) over the 50 mm gauge length. The ultimate tensile strength (UTS) was obtained from the data acquisition system of the MTS machine. The machine was calibrated each time before any testing was carried out. The average %El, YS and UTS values obtained from the five samples tested per alloy/condition were considered as the values representing that specified alloy/condition.

Figure 3.3 Servohydraulic MTS Mechanical Testing machine with data-acquisition system.

The tensile test data was analyzed employing Minitab and Six Sigma statistical software programs used in quality improvement projects by means of mathematical analysis and modeling.

3.6 METALLOGRAPHY

Samples for microstructural analysis were prepared from the castings obtained from the thermal analysis experiments as described in section 3.3.1, and also from tensile-tested bars ~10 mm below the fracture surface. In the latter case, the samples were examined in the as-cast and solution heat-treated (540ºC/5h and 540ºC/12h) conditions. The microstructures of the polished sample surfaces were examined using an optical microscope

linked to a Clemex image analysis system, as shown in Figure 3.4. A Hitachi SU-8000 field emission scanning electron microscope (FE-SEM), Figure 3.5, equipped with a standard secondary electron detector (SE), a backscatter electron detector (BSD) and Energy dispersive X-ray spectrometer (EDS) was used for examining the fracture surface. Line scans for Mg, Zn and Cu in the 7075 alloys, were obtained from the various heat-treated alloy samples using an electron probe microanalyzer, shown in Figure 3.6, equipped with EDX and WDS facilities.

Figure 3.4 Optical Microscope - Clemex Image Analyzer system.

Figure 3.5 Hitachi SU-8000 field emission scanning electron microscope used for the present study.

Figure 3.6 JEOL JXA-8900L electron probe microanalyzer used for the present study.

CHAPTER 4

MICROSTRUCTURE-TENSILE PROPERTIES RELATIONSHIP IN Al-Si-Mg CAST ALLOYS

CHAPTER 4

MICROSTRUCTURE-TENSILE PROPERTIES RELATIONSHIP IN Al-Si-Mg CAST ALLOYS

PART I

MICROSTRUCTURE CHARACTERISTICS

4.1 INTRODUCTION

The presence of magnesium in Be-free Al-7Si-Mg alloys [135] results in the formation of an undesirable iron-intermetallic known as the π-$Al_8FeMg_3Si_6$ phase. The effect of Mg, Fe and Be on the formation of π-$Al_8FeMg_3Si_6$ in both unmodified and Sr-modified Al-7Si-Mg-xFe alloys containing different levels of Mg (0.4-0.8 wt%) and Fe (0.1-0.8 wt%) was investigated in this study, in samples obtained at a slow cooling rate (sample DAS ~65 μm), close to near-equilibrium cooling conditions. A qualitative microstructural examination was carried out to study the effect of solution heat treatment on the decomposition of the π-$Al_8FeMg_3Si_6$ phase in Al-7Si-xMg-0.1Fe alloys containing different levels of Mg (0.4-1.0 wt%). The results obtained indicate that increasing Mg and Fe levels increases the amount of the π-$Al_8FeMg_3Si_6$ phase formed in all alloys investigated. Quantitative measurements revealed a reduction in the surface fraction of the π-$Al_8FeMg_3Si_6$ phase after solution heat treatment (540°C/8hr) in all alloys studied.

Different levels of decomposition of the π-phase into needles of β-Al_5FeSi iron intermetallic phase were observed at 0.4, 0.6 and 0.8 wt% Mg levels, after solution heat treatment.

It is inferred from the work of Elsharkawi and co-workers [136] on Al-7Si-Mg alloys that iron, as impurity, can form two different intermetallic compounds during solidification: β-Al_5FeSi and π-$Al_8FeMg_3Si_6$, which are known for their detrimental effect on the alloy ductility and strength. The impact and tensile properties of heat-treated Al-7Si-0.55Mg-0.1Fe (357 type) alloy samples were investigated in order to seek a correlation between said properties and the changes which occur in the micro-constituents, viz., the eutectic Si, and π-Fe and β-Fe phases, with prolonged solution treatment. Solution treatment was carried out at 540ºC for times of 2 to 100 h, followed by quenching in water at 60ºC, and artificial aging at 155ºC for 5 h. Results showed that the first 20 hrs of solution treatment are more sensitive to the changes occurring in the Si particle morphology than those in the π-phase. Decomposition of the π-phase significantly reduces the impact properties after prolonged solution times.

The work documented in this chapter is an extension of the studies that were carried earlier in order to correlate the precipitation of different phases during the solidification process and their decomposition during solution heat treatment with the tensile properties obtained from this type of alloys.

4.2 LOW COOLING RATE (DAS~65µm)

Samples for microstructural analysis were sectioned from the castings obtained from the thermal analysis experiments carried out for each alloy melt composition. Cylindrical specimens, 15 mm thick were sectioned off from the centre of each graphite mold casting close to the thermocouple tip for all of the compositions obtained. From these, samples (2.5 x 2.5 cm) were machined, mounted and polished for preparation of metallographic samples for qualitative and quantitative microstructural analysis.

4.2.1 Silicon Particle Characteristics

The silicon particle characteristics for the various alloy compositions investigated are summarized in Table 4.1. The Si particle measurements for the A1 base alloy, with low Mg and low Fe content, using the graphite mold sample (65 µm DAS) are listed in Table 4.1. It can be seen that the Si particle area decreased from 76.70 to 3.18 μm^2, the Si particle length decreased from 21.60 to 3.05 µm, the aspect ratio decreased from 3.52 to 2.11, while the roundness ratio increased from 28.4 to 46.0 % after Sr-modification, i.e. in the alloy A1S sample. In the case of Be addition (alloy A1B), the Si particle area decreased to 49.60 μm^2, the Si particle length to 15.20 µm, the aspect ratio to 2.85, while the roundness ratio increased to 33.8 %. The presence of both Sr and Be in alloy A1BS resulted in decreasing the Si particle area to 2.75 μm^2, decreasing the Si particle length to 3.00 µm, decreasing the aspect ratio to 2.18 and increasing the roundness ratio to 43.5 %. After increasing both Mg and Fe contents (alloy C3), the Si particle area decreased to 20.70 μm^2, the Si particle length decreased to 9.63 µm, the aspect ratio decreased to 2.86, while the roundness ratio

increased to 36.2 %. The combined effect of the four elements (alloy C3BS) resulted in decreasing the Si particle area to 3.38 μm^2, decreasing the Si particle length to 3.27 µm, decreasing the aspect ratio to 2.15 and increasing the roundness ratio to 43.9 %. The values listed in Table 4.1 reflect the modification effect of Sr and partial modification effects of Mg and Be; however, with increasing Fe levels it appears that most of the Be reacts with the Fe to form a Be-Fe phase (Al_8Fe_2BeSi), thereby reducing the partial modification effect attributed to Be. These results are supported by the optical micrographs shown in Figures 4.1 and 4.2.

Table 4.1* Silicon particle measurements for the as-cast 357 alloys using a graphite mold with a DAS of 65 µm

Alloy (Condition)	Area (μm^2)		Length (µm)		Roundness Ratio(%)		Aspect Ratio	
	Av.	SD	Av.	SD	Av.	SD	Av.	SD
A1 (non- mod.)	76.70	71.50	21.60	16.30	28.4	21.8	3.52	4.54
C3 (non- mod.)	20.70	22.70	9.63	7.98	36.2	21.4	2.86	5.84
A1B (Be mod.)	49.60	52.40	15.20	12.00	33.8	21.8	2.85	3.45
C3B (Be mod.)	13.60	14.30	6.75	5.08	43.7	22.2	2.27	1.15
A1S (Sr mod.)	3.18	3.21	3.05	2.16	46.0	19.2	2.11	2.14
C3S (Sr mod.)	4.48	4.78	3.82	3.07	43.4	21.5	2.46	3.87
A1BS (Be+Sr mod.)	2.75	2.94	3.00	2.38	43.5	19.5	2.18	2.25
C3BS (Be+Sr mod.)	3.38	3.97	3.27	2.69	43.9	19.8	2.15	1.32

* Codes A and C correspond to the Fe levels 0.09 and 0.6, respectively, while codes 1 and 3 correspond to the Mg levels 0.4 and 0.8, respectively; codes B and S represent Be addition and Sr modification, respectively.

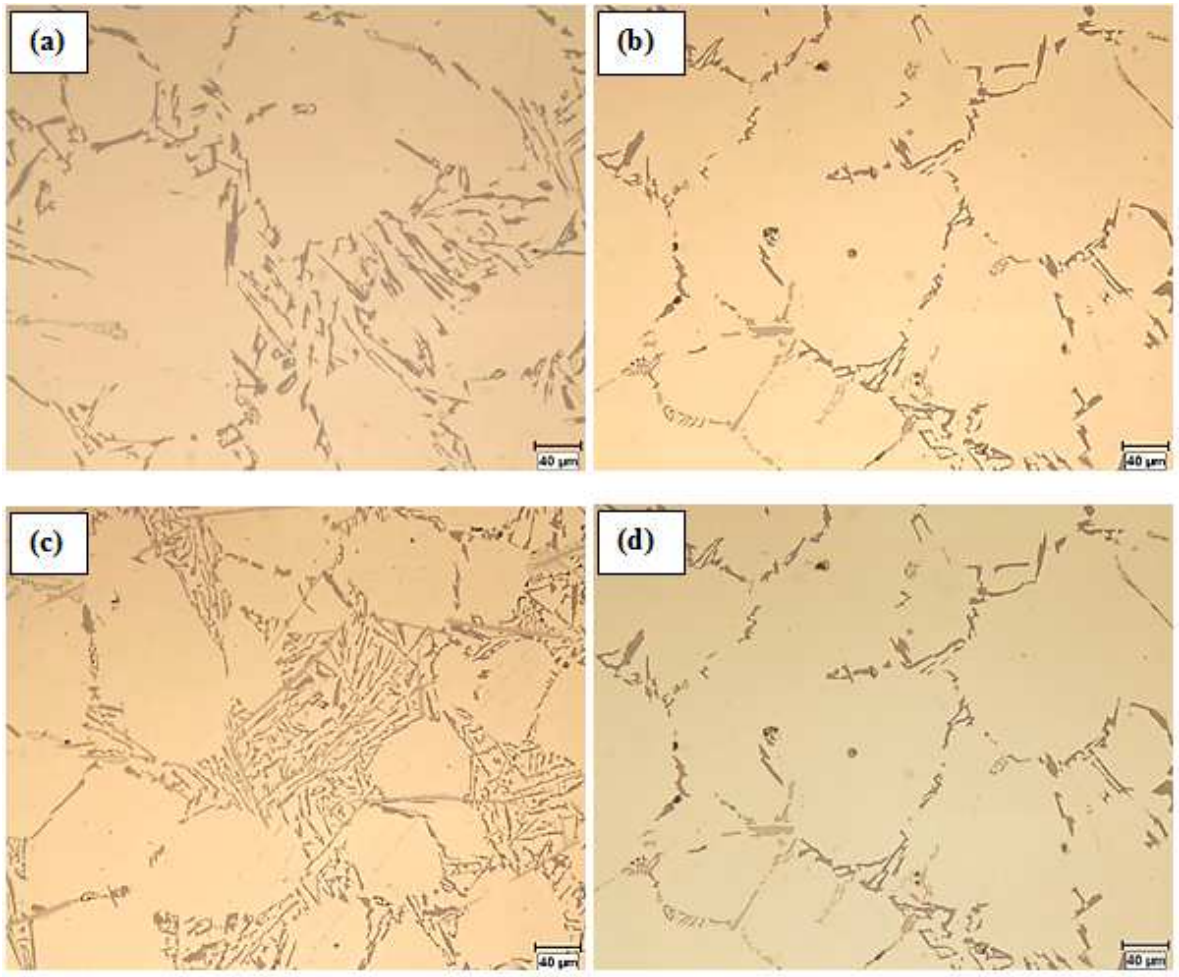

Figure 4.1 Silicon particle morphology and distribution in: (a) A1, (b) A1B, (c) A1S, and (d) A1BS alloys.

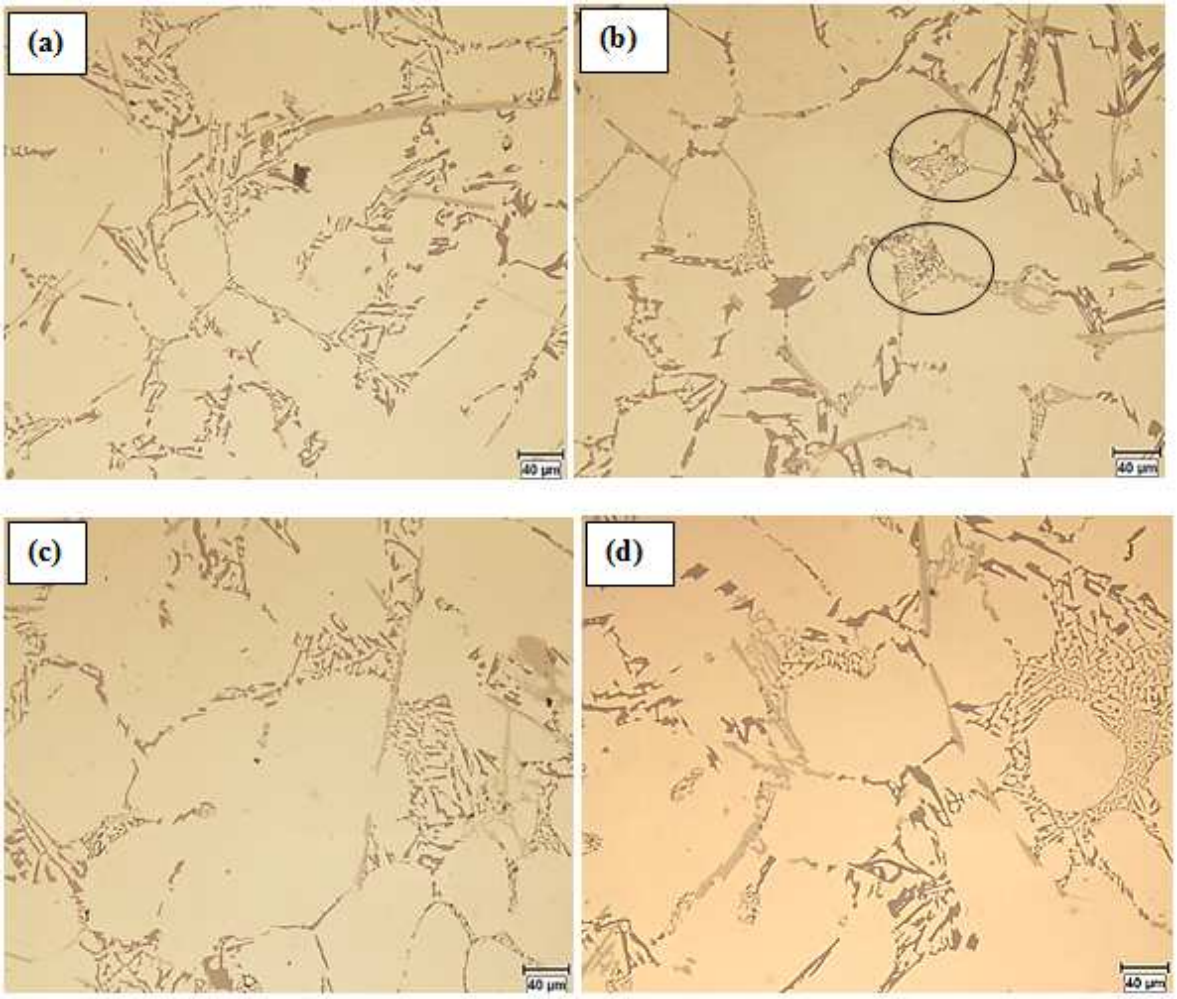

Figure 4.2 Silicon particle morphology and distribution in: (a) C3, (b) C3B, (c) C3S, and (d) C3BS alloys.

4.2.2 Fe-Based Intermetallic Phases

Thermal analysis was carried out to determine the precipitation sequence and formation temperature of the intermetallic phases observed in the 357 alloys containing different levels of Fe and Mg. In this respect, alloys A1, C3, C3BS and C3B were selected as examples. The reactions and corresponding temperatures observed in the cooling curves

for the alloys studied are summarized in Table 4.2. Figure 4.3(a) represents the cooling curve of the base alloy A1 showing the precipitation of α-aluminum (1), followed by formation of the Al-Si eutectic (2) together with the precipitation of the post-eutectic β-Al_5FeSi. It is expected that as solidification proceeds, the β-phase present will be transformed into the π-phase as a result of the pre-eutectic reaction (3), $L+Al_5FeSi \rightarrow Al+Si+Al_8FeMg_3Si_6$. The last reaction (4) is characterized by a wide peak, which may arise from two merged reactions, the first related to the formation of Mg_2Si, followed by the second which corresponds to the quaternary eutectic reaction,

$$L \rightarrow Al+Si+Mg_2Si+Al_8FeMg_3Si_6.$$

By comparing the first derivative curve in Figure 4.3(a) for alloy A1 (base alloy) with the one shown in Figure 4.4(a) for alloy C3, it will be seen that, at 0.09 wt% Fe, for the A1 alloy, the first derivative curve reveals four peaks, while at 0.6 wt% Fe (C3 alloy), a peak marked (2) may be observed before the eutectic reaction represented by the peak (3) in Figure 4.4(a). This peak corresponds to the formation of the pre-eutectic β-phase, while peak (4) corresponds to the precipitation of Mg_2Si phase. The presence of the π-phase noted in Figure 4.4(c) may be explained by the following reaction:

$$L+Al_5FeSi \rightarrow Al+Si+Al_8FeMg_3Si_6,$$

whereby the β-Al_5FeSi phase is transformed into the π-phase. Other reactions remain the same as those described for Figure 4.3(a).

To reach a better understanding of the effect of Fe content on the formation of intermetallic phases, it has been reported [137, 138] that increasing the Fe content from 0.09 wt% to 0.6 wt% changes the solidification sequence of the base Al-7Si-0.4Mg alloy (alloy

A1), which can be explained by the current cooling curves. At 0.09 wt% Fe, the β-phase precipitates at low temperatures together with the Al-Si eutectic and is characterized by fine platelets in the microstructure, as shown in Figure 4.3(b). At 0.6 wt% Fe, most of the β-phase will precipitate at higher temperatures before the Al-Si eutectic. This β-phase is characterized by its much larger size in the microstructure, as shown in Figure 4.4(b and c). As a result, increasing the Fe content will increase the size of the β-phase in the microstructure, which would have a negative effect on the alloy mechanical properties.

By comparing the first derivative curve in Figure 4.5(a) for alloy C3BS with those shown in Figures 4.3(a) and 4.4(a) for alloys A1 (base alloy) and C3, respectively, the reaction (5) in Figure 4.5(a) may be written as:

$$L+Al_5FeSi \rightarrow Al+Si+Al_8FeMg_3Si_{6,}$$

whereby β-Al_5FeSi phase is transformed into the π-phase. Other reactions for alloy C3BS remain the same as those observed in Figures 4.3(a) and 4.4(a).

Table 4.2 Main reactions observed from thermal analysis data of alloys A1, C3, C3BS and C3B

Alloy Code	Temp. (ºC)	Reaction [24]
A1 0.09%Fe-0.4%Mg (Figure 4.3)	612 (1)	- Formation of Al-dendritic network
	569 (2)	- Precipitation of Al-Si- eutectic - Precipitation of post-eutectic β-Al_5FeSi phase
	561 (3)	- Transformation of β-phase into π-$Al_8FeMg_3Si_6$ phase
	546 (4)	- Precipitation of Mg_2Si - Quaternary eutectic reaction*
C3 0.6%Fe-0.8%Mg (Figure 4.4)	613 (1)	- Formation of Al-dendritic network
	568 (2)	- Formation of pre-eutectic β-Al_5FeSi phase
	563 (3)	- Precipitation of Al-Si- eutectic - Precipitation of post-eutectic β-Al_5FeSi phase
	550 (4)	- Transformation of β-phase into π-$Al_8FeMg_3Si_6$ phase - Precipitation of Mg_2Si - Quaternary eutectic reaction*
C3BS 0.6%Fe-0.8%Mg-0.05%Be-0.02%Sr (Figure 4.5)	609 (1)	- Formation of Al-dendritic network
	568 (2)	- Formation of pre-eutectic β-Al_5FeSi phase
	561 (3)	- Precipitation of Al-Si- eutectic - Precipitation of post-eutectic β-Al_5FeSi phase
	550 (4)	- Transformation of β-phase into π-$Al_8FeMg_3Si_6$ phase - Precipitation of Mg_2Si
	540 (5)	- Quaternary eutectic reaction*
C3B 0.6%Fe-0.8%Mg-0.05%Be (Figure 4.6)	613 (1)	- Formation of Al-dendritic network
	611 (2)	- Formation of Be-Fe phase
	560 (3)	- Precipitation of Al-Si- eutectic - Precipitation of post-eutectic β-Al_5FeSi phase
	551 (4)	- Transformation of β-phase into π-$Al_8FeMg_3Si_6$ phase - Precipitation of Mg_2Si
	539 (5)	- Quaternary eutectic reaction*
*Quaternary eutectic reaction, $L \rightarrow Al+Si+Mg_2Si+Al_8FeMg_3Si_6$		

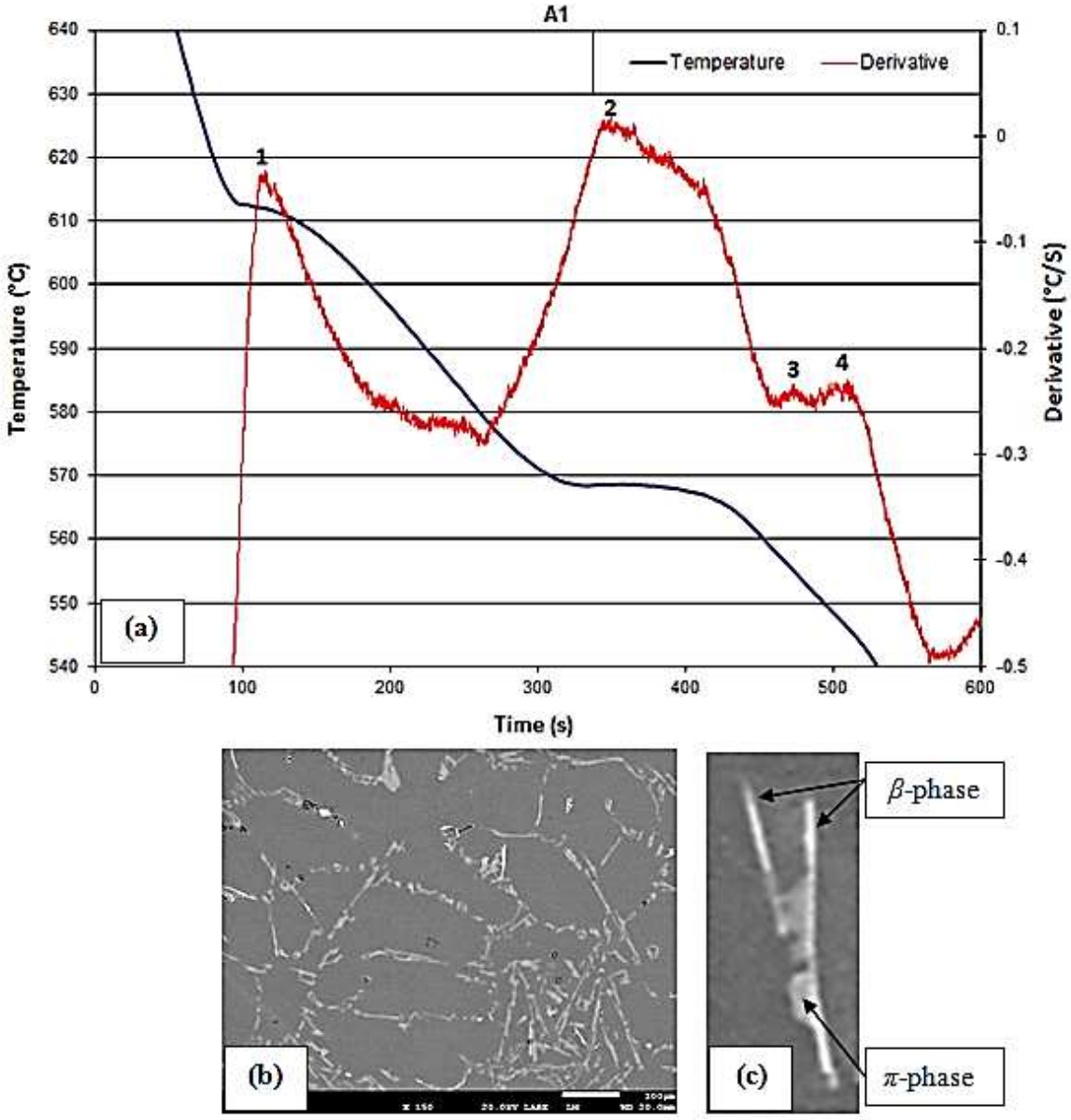

Figure 4.3 (a) Temperature-time cooling curve and its first derivative obtained from the base alloy A1 and (b) the corresponding microstructure showing the small size of the β-phase and π-phase particles, evidenced more clearly in the enlarged micrograph in (c).

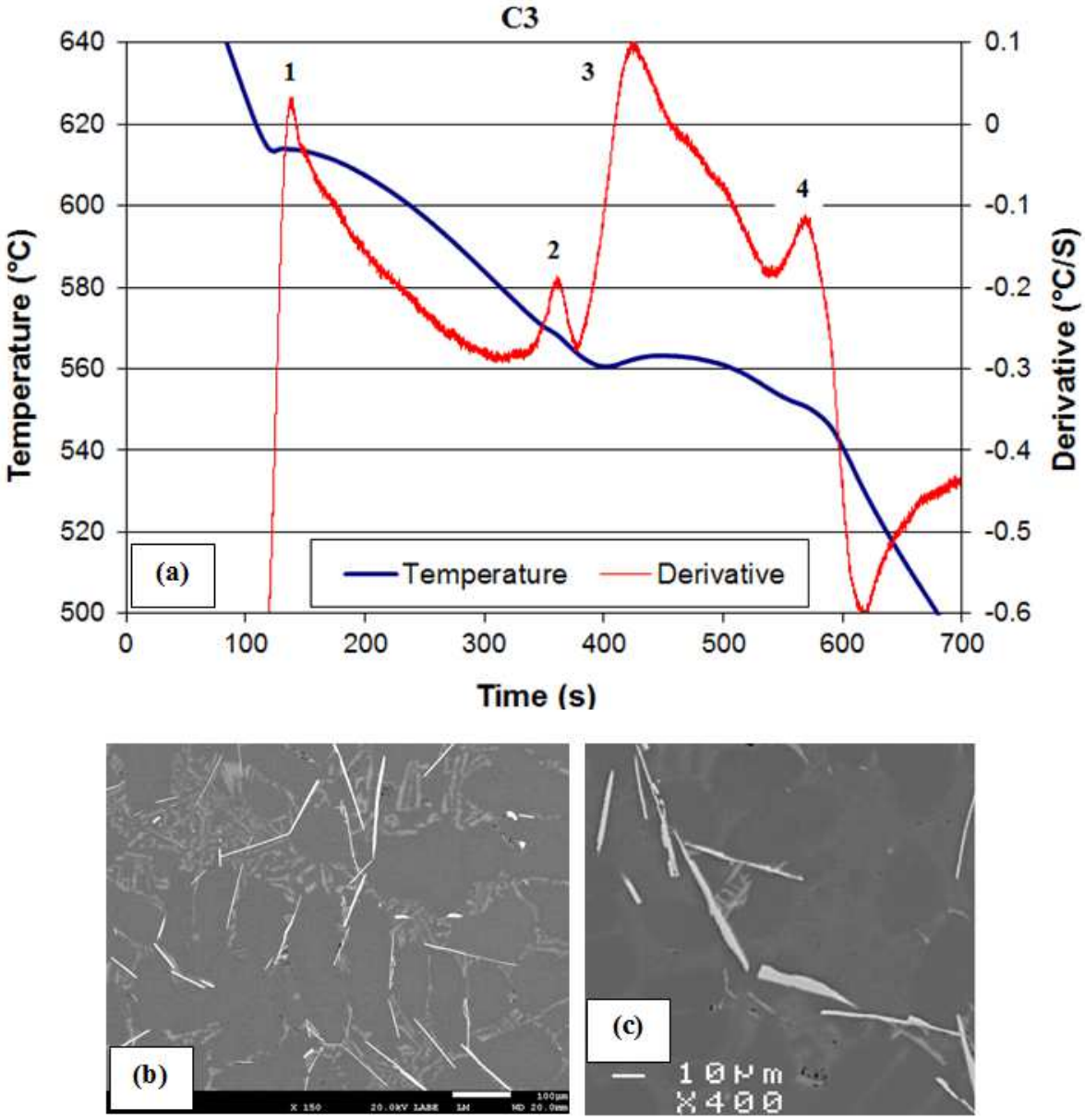

Figure 4.4 (a) Temperature-time cooling curve and its first derivative obtained from the non-modified alloy C3 and (b) the corresponding microstructure showing the larger size of the β-Al_5FeSi platelets in the enlarged image in (c) for this alloy.

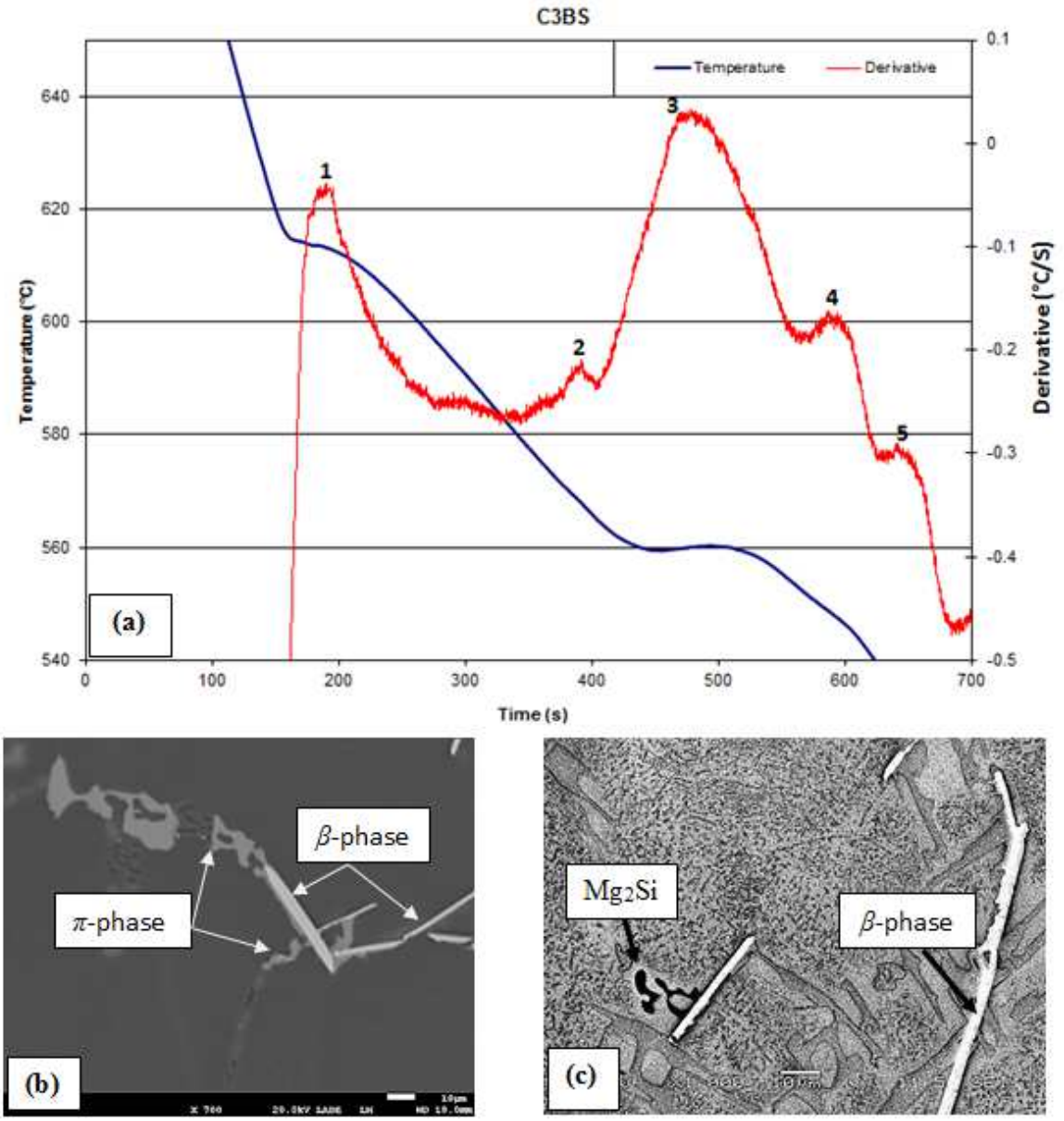

Figure 4.5 (a) Temperature-time cooling curve and its first derivative obtained from alloy C3BS, and corresponding microstructures showing (b) a much bigger size of the β-phase and π-phase particles, and (c) large β-phase and Mg_2Si particles.

For a clear understanding of the effects of Mg addition on the precipitation sequence and reaction temperature, the Mg content in the Sr-modified alloy C3BS (Figure 4.5), and also in the non-modified alloy C3B (Figure 4.6), was increased up to 0.8 wt%. Two separate peaks were identified corresponding to reactions (4) and (5) shown in Figures 4.5 and 4.6. The reactions and their corresponding formation temperatures during solidification of alloys C3BS and A1, containing high and low Mg levels, respectively, are listed in Table 4.2. There is a significant reduction in the eutectic temperature by ~10°C in the high Mg-containing alloys (C3, C3B and C3BS), compared to the low Mg-containing alloy (A1), which is in a good agreement with published findings. [139, 140] Moustafa *et al*. [140] reported that the observed reduction in eutectic temperature affects the modification of the eutectic Si particles.

From an extensive investigation of the microstructure, it is found that the π-$Al_8FeMg_3Si_6$ phase is often observed to be in close contact with the β-Al_5FeSi phase platelets. Figure 4.3(c) is an enlarged micrograph depicting the transformation of the β-phase to π-phase. Thus it may reasonable to assume that the β-Al_5FeSi phase will precipitate first, followed by the growth of the π-$Al_8FeMg_3Si_6$ phase from the surface of the β-Al_5FeSi thereafter.

4.2.3 Role of Beryllium Addition

The morphology of iron intermetallic phases in 357 alloys shows the precipitation of several types in Be-containing and Be-free alloys. The Fe intermetallics observed in the optical microstructure of the Al-7Si-0.8Mg-0.6Fe-0.05Be, C3B alloy, are (i) the nodular

Fe-Si-Al β-phase and (ii) Be-Fe phase (Al_8Fe_2BeSi) with a script-like morphology, as shown in Figure 4.6(c). This observation is in agreement with the reported microstructure of Be-containing B357 alloys. [57, 141, 142] It is shown in Figure 4.7 that the Be-Fe phase exists near or at the β-phase platelets. A similar observation can be made from the thermal analysis results of the C3B alloy (reaction marked (2)) as depicted in Figure 4.6(a). It is estimated that the formation temperature of this reaction is approximately 611°C which is close to the formation temperature of α-Al would facilitate the precipitation of the Be-Fe phase in the within the α-Al (Figure 4.6(b)). High temperature phases are typically overgrown by Al-dendrite arms and appear in the final microstructure to be embedded in the dendrites. [8, 57, 141, 142] Also, this temperature is higher than the formation temperature of the pre-eutectic β-Al_5FeSi phase marked as peak (2) in Table 4.2 for the Be-free A1 alloy and for the Sr-modified Be-containing C3BS alloy, as shown in Figures 4.3 and 4.5.

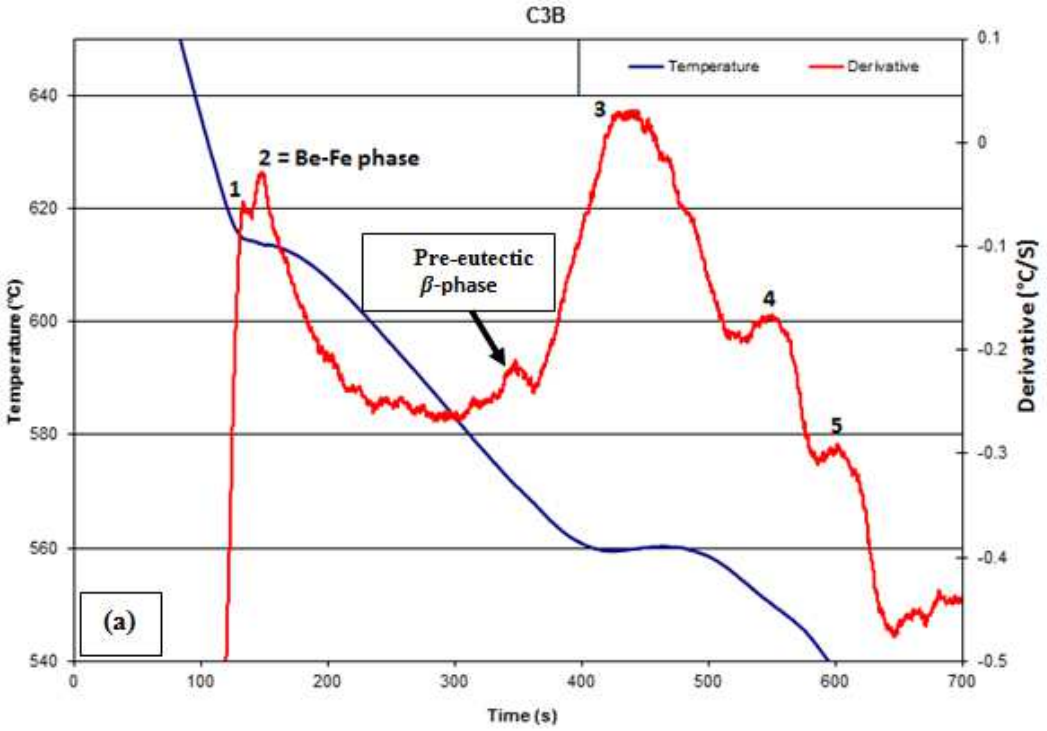
C3B
Temperature
Derivative
2 = Be-Fe phase
1
3
4
5
Pre-eutectic
β-phase
(a)
Temperature (°C)
Derivative (°C/S)
Time (s)
640
620
600
580
560
540
0.1
0
-0.1
-0.2
-0.3
-0.4
-0.5
0
100
200
300
400
500
600
700

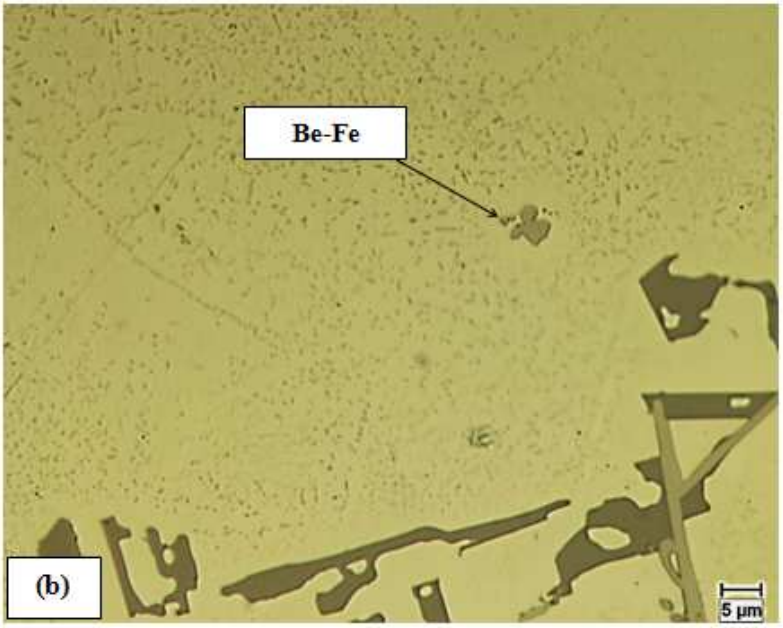
Be-Fe
(b)
5 µm

Figure 4.6

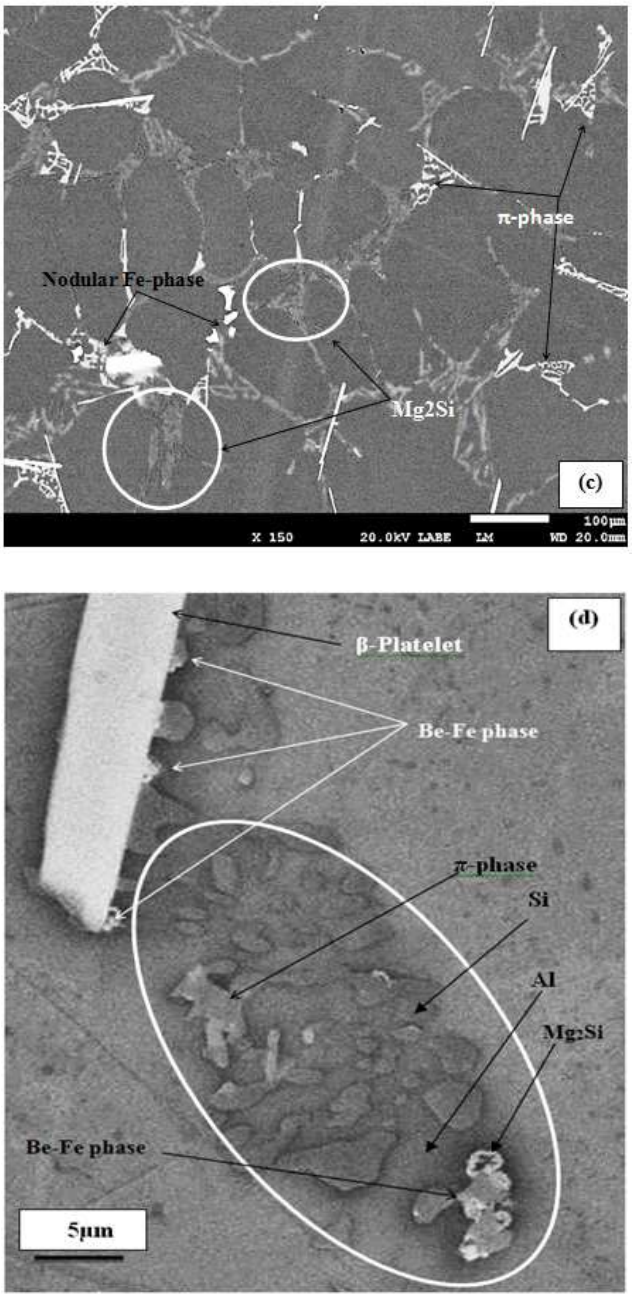

Figure 4.6 (a) Temperature-time cooling curve and its first derivative obtained from the non-modified alloy C3B, (b) optical micrograph showing precipitation of Be-Fe compound within the α-Al dendrite, (c) BSE image showing presence of nodular β-Al_5FeSi phase, π-$Al_8FeMg_3Si_6$phase,and Mg_2Si phase particles (arrowed) and (d) enlarged BSE image showing small Be-Fe phase particles growing out of the β-plate (white arrows) or formed as a result of the new quinary reaction (black arrows).

Based on the cooling curve data and the corresponding microstructures (Figures 4.6(b, c and d)), it may be noted that the addition of Be results in a change in the precipitation sequence of the iron intermetallics, where peak (2) in Figure 4.6(a) corresponds to the formation of the Be-Fe phase. This observation is supported by the work of Murali *et al.,* [8, 51, 55, 141] who carried out an interrupted quenching experiment to detect the formation temperature of the Be-Fe phase (Al_8Fe_2BeSi). They found that the Be-Fe phase exists in the microstructure at the point where the melt was quenched from the liquid at 607°C. In the present work, however, the exact composition of the Be-Fe phase could not be identified with certainty. Figure 4.6(a) indicates that the formation temperature of the Be-Fe phase may be somewhat greater than 607°C. The precipitation sequence and the corresponding temperatures for the Al-7Si-0.8Mg-0.6Fe Be-containing alloy, in both the non-modified and Sr-modified conditions (C3B and C3BS) are listed in Table 4.2. Figures 4.6(c) and 4.7(a) are microstructures of the Be-containing alloys showing nodular Al-Fe-Si, in addition to other phases. Figure 4.7(b) reveals the irregular shape of the β-phase platelets that may be caused by the addition of Be and its reaction with Fe.

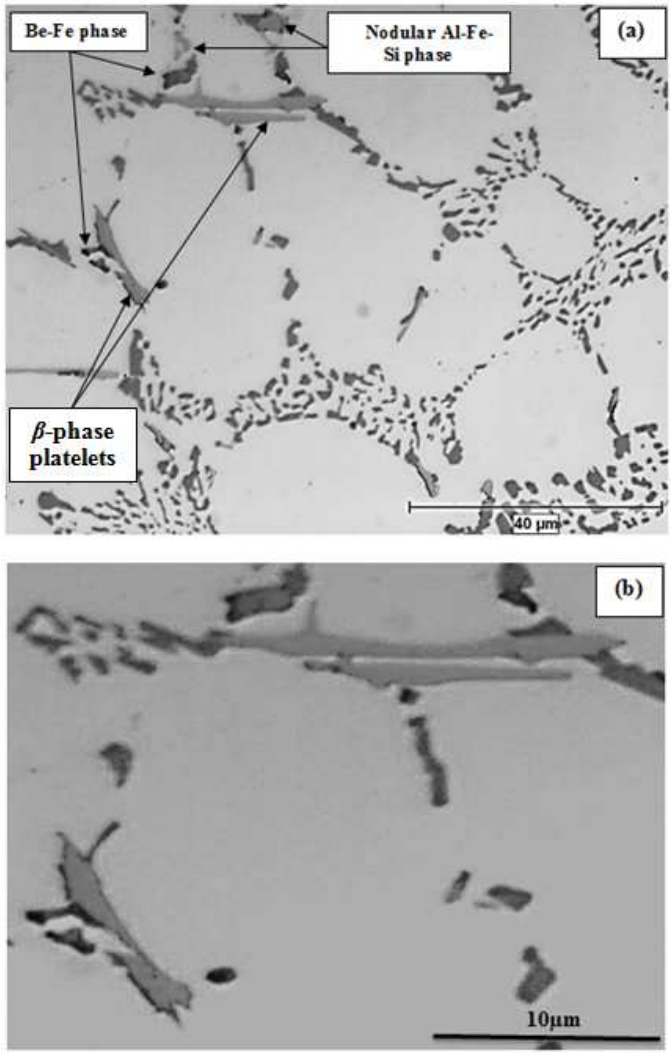

Figure 4.7 Optical microstructures of C3BS alloy showing (a) nodular Al-Fe-Si phase, β-Al_5FeSi phase platelets and Be-Fe phase; (b) enlarged portion of (a) revealing the irregular shape of the β-platelets.

Several attempts were made to obtain an EDS spectrum of the Be-Fe compound but with no success. The EDS spectra shown in Figures 4.8(a) and (b) correspond to Mg_2Si and π-Al_5FeSi phase particles, respectively. In order to confirm the effect of Be on the microstructure of the B357 alloys in the present study, the morphology of the iron

intermetallic phases and Mg_2Si particles were examined; the microstructures for alloys A1BS, C3, C3B and C3BS are shown in Figures 4.9(a) to (e). That of alloy A1BS shows large-sized Chinese-script Mg_2Si particles in conjunction with the nodular β-Al_5FeSi phase, whereas in the microstructure of the non-modified, Be-free C3 alloy, smaller-sized Mg_2Si particles and β-Al_5FeSi platelets were observed, compared to the size of the Chinese-script π-$Al_8FeMg_3Si_6$ phase. These compositions were confirmed by the associated element distributions corresponding to Figure 4.9. The smaller size of the Mg_2Si particles may be explained in terms of the consumption of the Mg content informing the π-phase. A comparison of Figures 4.9(a) and 4.9(b), clearly shows that Be has an effect on both size and morphology of the Fe- and Mg-containing phases.

In the case of the non-modified, Be-containing C3B alloy, where larger-sized Mg_2Si particles were reported, both nodular and small platelets of the β-Al_5FeSi and smaller π-$Al_8FeMg_3Si_6$ phases were observed, as displayed in Figures 4.9(c) and 4.9(d). The relatively small size of the β-Al_5FeSi and π-$Al_8FeMg_3Si_6$ phases may be attributed to the reaction of Be with Fe to form the Be-Fe phase. Also, by comparing these two figures with Figure 4.9(b), it may be seen that Be affects the size and morphology of the Fe-based intermetallic phases, whereas the formation of Mg_2Si remains unaffected by the presence of Be. These results agree with studies carried out by others. [56, 143]

Similar effects of Be on the microstructure of alloy C3BS were also observed as those in the case of alloy C3B (*cf.* Figures 4.9(c) and (d)) with Figure 4.9(e) for C3BS, except that the volume fraction of the nodular β-phase is much smaller in the case of alloy C3BS, whereas the opposite is true for the platelet β-phase in the alloy. This observation

may be attributed to a Be-Sr-reaction (forming $SrBe_3O_4$) or Be-Fe-Sr reaction; *i.e.* some of the Be reacts with Sr and the remaining amount is not enough for the nodular *β*-phase transformation from platelet *β*-phase particles to take place; thus the volume fraction of these platelets is much bigger.

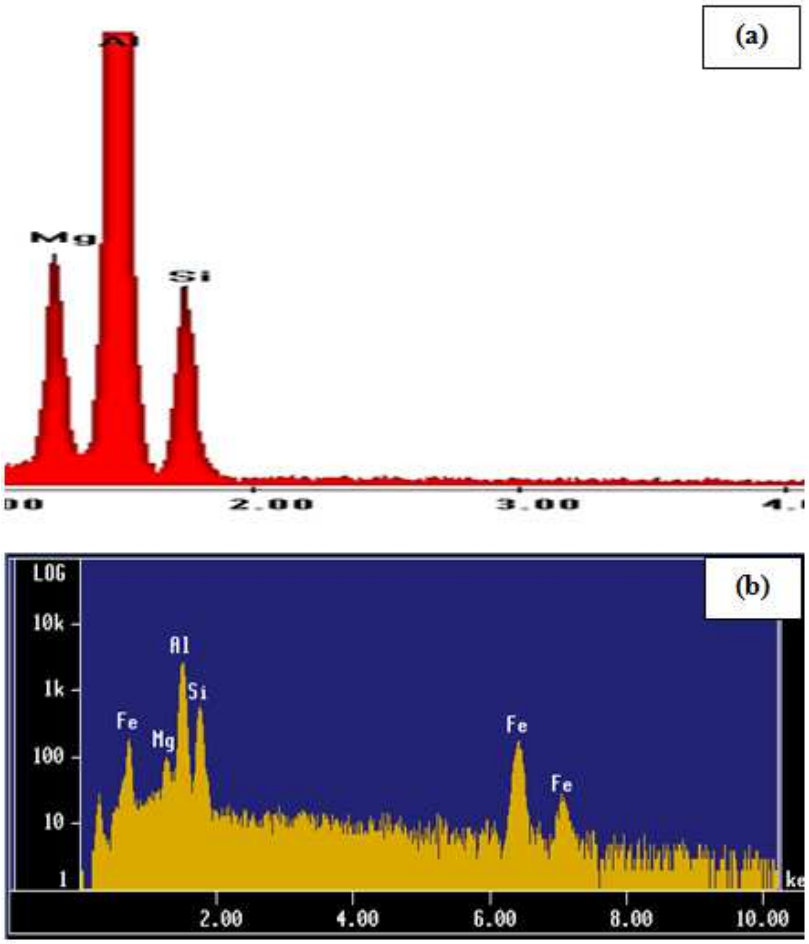

Figure 4.8 EDS spectra corresponding to: (a) Mg_2Si and (b) π-$Al_8FeMg_3Si_6$ phases observed in C3BS alloy.

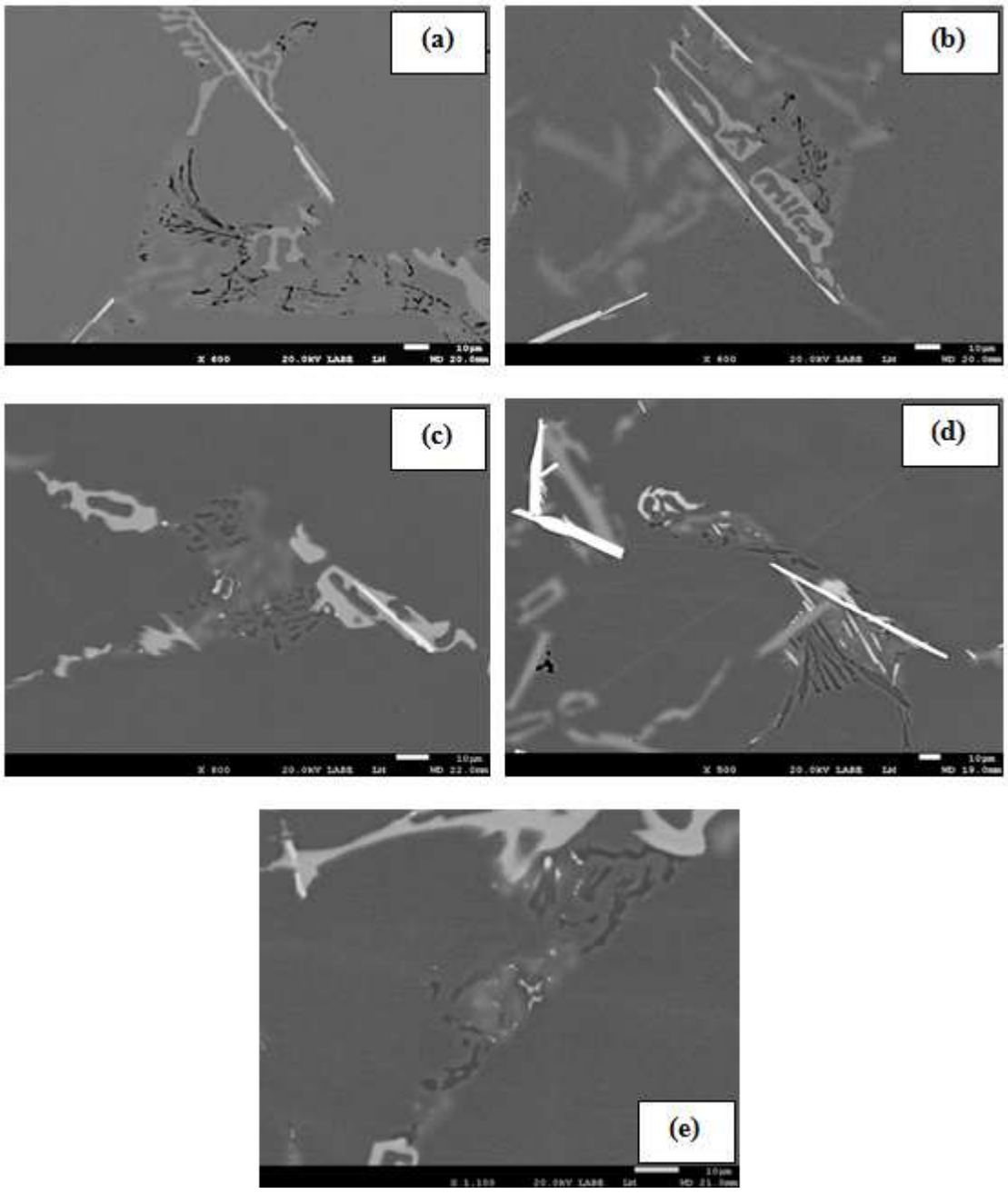

Figure 4.9 Backscattered electron images of: (a) A1BS, (b) C3, (c) C3B, (d) C3B, and (e) C3BS alloys.

4.2.4 Formation of a New Eutectic-Like Reaction

Figure 4.4 displays the cooling curve and its first derivative obtained from the C3 alloy. From an examination of the microstructures of alloys C3B and C3BS (containing higher levels of Mg and Fe), a new reaction was observed to take place towards the end of solidification at the low cooling rate (0.4ºC/s), as shown in Figure 4.10. This new reaction is composed of a mixture of phases that vary depending on the location of the reaction in the matrix, i.e. the examined cross-section. It should be mentioned here that this reaction was not detected in any of the cooling curves, since the heat associated with this reaction is apparently too low. Table 4.3 lists the solidification times obtained from the C3 series of alloys. As can be seen, the solidification time for the C3B alloy is ~29 seconds more than that of the C3 alloy. It may be suggested that this increase in the solidification time, due to the presence of Be, would result in the decomposition of the remaining liquid metal giving rise to the newly observed reaction, in accordance with the law of conservation of matter.[144] Figure 4.10(d) reveals the growth of the new reaction into the surrounding aluminum matrix. The presence of precipitate free zones (PFZ) surrounding the new reaction indicates that this reaction was formed in the molten state. Based on these observations, the new reaction may be considered to be a quinary eutectic-like reaction that could be described as:

$$L \longrightarrow Al + \pi\text{-phase} + Mg_2Si \text{ phase} + Si + (Be\text{-}Fe) \text{ phase}.$$

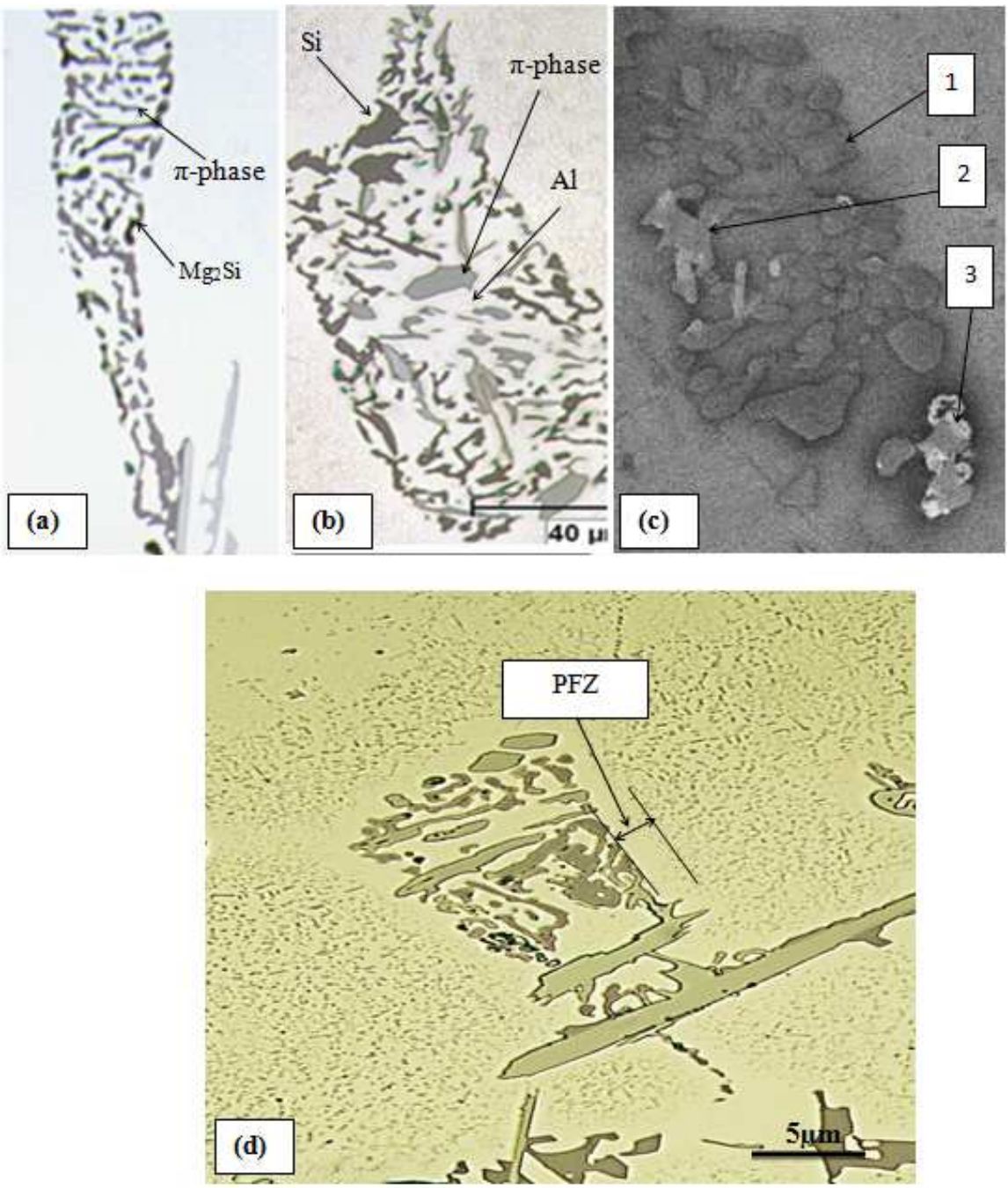

Figure 4.10 Different microstructures of the new reaction in Be-containing C3B alloy: (a) π-phase and Mg_2Si, (b) π-phase and Si, (c) Si (1) + π-phase (2) + (Be-Fe) phase (3), and (d) extension of the new reaction into the α-Al matrix, note the presence of precipitate free zones (PFZ).

Table 4.3 Solidification times of the A and C3 series of alloys obtained from the respective cooling curves. Each value is an average of five consecutive tests

Alloy Code	**A1**	**A1B**	**A1S**	**A1BS**	**C3**	**C3B**	**C3S**	**C3BS**
Solidification time (s)	452	464	472	474	463	492	510	504

Figure 4.11(a) displays an enlarged portion of the cooling curve shown in Figure 4.6(a). The new reaction is expected to take place in the temperature range 533-515°C (corresponding to precipitation of Mg_2Si phase reaction and end of solidification). Figure 4.11(b) shows large particles of Mg_2Si whereas Figure 4.11(c) shows ultra-fine particles of Fe, Be-Fe and Mg_2Si phases observed at the end of solidification.

Beryllium and strontium are the main parameters influencing the amount of this new reaction or precipitates formed. Table 4.4 summarizes the “area” and “intensity” measurements of the new reaction, the term “area” corresponding to the average area covered by the mix of the ultrafine Si, π, Mg_2Si and Be-Fe phase particles resulting from the reaction, and “intensity” representing the number of such reactions occurring in the sample area measured. It is found that addition of Sr to the non-modified, Be-containing C3B alloy decreased the reaction area by 44% and the intensity by 36%, respectively.

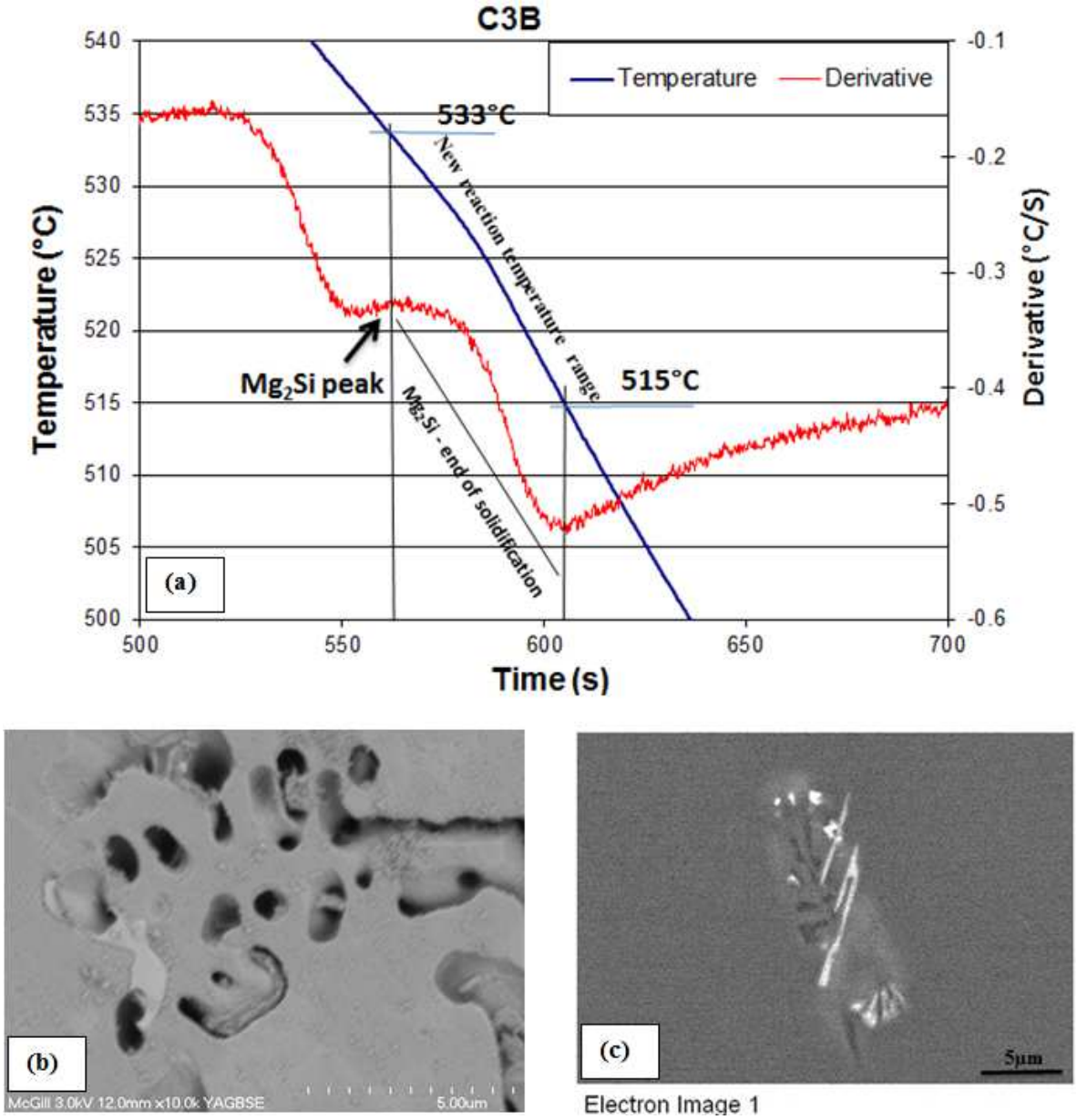

Figure 4.11 (a) An enlarged portion of the cooling curve shown in Figure 4.6(a) showing the temperature range of a new reaction, precipitation of Mg_2Si phase reaction, and end of solidification, (b) large Mg_2Si particles, and (c) an example of ultra-fine particles of Fe, Be-Fe and Mg_2Si phases observed at the end of solidification.

Table 4.4 Measurements of particles (mix of ultrafine Si, π, Mg_2Si and (Be-Fe) phases) resulting from the new eutectic-like reaction observed in as-cast C3 alloys containing Be

Alloy Code	Area (%)		Particle Area (μm^2)		Density (#Particles/field)
	Av.	SD	Av.	SD	
C3B	5.87	2.46	1155.2	1242.0	17.34
C3BS	3.30	1.64	662.8	805.5	11.22

Figure 4.12 shows an example of the distribution of elements within the area of the new reaction in the C3BS alloy sample. Figure 4.13(a) is a secondary electron image of C3B alloy exhibiting the presence of the new reaction consisting of fine Si particles and π-phase. Occasionally, some Be-containing phase particles were observed as well (Figure 4.6(d)). This reaction was noted to occur at the end of the solidification process or growing from the existing β-Al_5FeSi phase platelets. Figure 4.13(a) also reveals the precipitation of Mg_2Si in the matrix in two perpendicular directions caused by natural aging at room temperature for two years. [140] These precipitates seem to be associated with the formation of precipitate-free zones (PFZ) around the pre-existing components.

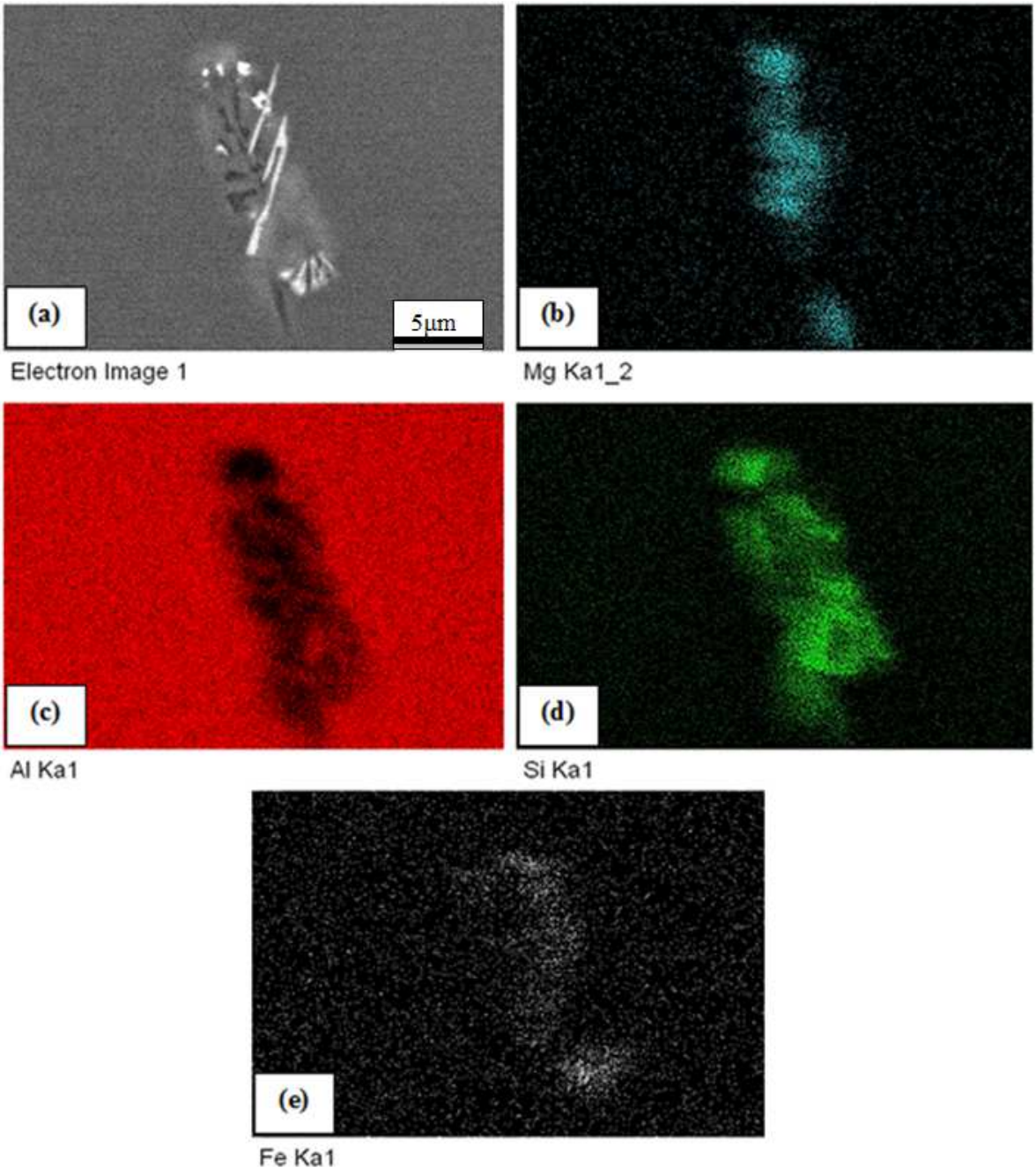

Figure 4.12 (a) Backscattered image of alloy C3BS showing an area containing the products of the new quinary reaction, and corresponding (b) Mg, (c) Al, (d) Si, and (e) Fe distributions.

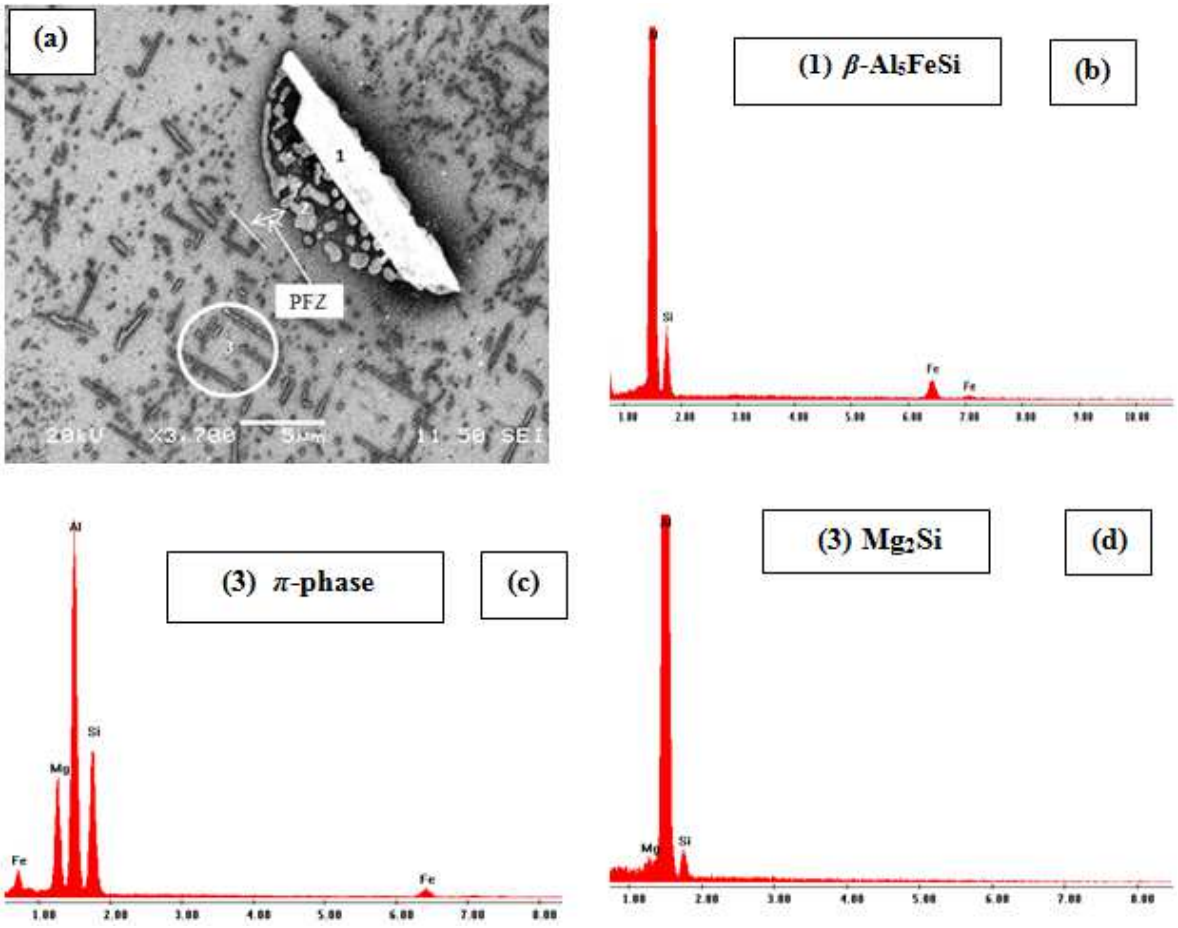

Figure 4.13 (a) Secondary electron image of Be-containing C3B alloy showing the formation of the new reaction on the β-phase platelet 1, (b) EDS spectrum corresponding to area marked 1 in (a), (c) EDS spectrum corresponding to π-phase precipitates marked 2 in the matrix in (a) and formation of precipitate free zone (PFZ), and (d) EDS spectrum corresponding Mg_2Si phase precipitates marked 3 in (a).

The histogram shown in Figure 4.14 illustrates the effects of Be, Sr, Mg and Fe additions on the length of the β-Al_5FeSi platelets. In the as-cast graphite mold samples (DAS of ~65 μm), Be addition reduces the length of the β-phase platelets by ~25% whereas introducing Sr shows further reduction (~37%); adding Be simultaneously with Sr

decreases the length of β-phase by ~50% regardless the levels of Fe or Mg in the alloy. This figure also illustrates how the addition of 0.02wt% Sr to Al-7Si-Mg-Fe alloys decreases the length or volume fraction of the β-phase, compared to the non-modified alloy. This may be explained in terms of the effect of Sr in breaking up the β-phase platelets as reported by Samuel *et al*., [33] thereby reducing the platelet length. In spite of the fact that increasing the Mg and Fe content increases the π-phase volume fraction, the length of β-phase particles is also observed to increase. This increase in β-phase length can be controlled through additions of Be and Sr.

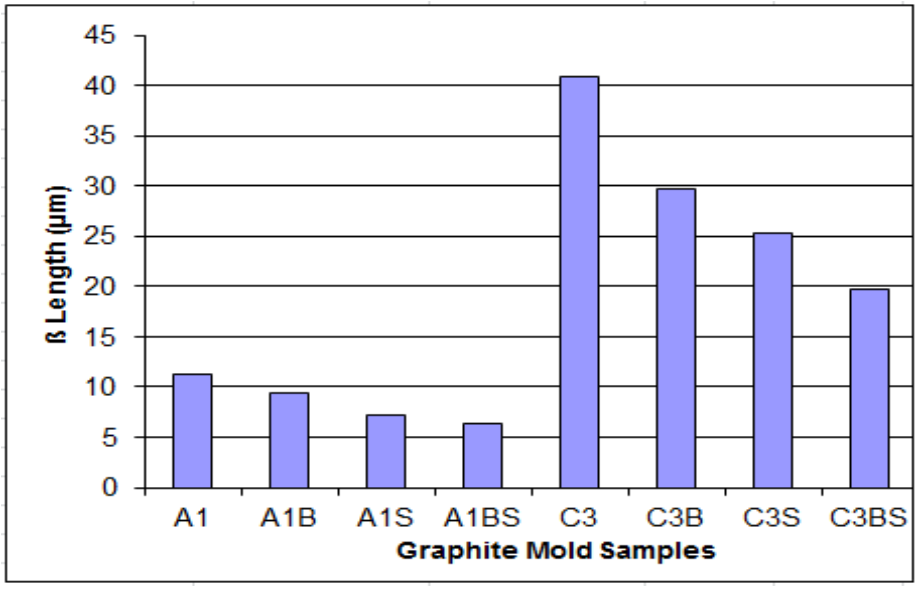

Figure 4.14 Histogram exhibiting the influence of alloy composition on the average length of β-Al_5FeSi phase platelets (sample DAS ~65µm).

4.3 HIGH COOLING RATE (DAS~24µm)

4.3.1 Silicon Particle Characteristics

Samples for microstructural analysis were sectioned from the tensile tested-bars ~10 mm below the fracture surface (away from the deformed portion of the tensile bar) to study each alloy in the as-cast and the two solution heat-treated conditions (540ºC/5h and 540ºC/12h). The dendrite arm spacing of these samples was about 24µm. The silicon particle characteristics of the as-cast alloys are presented in Table 4.5. Figures 4.15 through 4.17 show the eutectic Si particle characteristics in the as-cast and solution heat-treated conditions for the eight alloys investigated.

The Si particle measurements for the A1 base alloy, containing low Mg and low Fe, are listed in Table 4.5. In comparison, the average Si particle area decreased from 28.4 to 0.67 μm^2, the particle length decreased from 15.5 to 1.25µm, the aspect ratio decreased from 3.78 to 1.84, while the roundness ratio increased from 18.9 to 50.3% in the Sr-modified alloy (alloy A1S). In the case of Be addition (alloy A1B), the particle area decreased to 10.3 μm^2, the particle length decreased to 6.6 µm, the aspect ratio decreased to 2.73, while the roundness ratio increased to 35.7%. A combined Sr and Be addition (alloy A1BS) resulted in decreasing the Si particle area to 1.31 μm^2, the Si particle length to 1.84 µm, the aspect ratio to 1.94, and increased the roundness ratio to 47.6%. Increasing the Mg and Fe content (alloy C3), resulted in decreasing the Si particle area to 6.9 μm^2, the Si particle length to 6.44µm, the aspect ratio to 3.01, while increasing the roundness ratio to 24.6%. The combined effect of Sr, Be, Fe and Mg elements (alloy C3BS) resulted in decreasing the Si particle area to 1.53 μm^2, the Si particle length to 2 µm, the aspect ratio to

1.99, and increasing the roundness ratio to 46.7 %. These values reflect the modification effect of Sr and the partial modification effects of Mg and Be. For high Fe- and Mg-containing alloys, simultaneous addition of Be and Sr has less effect on the silicon particle characteristics than the addition of each element individually. The combined effect of addition of the four elements can easily be confirmed from the analysis of the microstructures and data listed in Tables 4.1 and 4.5. Comparing the data reported in the two tables shows that increasing the cooling rate causes significant improvement in the Si particle characteristics for all alloys containing Be, Sr or Be+Sr, as expected. The observed increase in the roundness and aspect ratio of Si particles reported in Table 4.1 for non-modified A1 and C3 alloys may be attributed to the longer cooling time needed for the samples to reach room temperature.

Table 4.5 Eutectic silicon particle measurements for as-cast 357 alloy samples (DAS ~24 µm)

Alloy (Condition)*	**Area (µm^2)**		**Length (µm)**		**Roundness Ratio(%)**		**Aspect Ratio**	
	Av.	**SD**	**Av.**	**SD**	**Av.**	**SD**	**Av.**	**SD**
A1 (non- mod.)	28.40	19.50	15.50	9.46	18.9	8.9	3.78	1.79
C3 (non- mod.)	6.90	6.40	6.44	4.35	24.6	10.5	3.01	1.07
A1B (Be mod.)	10.30	15.90	6.60	6.50	35.7	21.1	2.73	1.66
C3B (Be mod.)	3.17	6.21	2.98	3.40	46.9	21.4	1.99	0.93
A1S (Sr mod.)	0.67	1.04	1.25	1.07	50.3	17.9	1.84	0.70
C3S (Sr mod.)	1.44	2.30	1.91	1.88	47.2	19.7	1.99	0.92
A1BS (Be+Sr mod.)	1.31	1.94	1.84	1.66	47.6	18.8	1.94	0.81
C3BS (Be+Sr mod.)	1.53	2.20	2.00	1.76	46.7	18.9	1.99	0.93

*Codes A and C correspond to the Fe levels 0.09 and 0.6, respectively; while codes 1 and 3 correspond to the Mg levels 0.4 and 0.8, respectively; codes B and S represent Be additions and Sr modification, respectively.

After applying solution heat treatment, as shown in Figures 4.15 through 4.17, the results may be interpreted as follows: the fragmentation and spheroidization of the eutectic Si particles in the 357 base alloy A1 occurs as the alloy is subjected to solution heat treatment and continues as the solution treatment time increases from 5h to 12h, as reflected in the continual decrease in Si particle size and a corresponding increase in the particle roundness. The influence of alloying additions on the degree of refinement of the Si phase may be discerned from the particle characteristics observed for the various alloys in the as-cast condition. The greatest refinement is obtained for the Sr-modified alloy A1S, with A1BS and C3BS alloys displaying a close degree of refinement, whereas the addition of Be alone reduces the particle size in both A1B and C3B alloys, but not to the extent as that observed with a combined Be+Sr addition. Applying solution heat treatment thereafter produces only a very slight decrease in particle size, however, a slight increase is obtained for alloys A1BS and C3BS; this increase may be attributed to the coarsening of the Si particles with the increase in solution treatment time.

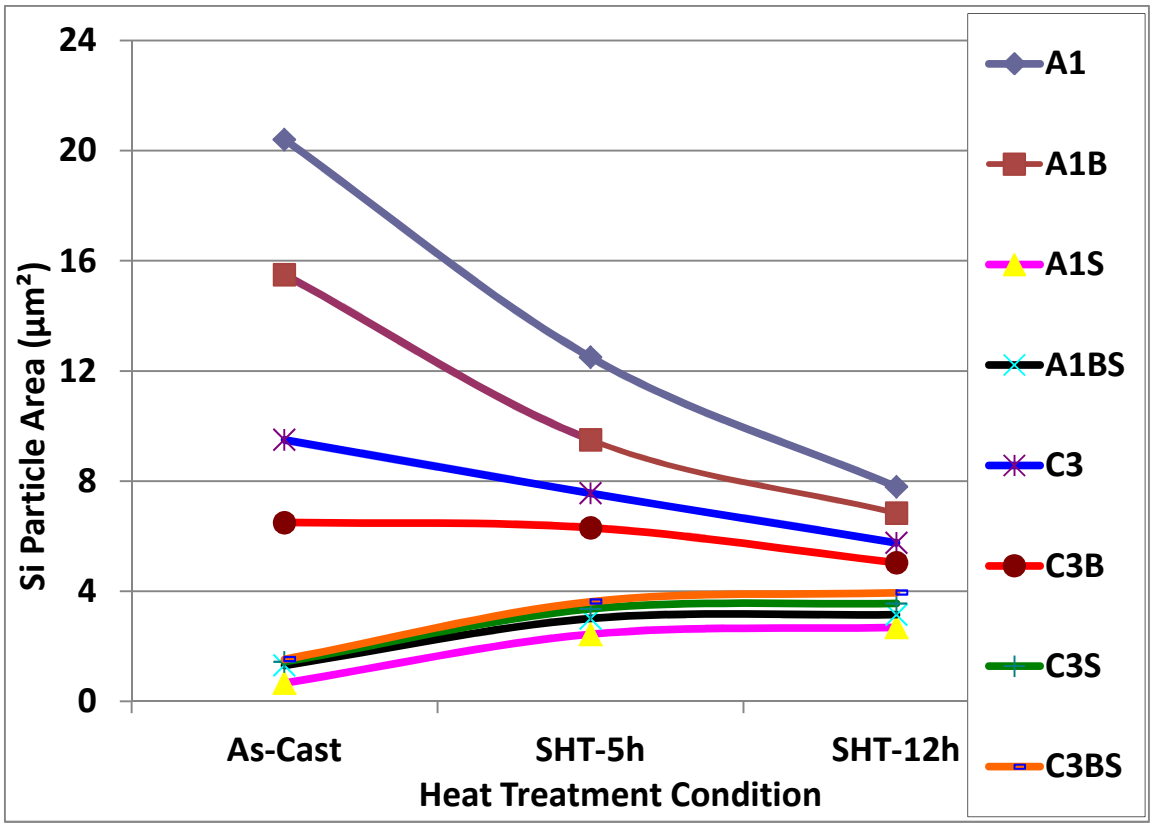

Figure 4.15 Average particle area of eutectic silicon as a function of heat treatment condition.

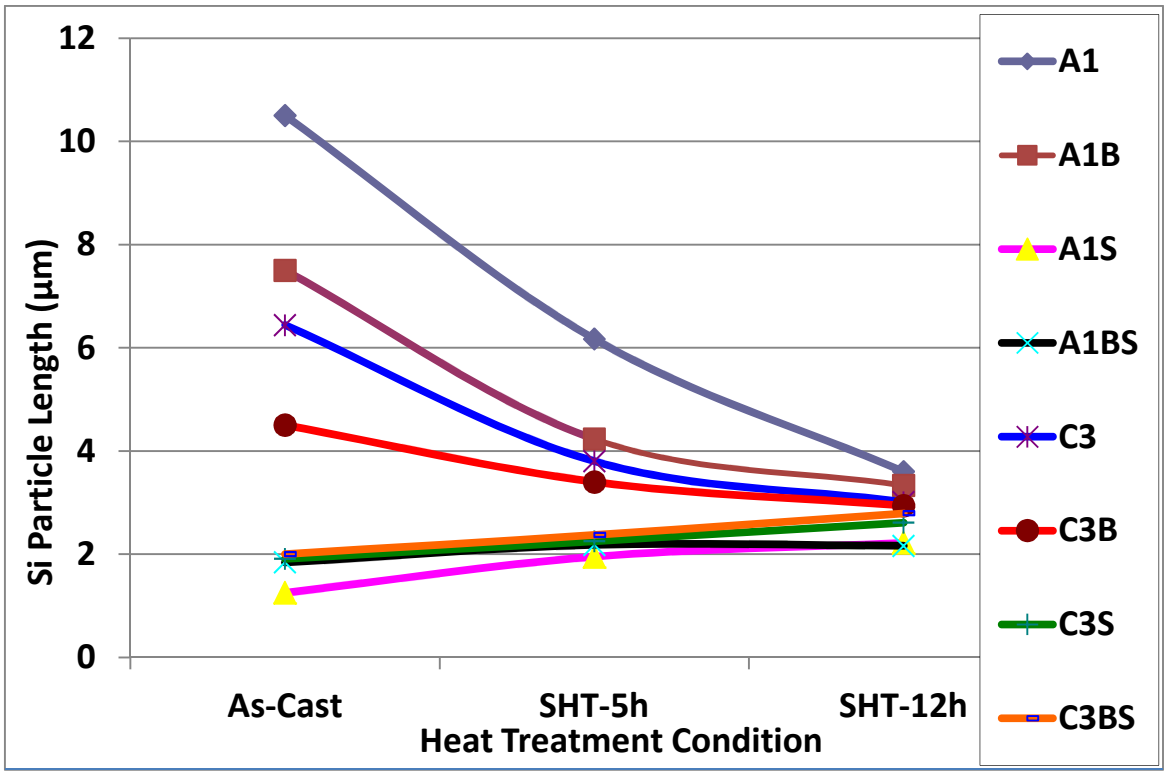

Figure 4.16 Average particle length of eutectic silicon as a function of heat treatment condition.

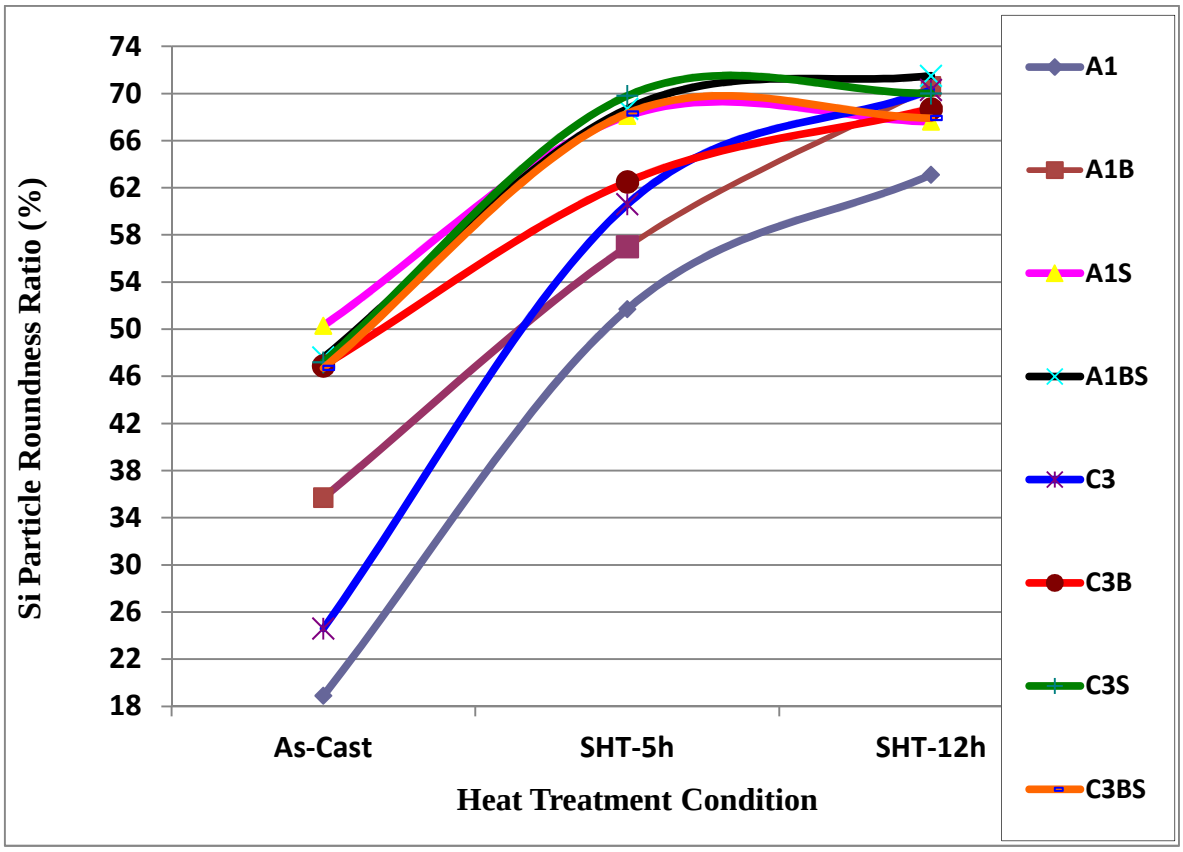

Figure 4.17 Average particle roundness of eutectic silicon as a function of heat treatment condition.

Figures 4.18 and 4.19 show the microstructures of selected as-cast and solution heat-treated samples of these alloys, to illustrate the changes in the morphology and size of the Si particles, depending on the alloying additions and heat treatment conditions. Increasing the solutionizing time from 5 to 12 hours also leads to further improvement in the morphology of eutectic silicon particles. The particle area in the C3 alloys containing higher levels of Mg and Fe was seen to decrease while for the A1 alloys with low Mg and low Fe, the particle area was seen to increase because of the coarsening brought about in

these particles following solution treatment for 12h at 540°C. Spheroidization of the Si particles may be clearly noted in Figures 4.18 (c, d) and 4.19 (c, d), for the long solution treatment time.

Compared to the microstructure of the as-cast base alloy A1 shown in Figure 4.18(a), the as-cast A1BS alloy sample displays on the whole fine Si particles in the interdendritic regions. The large standard deviation observed in Table 4.5 is due the presence of large Si particles indicated by the solid arrow in Figure 4.18(b) mixed with the fine Si particles (indicated by the broken arrow). The as-cast microstructure of alloy C3 in Figure 4.19(a) shows the presence of intermetallic phases due to the high Mg and Fe levels present in the alloy, while a number of long β-Al_5FeSi needles are observed in the as-cast structure of alloy C3BS, Figure 4.19(b).

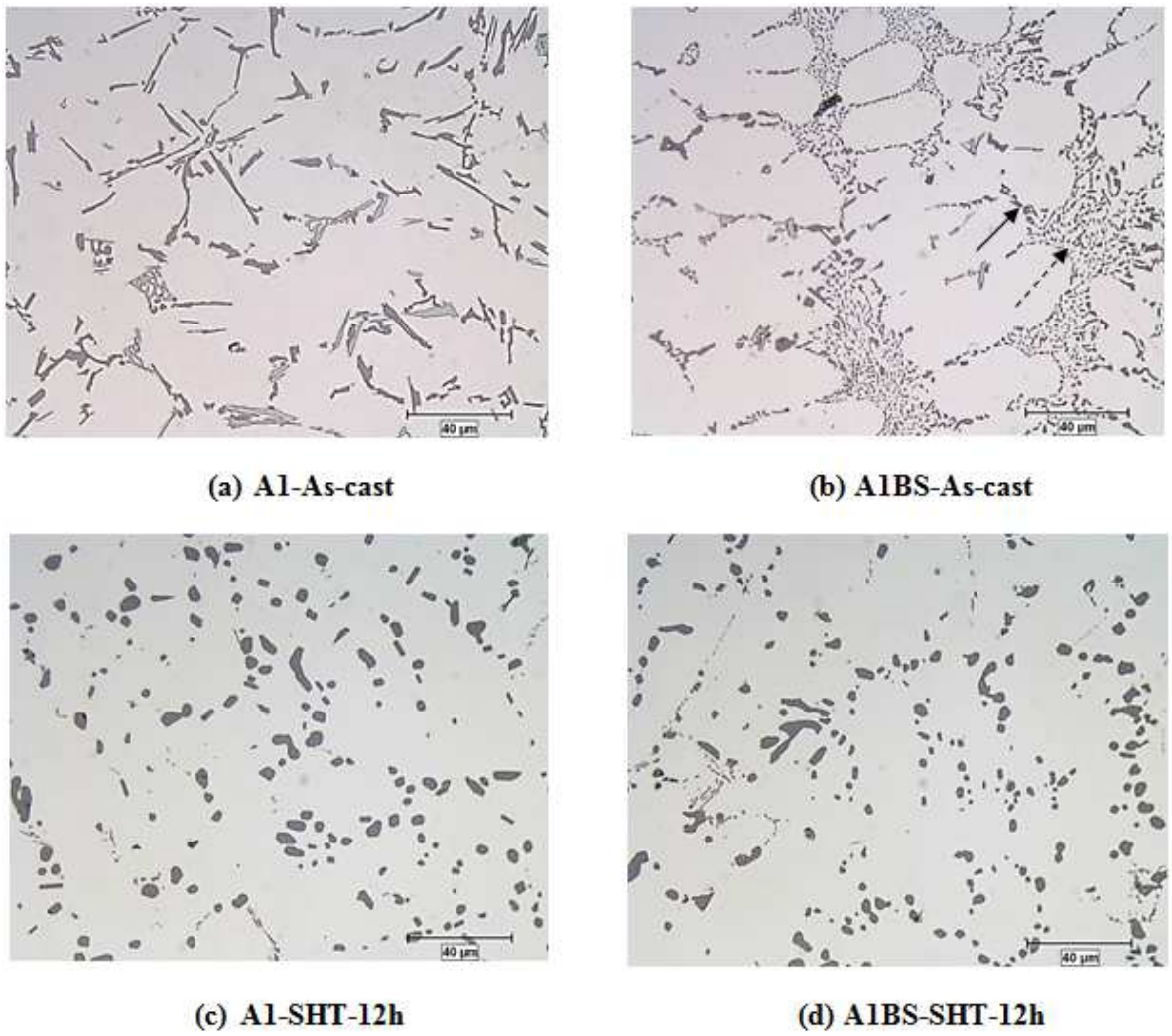

Figure 4.18 Morphology of eutectic silicon particles observed in 357 alloy samples under the following conditions: (a) and (c) base alloy A1 in as-cast and solution heat-treated conditions, respectively, (b) and (d) A1BS alloy in as-cast and solution heat-treated conditions, respectively (DAS 24 µm).

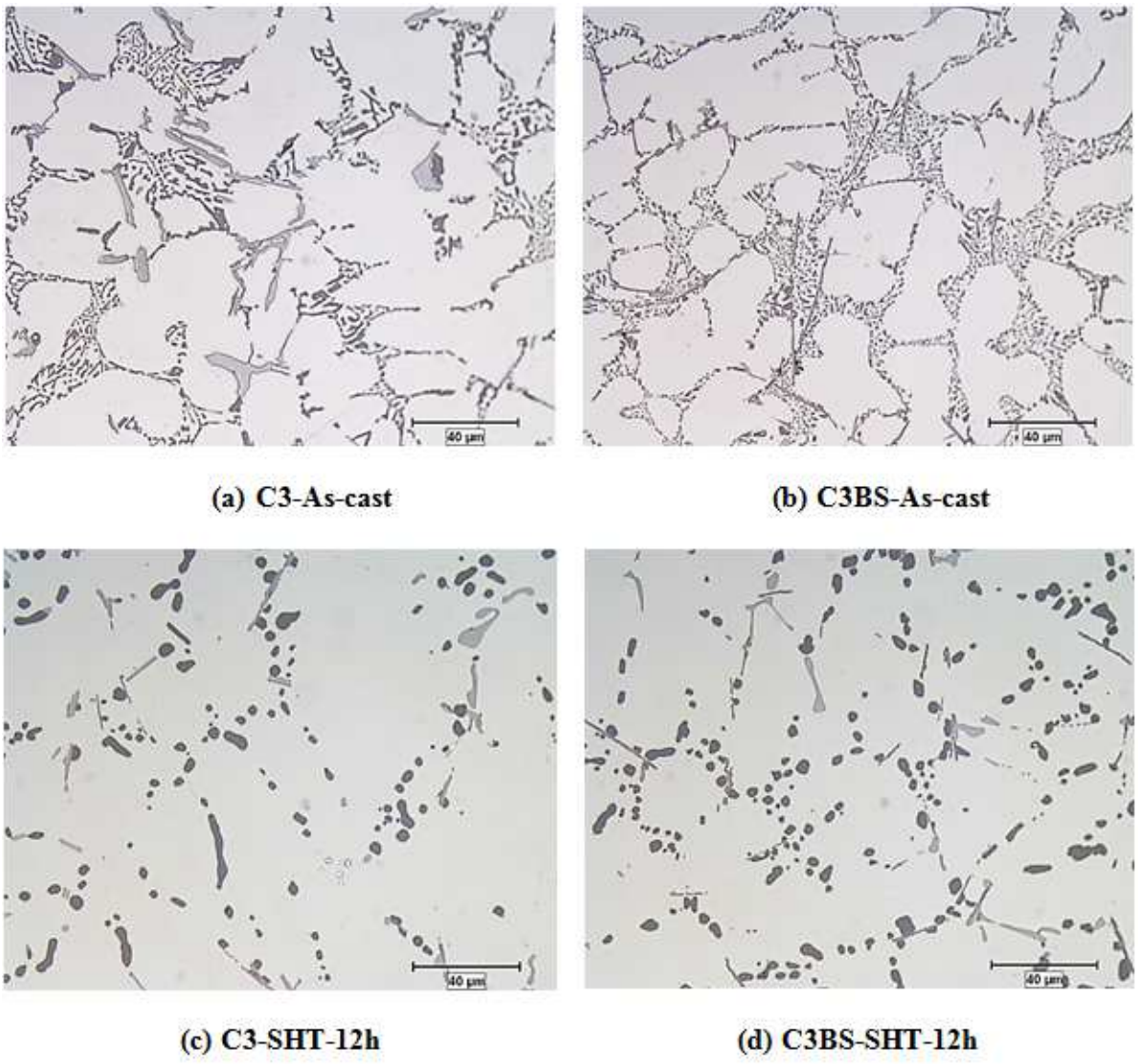

Figure 4.19 Morphology of eutectic silicon particles observed in the 357 alloy samples under the following conditions: (a) and (c) alloy C3 in as-cast and solution heat-treated conditions, respectively, (b) and (d) Sr-modified C3BS alloy in as-cast and solution heat-treated conditions, respectively (DAS 24 µm).

4.3.2 Characteristics of Iron Intermetallic Phases

4.3.2.1 As-Cast Condition

Mathematically, the volume fraction or percentage of a phase may be represented by the average particle size (length or area) of that phase times the number of particles. The histogram shown in Figure 4.20 demonstrates the effects of alloy Fe and Mg content, and Sr and Be additions on the volume fraction of the β-Al_5FeSi iron intermetallic phase, as represented by the average β length for as-cast alloy samples obtained from the preheated (600ºC) graphite mold castings (DAS ~65μm), and from the metallic ASTM-B108 mold castings (DAS ~24μm), microstructures of which are shown in Figure 4.21 and Figure 4.22, respectively. As may be seen, the increase in cooling rate on going from the graphite to the metallic mold reduces the β-phase length by ~50%. A similar reduction in β-phase length can also be obtained by adding Be and/or Sr. Increasing Mg to 0.8 wt% and Fe to 0.6 wt% similarly resulted in reducing the β-phase length and hence the β-phase volume fraction. Increasing latter two elements also increases the π-phase volume fraction, as shown in Figure 4.22. These results agree with those reported by Elsharkawi. [56]

Figure 4.20 also illustrates how the addition of 0.02 wt% Sr to Al-7Si-Mg-Fe alloys resulted in slight decrease in the β-phase length, compared to non-modified alloys. This may be explained in terms of the presence of Sr which results in breaking up the β-phase platelets as reported by Samuel *et al*. [145] The authors reported that Sr is absorbed by the β-phase platelets, leading to their destabilization and fragmentation. In the present context, this may contribute to an increase in the number of β-platelets available for the pre-eutectic reaction to occur, leading thereby to the formation of further amounts of the π-phase.

Figure 4.23 shows examples of β-phase platelets present in the microstructures of alloys A1 and C3BS obtained from samples cast in metallic mold, respectively. These results agree with those reported in the literature. [143, 145]

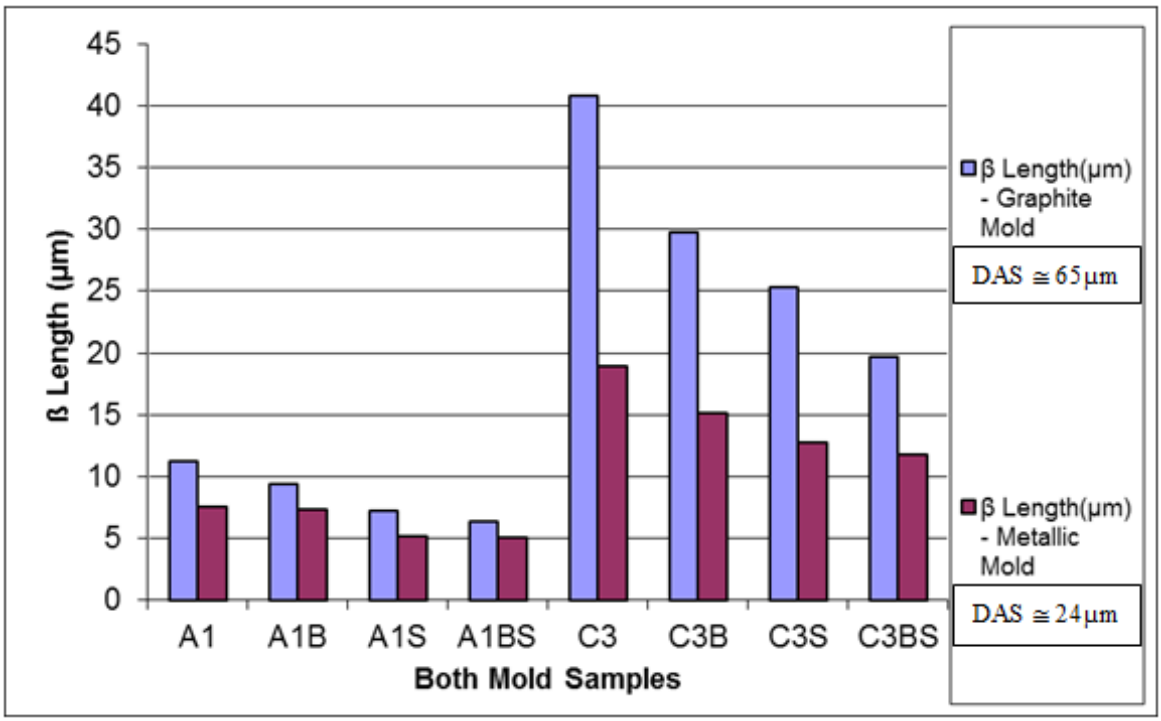

Figure 4.20 Histogram showing how the β-Al_5FeSi phase length is affected by cooling rate and alloy composition.

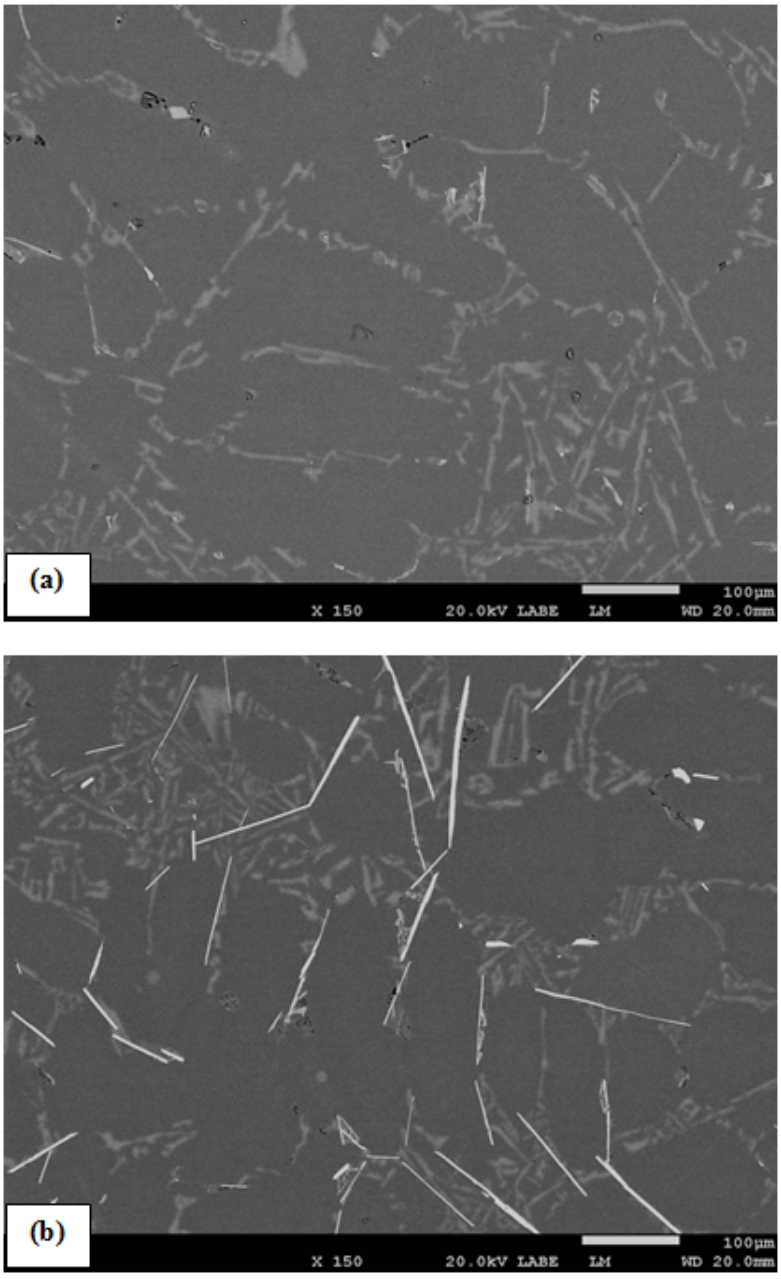

Figure 4.21 Microstructures of as-cast samples of (a) A1, and (b) C3BS alloys (DAS ~65µm).

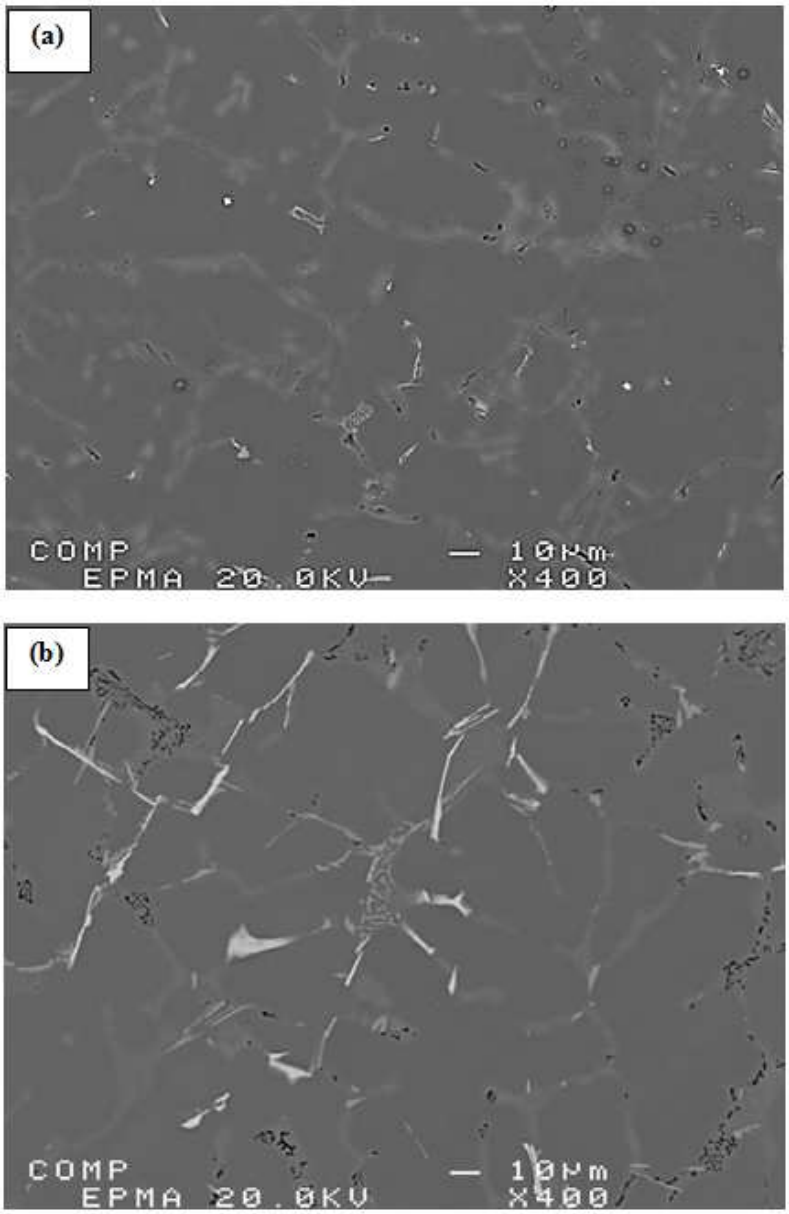

Figure 4.22 Examples of π-$Al_8FeMg_3Si_6$ phase observed in (a) A1, and (b) C3 alloys (DAS ~24µm).

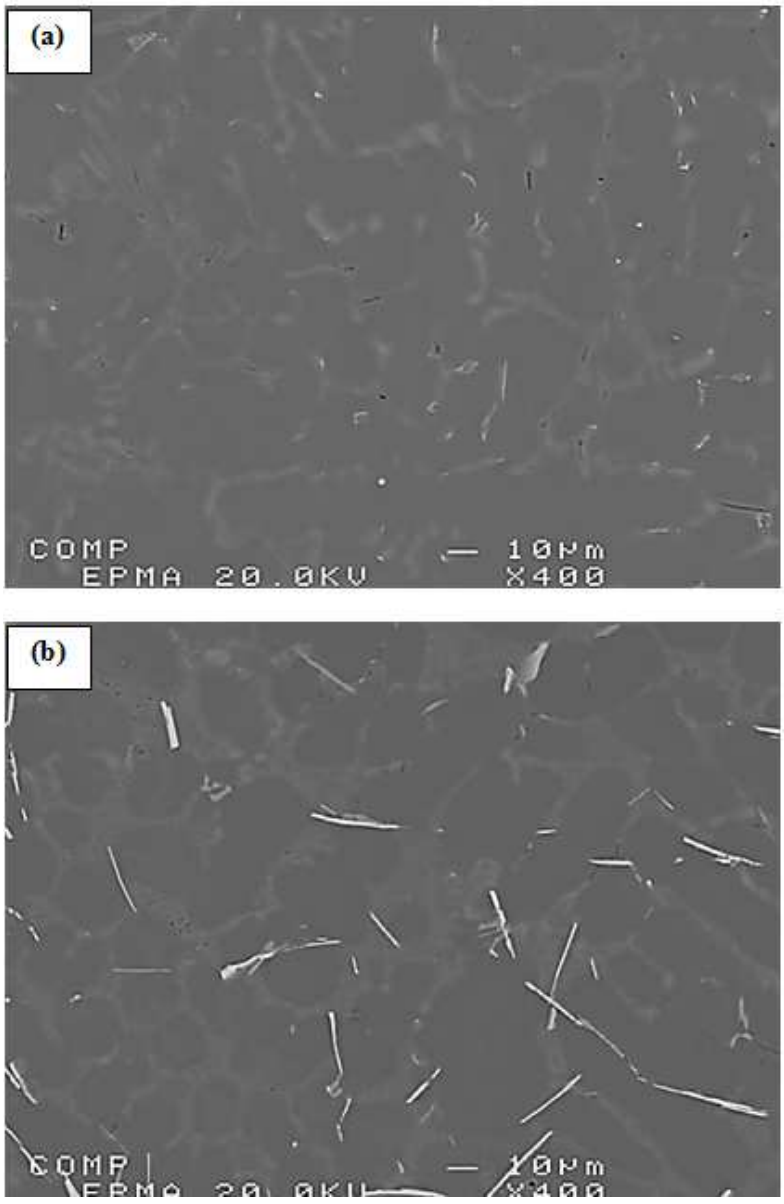

Figure 4.23 Microstructures of as-cast samples of (a) A1, and (b) C3BS alloys (DAS ~24µm).

4.3.2.1 After Solution Heat Treatment

The effects of solution treatment on the π-phase in Al-Si-Mg 357-type alloys were extensively investigated. [56, 135, 136] It was concluded that after applying the recommended solution treatment, the Chinese-script π-phase is more or less decomposed completely to fine platelets of the β-phase in 0.4 wt% Mg-containing alloys. However, only partial decomposition is observed at higher Mg contents, namely 0.6-0.8 wt%. Addition of 500 ppm Be reduces the amount of the π-phase formed in Al7Si*x*Mg-0.1Fe alloys. Addition of Be also facilitates the decomposition of the π-phase into the β-phase, particularly at higher Mg content. Also long solutionizing times lead to a significant reduction in the volume fraction of the π-phase through the dissolution and decomposition of the π-phase into fine β-phase platelets. [56] Together with the π-phase, it is also important to focus on investigating the characteristics of β-phase due to its negative effect on the mechanical properties. [30, 33] Solution heat treatment time and temperature have a significant effect on solubility of both soluble and partially soluble phases. The area percentage of the partially soluble intermetallic phases, particularly the β-phase, was observed to decrease with an increase in the solutionizing time, as illustrated in Figure 4.24. Reduction of ~25% after 5 hours, and ~40% after 12 hours solution treatment were observed. The principal partially soluble phases which formed in the 357 casting alloys, for example the C3BS alloy, were the β-Al_5FeSi and π-$Al_8FeMg_3Si_6$ phases. The major phases observed in the as-cast structure, however, are β-Al_5FeSi and π-$Al_8FeMg_3Si_6$, as shown in Figure 4.22.

The area percentages of β-phase platelets seen in Figure 4.24 for the different alloys studied may be divided into two groups: low ~0.3% and high ~2%. Since the curves lie

close to these two points, it may be more effective to examine the changes in the β-phase platelets in terms of their lengths to compare the effects of each alloying element added, especially Be, on the characteristics of iron intermetallic phases. Not all π-phase particles, however, undergo complete decomposition even after 100 hours of solution treatment. [56]

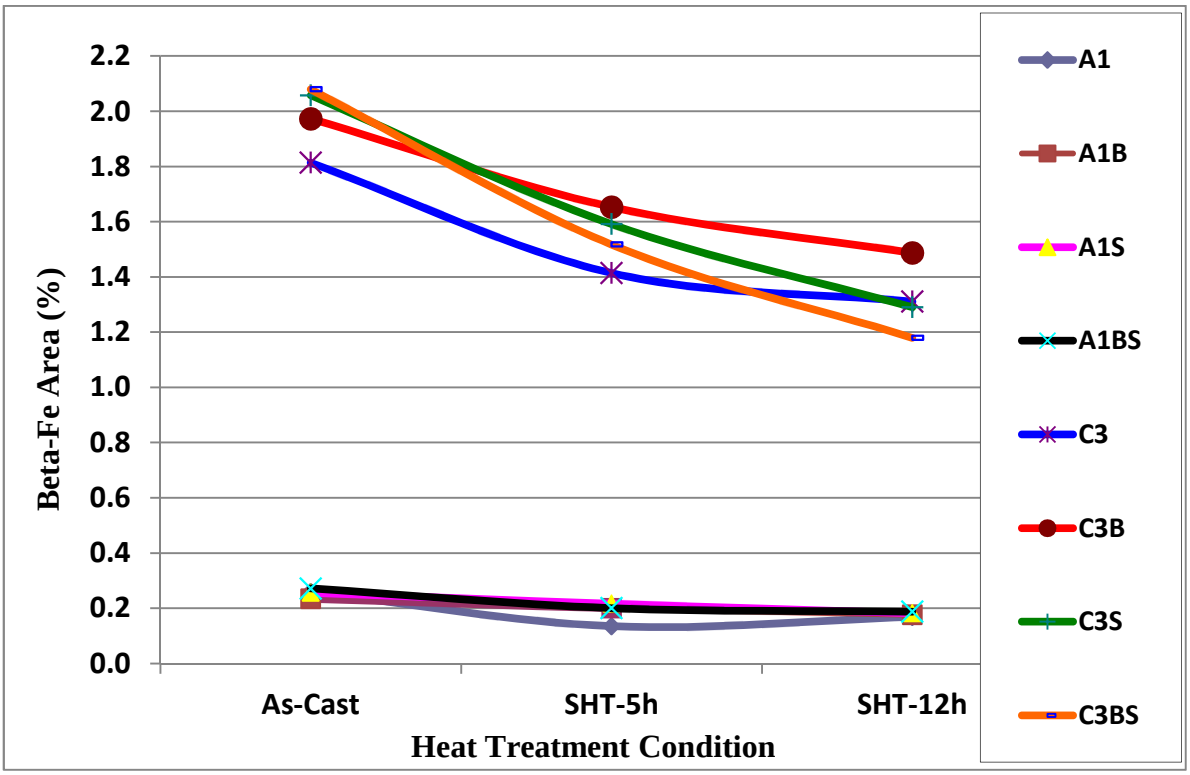

Figure 4.24 Average area percentage of β-phase observed in the 357 alloys studied (DAS ~24µm).

Figure 4.25 shows the average β-phase platelet length as a function of solution heat treatment time. As may be noted, the presence of Be decreases the β-phase length considerably; this effect is limited by adding Sr.

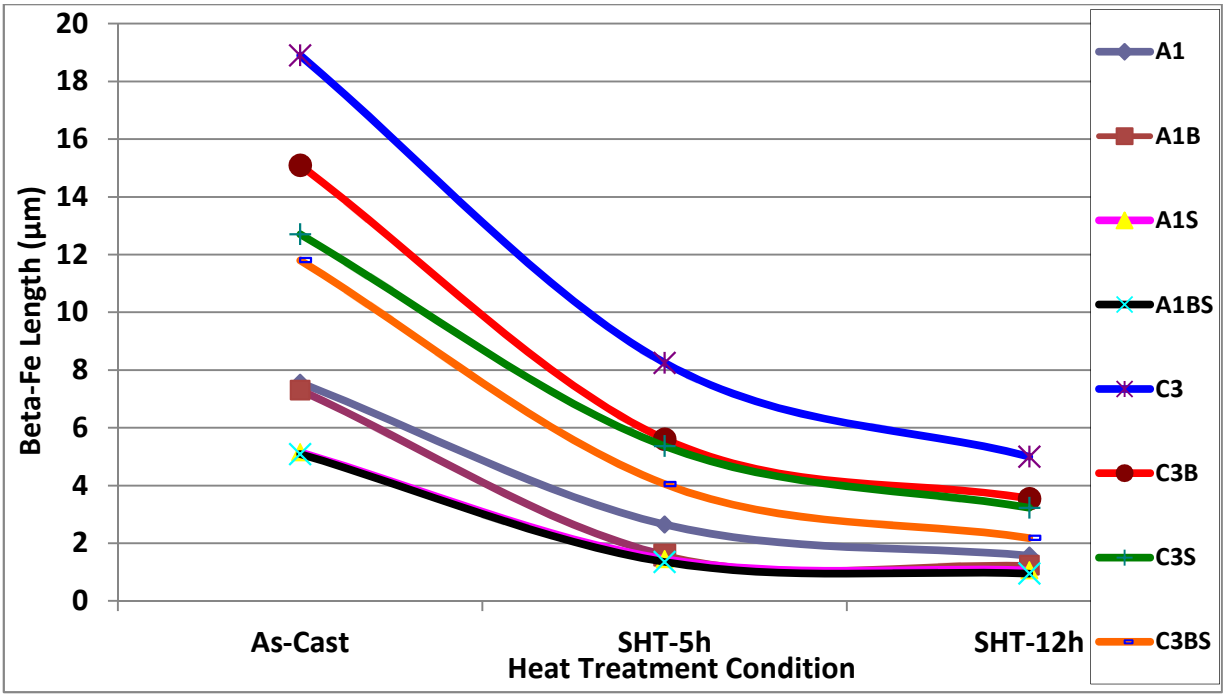

Figure 4.25 Characteristics of average β-phase length of the 357 alloy samples (DAS ~24 µm).

Figure 4.26 illustrates the microstructures of alloys A1, C3, A1BS and C3BS alloy samples in the as-cast condition, cast in the ASTM-B108 mold. Both *β*-platelets and Chinese-script*π*-phase in their regular morphology are observed in the four microstructures, as well as the Chinese-script Mg_2Si phase. With the application of solution treatment, the *β*-phase platelets were observed to undergo changes in their morphology due to the dissolution, thinning, necking and fragmentation of these platelets with increase in solution time. The changes in the size and morphology of the Fe-bearing phases become apparent upon increasing the solution time up to 12 hours, as shown in Figures 4.27(a) through (e). Figure 4.27(e) shows an enlarged particle of *β*-phase undergoing changes in its morphology through dissolution, necking and fragmentation. Such changes in morphology of the *β*-phase were also mentioned in other studies. [146-148] All Mg_2Si particles were completely dissolved while most of *π*-phase was decomposed to *β*-phase and went to the fragmented form. The π-phase was observed to dissolve and/or transform into a cluster of very fine *β*-phase platelets. Similar observations regarding the transformation of the *π*-phase have been reported in the literature. [56, 149-153]

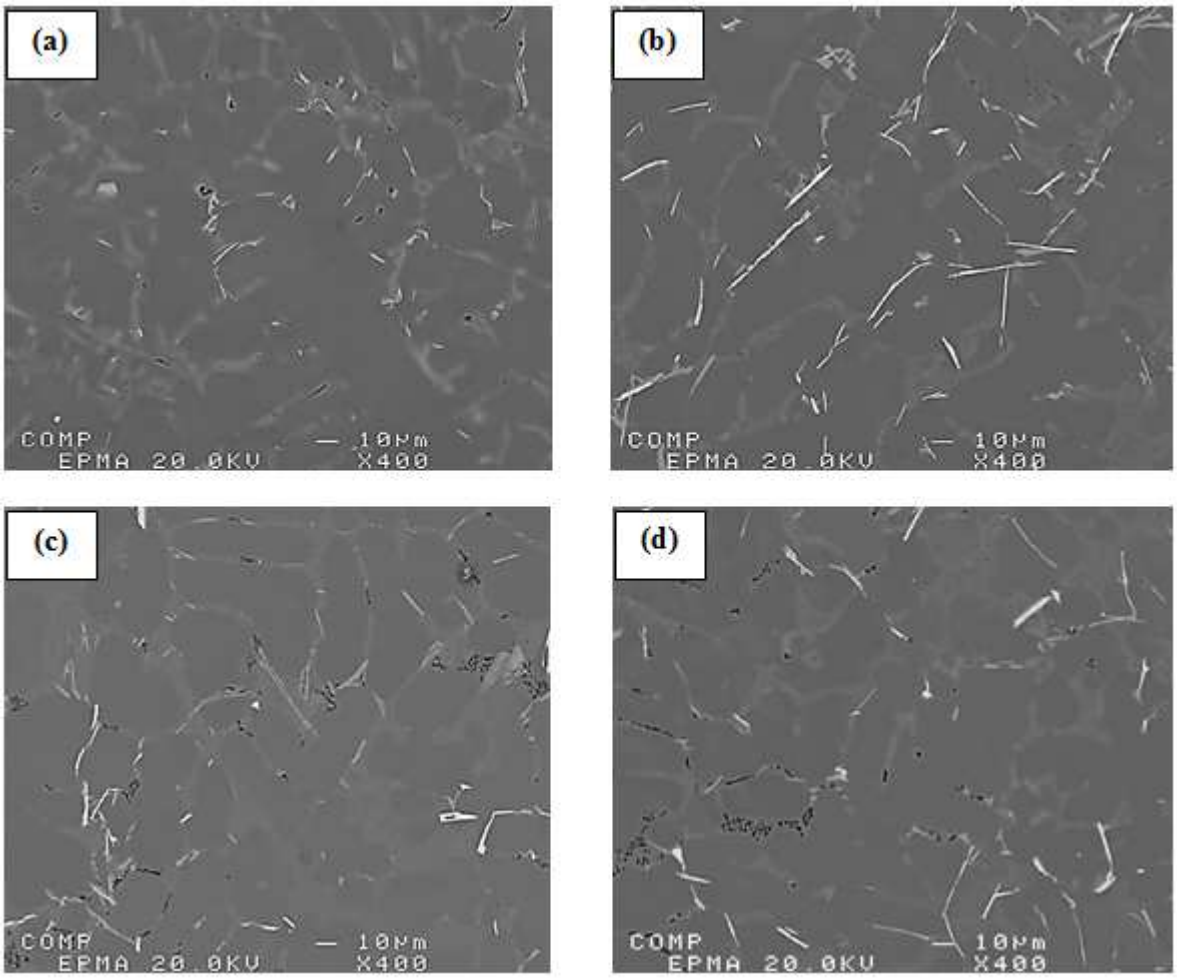

Figure 4.26 The as-cast microstructure of (a) A1, (b) C3, (c) A1BS and (d) C3BS alloy samples (DAS ~24 µm).

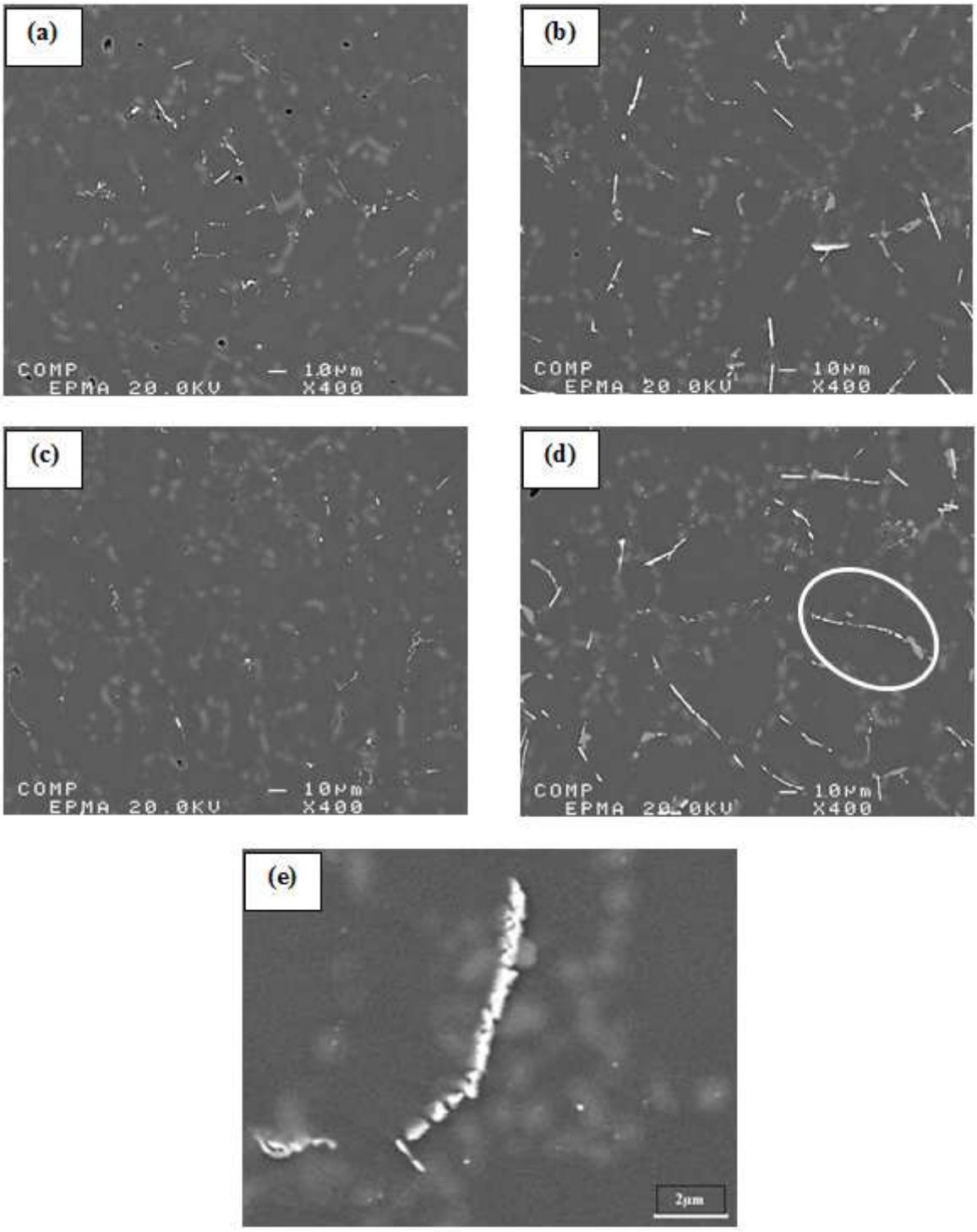

Figure 4.27 Microstructures of alloys: (a) A1, (b) C3, (c) A1BS, (d) C3BS, alloy samples solutionized for 12h at 540ºC (DAS ~24 µm), and (e) enlarged area of encircled area in (d).

4.4 CONCLUSIONS

Based on the microstructural results presented in this study from samples obtained from thermal analysis experiments (DAS ~65µm) and those obtained from tensile bars (DAS ~24µm), the following conclusions may be drawn:

1. Beryllium causes partial modification effect of eutectic Si particles similar to that reported for magnesium addition.
2. Addition of 0.8wt% Mg reduces the eutectic temperature by ~10°C, *i.e.* 1.3°C/0.1 wt% Mg.
3. During solidification of alloys containing high levels of Fe and Mg without Sr, a peak corresponding to the formation of Be-Fe phase (Al_8Fe_2BeSi) is detected at 611°C, which is close to the formation temperature of α-Al.
4. The beryllium-iron phase precipitates in the form of script-like morphology close to other Fe-phases.
5. A new eutectic reaction is observed to take place near the end of solidification of high-Mg, high-Fe, Be-containing alloys. The volume fraction of this reaction decreases with the addition of Sr. The new eutectic reaction is composed of fine particles of Si and π-Fe phases.
6. Addition of Be has a noticeable effect on decreasing the β-phase length, or volume fraction, this effect may be limited in the presence of Sr.
7. Beryllium addition also results in the precipitation of β-phase in the nodular form, which would decrease the harmful effects of these intermetallics on the alloy mechanical properties.

8. Increasing both Mg and Fe levels leads to an increase in the amount of the π-phase.
9. Increasing the iron content leads to an increase in the volume fraction of the partially soluble β- and π-phases, whereas Mg_2Si particles are completely dissolved.
10. The β-phase platelets are observed to undergo changes in their morphology with increasing solution treatment time due to the dissolution, thinning, necking, and fragmentation of these platelets with the progress of solution treatment.
11. The π-phase is observed to dissolve and/or transform into a cluster of very fine β-phase platelets.

PART II

ASSESSMENT OF MECHANICAL PROPERTIES

4.5 INTRODUCTION

Strength and alloy quality are the factors used to determine how a particular metal behaves under a tensile load. Any improvement in these mechanical properties is attributed to an increase of the tensile values observed. The chemical composition of the alloy, the presence of porosity and/or non-metallic inclusions, solidification rate and heat treatment conditions applied constitute the primary variables which affect the tensile properties and quality of aluminum alloy castings. The most common aluminum casting alloys are listed in Table 4.6. [1, 154] Among these, Al-Si alloy castings constitute 85 to 90% of all aluminum cast parts produced.

Table 4.6 Chemical compositions of common types of Al-Si casting alloys (a) [1, 154]

Alloy	Elements (wt. %)						
	Method(b)	Si	Cu	Mg	Fe	Zn	Others
319.0	S, P	6.0	3.5	<0.10	<1.0	<1.0	
332.0	P	9.5	3.0	1.0	1.2	1.0	
355.0	S, P	5.0	1.25	0.5	<0.06	<0.35	
A356.0	S, P	7.0	<0.20	0.35	<0.2	<0.1	
A357.0	S, P	7.0	<0.20	0.55	<0.2	<0.1	0.05 Be
380.0	D	8.5	3.5	<0.1	<1.3	<3.0	
383.0	D	10.0	2.5	0.10	1.3	3.0	0.15 Sn
384.0	D	11.0	2.0	<0.3	<1.3	<3.0	0.35 Sn
390.0	D	17.0	4.5	0.55	<1.3	<0.1	
413.0	D	12.0	<0.1	<0.10	<2.0	-	
443.0	S, P	5.25	<0.3	<0.05	<0.8	<0.5	

(a) Remainder: Aluminum and other impurities
(b) S, Sand Casting; P, Permanent Mold Casting; D, High Pressure Die Casting

Quality index charts, as will be seen later in this chapter, are used in selecting the optimum test conditions in order to enhance tensile properties and quality in Al-Si alloys, particularly the Al-Si-Mg family of casting alloys. Based on the information presented in Table 4.6, the Al-Si-Mg (356 and 357) alloys will be examined according to their Mg and Fe levels, as well as Be additions.

4.6 RESULTS AND DISCUSSION

The 356 and 357 (Al-Si-Mg) alloys investigated in the present work were classified into six categories by considering the base alloy A1 (low Mg - low Fe), alloy A3 (high Mg - low Fe), and alloy C3 (high Mg - high Fe), under different heat treatment conditions, as the reference alloys based on which any changes in tensile properties will be discussed. The six categories selected were: (i) A1 series taking alloy A1 as reference alloy to understand the influence of Be and Sr additions in the case of low Mg-containing alloys, (ii) A3 series using alloy A1 as reference alloy to investigate the effect of increasing the Mg content, (iii) A3 series taking alloy A3 as reference alloy to discuss how Be and Sr additions affect the high Mg-containing alloys, (iv) C3 series using alloy A3 as reference alloy to study the influence of increasing Fe levels, (v) C3 series taking alloy C3 as reference alloy to determine the effects of adding Be and Sr to high Mg- and high Fe-containing alloys, and (vi) C3 series using alloy A1 as reference alloy to elaborate upon the combined effects of different Mg and Fe contents, with other alloying elements, on the alloy mechanical properties. Tensile properties of the reference alloys A1, A3 and C3 in the as-cast and heat-treated conditions are summarized in Table 4.7.

Table 4.7 Tensile properties of reference alloys A1, A3 and C3 of the as-cast and heat-treated conditions

Alloy Code	**Mechanical Property**	**As-cast**	**SHT 5h**	**Aging time (h)**				
				2	**4**	**6**	**8**	**12**
A1	UTS(MPa)	203.8	262.2	342.2	358.0	361.0	354.0	360.3
	YS (MPa)	97.1	115.9	237.2	266.9	277.2	281.5	291.7
	El (%)	6.5	159	9.9	8.7	8.1	6.2	6.5
A3	UTS(MPa)	204.3	263.0	343.3	357.8	380.8	382.9	386.2
	YS (MPa)	114.1	140.9	254.0	291.5	329.6	332.5	347.5
	El (%)	3.4	7.2	6.0	4.3	3.1	2.7	2.0
C3	UTS(MPa)	200.9	239.3	319.9	328.2	366.2	365.7	360.4
	YS (MPa)	116.0	135.3	269.7	296.6	345.2	350.4	356.8
	El (%)	2.6	4.8	1.7	1.0	0.9	0.9	0.7
Alloy Code	**Mechanical Property**	**As-cast**	**SHT 12h**	**Aging time (h)**				
				2	**4**	**6**	**8**	**12**
A1	UTS(MPa)	203.8	255.0	340.3	356.0	359.9	362.3	361.6
	YS (MPa)	97.1	107.5	228.7	273.5	284.3	274.1	279.6
	El (%)	6.5	17.6	12.3	9.9	8.7	9.4	8.5
A3	UTS(MPa)	204.3	287.4	351.3	368.1	381.9	382.0	384.5
	YS (MPa)	114.1	154.0	265.7	294.8	321.1	336.4	353.0
	El (%)	3.4	9.7	6.5	3.6	3.9	2.7	2.0
C3	UTS(MPa)	200.9	250.4	316.5	334.4	337.4	335.3	334.2
	YS (MPa)	116.0	151.8	294.2	301.3	317.0	326.0	327.0
	El (%)	2.6	4.3	1.0	1.1	0.8	0.7	0.7

In the as-cast samples, raising the Mg content from 0.4wt% (alloy A1) to 0.8wt% (alloy A3) slightly increased the alloy strength due to the partial modification effect of Mg, as well as the transformation of the β-phase into the π-phase (most of the Fe-intermetallic phases precipitated in the form of the π-phase, despite the low amount of Fe (0.09 wt%)

present), whereas raising the Fe level up to 0.6wt% in the high Mg-containing alloy C3 led to a decrease in the UTS due to the formation of Fe-intermetallics. For all the three reference alloys, the percent elongation decreased.

Applying a 5-hour solution heat treatment at 540°C raised the UTS by 59 MPa for alloys A1 and A3, and by 39 MPa for alloy C3. The fragmentation and spheroidization of Si particles, the spheroidization of undissolved π-phase particles, the dissolution of Mg_2Si in the matrix and decomposition of the π-phase to the β-phase, which was fragmented during solution heat treatment, all helped to improve the tensile properties.

It was observed that a higher solution heat treatment time (12 hours) led to further improvement of the UTS (60 MPa for alloys A1 and A3, and 50 MPa for alloy C3). This is due to the increase in fragmentation and spheroidization of Si particles and decomposition of the π-phase to the β-phase or further fragmentation of β-phase platelets. For both solution times (5h and 12h), the percent elongation was much greater than that in the as-cast condition for alloys A1, A3 and C3, indicating improved ductility. [155,156]

The micrographs in Figures 4.28 and 4.29 demonstrate how the tensile properties shown in Table 4.7 were affected by Mg content and solution heat treatment. Those presented in Figure 4.30 demonstrate how the microstructures, and consequently the tensile properties, were affected by raising the Mg and Fe levels, in addition to the solution heat treatment used. [157, 158]

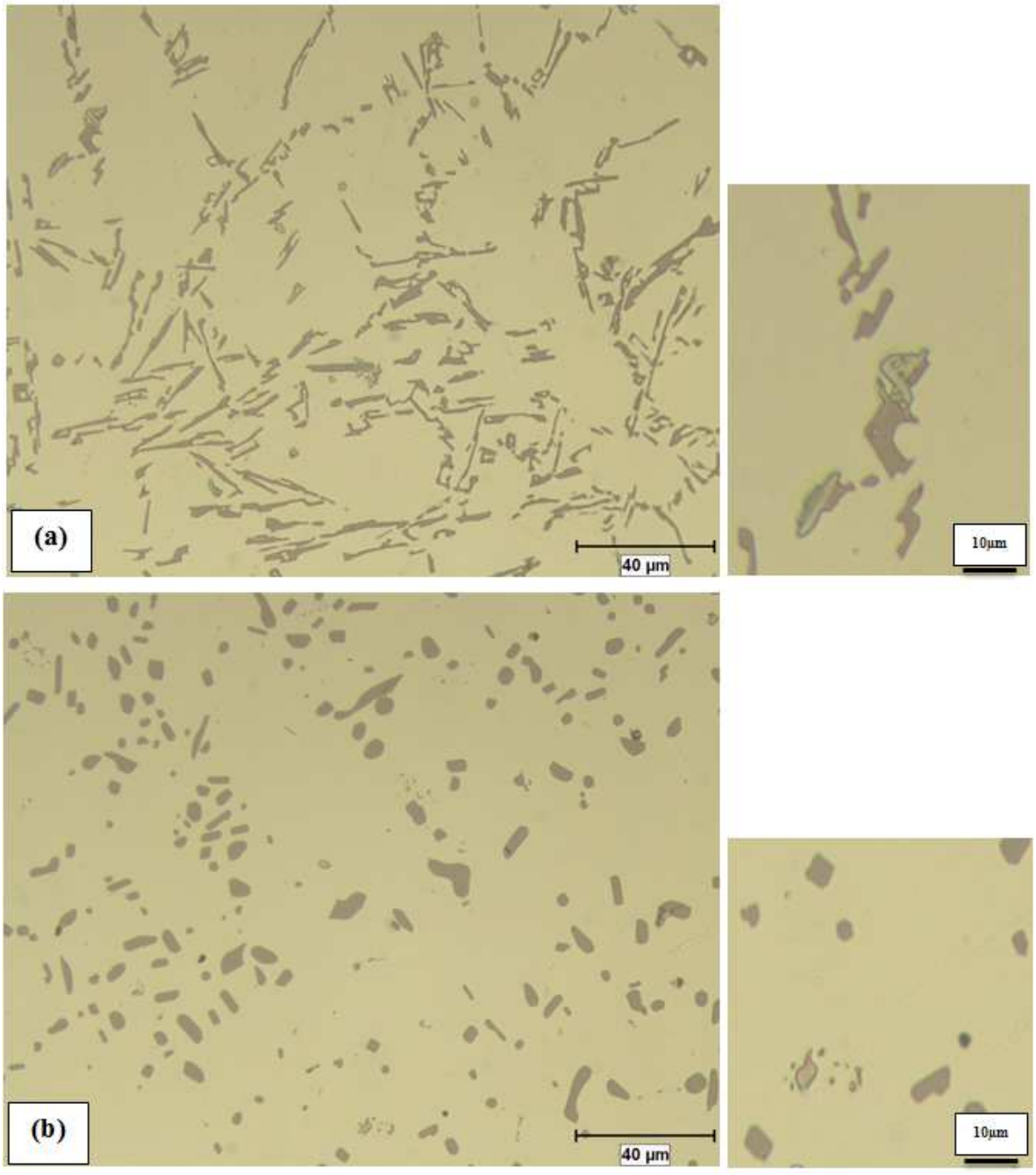

Figure 4.28 Optical microstructures of the low Mg- and low Fe-containing base alloy A1: (a) as-cast sample showing small particles of β- and π-phases, and (b) after a 12h solution heat treatment showing fragmentation of the β-phase as well as spheroidization of the π-phase particles.

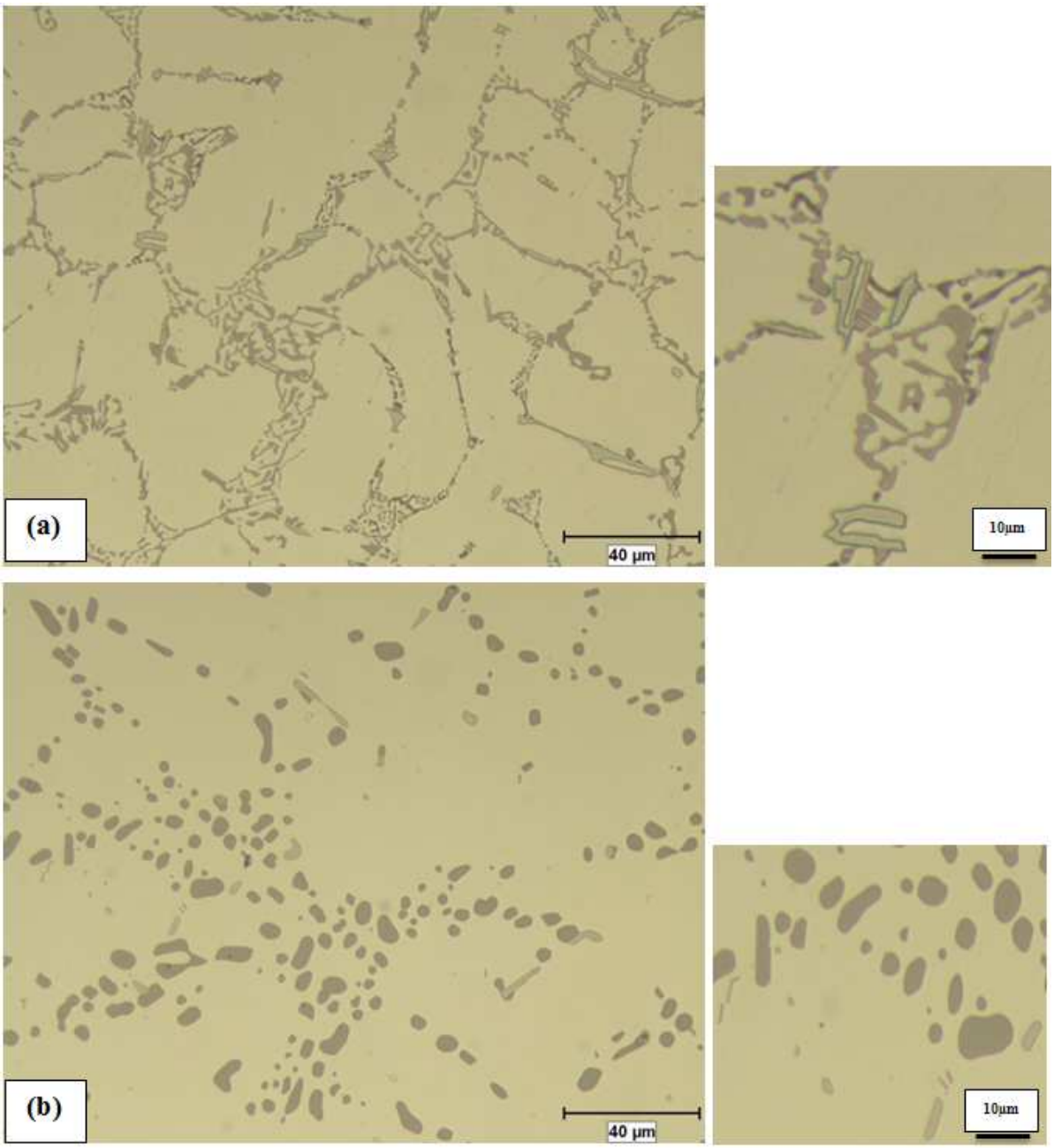

Figure 4.29 Optical microstructures of the high Mg- and low Fe-containing alloy A3: (a) as-cast sample showing larger particles of β- and π-phases, and (b) after a 12h solution heat treatment showing fragmentation of the β-phase as well as spheroidization of the π-phase particles.

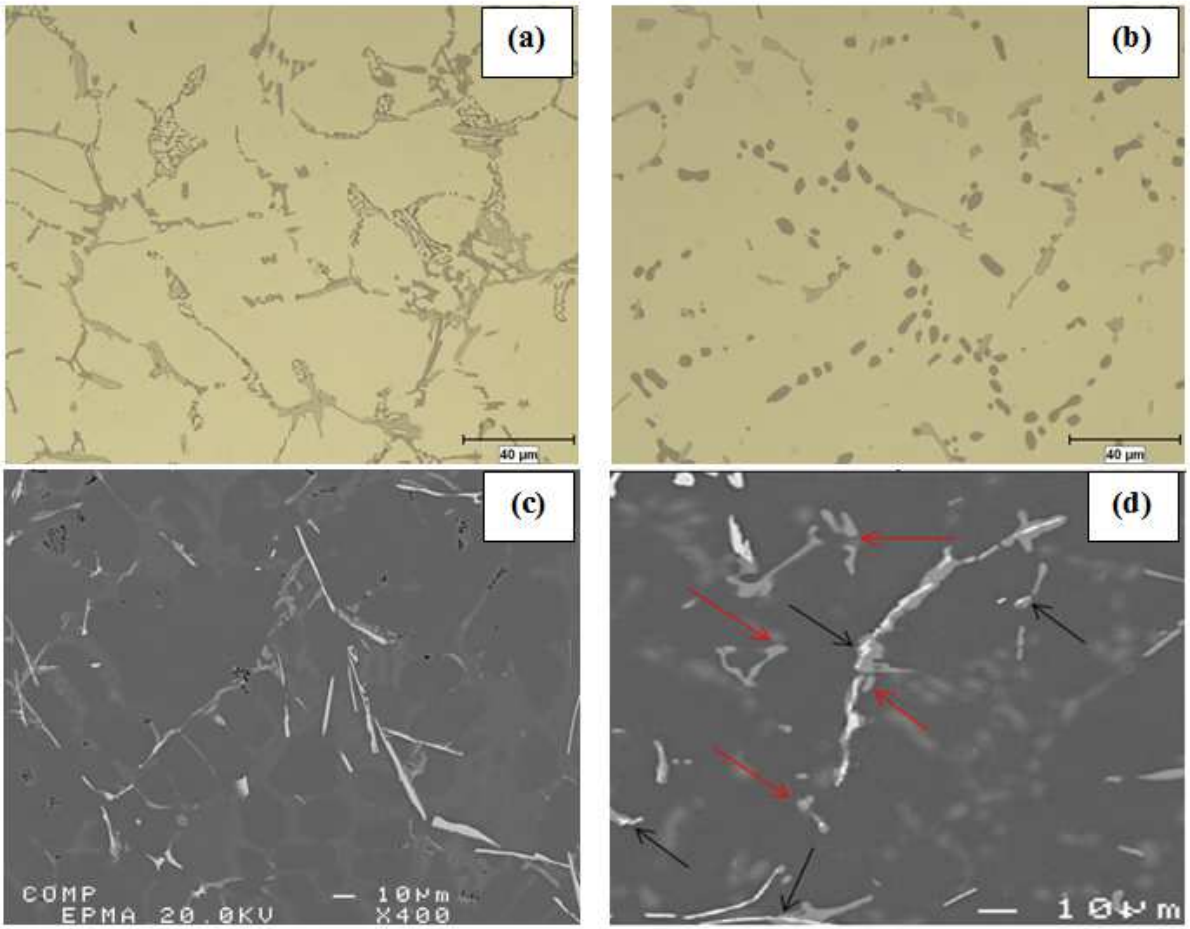

Figure 4.30 Optical microstructures of the high Mg- and high Fe-containing alloy C3: (a) as-cast sample showing larger particles of β- and π-phases, (b) after a 12h solution heat treatment showing fragmentation of the β-phase as well as spheroidization of the π-phase particles, (c) and (d) backscattered images of both conditions, respectively; image (d) shows decomposition of the π-phase into the β-phase, fragmentation of the β-phase (black arrows), as well as spheroidization of the π-phase (red arrows).

Figure 4.30(d), in particular, is an excellent example showing the decomposition of the π-phase and fragmentation of the β-phase (black arrows), as well as spheroidization of the π-phase (red arrows). Figures 4.28 through 4.30 show a complete dissolution of the Mg_2Si phase and the influence of solution heat treatment on the eutectic Si particles, which

appear in fragmented, spheroidized and coarsened forms. [159, 160] Complete dissolution of the Mg_2Si phase and thermal modification of the eutectic Si particles has a marked effect in increasing the alloy mechanical properties. These results agree with the work carried out by Elsharkawi *et al.* [135, 136]

Coarsening of the Si particles during solution heat treatment can be explained by Ostwald ripening, [161, 162] where this mechanism describes the change of an inhomogeneous structure over time, *i.e.*, small crystals or particles dissolve, and redeposit onto larger crystals or particles, as shown schematically in Figure 4.31. [162] The Si particles will increase in size provided their size is greater than the critical volume, while smaller particles will dissolve into the larger particles. Subsequently, the average size and spacing of the Si particles will increase, while the particle density will decrease during the coarsening stage. This mechanism of Si particle coarsening was observed for the three reference alloys (A1, A3 and C3) after solution heat treatment was applied.

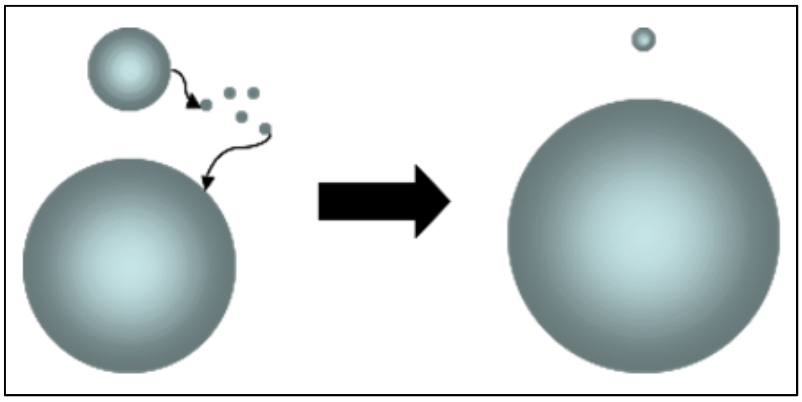

Figure 4.31 Basic representation of the coarsening mechanism as proposed by Ostwald.[162]

The same phenomenon was observed for Mg_2Si precipitates when aged at 160°C for up to 12 hours. Coarsening of the Mg_2Si precipitates became more pronounced when the Mg content was increased from 0.4wt% (alloy A1) to 0.8 wt% (alloy A3). It should be pointed out that the original Mg_2Si volume fraction formed during quenching from the solution temperature was increased, as observed in the backscattered images presented in Figure 4.32(a, b). Some examples of Mg_2Si coarsening precipitates are shown in the areas circled in Figure 4.32(c).

The base A1 alloy was aged at 160°C for 2, 4, 6, 8 and 12 hours, following a solution treatment at either 5 or 12 hours. The ultimate tensile (UTS) and yield strength (YS) values were markedly improved with increase in aging time up to the point of peak aging due to the presence of more precipitates of Mg_2Si which were dissolved after increasing the solution heat treatment time. The maximum UTS values reported for the A1 base alloy were 361 MPa (5 hours solution heat treatment, 6 hours of aging) with further increase in the yield strength (YS) after 6 hours of aging, and 362 MPa (12 hours solution heat treatment, 8 hours of aging) with continuous increase in the yield strength after 8 hours of aging as well. Thus it is difficult to determine the peak aging point exactly and prolonged aging times beyond 12 hours may be recommended.

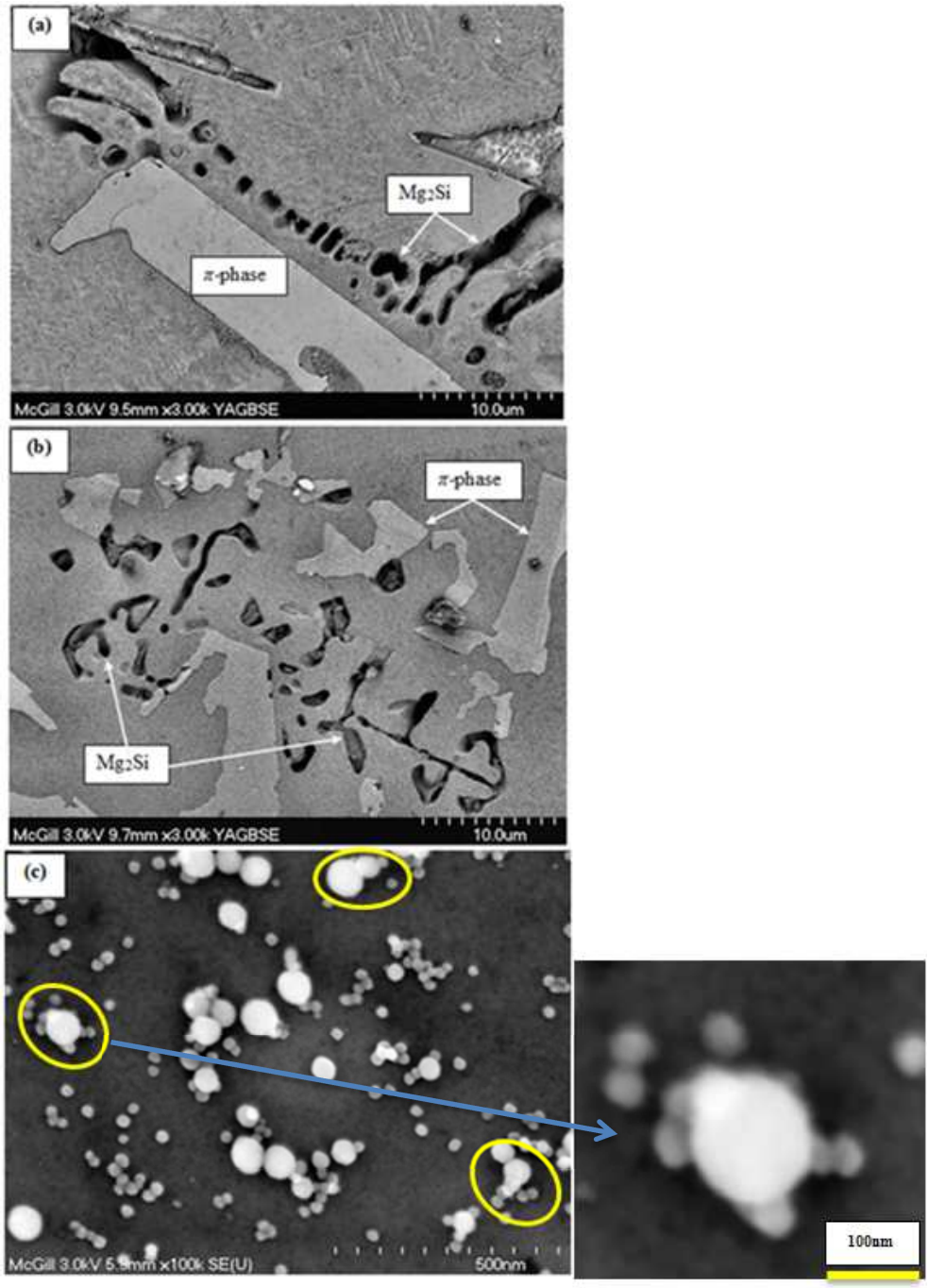

Figure 4.32 (a) and (b) Backscattered images of the as-cast microstructures of the A1 and A3 alloys, and (c) fine and coarse Mg_2Si precipitates observed in the solution heat-treated A1 base alloy. The areas circled in (c) are some examples of Mg_2Si precipitate coarsening. The enlarged area of (c) shows the dissolving of some small particles and re-deposition onto a larger one, resulting in coarsening.

Upon T6-heat treating the high Mg-containing A3 alloy, It was observed that increasing the Mg content encourages the amount of Mg_2Si precipitation and, as a result, the UTS may go up with aging time. Peak aging was observed after 12 hours aging time for the two applied solution heat treatment times, *i.e.* 5 and 12 hours. The UTS obtained in the peak-aged condition for the A3 alloy was 386 MPa (5 hours solution heat treatment, 12 hours of aging) and 385 MPa (12 hours solution heat treatment, 12 hours of aging).

The high Mg- and Fe-containing C3 alloy was also T6-treated as for reference alloys A1 and A3. Again, it was observed that increasing the Mg content encourages the precipitation of Mg_2Si and, as a result, the UTS increases with aging time. However, this increase in UTS was found to be limited, given that the high Fe and Mg contents lead to a stronger presence of the π-$Al_8FeMg_3Si_6$ phase. Peak aging was observed at 6 hours aging time for both solution heat treatment times. These results demonstrate that the amount of Mg_2Si is the primary variable responsible for the 357 alloy strength. The highest UTS values observed for the C3 alloy were 366 MPa (5 hours solution heat treatment, 6 hours of aging) and 337 MPa (12 hours solution heat treatment, 6 hours of aging).

The results shown in Table 4.7 indicate that: (i) greater levels of Mg increase the peak aging time and UTS value, (ii) greater Fe levels, with or without an increase in Mg content, increase the peak aging time and noticeably decrease the corresponding strength, and (iii) the UTS increases with longer solution heat treatment and aging times, especially in the case of the high Mg- and low Fe-containing alloys. [163]

For aged samples, once past the point of peak aging, softening was noted to occur. This is attributed to the coarsening of the Mg_2Si precipitates by either clustering, as shown in Figures 4.33 (alloy A1) and 4.34 (alloy A3), or by the Ostwald ripening mechanism. Figure 4.33(a) shows how the Mg_2Si precipitates initiate clustering during 2 hours of aging. The circled areas in these two figures reveal the tendency for growth of the Mg_2Si cluster with increase in aging time, from 2 to 12 hours (Figures 4.33 (a) and (b)), or with increased Mg content for the same aging time of 12 hours (Figure 4.33(b) and Figure 4.34(a)). When comparing these last two figures, it is observed that raising the Mg content increases the density of the Mg_2Si precipitates. The clustering of the Mg_2Si precipitates and the associated growth is shown in Figure 4.35.

In a previous investigation of the aging behavior of 357 alloys, a noticeable reduction in the strength (commencement of softening) of the alloys examined upon increasing the aging time or temperature, was reported to be related to the formation of coarser precipitates in the matrix, displaying large inter-particle spacing, as shown in Figure 4.36. This facilitates dislocation motion and results in softening, thereby reducing the alloy strength and, consequently, the quality index values, as will be explained later in this chapter, of the castings being studied. [153]

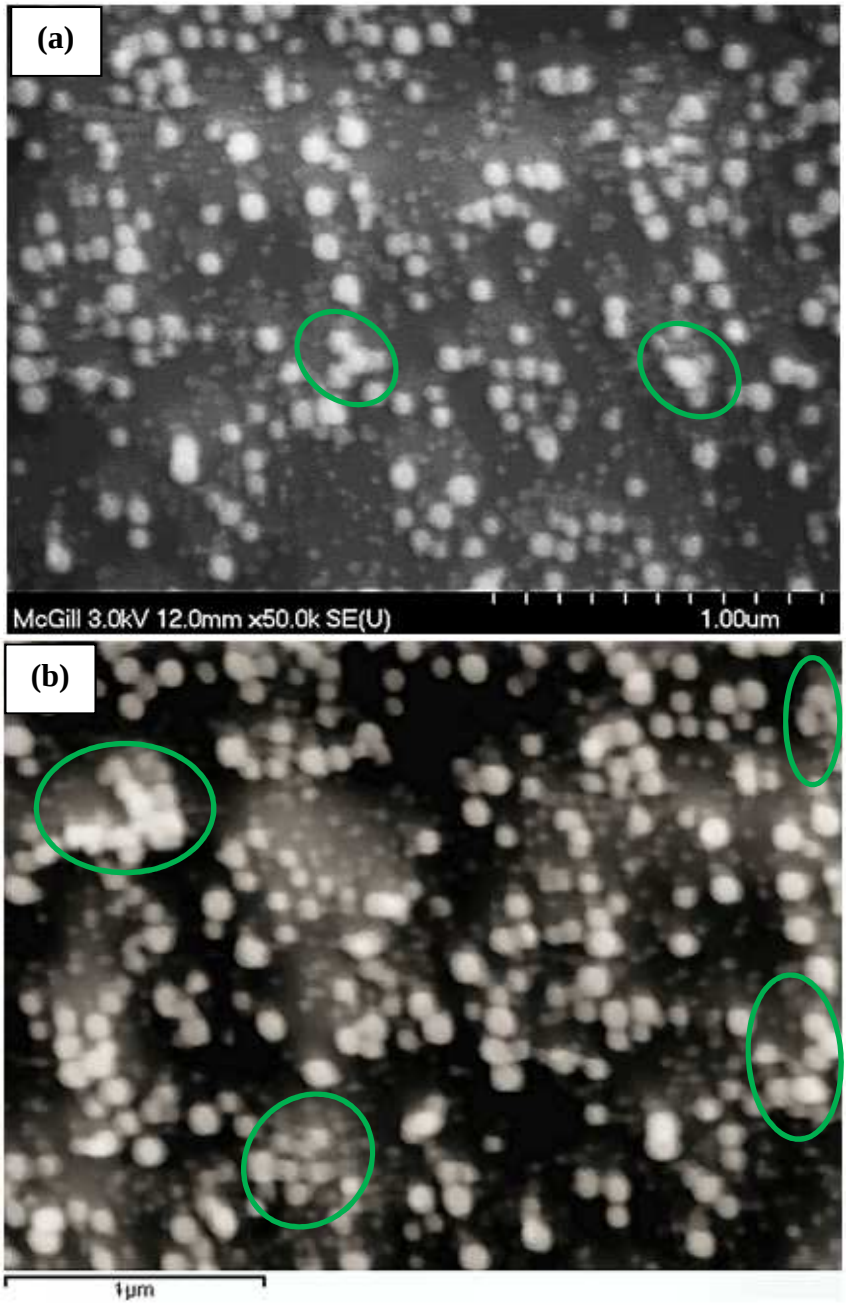

Figure 4.33 Backscattered images of the base A1 alloy after aging at 160°C for: (a) 2 hours and (b) 12 hours, showing an increase in the amount of clustered Mg_2Si precipitates with increasing aging time.

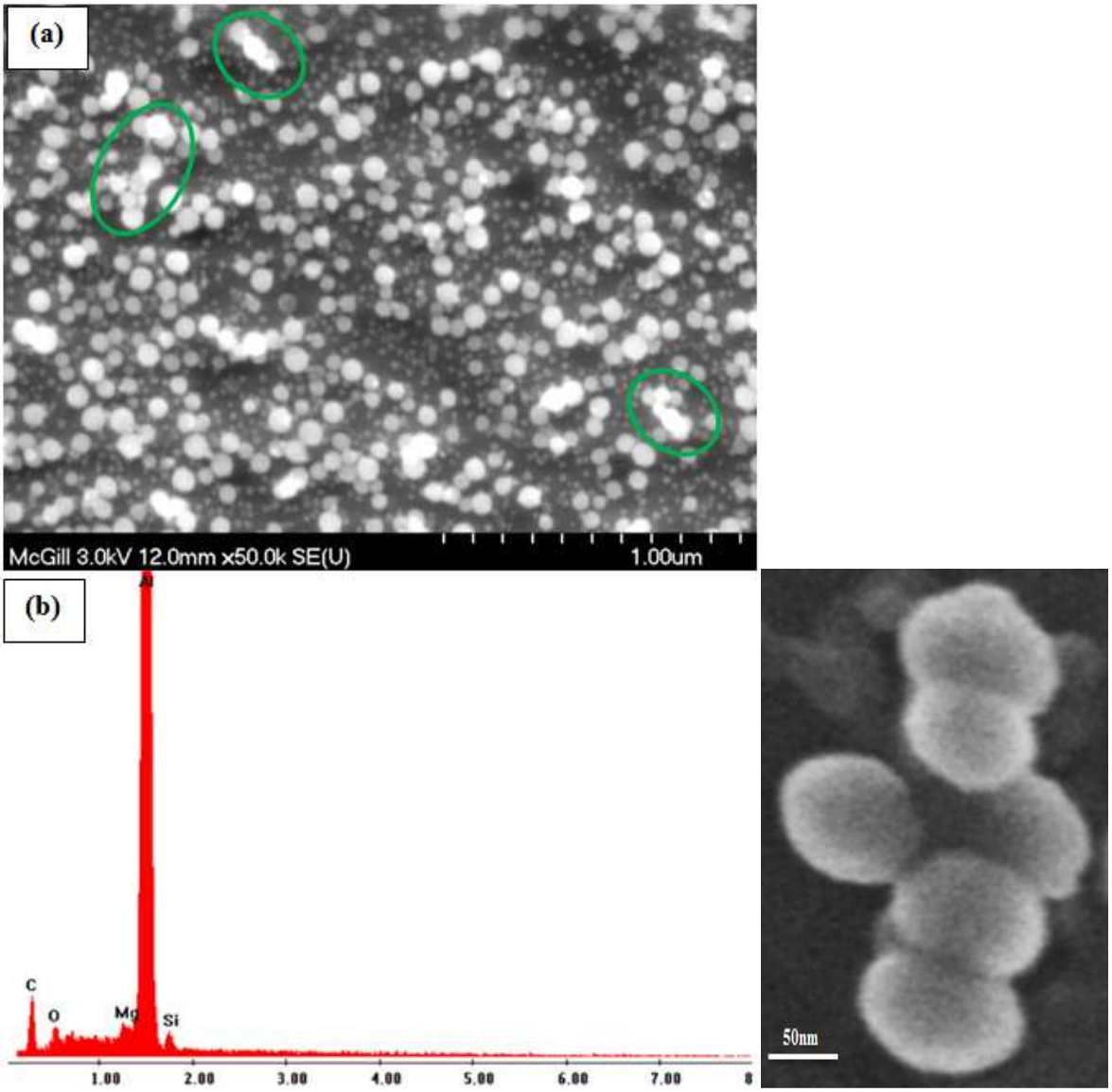

Figure 4.34 (a) Backscattered image of the high Mg-containing A3 alloy after aging at 160°C for 12 hours which shows a high density of Mg_2Si precipitates, as well as more of the clustered precipitates, and (b) EDS spectrum of clustered Mg_2Si precipitates. The enlarged area of (a) shows the onset of precipitate clustering.

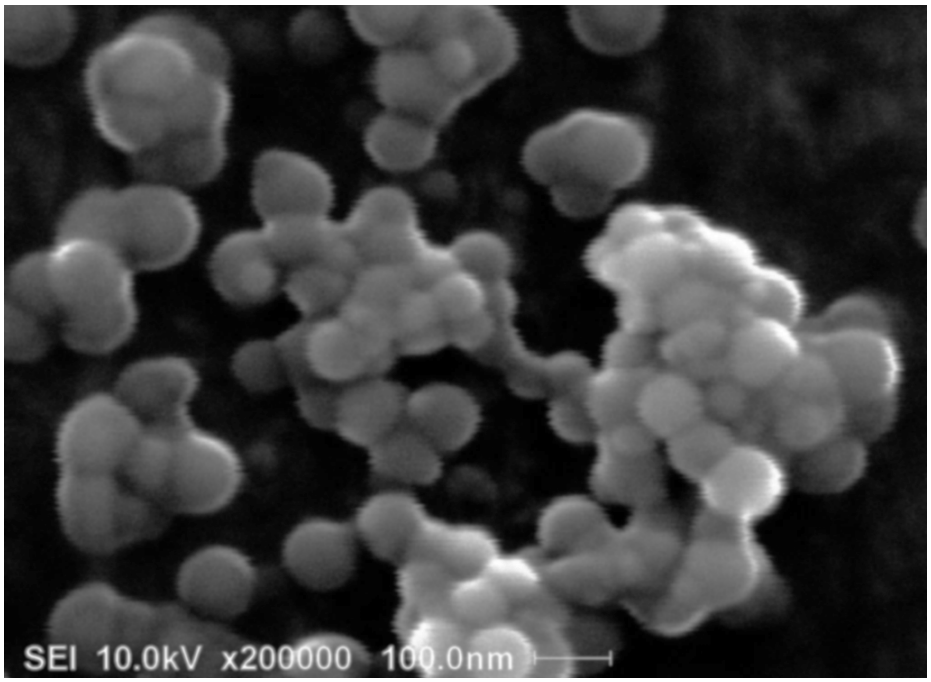

Figure 4.35 Clustering of Mg_2Si during precipitation hardening of the high Mg-containing A3 alloy at 160°C for 12 hours, after being solution heat-treated for 12 hours.

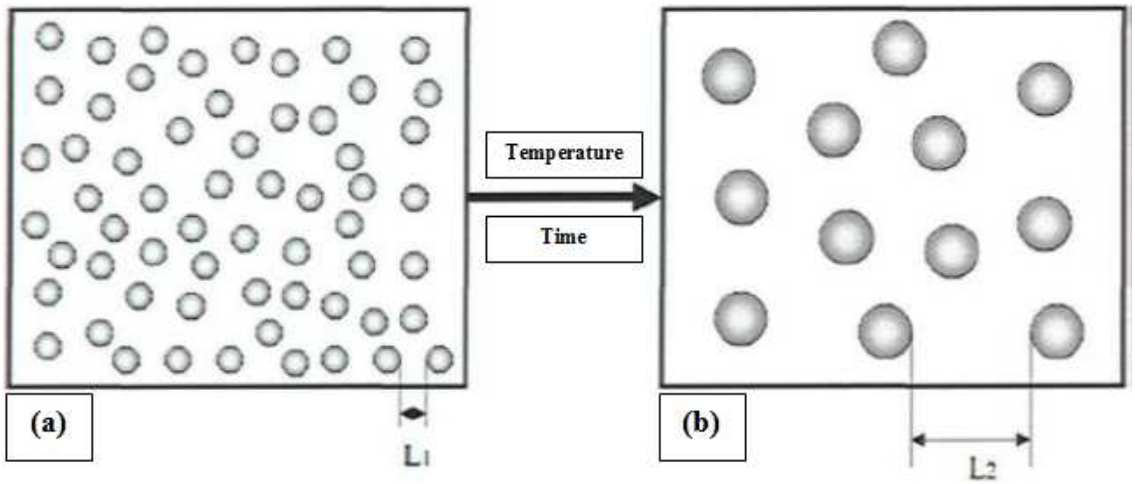

Figure 4.36 Schematic representation showing the influence of increasing aging temperature/time on the size, density, and inter-particle spacing of the hardening precipitates: (a) at low aging temperature/time, and (b) at high aging temperature/time. L1 and L2 indicate the inter-particle spacing in each case. [153]

Based on the above-mentioned observations, coarsening of precipitates may take place either by dissolution and re-deposition or clustering of fine particles prior to becoming large ones leading to commencement of softening. The observed clustering may be explained in terms of precipitation of Mg_2Si particles on the pre-existing Mg_2Si particles leading ultimately to coarsening with increase in aging time. However, more work is needed to arrive at a better understanding of this observation and the exact coarsening mechanism.

From an engineering point of view, yield strength is the main parameter on which design considerations are based, given that YS is more sensitive to alloying additions than UTS. From the values listed in Table 4.7, the YS increased in the cases of: (i) increased Mg levels, as well as increased Fe contents (from 0.09wt% in A alloys to 0.6wt% in C alloys, alloy C3 being an example of an alloy with increased Fe content), (ii) after solution heat treatment, and (iii) with increasing aging time.

Increasing the Mg levels in the as-cast condition raised the YS by 17 MPa and by 19 MPa when the Fe content was also raised. When solution heat treatment was applied to the base A1 alloy, the YS was seen to increase by 19 MPa for a 5-hour solution treatment and 10 MPa for a 12-hour solution treatment. In the case of alloy A3, the YS was seen to increase by 26 MPa for a 5-hour solution treatment and 40 MPa for a 12-hour solution treatment. A reduced degree of improvement in the yield strength was reported for either solution treatment time in the case of the high Fe-containing C3 alloy.

Aging time was also observed to be a significant factor affecting the yield strength, where longer aging times led to greater YS values. Maximum YS values of 292, 347 and 357 MPa for alloys A1, A3 and C3, respectively, were observed after prolonged aging. Ductility, as measured by percent elongation, is inversely proportional to strength, particularly the yield strength. However, improvement of the alloy ductility is as important as improvements in the strength. As shown in Table 4.7, alloy ductility was improved at greater Mg levels and/or solution treatment time, whereas it decreased with increase in Fe content.

Magnesium and iron have been observed to affect the strength, ductility and quality of the 357 alloys studied. Figure 4.37 shows the quality chart, which was generated to represent the effects of Mg and Fe content on the tensile properties of the alloys under investigation.

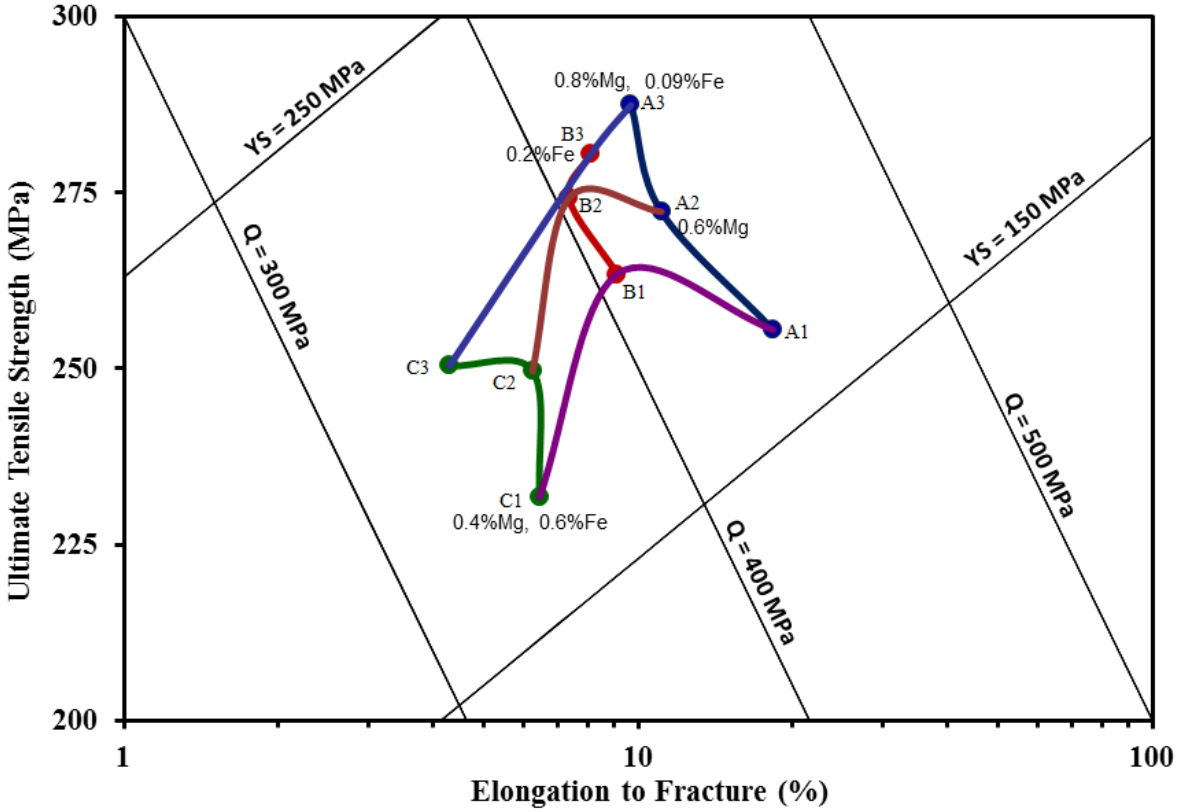

Figure 4.37 Quality chart generated using equations (1) and (2), showing the effects of adding Mg and Fe. Samples were solution heat-treated for 5h at 540°C, followed by quenching in warm water and no aging.

As can be seen from the figure, when the Fe level is increased from 0.09 wt% (alloy A3) to 0.2 wt% (alloy B3) and further to 0.6 wt% (alloy C3), the alloy strength and ductility are decreased and the alloy quality is diminished. This detrimental effect is caused by an increased presence of brittle, undissolved Fe-intermetallic phases. Similar observations were made when the Fe content was increased from alloy 0.09 wt% (A2) to 0.2 wt% (alloys B1 and B2) and, finally, to 0.6 wt% (alloys C1 and C2). Since these alloys contain different levels of Mg (0.4, 0.6 and 0.8 wt%), it can be seen that a high Fe content will bring about a noticeable reduction of the alloy mechanical properties, regardless of the Mg content.

When increasing the Fe-level, the Fe series presented in Figure 4.37 shift virtually parallel to the iso-Q lines toward the lower left-hand portion of the figure, where all alloy properties are lowered. The yield strength, however, revealed no significant changes when increasing the Fe-level from 0.09 to 0.6% (Figure 4.37), where each Mg line, which represents three levels of Fe, is more or less parallel to the iso-yield strength lines or iso-flow lines. Yield strength is independent of impurity elements such as Fe but is strongly affected by the addition of hardening elements or by the application of a suitable aging step.

The increase in the Mg content from 0.4 wt% (alloy A1) to 0.6 wt% (alloy A2) leads to an improvement in the strength of the castings by about 12 MPa, and to a corresponding decrease in ductility without any decrease in the quality (Figure 4.37). Further improvements (32 MPa) were observed when raising the Mg level up to 0.8 wt% (alloy A3). Positive effects were also observed when raising the Mg levels from alloys B1 and C1 (0.4 wt%) to alloys B2 and C2 (0.6 wt%) and B3 and C3 (0.8 wt%). Since these alloys have different levels of Fe (0.09, 0.2and 0.6 wt%), then greater Mg contents yield a noticeable improvement of the alloy mechanical properties, in spite of the presence of Fe. These observations relate to the fact that the amount by which the strength of the alloy is increased compensates for the amount by which the ductility is reduced. The improved strength of the castings obtained by increasing the Mg content is related to the precipitation of the Mg_2Si phase, where the greater Mg content will yield a higher density of this phase. However, a higher Mg level will also lead to the precipitation of the π-$Al_8FeMg_3Si_6$ phase, which has a deleterious effect on both strength and ductility, in other words, the quality, of the castings. [89, 90]

It was observed that adding Be improved the tensile properties and quality of the alloys containing various levels of Mg and Fe (in this case, alloys A1B, A2B, A3B, B1B, B2B, B3B, C1B, C2B and C3B). As may be seen from Figure 4.38, the addition of Be shifts the quality index values towards the upper right portion of the chart, *i.e.* in the direction of improved alloy quality. From the figure, the yield strength is shown to increase, as indicated by the shift of the Mg lines towards the direction of higher YS. The improvement in tensile properties through the addition of Be stems from two sources: (i) during casting, the presence of Be helps to prevent the oxidation of Mg, and (ii) changing the morphology and chemistry of the β-Fe phase platelets to smaller nodular-shaped β-phase particles, accelerating the π-phase decomposition to the β-phase and forming a Chinese-script Be-Fe phase (Al_8Fe_2BeSi). [51, 54, 57]

For different levels of Fe and Mg (in this case, alloys A1S, A2S, A3S, B1S, B2S, B3S, C1S, C2S and C3S), the addition of Sr improved the tensile properties and quality index values of the modified alloys compared to the non-modified alloys (without Sr), as shown in Figure 4.39. The addition of Sr also helped reduce the harmful effect of the β-phase by transforming it into the script-like α-Al_8Fe_2Si phase.[30]

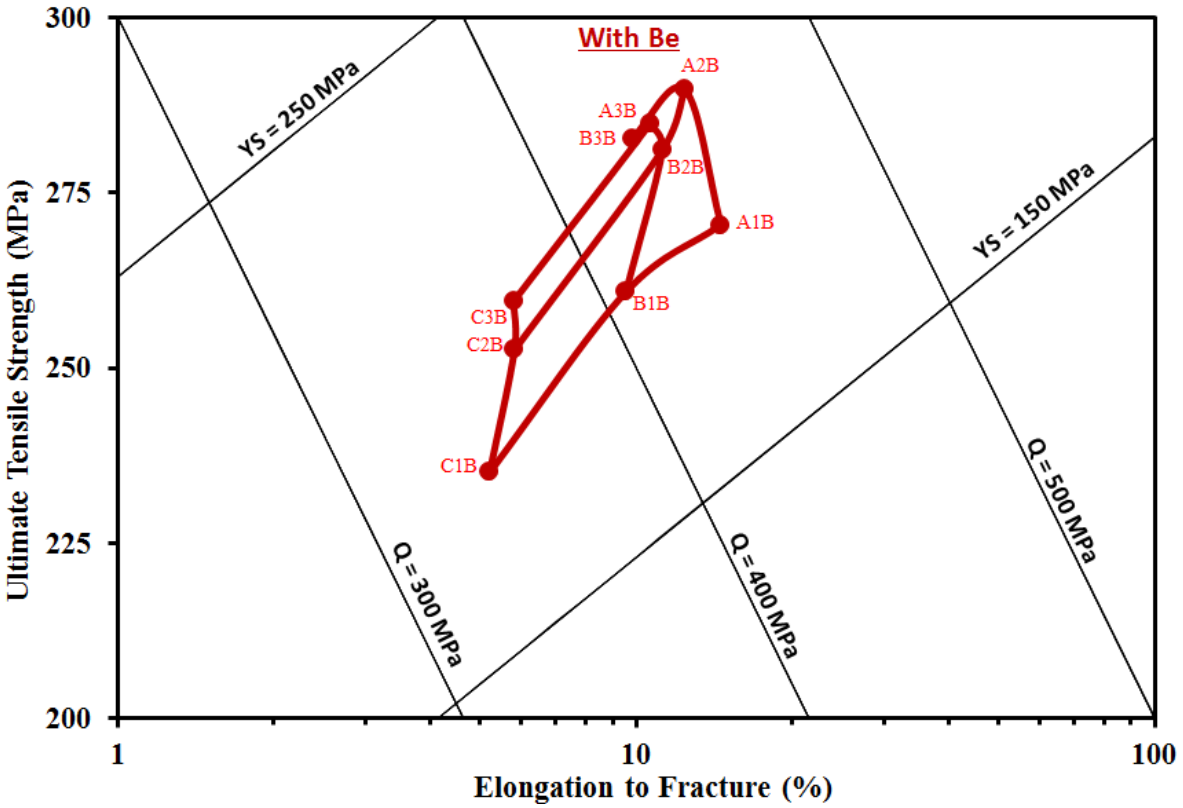

Figure 4.38 Quality chart generated using equations (1) and (2), showing the effects of adding Be, Mg and Fe. Samples were solution heat-treated for 5h at 540°C, followed by quenching in warm water and no aging.

The combined effect of adding both Be and Sr to the alloys investigated yielded a noteworthy increase in the tensile properties and quality index values of the alloys containing both Fe and Mg (for example, alloys A1BS, A2BS, A3BS, B1BS, B2BS, B3BS, C1BS, C2BS and C3BS), as compared to the reference alloys (without Be or Sr). Figure 4.40 illustrates the quality chart pertaining to the combined effects of Be and Sr on the tensile properties of the alloys examined. When adding Be and Sr, the Fe series shifts toward the upper right-hand portion of the figure, parallel to the iso-Q lines.

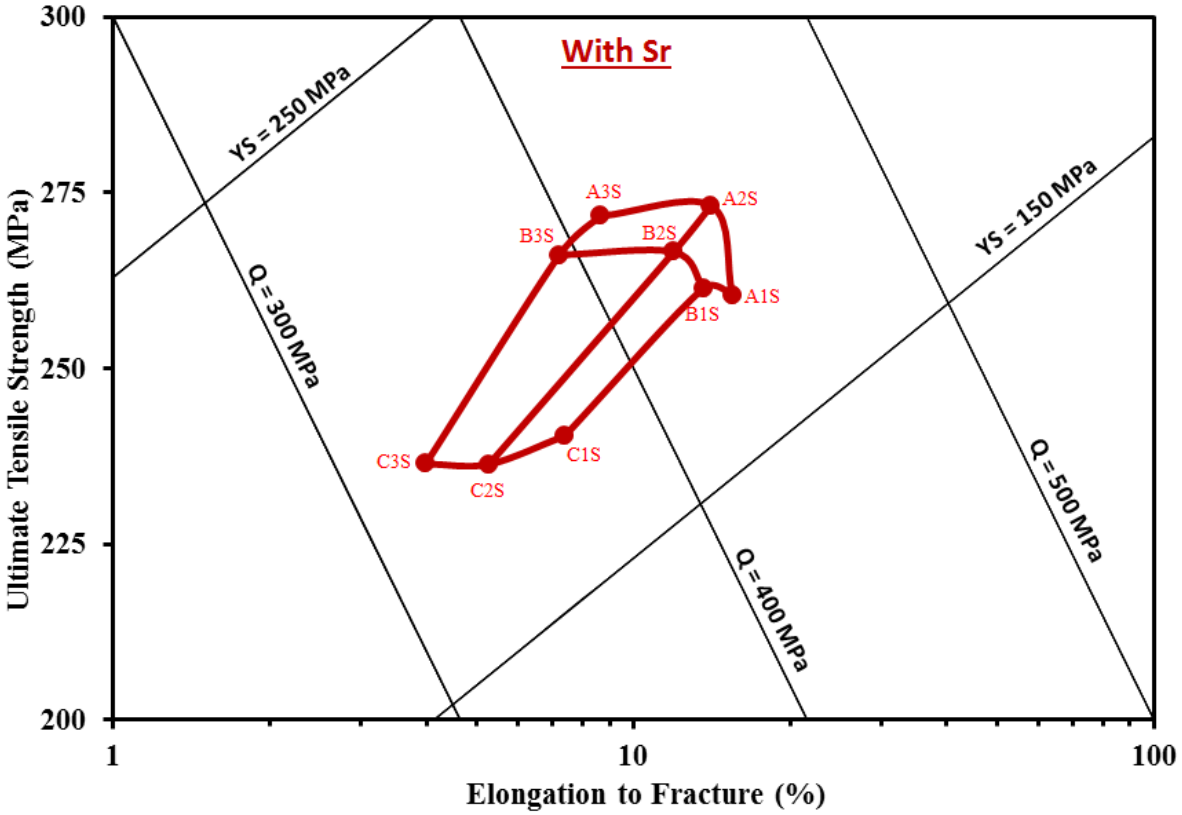

Figure 4.39 Quality chart generated using equations (1) and (2), showing the effects of adding Sr, Mg and Fe. Samples were solution heat-treated for 5h at 540°C, followed by quenching in warm water and no aging.

The yield strength exhibited a marked increase when both Be and Sr were added, as may be observed in Figure 4.40, where each Mg line, which represents three levels of Fe, shifts more or less parallel to the iso-yield strength or iso-flow lines in the direction of higher yield strength. The only negative effect reported associated with adding both Be and Sr was the formation of the Be-Sr phase ($SrBe_3O_4$) [61] which limits improvements in the yield strength.

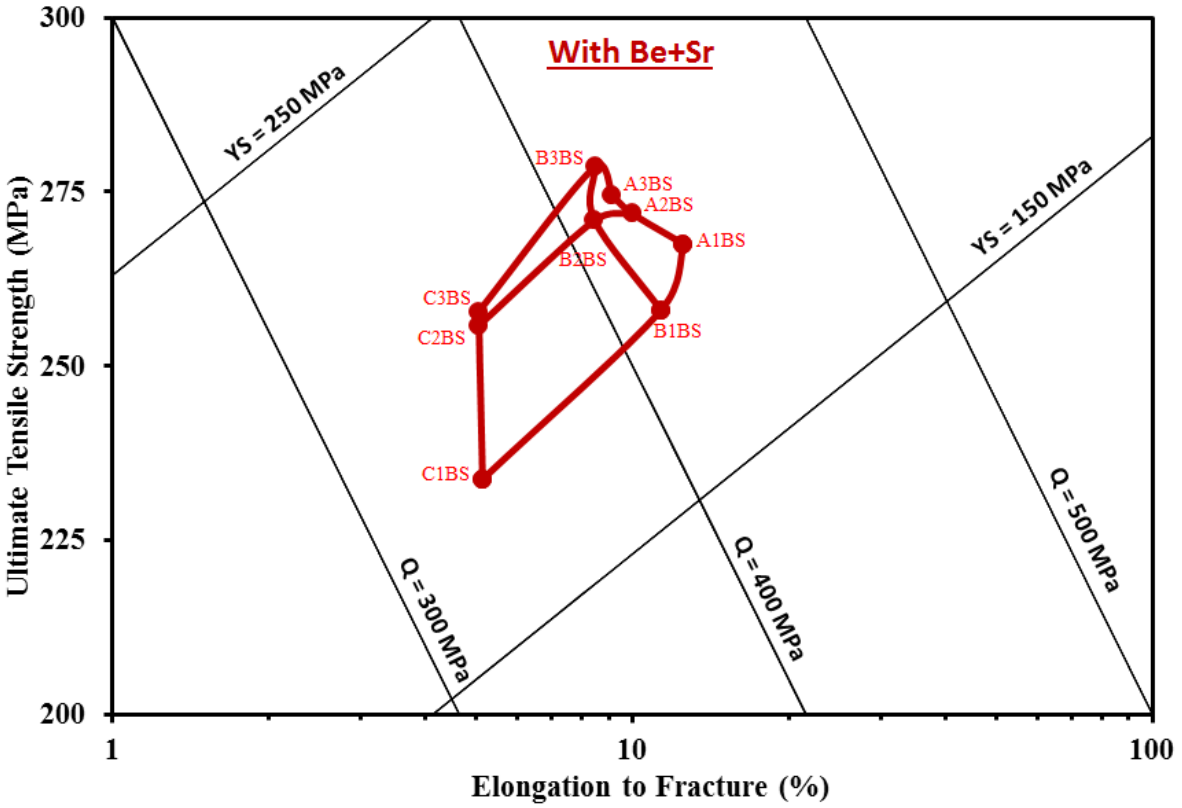

Figure 4.40 Quality chart generated using equations (1) and (2), showing the effects of adding Be, Sr, Mg and Fe. Samples were solution heat-treated for 5h at 540°C, followed by quenching in warm water and no aging.

Increasing the solution heat treatment time to 12 hours further improves in the tensile properties and quality index values of the alloys as observed in Figures 4.41 through 4.44. With respect to the three reference alloys A1, A3 and C3, the improvement in quality results from: (i) a larger density of precipitates of completely dissolved Mg_2Si, (ii) further decomposition of the π-phase into the β-phase, (iii) higher fragmentation rate of the β-phase, and (iv) more spheroidization of the Si and π-phases as shown previously in Figures 4.28 through 4.30. These observations were noted to increase with longer solution heat

treatment times. [163, 164]

Figure 4.41 shows the quality charts representing the effects of iron level and magnesium content on the properties of the 357 alloys after 12h solution treatment. When the Fe level in these alloys is increased from 0.09 wt% (alloy A3) to 0.2 wt% (alloy B3), strength is decreased, ductility is reduced, and the alloy quality is diminished. This was attributed to an increased density of brittle, undissolved Fe-intermetallic phases. Negative effects were also observed when the Fe content was increased to 0.6 wt% in alloy C3. Since these alloys have different levels of Mg (0.4, 0.6 and 0.8 wt%), it may be said that increasing Fe contents noticeably reduce the mechanical properties, regardless of the alloy Mg levels.

When increasing the Fe level, the Fe series shown in Figure 4.41 are seen to shift virtually parallel to the iso-Q lines toward the lower left-hand portion of the figure. The yield strength, however, revealed no significant changes when increasing the Fe level from 0.09% to 0.6%, as shown in Figure 4.40, where each Mg line, which represents three levels of Fe, is more or less parallel to the iso-yield strength or iso-flow lines. Yield strength is thus independent of impurity elements such as Fe.

The increase in the Mg content from 0.4wt% (alloy A1) to 0.6wt% (alloy A2) leads to an improvement of about 10 MPa in the strength of the castings and to a slight decrease in ductility, but without a noticeable reduction of quality, as may be seen from Figure 4.41. Further improvements were observed by increasing the Mg level up to 0.8wt% (alloy A3).

Similarly, positive effects were obtained with increase in Mg levels, This may attributed to the fact that the amount by which the strength of the alloy is increased compensates for the amount by which the ductility is decreased. The improved strength of the castings obtained by increasing the Mg-level is directly related to the precipitation of Mg_2Si. A higher Mg content will yield a higher density of this hardening phase. On the other hand, a higher Mg content will also bring about the precipitation of a large volume fraction of the π-$Al_8FeMg_3Si_6$ phase which ultimately has a deleterious effect on both the strength and the ductility of the alloys and consequently on their quality. Comparison of Figure 4.41 with Figure 4.37 reveals that increasing the solution heat treatment time shows no observable effect on improving the mechanical properties and quality index values of alloys containing only Fe and Mg, without additions of Be and Sr. [165-167]

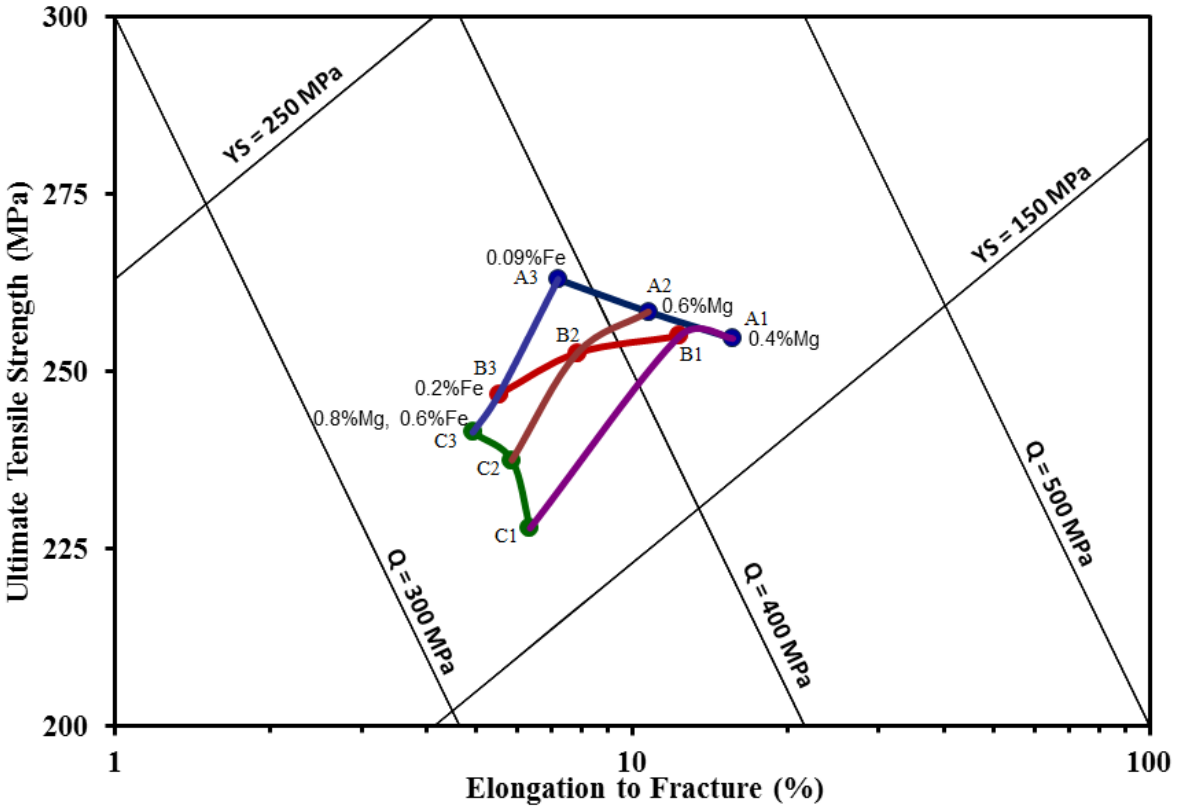

Figure 4.41 Quality chart generated using equations (1) and (2), showing the effects of adding Mg and Fe. Samples were solution heat-treated for 12h at 540°C, followed by quenching in warm water and no aging.

Beryllium additions improved the tensile properties and quality index values of the alloys containing Mg and Fe and resulted in shifting the quality index values towards the upper right corner of the chart shown in Figure 4.42. The yield strength is also observed to increase as indicated by the shift of the Mg lines towards the direction of higher yield strength. The improvement in mechanical properties stems from two sources: (i) retention of more Mg in the molten metal resulting from the effect of Be in protecting Mg from oxidation by forming the Be-Mg phase ($MgBe_{13}$), [64-66] and (ii) changes in the morphology and chemistry of the β-Fe phase from platelets to much smaller nodular-shaped β-Fe

particles, an acceleration in the decomposition of the π-phase into the β-phase, and formation of the Chinese-script Be-Fe phase (Al_8Fe_2BeSi). [51, 55]

By comparing Figures 4.42 and 4.38 it may be seen that Be greatly improves the mechanical properties and quality index values, particularly at higher solution treatment times.

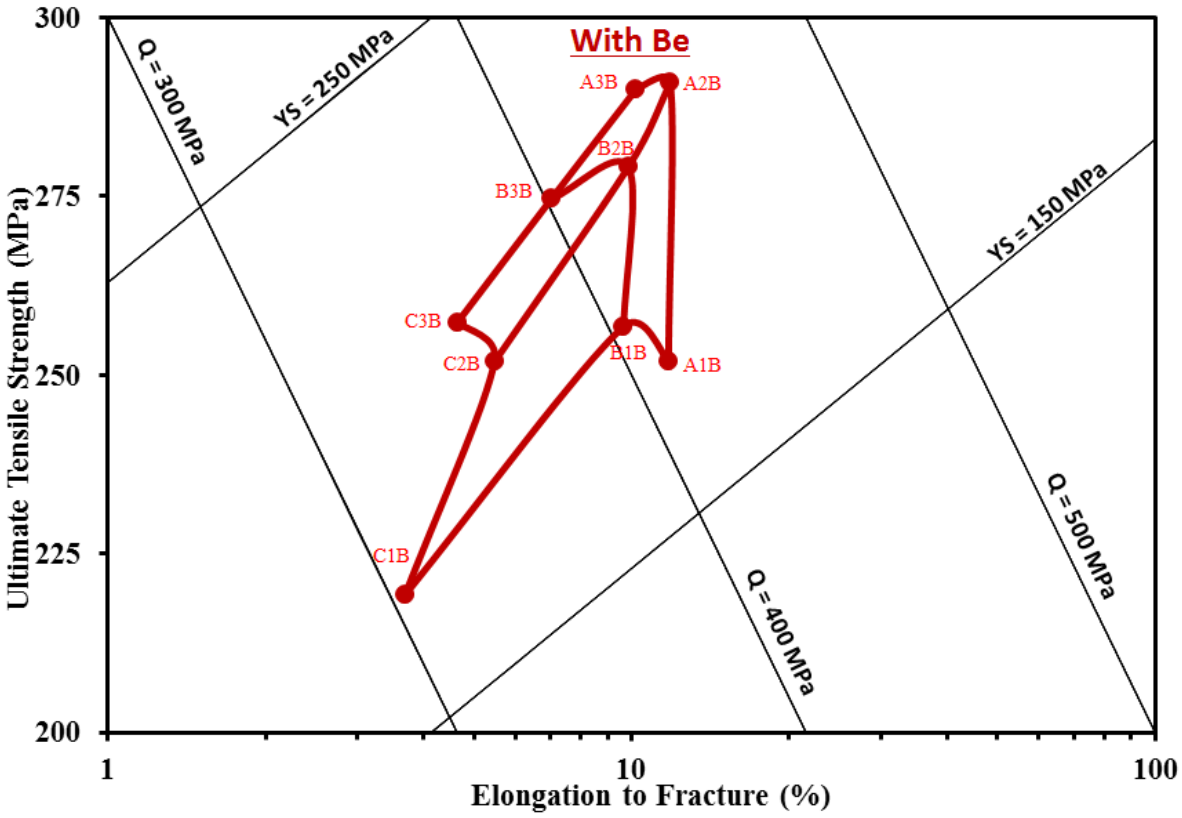

Figure 4.42 Quality chart generated using equations (1) and (2), showing the effects of adding Be, Mg and Fe. Samples were solution heat-treated for 12h at 540°C, followed by quenching in warm water and no aging.

For a 12-hour solution heat treatment time, and for the different levels of Fe and Mg used, the addition of Sr improved the tensile properties and quality index values of the modified alloys (namely, alloys A1S, A2S, A3S, B1S, B2S, B3S, C1S, C2S and C3S), compared to the non-modified alloys, as shown in Figure 4.43. [168] This improvement in mechanical properties is related to the change in the eutectic Si morphology from acicular to fibrous type, and to the role of Si in reducing the harmful effect of the β-phase by transforming it into the α-Al_8Fe_2Si script-like phase.

For the 12-hour solution heat-treated samples, the combined addition of both Be and Sr yielded a significant increase in the tensile properties and quality index values of the alloys A1BS, A2BS, A3BS, B1BS, B2BS, B3BS, C1BS, C2BS and C3BS, compared to the reference alloys (without Be or Sr). As strength and ductility are both increased, the quality is also improved, as seen in the quality chart of Figure 4.44. With the addition of Be and Sr, the Fe series shown in Figure 4.44 shifts parallel to the iso-Q lines toward the upper right-hand portion of the figure, in the direction where the desired properties are enhanced.[169,170]

The yield strength experienced a significant increase when adding both Be and Sr, as may be observed in Figure 4.44, where each Mg line, which represents three levels of Fe, is shifted more or less parallel to the iso-yield strength or iso-flow lines in the direction of higher yield strength. The only negative effect reported with respect to adding both Be and Sr was the formation of the Be-Sr phase ($SrBe_3O_4$) which limits improvements in the YS.

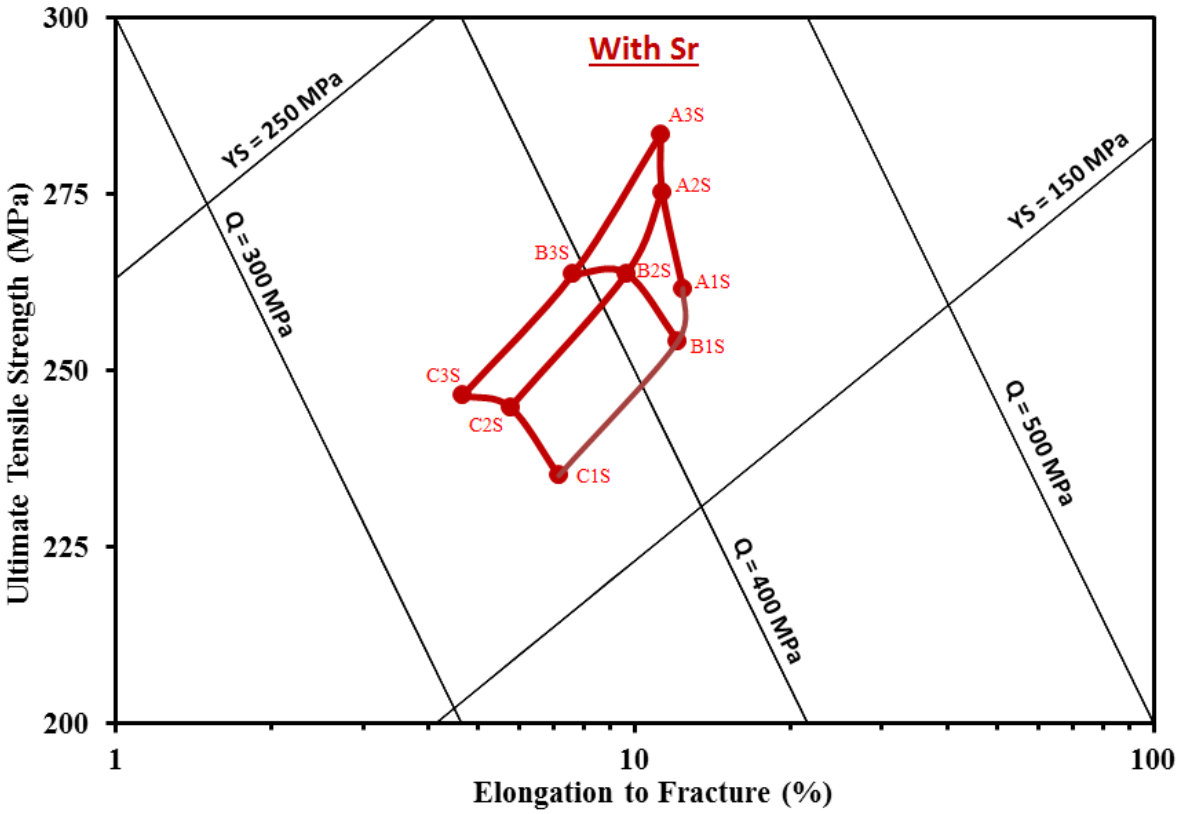

Figure 4.43 Quality chart generated using equations (1) and (2), showing the effects of adding Sr, Mg and Fe. Samples were solution heat-treated for 12h at 540°C, followed by quenching in warm water and no aging.

A comparison of Figures 4.44 and Figure 4.40 confirmed that Be and Sr have a noteworthy combined effect in improving the mechanical properties and quality index values with increased solution heat treatment time. The results observed in this study with respect to the mechanical properties and quality index values of 357 alloys are in good agreement with those reported in the literature. [89, 90, 171-173]

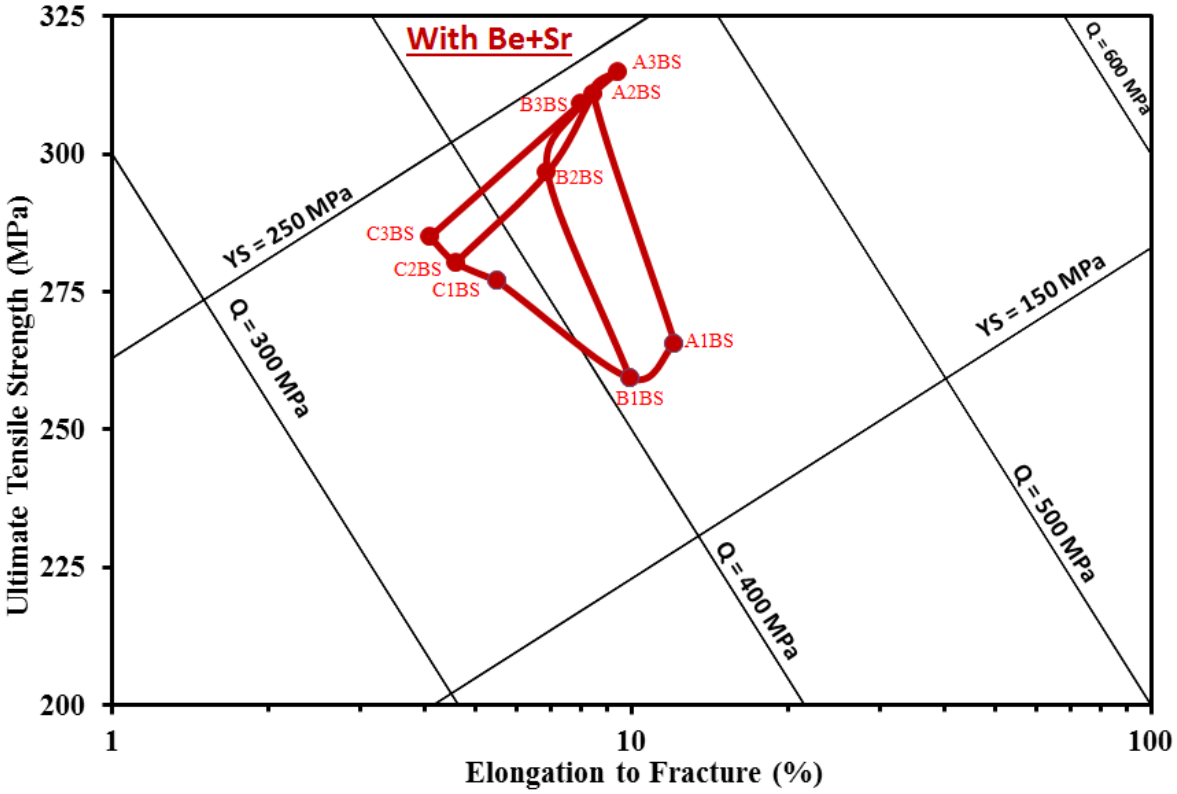

Figure 4.44 Quality chart generated using equations (1) and (2), showing the effects of adding Be, Sr, Mg and Fe. Samples were solution heat-treated for 12h at 540°C, followed by quenching in warm water and no aging.

In order to better understand the effects of Mg, Fe, Be and Sr interactions on the tensile properties of the alloys used in this study were examined in terms of alloy A1 (base alloy containing low Mg and low Fe content), alloy A3 (which has high Mg and low Fe) and alloy C3 (high amounts of both Mg and Fe) were selected as reference alloys. The changes (ΔP) in tensile properties (UTS, YS and %El) were noted for the alloys studied with respect to these reference alloys as follows:

(i) ΔP is defined as the change in ultimate tensile strength (UTS) of a given alloy, with respect to its reference alloy;

(ii) ΔPY is defined as the change in yield strength (YS) of a given alloy, with respect to its reference alloy; and

(iii) ΔPE is defined as the change in percent elongation (%El) to fracture of a given alloy, with respect to its reference alloy.

The influence of adding Be, Sr, or both to the low Mg- and low Fe-containing base alloy, A1, with respect to tensile properties is presented in Figures 4.45 to 4.47. Adding 0.05wt% Be to the base alloy, thus producing alloy A1B, led to small loss (~10 MPa with respect to the base alloy A1) in the as-cast, solution heat-treated and aged conditions, as shown in Figure 4.45. A slight increase in the UTS was observed in alloy A1B after a 12-hour solution heat treatment. This may be attributed to the role of Be in preventing Mg of oxidation during casting, thereby increasing the amount of Mg available for the precipitation of the Mg_2Si phase.

An addition of 200 ppm Sr to the base alloy A1 (thus producing alloy A1S) has a similar impact on the UTS as that observed after introducing Be to the alloy. This increase in the UTS may be due to the change in the shape and distribution of the eutectic Si particles caused by the Sr-addition. When Be and Sr were added to the base alloy (giving alloy A1BS), further positive changes in the UTS were obtained.

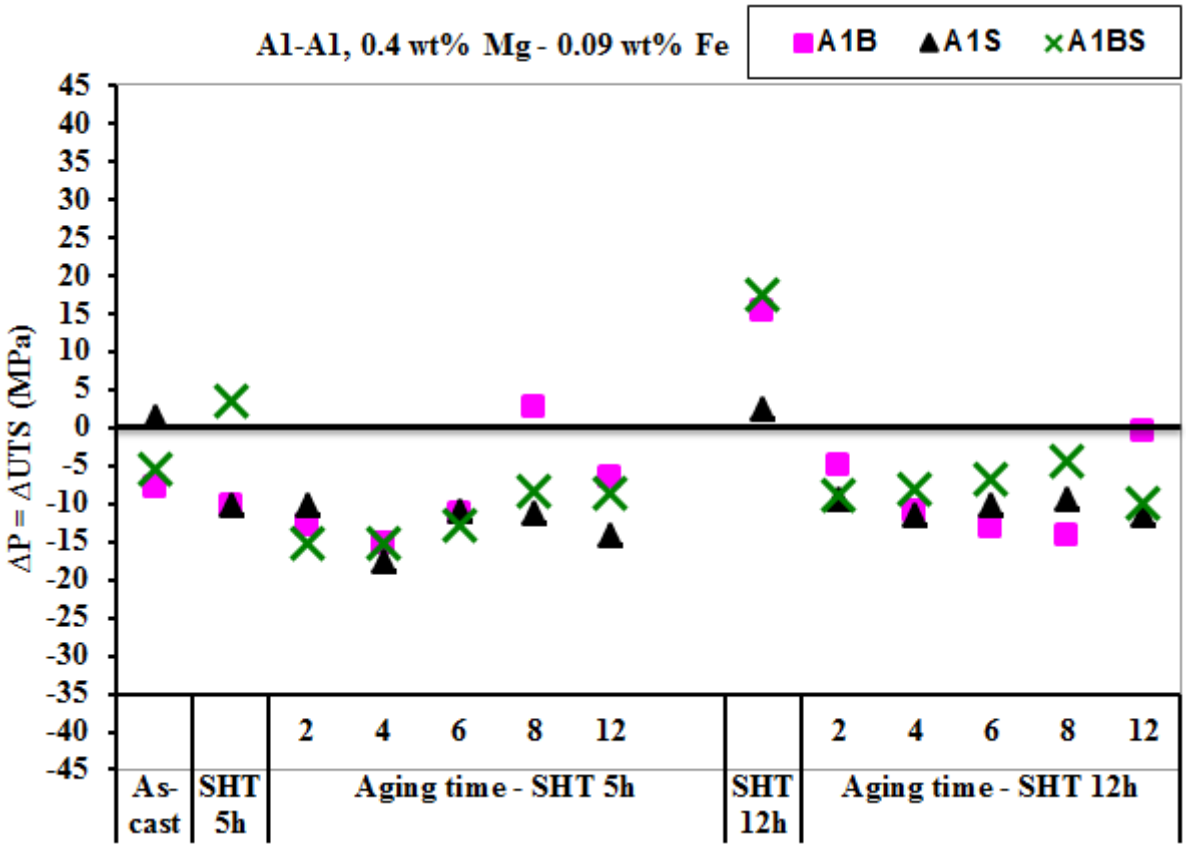

Figure 4.45 Changes in ultimate tensile strength of low Mg- and low Fe-containing A1 alloys with respect to base alloy A1.

The yield strength was observed to increase by ~15 MPa for the alloy A1B, as shown in Figure 4.46. This was especially noticeable in two cases: (i) after 12 hours of solution heat treatment and (ii) with increasing aging time. A marked improvement in the YS (~25 MPa) was noted with increasing aging time, from 4 to 12 hours, for the 12-hour solution heat-treated A1B alloy, as a result of the enhanced precipitation of the Mg_2Si hardening phase or the spheroidized π-phase particles. The addition of Sr yielded similar results as that of Be on the YS, while introducing both Be and Sr further increased the YS by ~30 MPa.

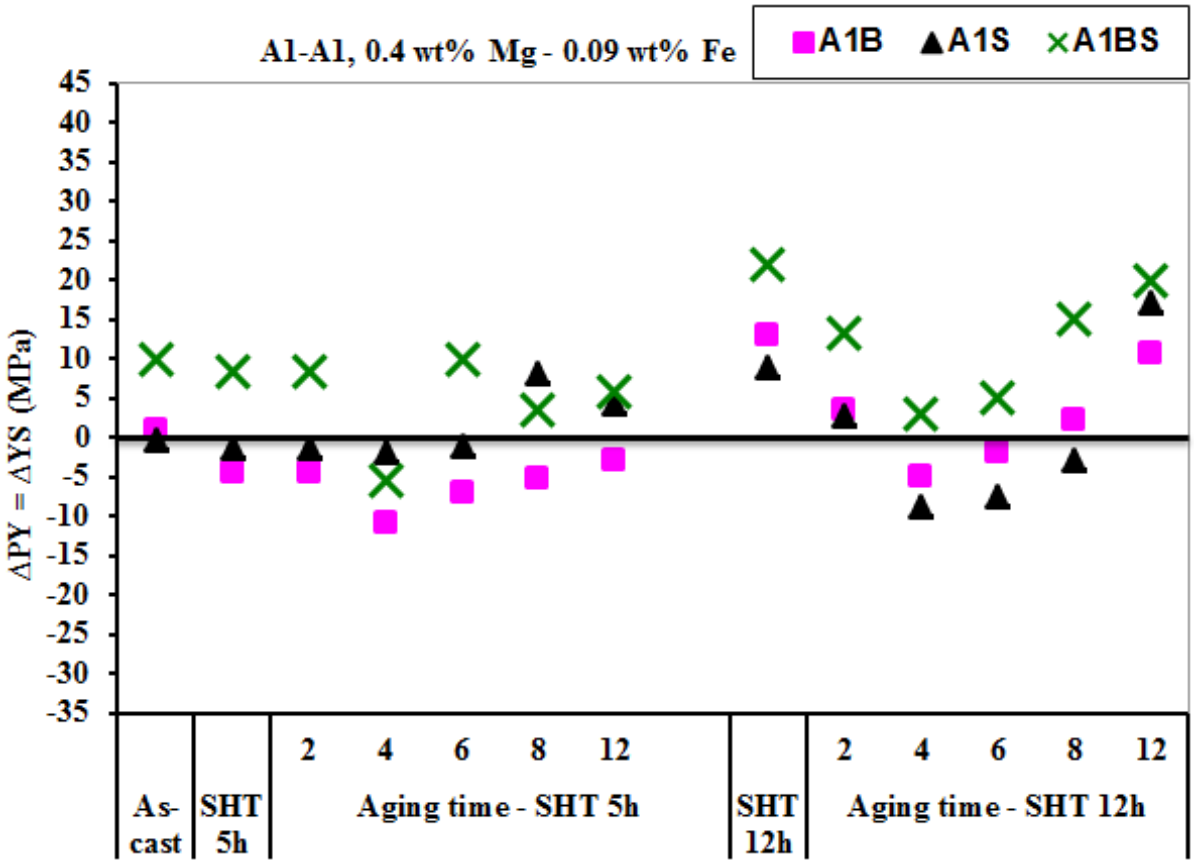

Figure 4.46 Changes in yield strength of low Mg- and low Fe-containing A1 alloys with respect to base alloy A1.

Percent elongation in the Be-modified alloy, A1B, was not affected by increasing either the solution heat treatment time or aging time, as presented in Figure 4.47. With respect to changes in the alloy tensile properties due to Be and/or Sr additions to base alloy, it appears that yield strength is most sensitive to these additions, in a positive way.

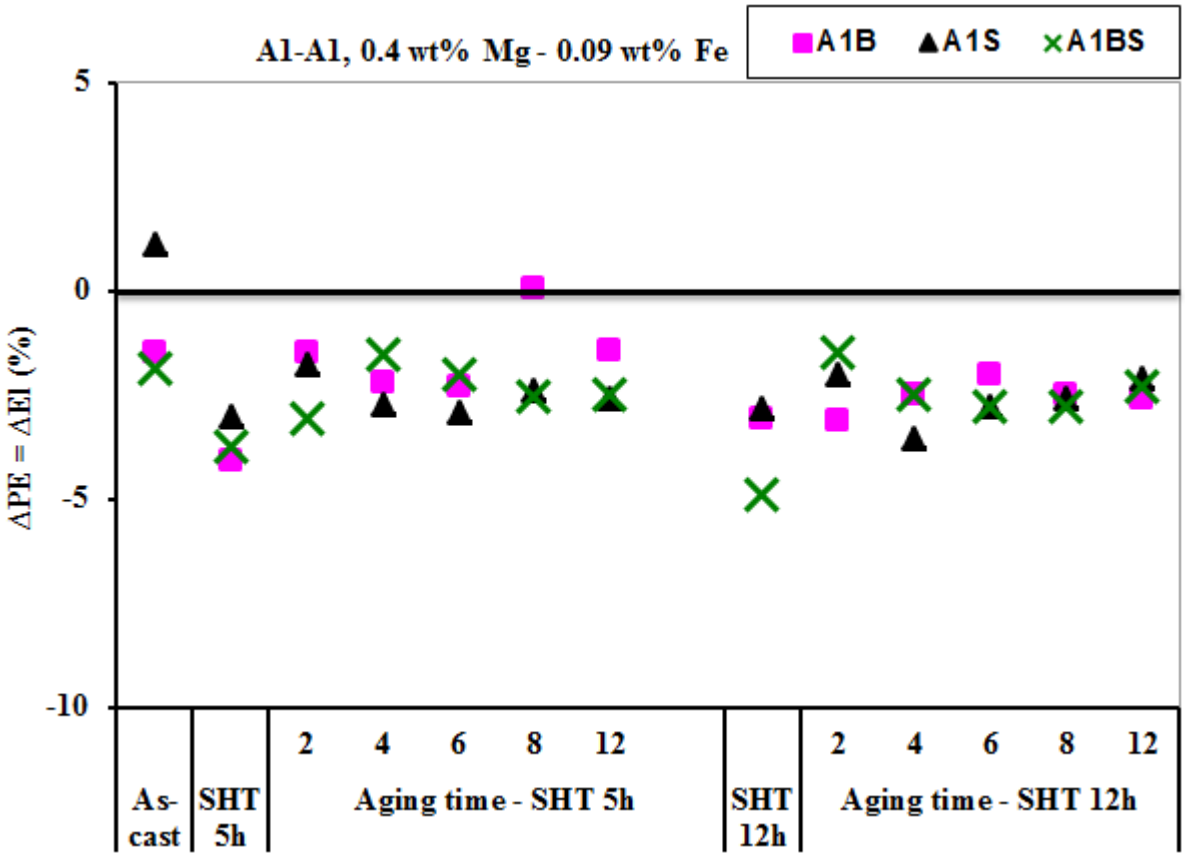

Figure 4.47 Changes in percent elongation of low Mg- and low Fe-containing A1 alloys with respect to base alloy A1.

Increasing the level of Mg in the base A1 alloy to 0.8 wt% produces alloy A3. The effects of adding Be or Sr (or both) to alloy A3, with respect to tensile properties are shown in Figures from 4.48 to 4.50, with alloy A1 serving as the reference alloy. The high Mg level led to an increase in UTS of up to 35 MPa, for samples exposed to a long solution heat treatment time. [174, 175] Adding 500ppm of Be to alloy A3 (producing alloy A3B) also revealed a noticeable increase in UTS, of ~30 MPa, with respect to the base A1 alloy, for samples exposed to a 12-hour solution heat treatment time and subsequently aged, as shown in Figure 4.48.

Raising the Mg content increases the formation of the π-phase, which, in turn, will provide more spheroidized of the π-phase particles, ultimately increasing the alloy UTS. The increase in UTS may also be attributed to the role of Be in enhancing the precipitation of the Mg_2Si hardening phase, by preventing the oxidation of Mg during casting. [176, 177] Adding 200ppm Sr to the base alloy A3 (producing alloy A3S) produced similar observations on the UTS as that observed with Be addition.

When Be and Sr were both added to the A1 alloy (producing alloy A3BS), negative changes in the UTS were observed, reported to be due to interaction of Be with Mg and Sr, leading to the formation of Be-Mg ($MgBe_{13}$) and Be-Sr ($SrBe_3O_4$) phases; it appears that the latter phase, $SrBe_3O_4$ has a negative effect on the alloy mechanical properties in that it reduces the amount of free Be. This reaction is expected to take place near the melt surface.[61, 64-66]

When comparing the high Mg-containing alloy, A3, with the base A1 alloy, the yield strength was observed to increase by ~40 MPa for the cases of increased Mg (0.8 wt%) content, Be-addition (alloy A3B), Sr-modification (alloy A3S), and (Be+Sr) addition (alloy A3BS), as presented in Figure 4.49, especially for long aging times. These observations demonstrate that the Mg_2Si precipitates serve as the primary hardening agent in these alloys.

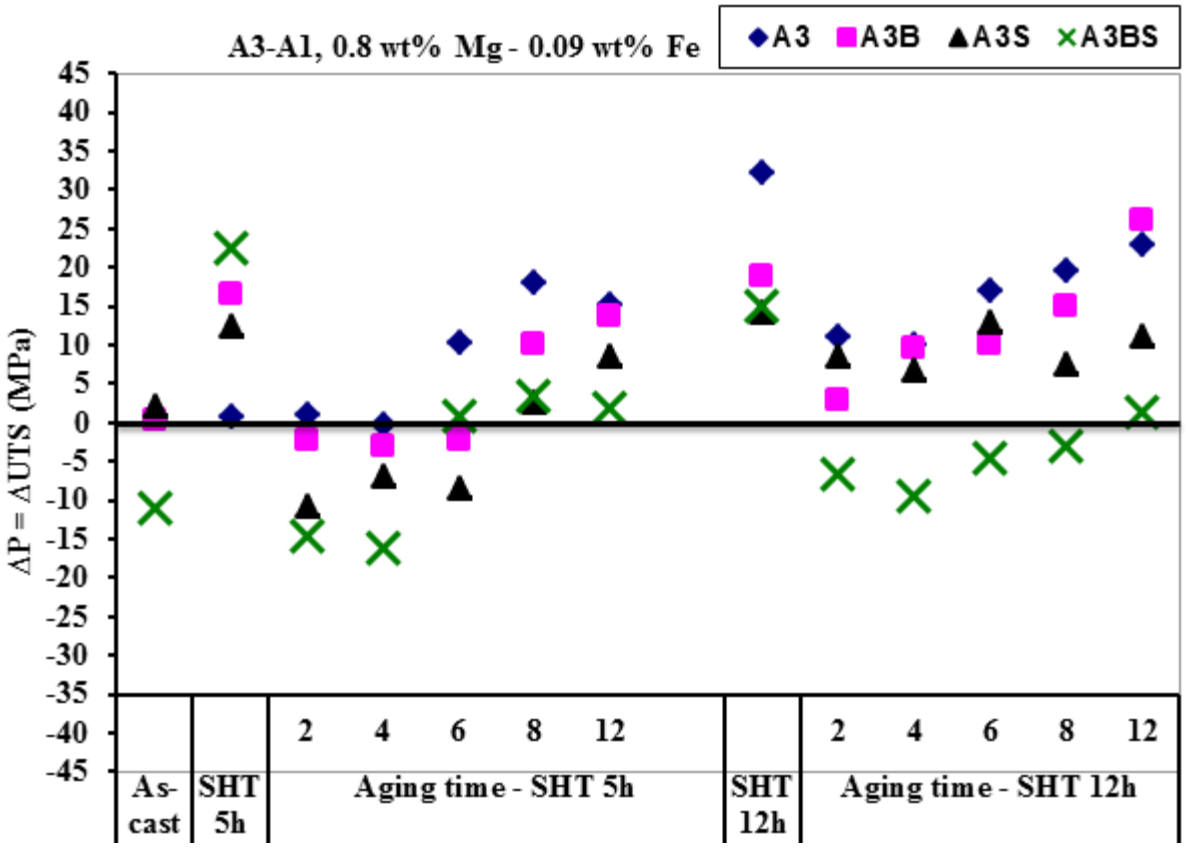

Figure 4.48 Changes in ultimate tensile strength of high Mg- and low Fe-containing A3 alloys with respect to base alloy A1.

Percent elongation was observed to improve with increased aging time for the high Mg-containing alloys (A3, A3B, A3S and A3BS), as shown in Figure 4.47. [178] As in the case of the A1 alloys, for the A3 alloys also, it was observed that yield strength is the tensile property most sensitive, in a positive way, to additions of Mg, Be and Sr.

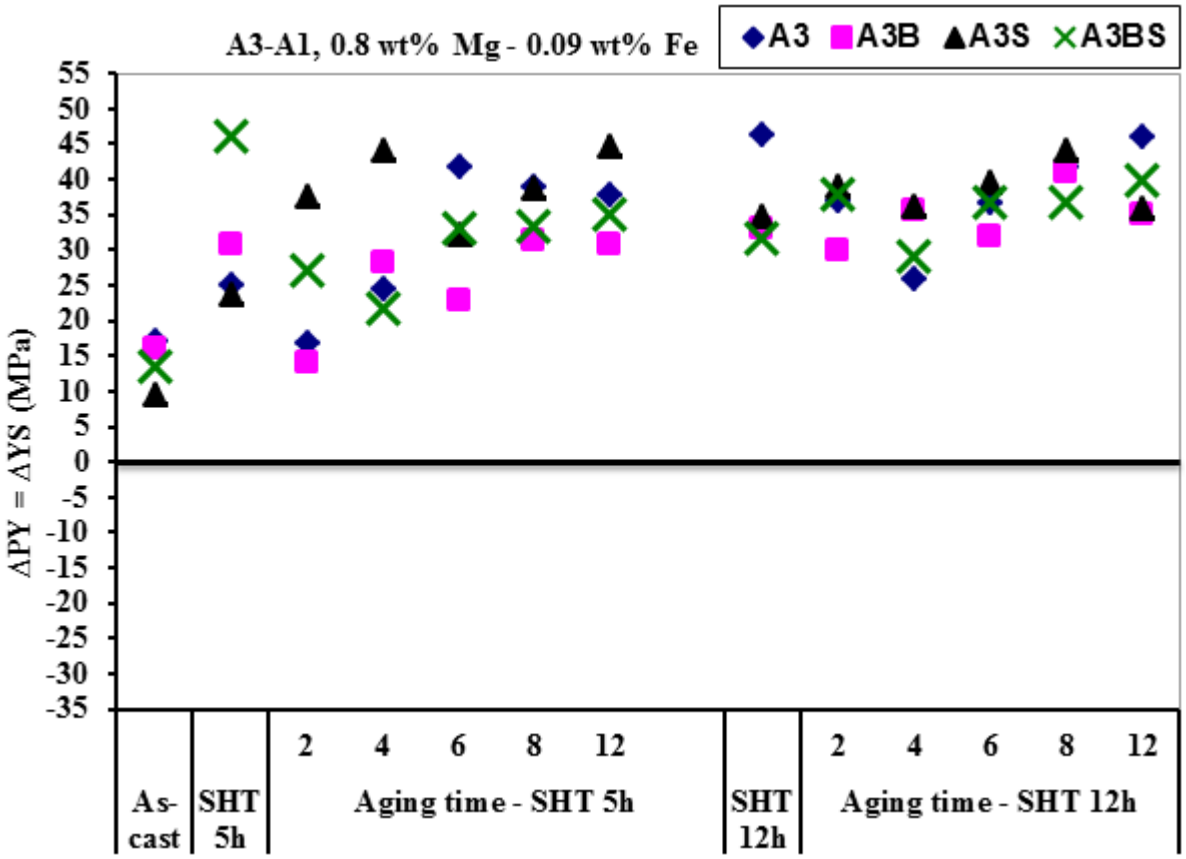

Figure 4.49 Changes in yield strength of high Mg- and low Fe-containing A3 alloys with respect to base alloy A1.

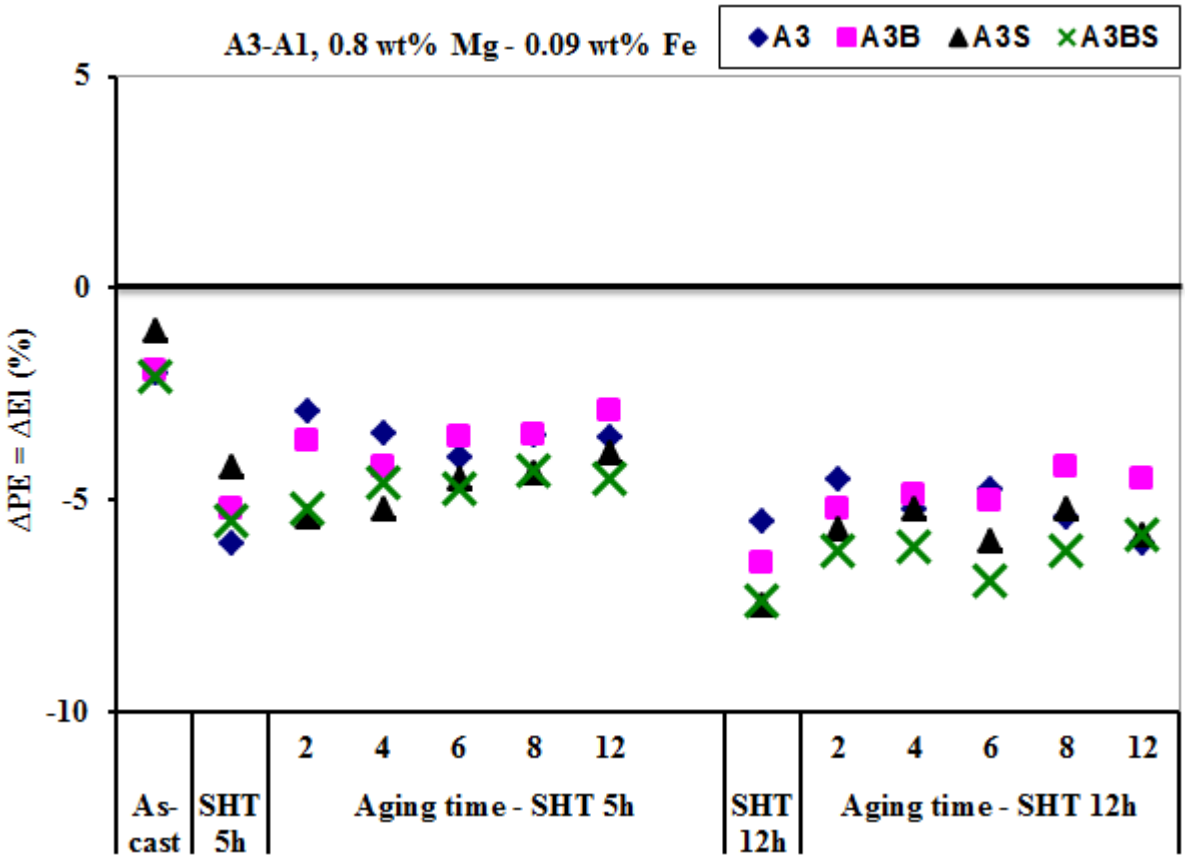

Figure 4.50 Changes in percent elongation of high Mg- and low Fe-containing A3 alloys with respect to base alloy A1.

Consider the high Mg-containing alloy, A3, as a reference alloy with which to study the effects of Be and Sr interactions on tensile properties (Figures 4.51 to 4.53). Adding Be (A3B) or Sr (A3S) or both (A3BS) to the A3 alloy did not produce any noticeable effects on the UTS values, except for a slight improvement with aging time, regardless of the solution heat treatment time used (Figure 4.51). [178] The noted improvement in UTS was attributed to further precipitation of the Mg_2Si hardening phase with further aging of the alloy. No observed effects on yield strength values were reported, with the exception of a

slight increase at low aging time (less than 6 hours), irrespective of the solution heat treatment time used (Figure 4.52).

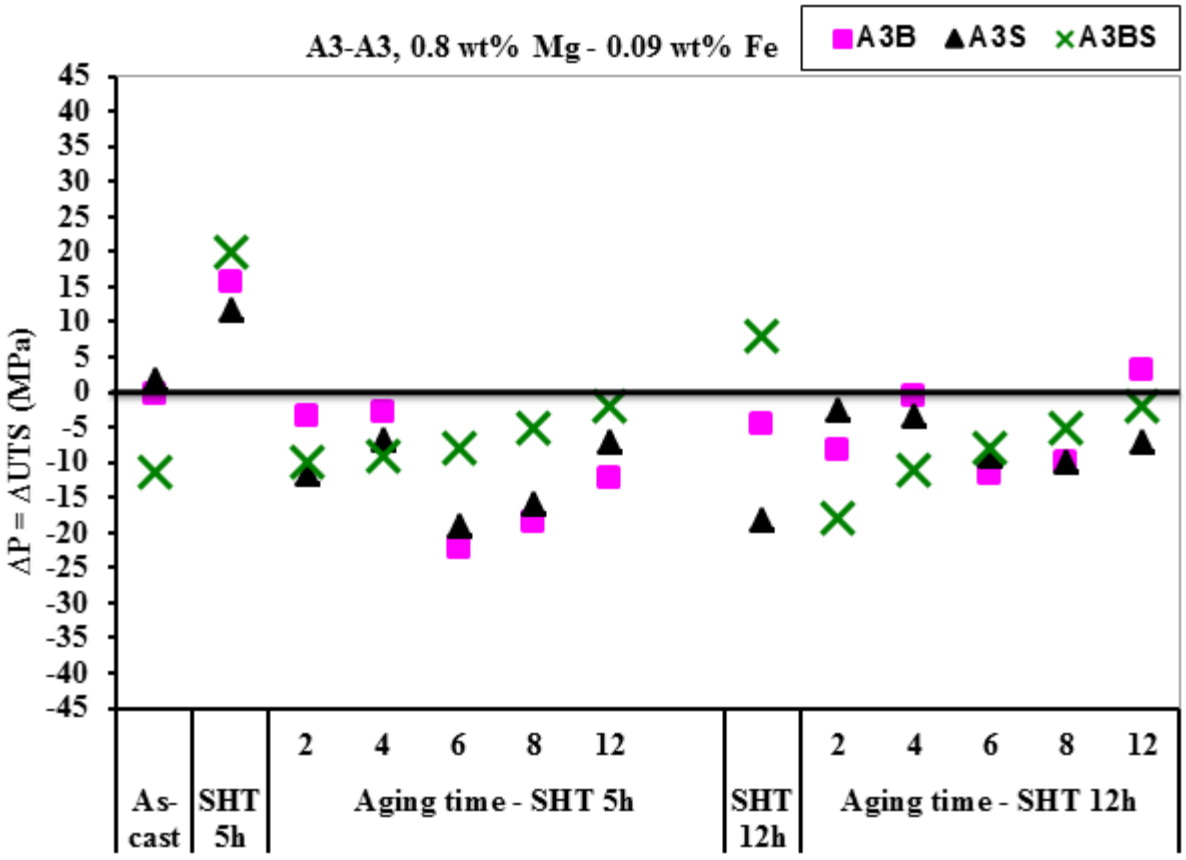

Figure 4.51 Changes in ultimate tensile strength of high Mg- and low Fe-containing A3 alloys with respect to alloy A3.

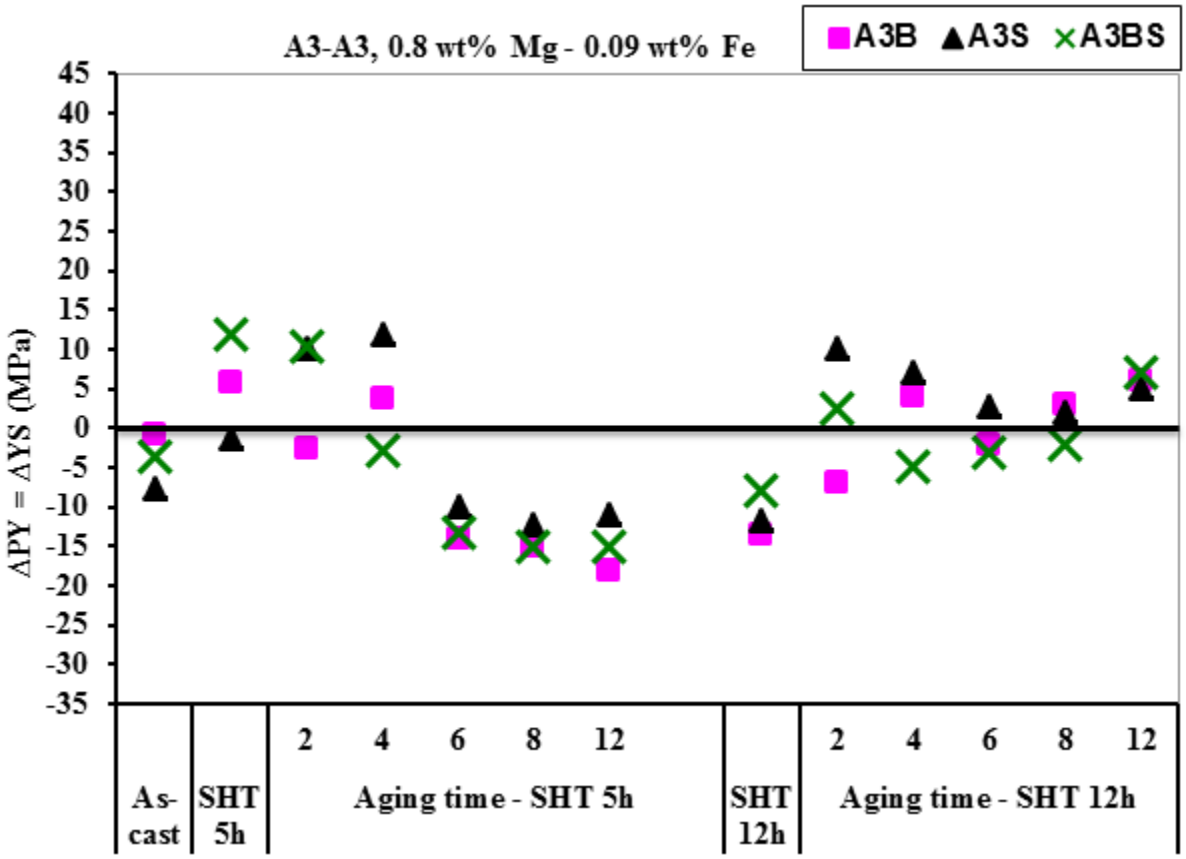

Figure 4.52 Changes in yield strength of high Mg- and low Fe-containing A3 alloys with respect to alloy A3.

Percent elongation was improved by adding Be, Sr, or both, especially at higher aging times, as shown in Figure 4.53. From the results shown for the high Mg- and low Fe-containing A3 alloys, Be and Sr interactions appear to have no noticeable effects on the alloy mechanical properties. Once again, Mg_2Si precipitates were confirmed to be the main hardening agent in these alloys.

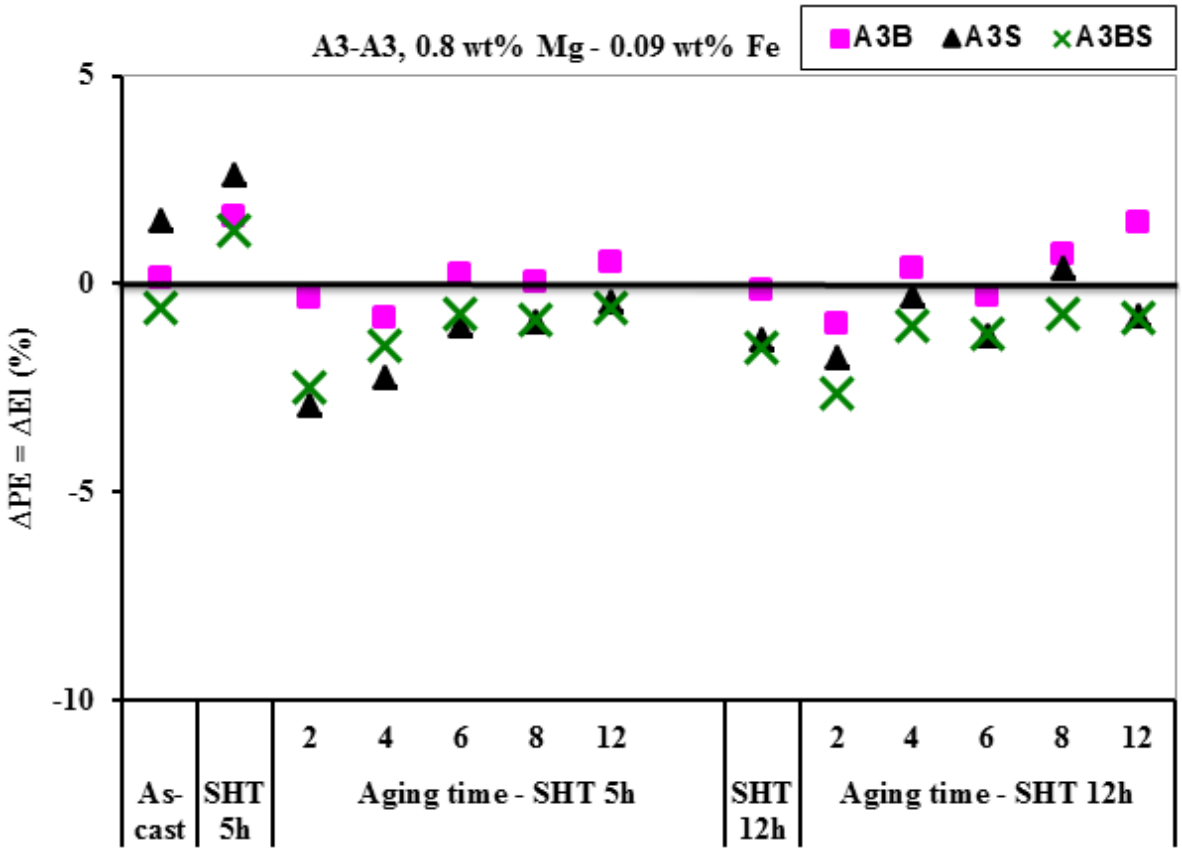

Figure 4.53 Changes in percent elongation of high Mg- and low Fe-containing A3 alloys with respect to alloy A3.

The high Mg- and low Fe-containing A3 alloy was used as a reference alloy in order to study the effects of a high Fe content, as well as Be and Sr interactions, on the tensile properties of C3, C3B, C3S and C3BS alloys, as shown in Figures 4.54 to 4.56. As expected, high levels of Fe lower the UTS, and regardless of the addition of effective alloying elements or the type of heat treatment applied, the alloy strength remains diminished.

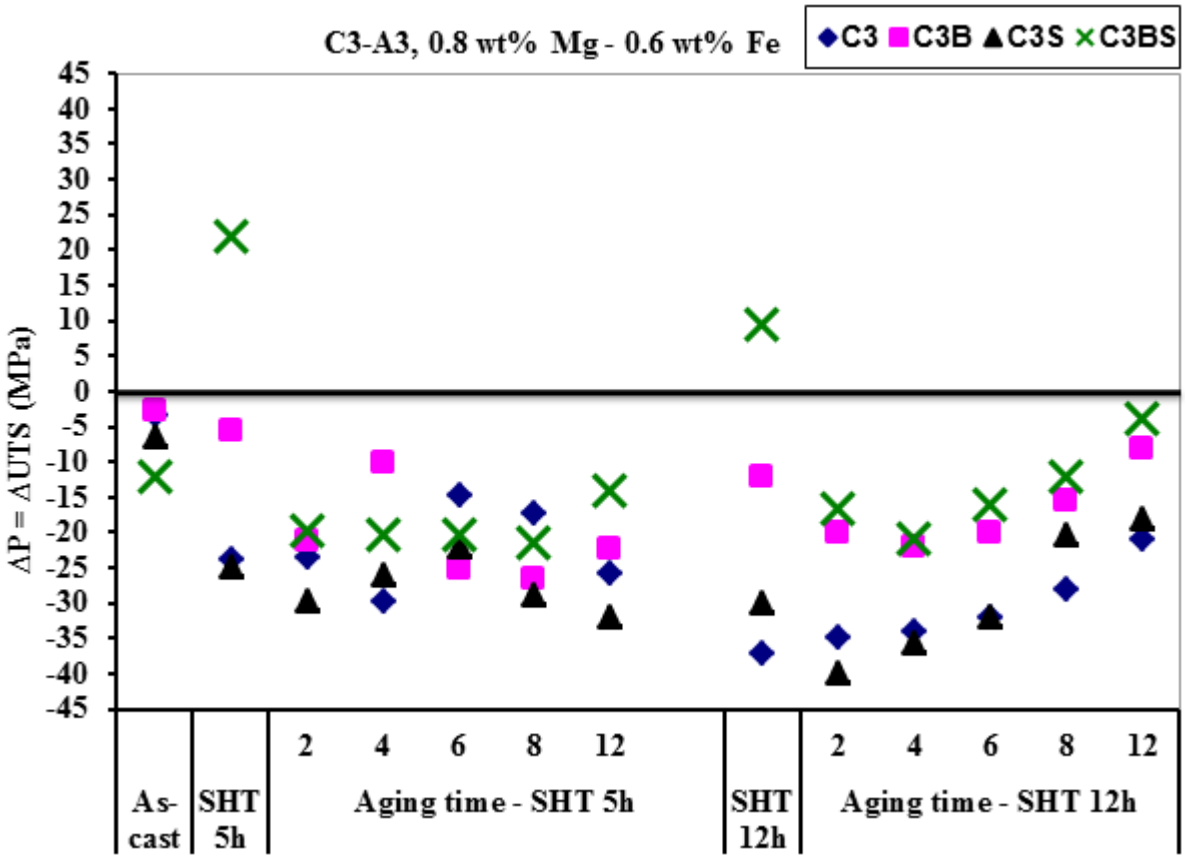

Figure 4.54 Changes in ultimate tensile strength of high Mg- and high Fe-containing C3 alloys with respect to alloy A3.

The yield strength was found to increase with increasing aging time regardless solution heat treatment time, and appeared to be more sensitive to Mg, Be and Sr effective additions. The increase in yield strength values with increasing aging time confirms that the Mg_2Si precipitates are mainly responsible for hardening in these alloys. Percent elongation was observed to improve with increasing aging time for high Mg-and high Fe-containing alloys C3, C3B, C3S and C3BS as shown in Figure 4.56.

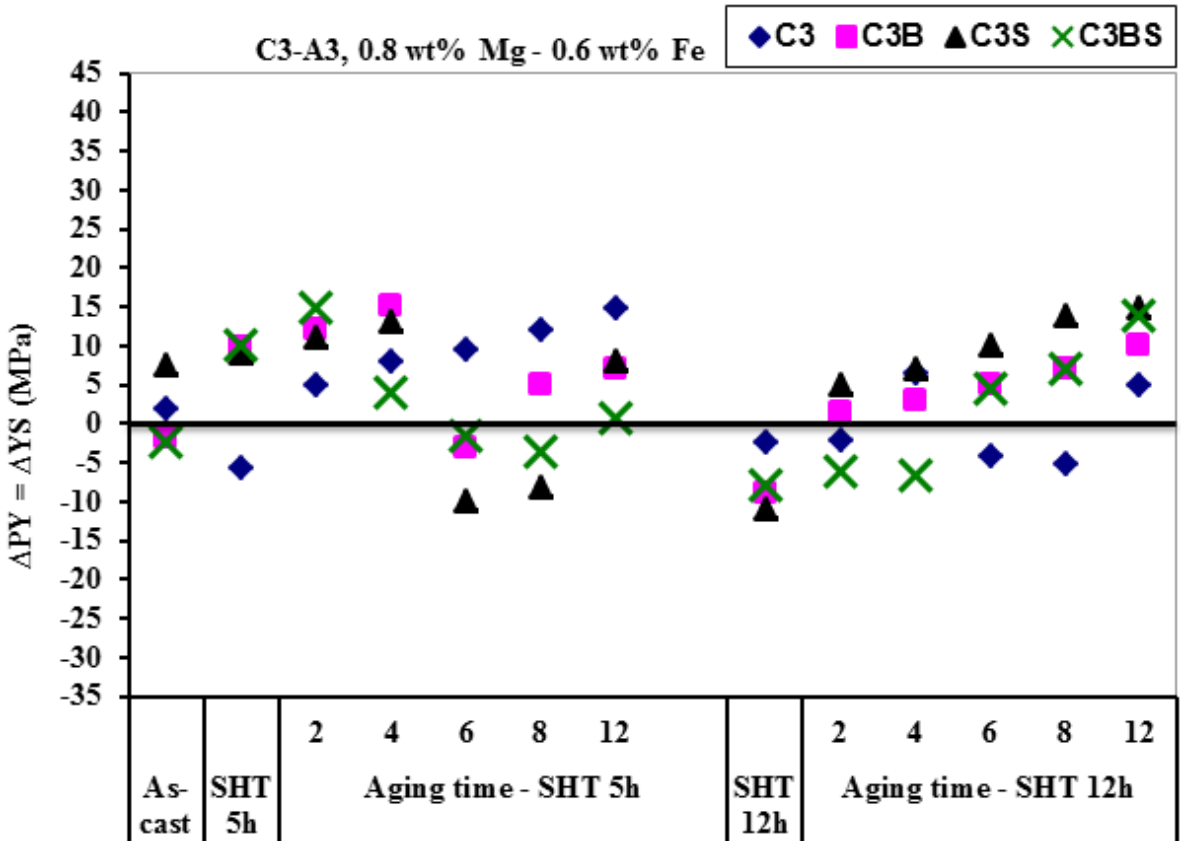

Figure 4.55 Changes in yield strength of high Mg- and high Fe-containing C3 alloys with respect to alloy A3.

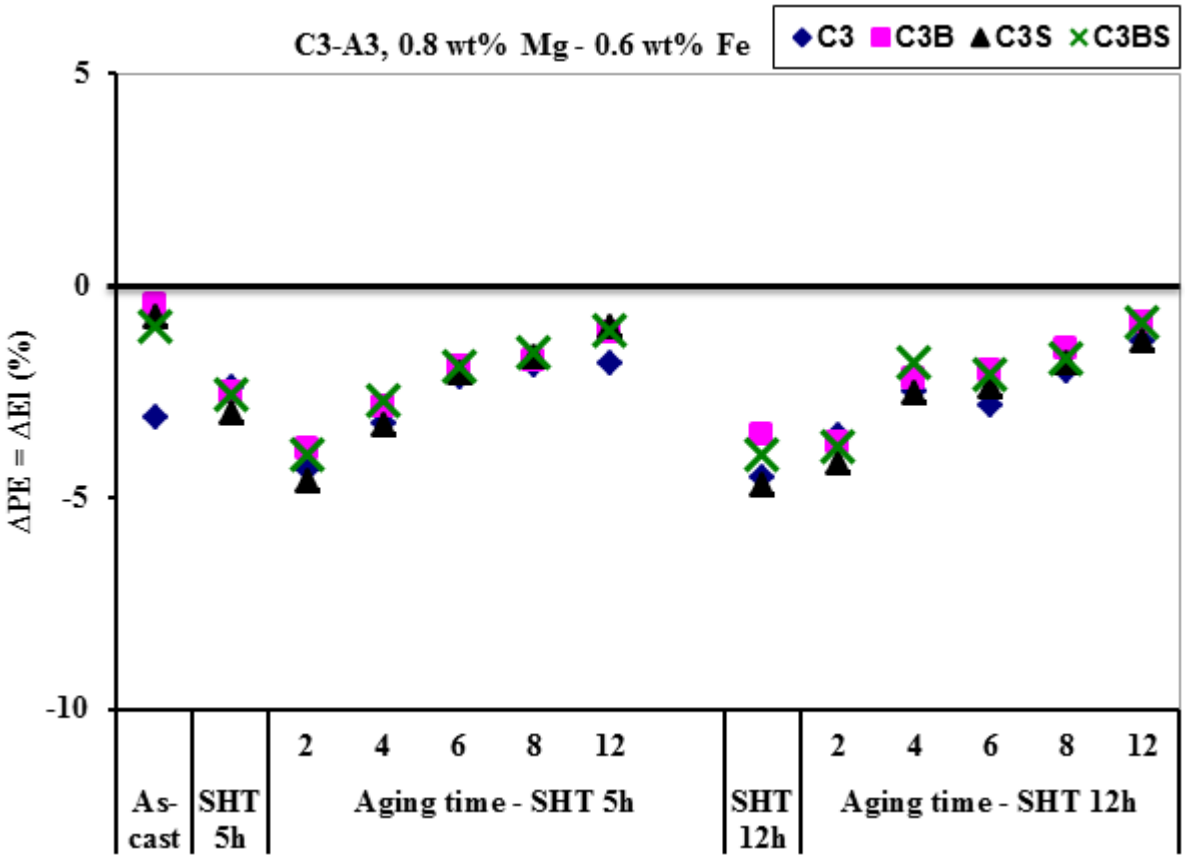

Figure 4.56 Changes in percent elongation of high Mg- and high Fe-containing C3 alloys, with respect to alloy A3.

With respect to industrial practices, the permitted use of Be should not exceed 500 ppm. However, this amount is not sufficient to provide both the beneficial effects of Be and to counter the expected interactions of Be with Fe, Mg and Sr. Further investigations are required to arrive at a more accurate level of Be that could be applied to enhance the mechanical properties.

Figures 4.57 to 4.59 present the changes in tensile properties in the C3 alloys using alloy A1 as the reference alloy.

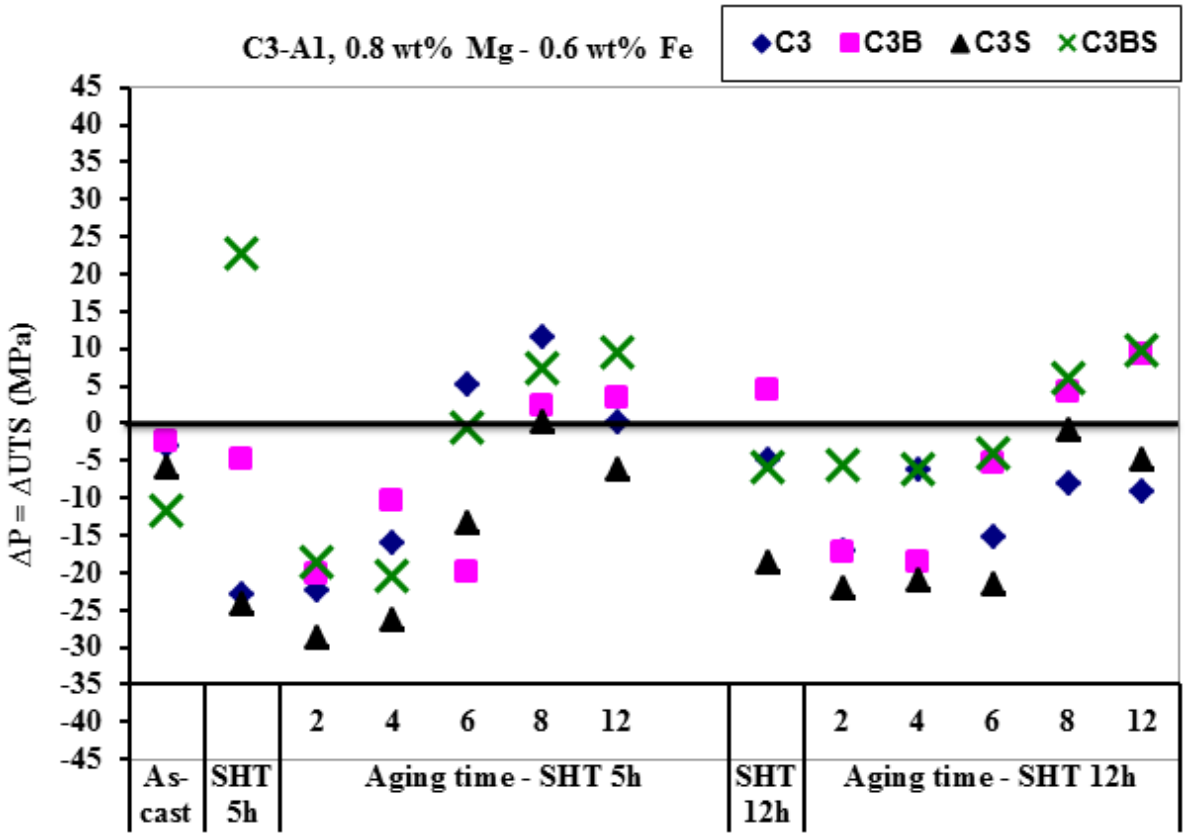

Figure 4.57 Changes in ultimate tensile strength of high Mg- and high Fe-containing C3 alloys, with respect to base alloy A1.

As may be seen, the increased Fe level in alloy C3 is the main factor that reduces the alloy mechanical properties. [187-180] Adding Be (C3B alloy), Sr (C3S alloy), or both (C3BS alloy) lowers the detrimental effect of the high Fe content on the UTS, for aging times greater than 6 hours. The results shown in Figure 4.57 demonstrate that adding 500 ppm of Be, 200 ppm of Sr, or both, as well as applying solution heat treatment and aging steps, help to improve the UTS in such high Fe-containing alloys.

Figure 4.58 shows that marked improvements in yield strength (~40 MPa) were noted for larger Mg contents, as well as with additions of Be, Sr, or both, in all heat-treated samples, in spite of the high Fe level. This reaffirms that yield strength is very sensitive to the use of alloying element additions and heat treatment.

Percent elongation was observed to improve with aging time in the case of the high Mg-and high Fe-containing C3 alloys, as shown in Figure 4.59. As may be seen, percent elongation is mainly affected by increase in Mg content and with increasing aging time, regardless the addition of Be or Sr.

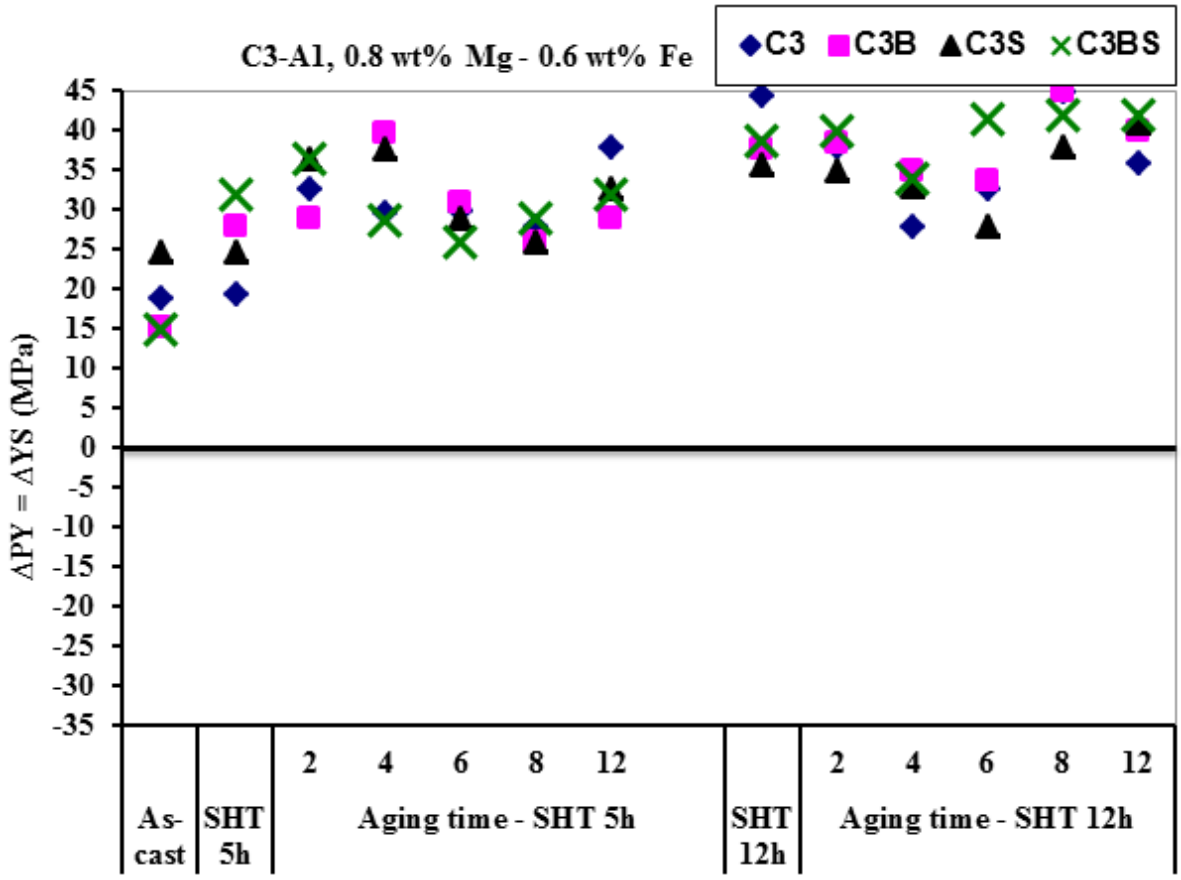

Figure 4.58 Changes in yield strength of high Mg- and high Fe-containing C3 alloys with respect to base alloy A1 in the corresponding conditions.

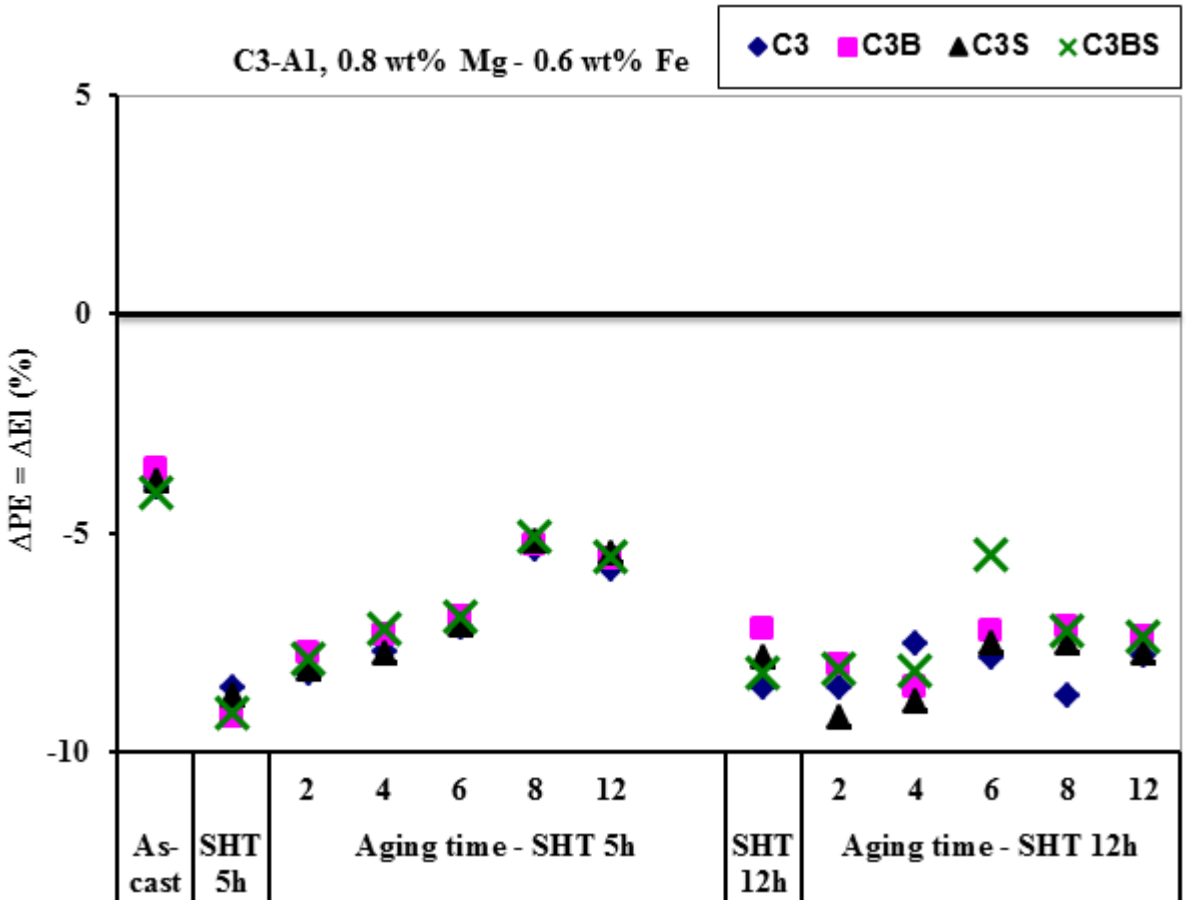

Figure 4.59 Changes in percent elongation of high Mg- and high Fe-containing C3 alloys with respect to base alloy A1.

Using C3 alloy as the reference alloy, an examination of the effects of adding 0.05 wt% Be, 0.02 wt% Sr, or both, on the tensile properties of the C3 alloys is shown in Figures 4.60 through 4.62. The addition of Be, Sr or both, improves the UTS values of the solution treated and aged samples, as shown in Figure 4.60.

As Figure 4.61 shows, yield strength is sensitive to alloying additions and heat treatment conditions. The yield strength decreases with increase in aging time, for samples that were solution heat-treated for 5 hours. Two reasons for this can be supposed: (i) a 5-hour solution time is not enough to fully dissolve the Mg_2Si, decompose the π-phase into the β-phase or fragment the β-phase, and (ii) increased volume fraction of Be-, Sr-, and Mg-containing intermetallics, which may bring about a decrease in yield strength or the alloy mechanical properties in general. [180, 181]

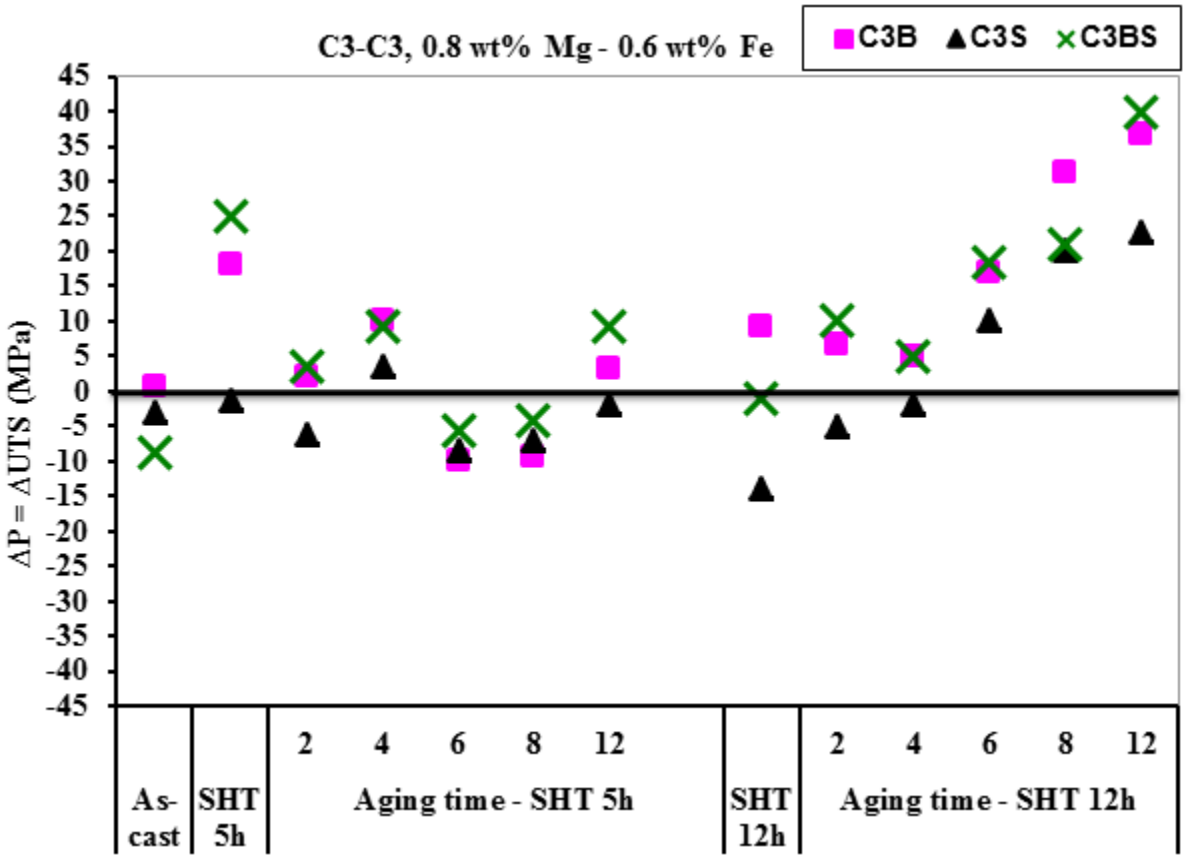

Figure 4.60 Changes in ultimate tensile strength of high Mg- and high Fe-containing C3 alloys, with respect to alloy C3.

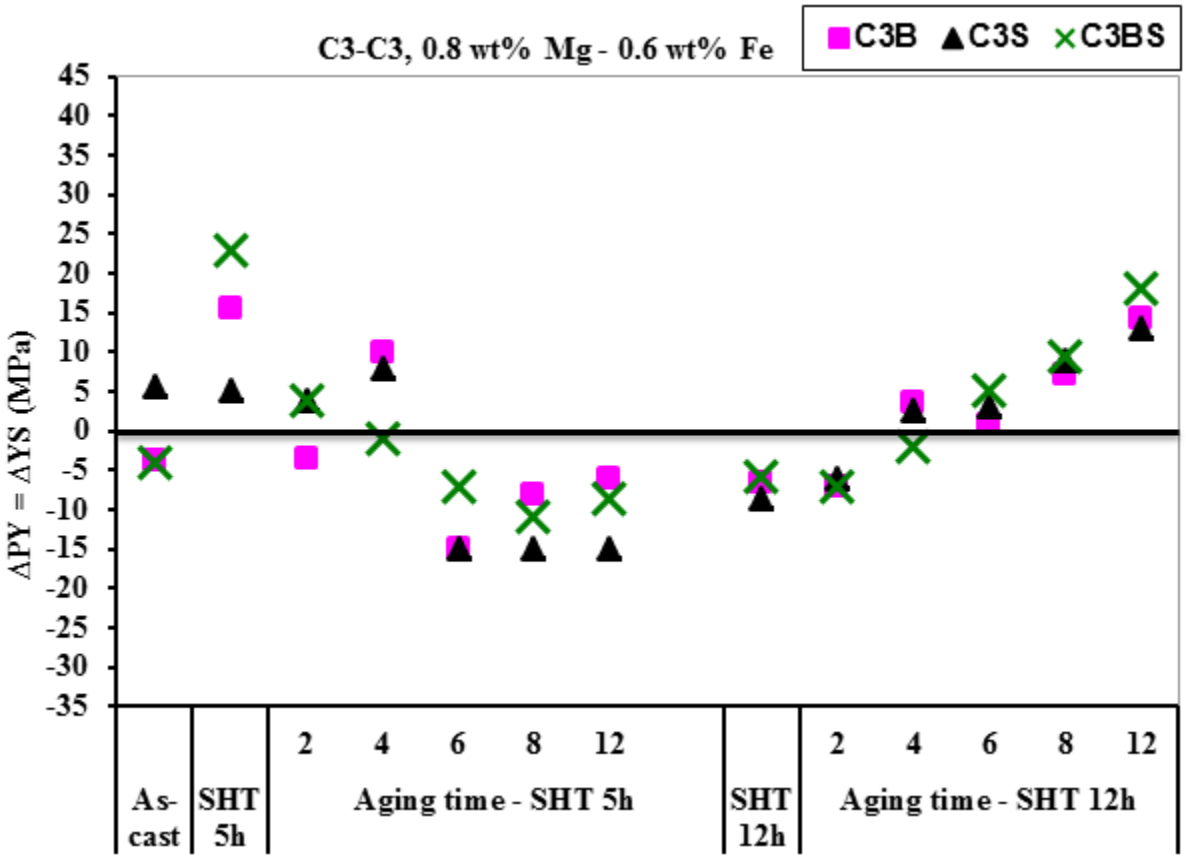

Figure 4.61 Changes in yield strength of high Mg- and high Fe-containing C3 alloys, with respect to alloy C3.

Percent elongation was not affected by the interaction of alloying elements or by the heat treatment parameters used, as shown in Figure 4.62. [180,181]

The tensile test data obtained for the various 357 alloys investigated in this study were presented in different formats, using alloy A1, alloy A3, and alloy C3 as the reference alloys, with the intention of bringing out the effects of (a) each addition/level, (b) interactions between added elements, as well as (c) the heat treatment conditions applied. The results obtained are in good agreement with those reported by other researchers. [182-184]

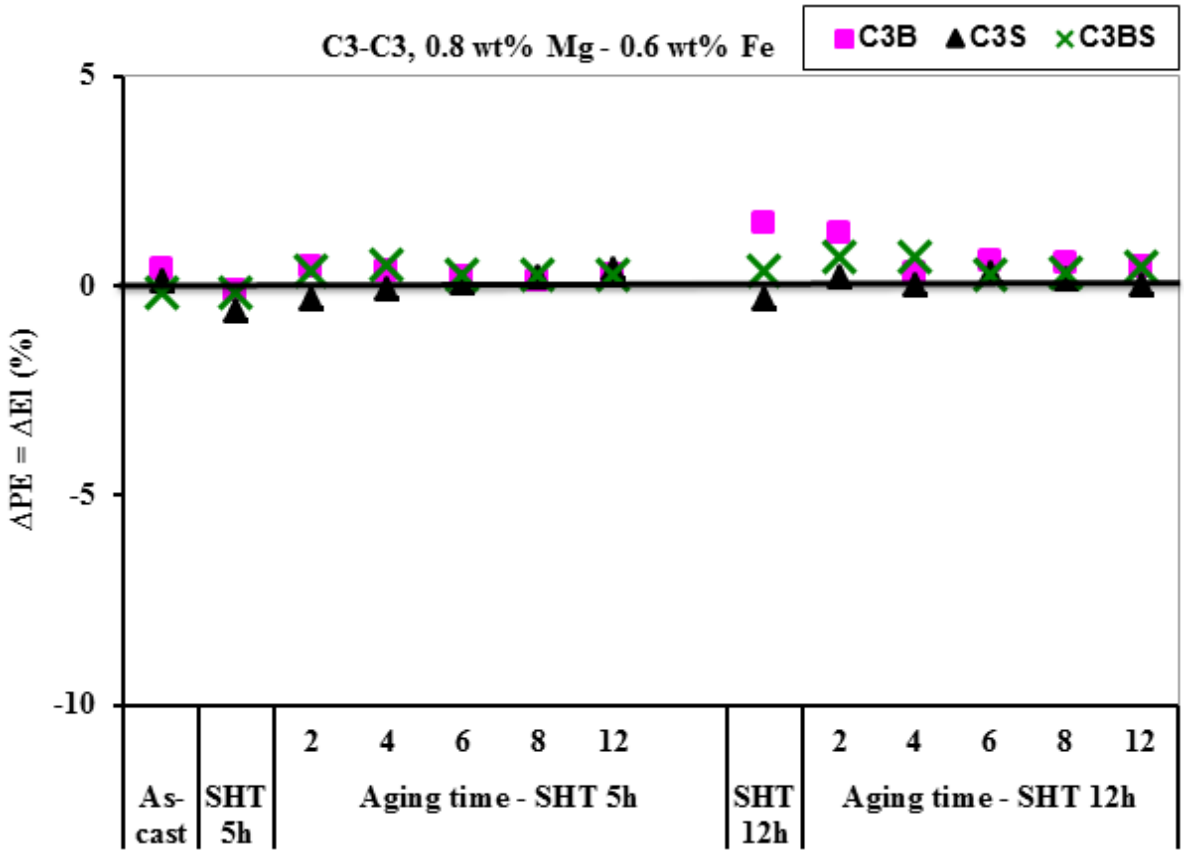

Figure 4.62 Changes in percent elongation of high Mg- and high Fe-containing C3 alloys, with respect to alloy C3.

4.7 CONCLUSIONS

Based upon the results discussed in this chapter, the following conclusions may be drawn:

1. In the as-cast condition, increasing the Mg content leads to further transformation of the β-phase platelets to a Chinese-script π-phase, regardless of the Fe content, decreasing the harmful effect of the β-phase.
2. Increasing the solution heat treatment time leads to further decomposition of the π-phase, fragmentation of the β-phase and spheroidization of the eutectic Si, resulting in an improvement of the alloy tensile properties.
3. Two mechanisms of Mg_2Si precipitate coarsening were observed to take place: Ostwald ripening and clustering. The rate of coarsening is higher when both aging time and Mg content are raised.
4. Increasing the Fe level decreases the alloy quality index (Q) values, whereas the addition of Mg increases the Q-values.
5. Introducing Be, Sr, or both, improves the alloy quality index, regardless of the levels of Fe and Mg present.
6. Quality index values increase with solution heat treatment time from 5 to 12 hours.
7. Raising the Mg content leads to an increase in tensile parameters. Raising the Fe levels, however, leads to a drastic decrease in these properties.
8. For the same levels of Fe and/or Mg, Be and Sr help to improve the alloy mechanical properties. This is more prominent at low levels of Fe with high levels of Mg.

9. Addition of Be is beneficial in the case of high Fe content in the context of reducing the harmful effects of Fe-phases through the formation ofAl-Fe-Be phases.
10. In the case of alloys containing high amounts of Fe, it was observed that the simultaneous addition of Be and Sr has a negligible effect on tensile properties. The addition of 500 ppm of Be, for example, appears insufficient, considering interactions with other alloying elements.
11. The role of Be is not only in minimizing Mg oxidation but in changing the Fe-intermetallic chemistry and morphology, as reflected by the improved tensile properties of the Be-containing alloys.
12. Partial modification of the eutectic Si particles by Mg and Be may contribute to some extent to improvements in the tensile properties.
13. Solution heat treatment and aging time are the main parameters to consider in terms of controlling the alloy tensile properties.
14. Precipitation of the Mg_2Si phase was confirmed to be the main hardening agent of 356 and 357 alloys investigated in the present work.
15. Yield strength increases with raised Mg levels, reduced Fe levels, Be additions, Sr-modification, solution treatment time and aging time. Increase in the YS is an important factor from a design point of view.
16. The combined addition of Be and Sr, coupled with long solution times (e.g. 12hours) at 540°C, improves the yield strength, regardless of the alloy composition.
17. Increasing the amount of added Fe in high Mg-containing alloys improves the percent elongation with increase in aging time regardless the addition of Be or Sr.

CHAPTER 5

OPTIMIZING THE HEAT TREATMENT OF HIGH STRENGTH Al-Cu-Mg-Zn ALLOYS: A PRELIMINARY STUDY

CHAPTER 5

OPTIMIZING THE HEAT TREATMENT OF HIGH STRENGTH Al-Cu-Mg-Zn ALLOYS: A PRELIMINARY STUDY

5.1 INTRODUCTION

The design of aerospace aluminum alloys is mainly rooted in optimizing the strength and ductility, both of which can be enhanced by controlling the added alloying elements as well as the heat treatment conditions. Aluminum-copper-magnesium-zinc (Al-Cu-Mg-Zn) alloys belong to the 7xxx series of aluminum wrought alloys used for such critical applications. The Al-Cu-Mg-Zn 7075- and 7475- type aeronautical alloys were investigated in this preliminary study. The objective was to optimize both the heat treatment techniques and the strength of a 7075 alloy, whose tensile properties exceed 500 MPa, depending on the production procedures and heat treatment techniques applied. Moreover, these alloys have other favorable properties such as resistance to stress-corrosion cracking and fracture toughness.

Farhadi *et al*. [134, 185, 186] carried out a detailed study on the effects of small additions of Be and Sr on the microstructure and tensile properties of experimental 6xxx alloys. Their results showed that for 0.02% Be addition, the iron intermetallics precipitate

in the form of small, globular α-Al_8Fe_2SiBe particles in the interdendritic regions. Combined addition of Be and Sr leads to the precipitation of α-Al_8Fe_2SiBe phase as very fine, broken particles which markedly enhances the alloy formability. The authors also found that addition of 0.02% Be reduces the possibility of hot tearing during solidification and protects the outer surfaces of the cast test bars from oxidation during solution heat treatment at high temperatures.

This chapter is an extension of these studies [134, 185, 186] and focuses on the influence of alloying elements, mainly Fe, Be, Mg, Zn and Cu, interactions and intermetallic phases formed during solidification as well as heat treatment conditions applied on the microstructure and tensile properties of Al-Cu-Mg-Zn wrought alloys. These variables, in turn, can affect the mechanical properties and the fracture behavior of an alloy. The effects of the above-mentioned parameters on the tensile properties and fracture behavior of the Al-Cu-Mg-Zn alloys investigated in this study will be elaborated upon. Adjusting the chemical composition and optimizing both the heat treatment sequence and parameters are the two valuable topics which will be highlighted here in the second part of this thesis.

5.2 RESULTS AND DISCUSSION

5.2.1 Correlation of Microstructure and Mechanical Properties

In the present work, the effects of alloying elements and the heat treatment conditions applied are explained and confirmed by the tensile properties summarized in Table 5.1. Based on the present results, the maximum attainable ultimate tensile strength

(UTS) was 580 MPa for samples of the base alloy (A alloy) subjected to single aging at 120ºC/24h, which is normally higher than that obtained for the solution heat-treated alloy (429 MPa), while the minimum UTS reached was 312 MPa for samples subjected to retrogression and re-aging at 280ºC/8h, followed by 120ºC/24h, as a result of over-aging, dissolution of phases in the matrix during retrogression treatment and particle segregation at the grain boundaries. The best aging condition, as recommended in the literature, was single aging at 120ºC/24h. Compared to the base 7075 alloy (A alloy) used in the current study, the B alloy after homogenization and stretching displayed a UTS of 597 MPa (~600 MPa) while, after the proposed aging process, the UTS value further increased to 980 MPa (~1 GPa) which renders this alloy in the category of super strong alloys. Over-aging the B alloy resulted in a decrease in the ultimate tensile strength and yield strength (YS) with an increase in the alloy ductility. Figure 5.1 displays the stress-strain diagrams obtained from the newly developed alloy (B alloy) under different heat treatment/aging conditions.

Table 5.1 Tensile properties values for alloys/conditions studied

Alloy Code and Condition / Tensile Properties	YS (MPa)	UTS (MPa)	El (%)
A / Solution heat treatment (8h @ 470°C)	267	429	4.63
A / Single aging (24h @ 120°C)	566	580	1.01
A / Single aging (8h @ 280°C)	240	386	4.16
A/Double aging (24h @ 120°C + 8h @ 180°C)	518	525	0.92
A/Double aging (8h @ 180°C + 24h @ 120°C)	483	496	1.02
A/Double aging (8h @ 280°C + 24h @ 120°C)	201	312	3.50
B / Homogenization and stretching	495	597	3.62
B / Proposed new aging process	970	980	1.13
B / over-aging	597	617	3.17

The work was extended to include a commercial 7475 alloy, the composition of which comprised approximately 0.03%Si, 0.06%Fe, 1.6%Cu, 2.4%Mg, 0.2%Cr, 5.8%Zn and 0.015%Ti, in addition to some other minor elements. The obtained stress-strain curves (at 10% deformation) are shown in Figures 5.1(d) and (e). As can be seen in Figures 5.1(d) and (e), by adjusting the alloy chemistry and heat treatment parameters, the as-received strength increased from 403 MPa (YS) and 463 MPa (UTS) to 774 MPa (YS) and 842 MPa (UTS), respectively.

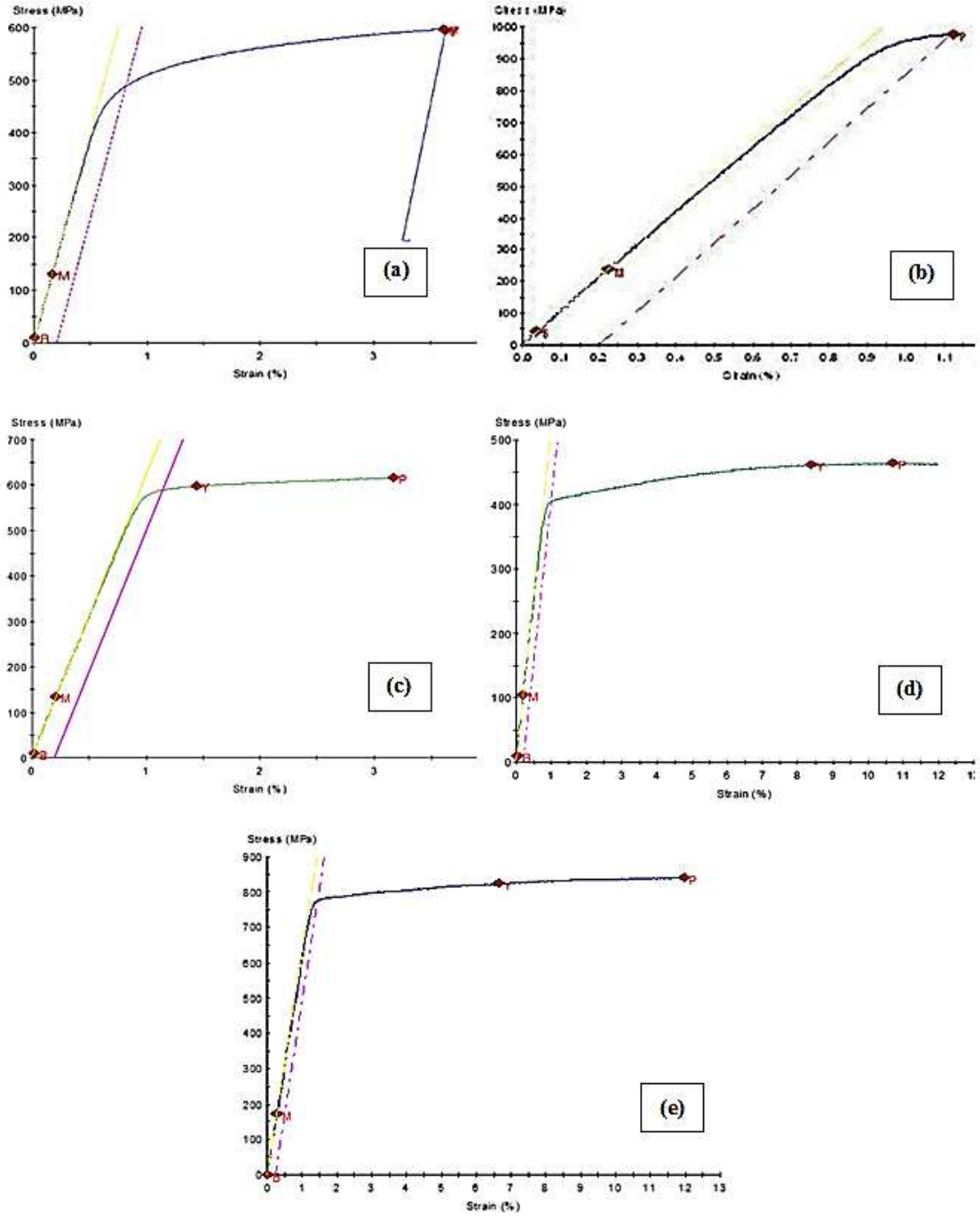

Figure 5.1 Stress-strain diagrams obtained from experimental alloy test bars of: (a) B alloy after homogenization, (b) B alloy after aging, and (c) B alloy after over-aging, (d and e) results obtained from the modified commercial 7475 alloy (at 10% deformation).

Figure 5.2 shows the equiaxed microstructure of the as-cast base alloy, and illustrates the different micro constituents observed therein. Figures 5.3 through 5.5 present the changes in the microstructure of the base alloy upon solution heat treatment in the temperature range 460-485°C (solutionizing time was 48h in all cases). These figures reveal that solution heat treatment resulted in the dissolution of the Al_2Cu, Mg_2Si, Mg_2Zn and α-Fe phases. When the solution temperature was as high as 485°C, incipient melting took place leading to the formation of spherical pores.

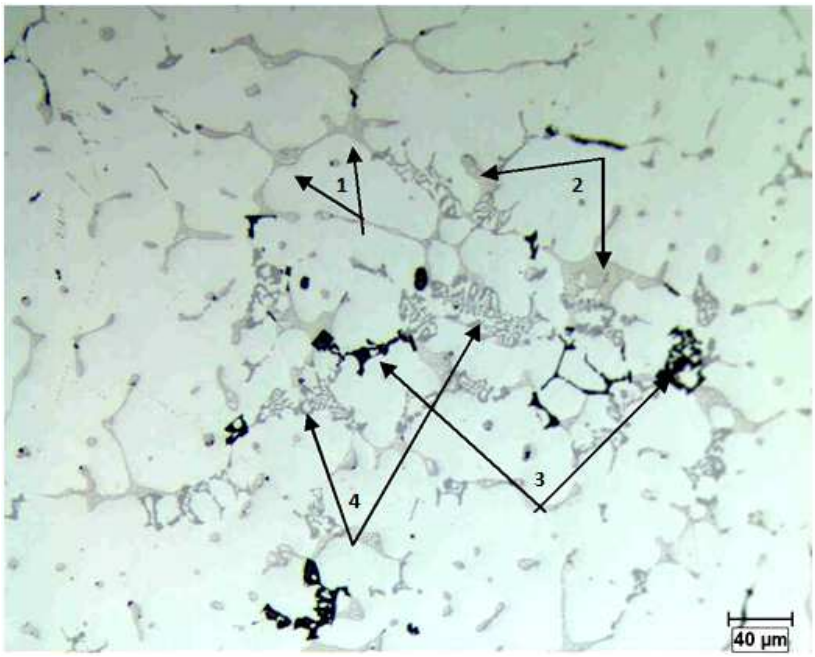

Figure 5.2 Optical microstructure of the base alloy in the as-cast condition: showing the different micro constituents: 1) Zn-, 2) Cu-, 3) Mg- and 4) Fe- rich phases.

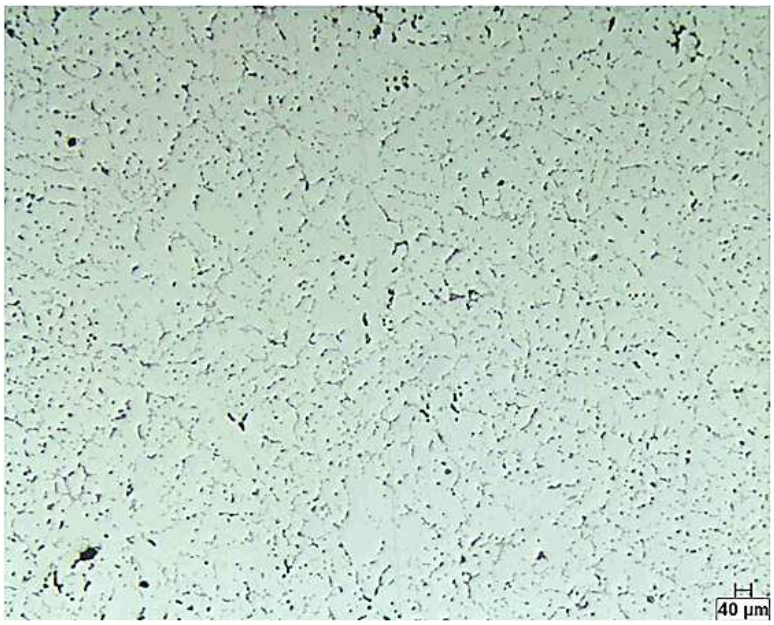

Figure 5.3 Optical micrograph showing progress of the dissolution of Zn- and Cu-rich phases in base alloy A after 48h solution treatment at 460°C.

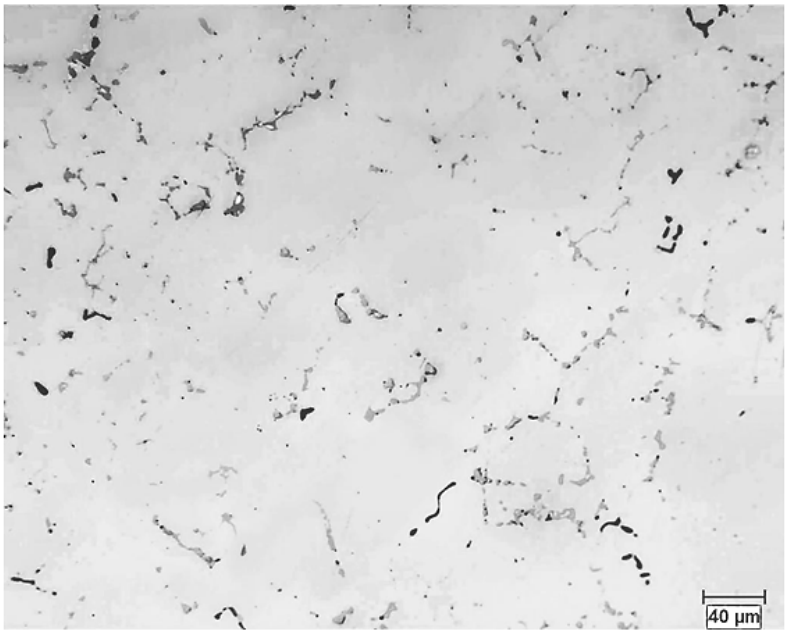

Figure 5.4 Optical micrograph of base alloy sample after 48h solution treatment at 470°C, showing the persistence of Fe-rich phases.

Figure 5.5 Optical micrograph of base alloy A after 48h solution treatment at 485°C showing commencement of incipient melting. Note the presence of solidified material in the interiors of the melted areas (arrowed).

Figure 5.6(a) shows a backscattered image of the as-cast microstructure of the base alloy; a higher magnification image of the same is provided in Figure 5.6(b), where the AlFeCuZn phase is observed precipitated on the grain boundaries as well as within the grains in the form of spherical particles. Figures 5.6(c) is an EDS spectrum corresponding to the AlMgCuZn phase in the as-cast structure. Figure 5.7 shows another backscattered image of the as-cast microstructure at high magnification, where the AlFeCuZn, AlFeSi and AlMgCuZn phases were detected. Figures 5.7 (b, c, and d) are the EDS spectra corresponding to these three phases. Figure 5.8(a) shows a backscattered image of the microstructure of the base alloy after solution treatment; the high magnification image of Figure 5.8(b) reveals the presence of the α-Fe and AlFeCu insoluble phases. The EDS spectrum corresponding to the AlFeCu phase detected in the homogenized structure is

shown in Figure 5.8(c). Table 5.2 summarizes the compositions of the phases observed in Figures 5.7 and 5.8, which in good agreement with those reported in the literature.

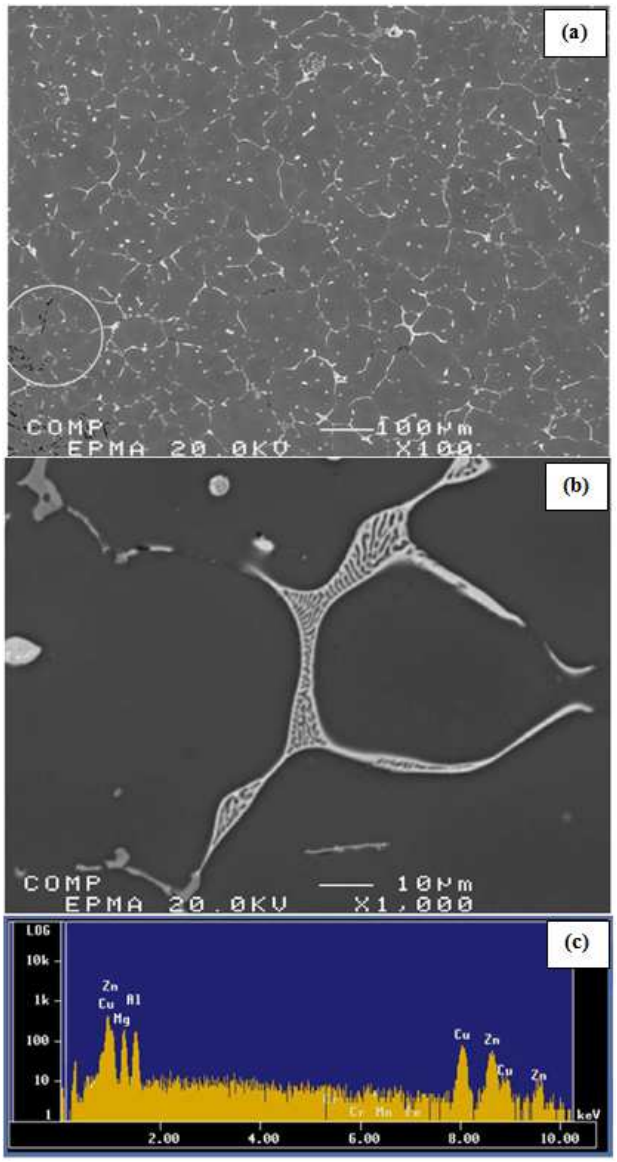

Figure 5.6 Backscattered electron images showing the micro-constituents in base alloy A in the as-cast condition: (a) low magnification image, note the presence of fine cracks in the white circle due to shrinkage; (b) high magnification image illustrating the details of the eutectic structure of AlMgCuZn phase- note that the spherical particles in the middle of the grain have the same composition; (c) EDS spectrum obtained from the eutectic region in (b) displaying strong peaks due to Al, Mg, Cu and Zn.

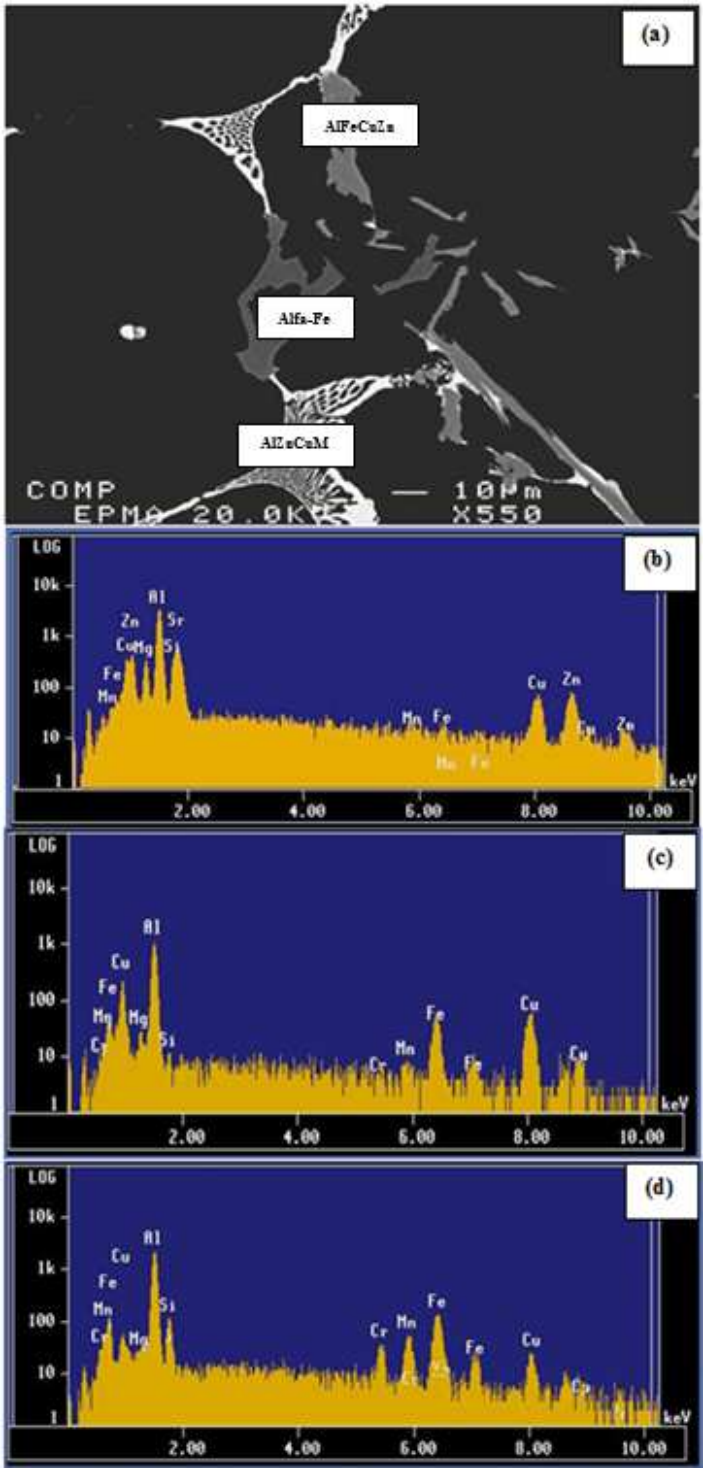

Figure 5.7 (a) Backscattered electron image of the as-cast microstructure of base alloy A, and respective EDS spectra corresponding to the (b) AlFeCuZn, (c) AlFeSi and (d) AlMgCuZn phases shown in (a).

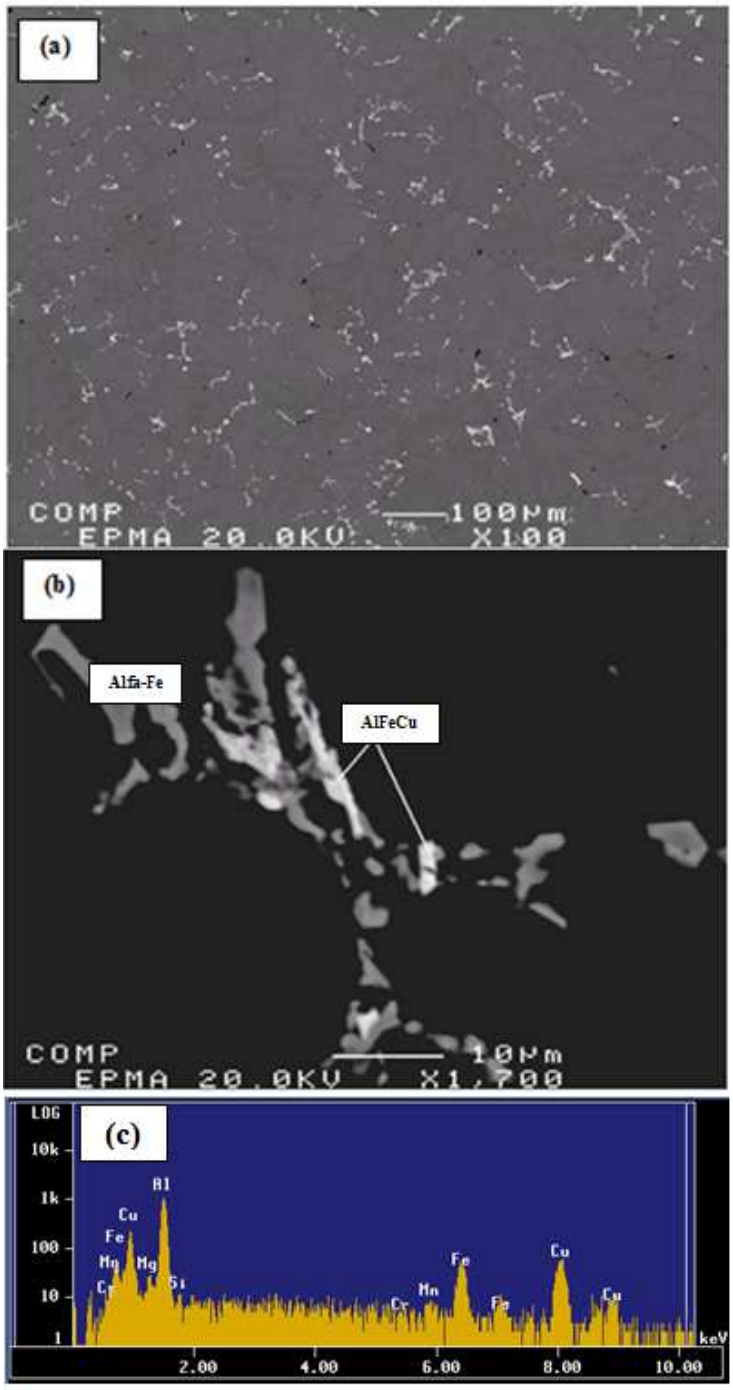

Figure 5.8 (a) Backscattered electron image of base alloy A after solution heat treatment, (b) high magnification image showing the presence of AlFeCu and α-Fe intermetallic phases in the microstructure, and (c) EDS spectrum corresponding to the AlFeCu phase in (b).

Table 5.2 Identification of phases shown in various figures

Figure No.	**Element (at%)**								**Approximate Composition**
	Si	Al	Fe	Cr	Cu	Mg	Mn	Zn	
5.7(a, b)	0.140	26.827	0.168	0.009	21.078	34.271	0.040	17.42	$T(Al_3Cu_2Mg_4Zn_2)$
5.8(b)	0.617	75.332	16.755	0.968	2.311	0.049	3.310	0.554	$Al_3(Fe,Cu,Mn,Cr)$
5.8(b)	3.683	77.508	11.006	2.485	0.717	0.079	3.918	0.578	$Al_8(Fe,Mn,Cr)_2Si/Al_{15}(Fe,Mn,Cr)_3Si_2$

For all microstructures studied, line scans were used to investigate the distribution of alloying elements before and after solution heat treatment for both the base and the B alloys. Figure 5.9 shows the distribution of the three common elements Mg, Cu and Zn in the 7075 alloy. The peaks in Figure 5.9 (a, b and c), corresponding to the Mg, Cu, and Zn concentrations in the as-cast sample, disappear after solution treatment, reflecting the optimized homogeneity of the matrix in the solution-treated alloys. Conventional and/or commercial heat treatment of 7075 alloy resulted in a maximum UTS of 580 MPa.

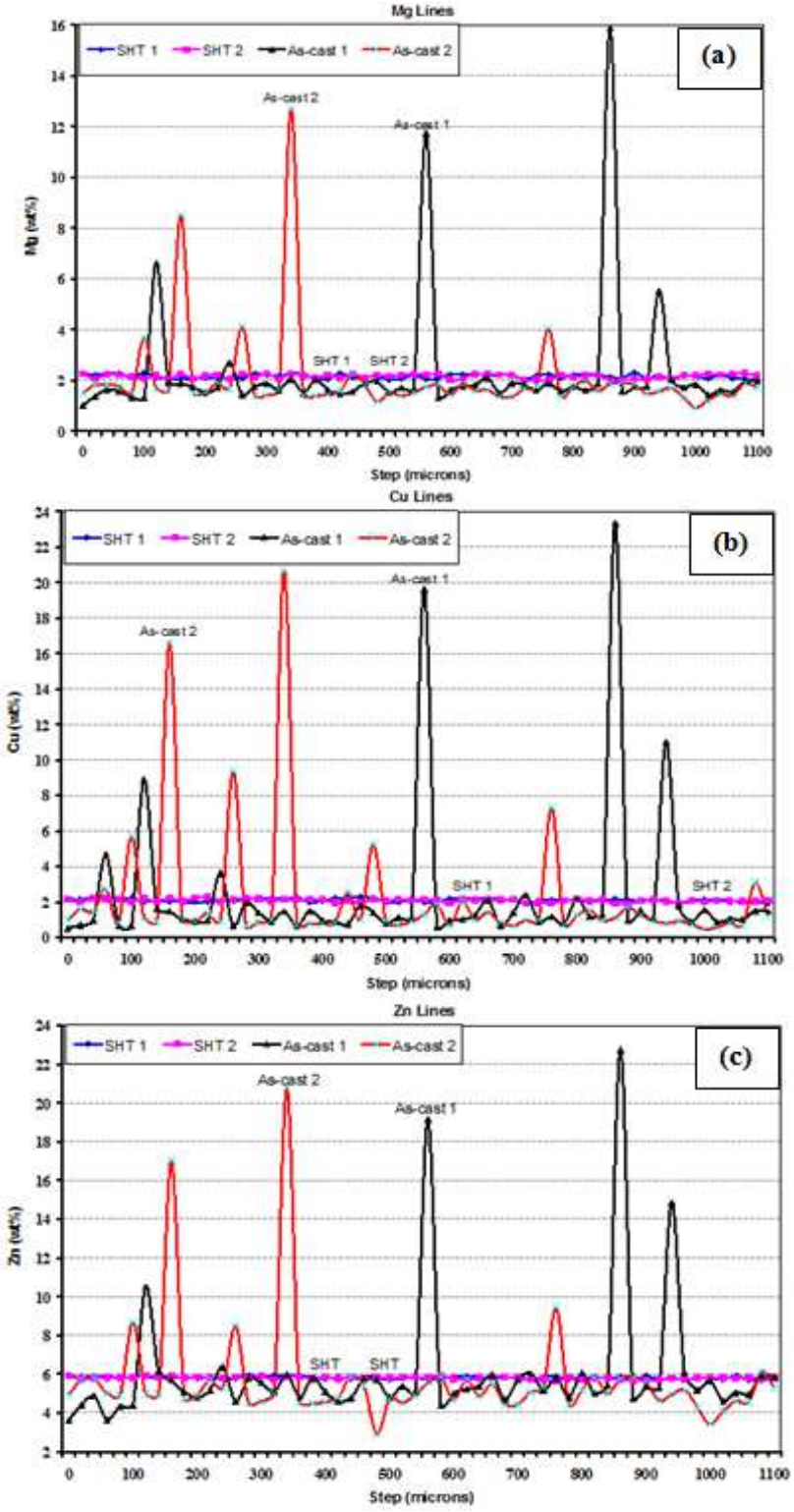

Figure 5.9 Line scans taken from as-cast and heat-treated samples of A alloy showing element distributions of (a) Mg, (b) Cu, and (c) Zn.

In order to arrive at a better understanding of the precipitation sequence in the newly developed B alloy, samples for SEM examination were cut from the tensile-tested bars. The polished samples were examined using a Hitachi SU-8000 FE-SEM operating at 5kV, and equipped with an EDS system. Figure 5.10(a) is a backscattered electron image of an as-cast sample of the B alloy, showing a few rod-like shaped particles. These particles were identified as being mostly Al_2Cu phase from the corresponding EDS spectrum, Figure 5.10(b), together with some α-Fe intermetallic phase particles, Figure 5.10(c). As may be observed from Figure 5.11(a), most of the Al_2Cu phase particles have dissolved in the aluminum matrix after the homogenization and quenching treatment, with fragments of α-Fe $Al_{15}(Fe,Mn)_3Si_2$ phase particles still present in the matrix, as seen from the EDS spectrum of Figure 5.11(b).

Double aging treatment of 24h at120ºC followed by 8h at 180ºC resulted in intense precipitation of ultrafine particles with two distinct morphologies: spherical (encircled) and rod-like, due to their precipitation at two different temperatures, Figure 5.12(a). Aging the B alloy using the new technique resulted in a dense precipitation of the spherical particles throughout the matrix, Figure 5.12(b). These precipitates were mainly Al_2Cu phase particles as confirmed by the associated EDS spectrum displayed in Figure 5.12(c). These precipitates are believed to be the reason for the observed high strength achieved in the new alloy at 120ºC/24h (580 MPa), which is normally higher than that of the solution heat-treated alloy (429 MPa), while the minimum UTS reached was 312 MPa for samples subjected to retrogression and re-aging at 280ºC/8h, followed by 120ºC/24h, as a result of over-aging, dissolution of phases in the matrix during the retrogression treatment, and

segregation of some particles at the grain boundaries. The best aging condition was, as recommended in the literature, single aging at 120ºC/24h. Compared to the 7075 alloy, the base alloy in the current study, the B alloy after homogenization and stretching displayed in a UTS of 597 MPa (~600 MPa) while, after the proposed aging process, the strength increased to 980 MPa (~1 GPa) which renders this alloy in the category of a super strong alloy.

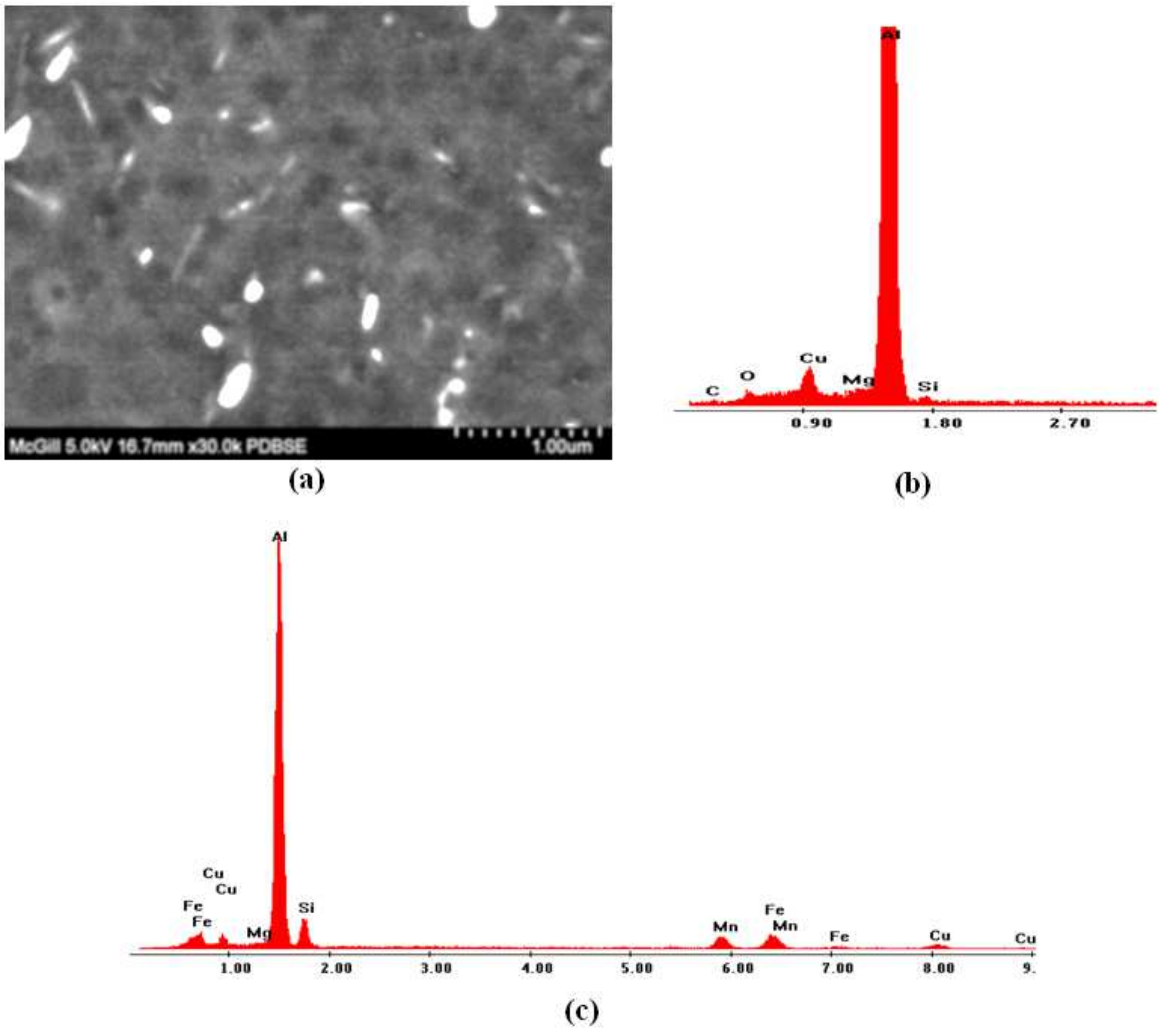

Figure 5.10 (a) Backscattered electron image of the new alloy in the as-cast condition, (b) EDS spectrum corresponding to Al_2Cu phase, and (c) EDS spectrum corresponding to α-$Al_{15}(Fe, Mn)_3Si_2$ phase.

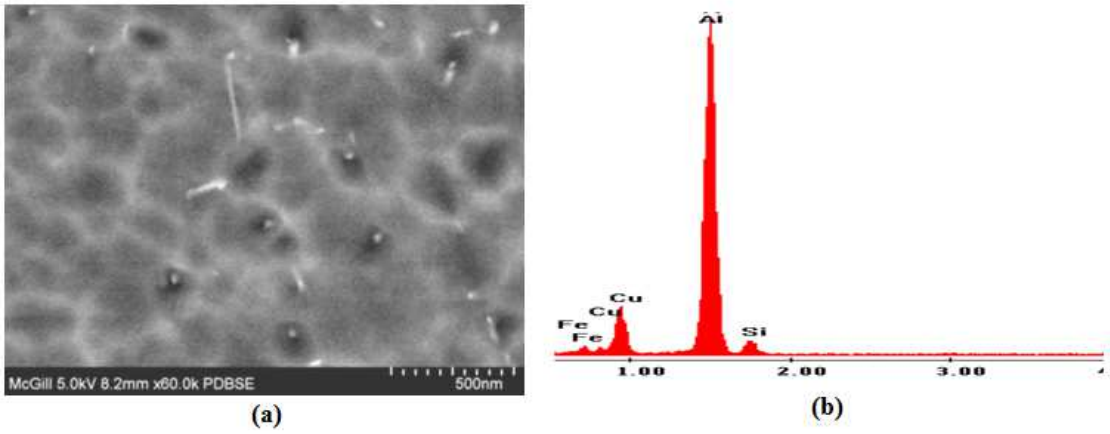

Figure 5.11 (a) Backscattered electron image of the new alloy after solution heat treatment and (b) EDS corresponding to (a), showing the presence of Cu and Fe peaks.

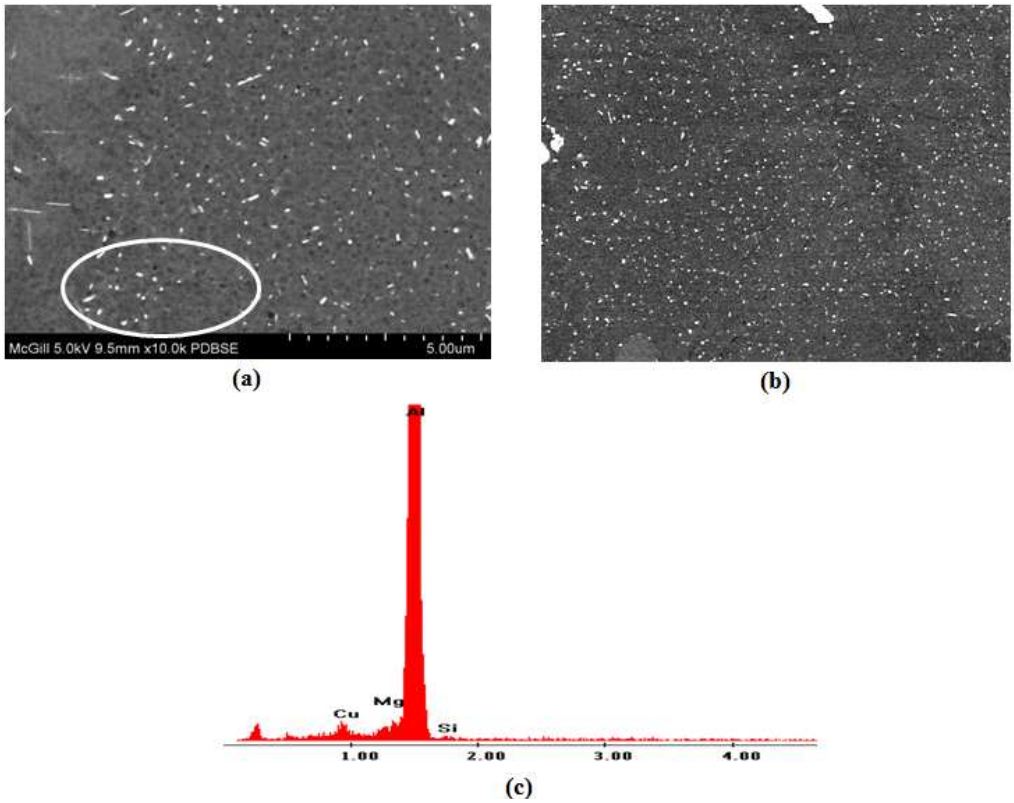

Figure 5.12 Backscattered electron images showing precipitation in the new alloy under different conditions: (a) homogenization and stretching (b) double aging (24h/120ºC + 8h/180ºC), and (c) EDS spectrum corresponding to (a) showing reflections mainly due to Al and Cu elements.

5.2.2 Fractography

The fracture surfaces of the four heat-treated samples shown in Figure 5.1 were examined using an FE-SEM. The backscattered image of Figure 5.13 (a) shows the fracture of the undissolved intermetallic phases in alloy A after applying the recommended solution heat treatment (see Table 5.1). The corresponding EDS spectra taken from various areas in Figure 13(a) revealed the following:

(i) Dissolution of large proportions of Mg, Cu, and Zn in the aluminum matrix, Figure 5.13(b). [116-122]

(ii) Persistence of the Fe-based intermetallics, mainly the Al-Fe-Mn phase, Figure 5.13 (c). Since these EDS spectra were generated from fractured surfaces, the element percentages could not be used to identify their chemical compositions with certainty. [187]

(iii) The interaction between Cu and Fe resulted in the presence of a large amount of undissolved Cu-based intermetallic phase particles, Figure 5.13(d). [188, 189]

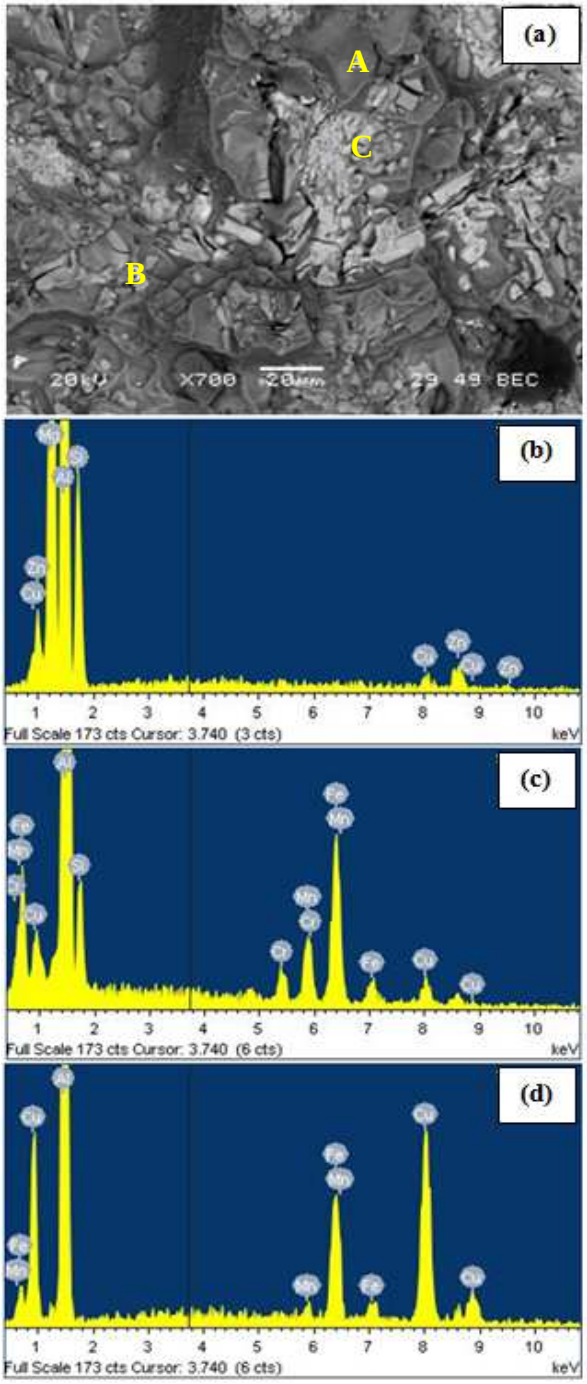

Figure 5.13 (a) Backscattered electron image of the fracture surface of the sample corresponding to Figure 5.1(a), (b) EDS spectrum taken from area marked A in (a) revealing peaks corresponding to Al, Cu, Mg, and Zn, (c) EDS spectrum taken from area marked B in (a) showing reflections due to Al, Fe and Mn and (d) EDS spectrum taken from area marked C in (a) displaying peaks corresponding to Al, Cu, and Fe.

Applying the new solution heat treatment resulted in the dissolution of a noticeable amount of the Cu-rich phases as indicated by the residual fragments in the circled areas in Figure 5.14(a). The presence of several cracks (blue arrows) clearly visible in the interiors of the undissolved intermetallic particles observed in the figure indicate the improvement in the alloy strength as reflected in Figure 5.1(b). The EDS spectrum taken from the area marked by the thick blue arrow in Figure 5.14(a) may be due to the π-phase, [190] see Figure 5.14(b).

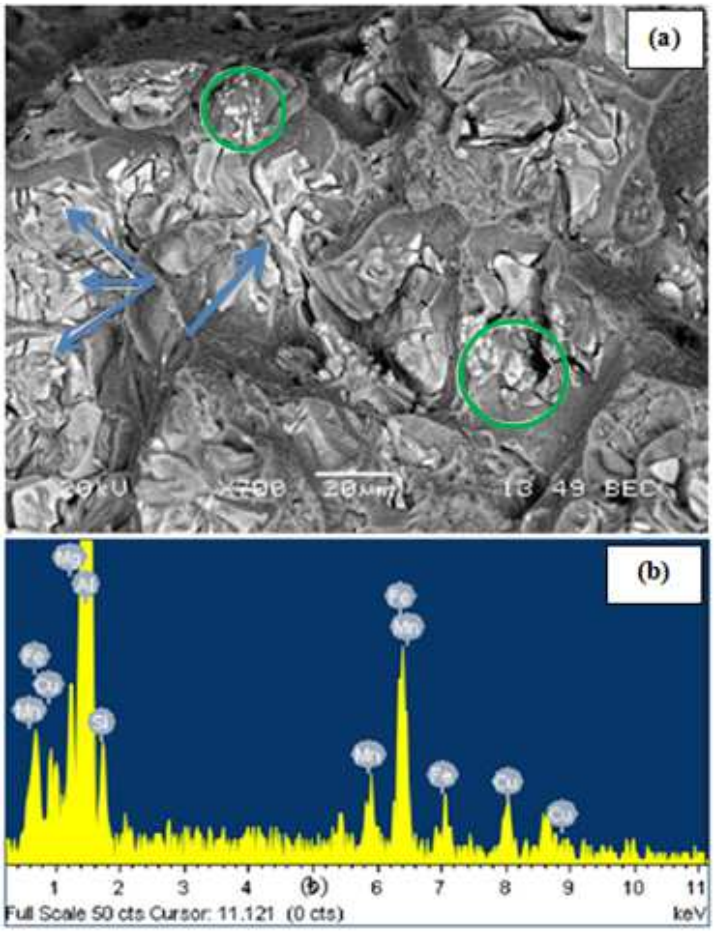

Figure 5.14 (a) Backscattered electron image of the newly developed B alloy sample treated using the new solution heat treatment, (b) EDS spectrum corresponding the phase marked by thick blue arrowed showing reflections due to Al, Mg, Si and Fe elements.

Figure 5.15 (a) presents the fracture surface of the newly developed alloy after homogenization treatment. Large deep dimples could be seen throughout the surface with broken particles at their interiors. The corresponding EDS spectrum, Figure 5.15(b), reveals that these particles are mainly Fe-based intermetallic phases.

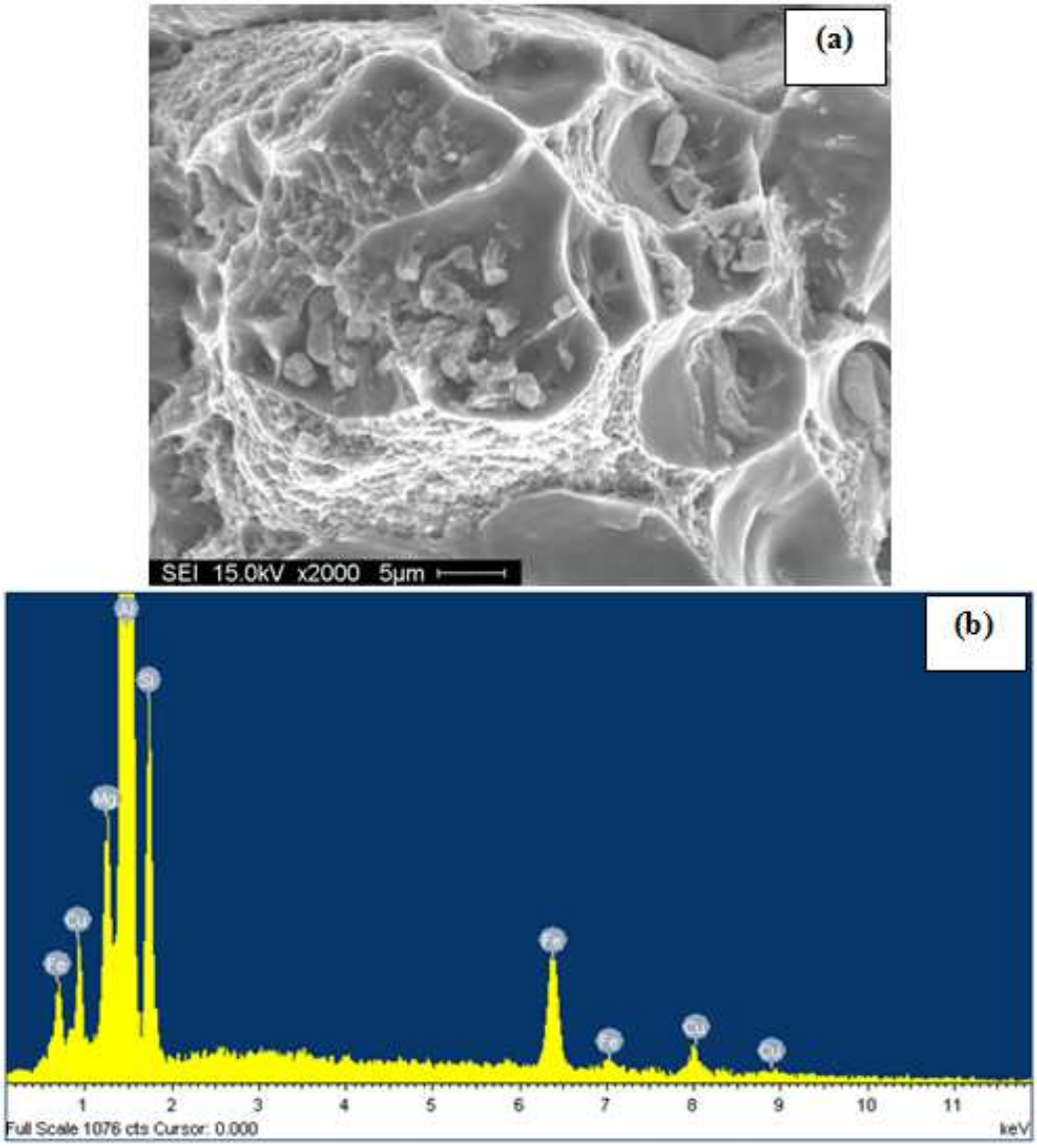

Figure 5.15 (a) Fracture surface of new alloy after homogenization, and (b) EDS spectrum corresponding to the particles within the dimples in (a) revealing Al, Mg, Fe and Cu peaks.

The fracture surface of alloy A after aging for 24 hours at 120°C is shown in Figure 5.16. The increase in the alloy strength (UTS) from 470MPa to 580MPa (see Table 5.1) appears to be related to the formation of an ultra-fine dimpled structure (circled in Figure 5.16) caused by precipitation of age-hardening phases. Another important observation is cleavage fracture of the grains (thick white arrows) leading to the reported brittle failure of this alloy. Figure 5.17 presents the fracture surface of the B alloy after aging exhibiting the fracture of an α-Fe Chinese script phase particle, as evidenced from the associated EDS spectrum of Figure 5.17(b), with several cracks in its interior. The open arrow in (a) points to the formation of a large number of slip bands that formed during the plastic deformation process. [191]

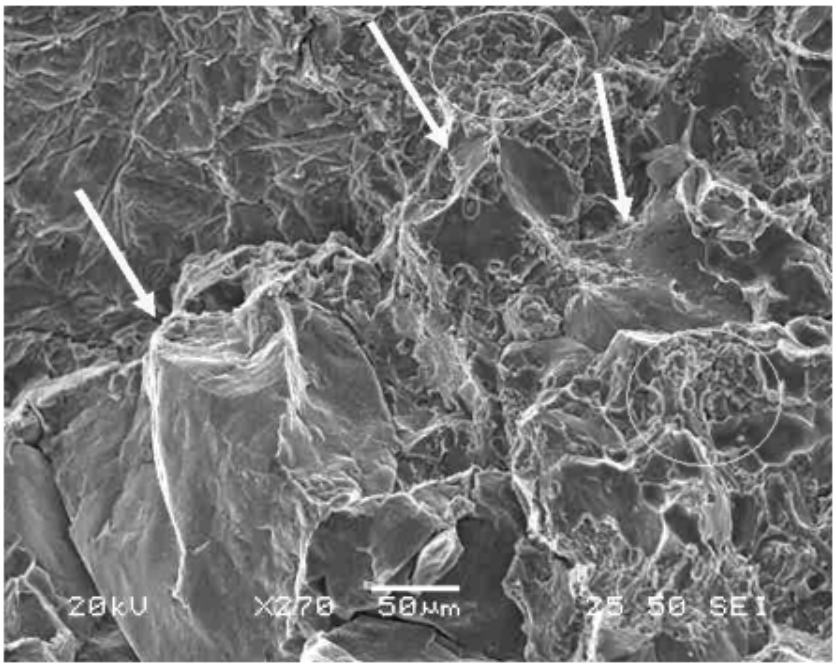

Figure 5.16 Secondary electron image of A alloy aged at 120°C for 24h.

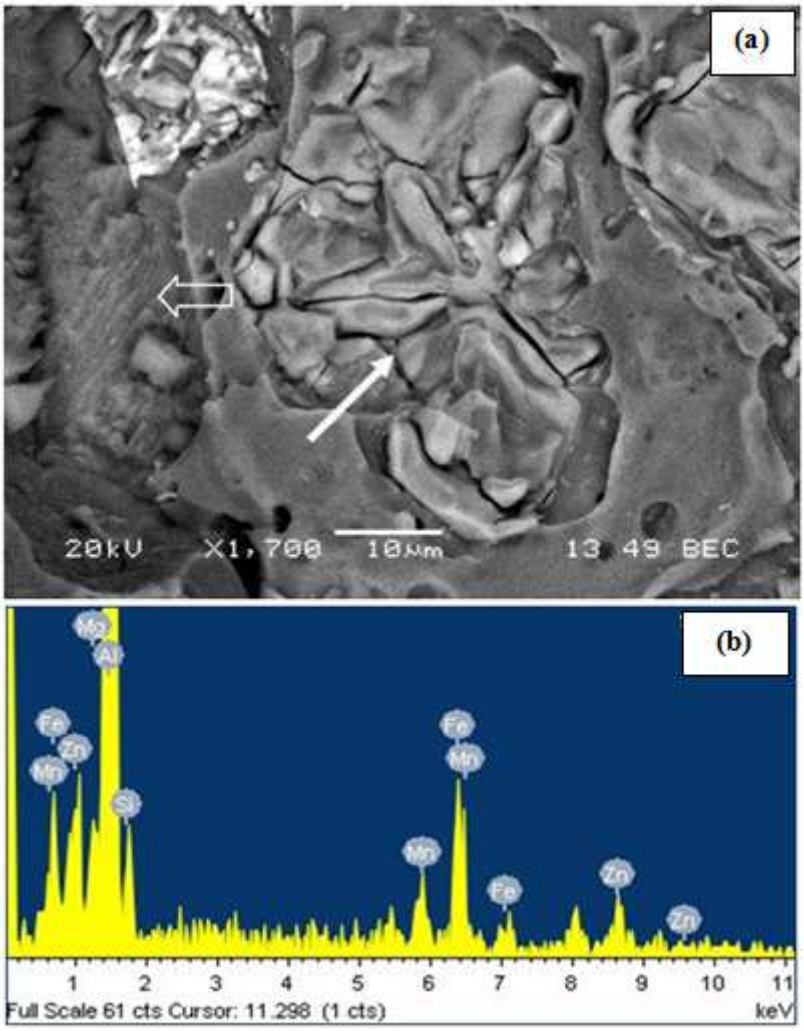

Figure 5.17 (a) Backscattered electron image of the newly developed B alloy after aging and (b) EDS spectrum corresponding to the arrowed area in (a), showing reflections due to Al, Si, Fe and Mn.

Although the ductility of this alloy is very low, the considerable increase in the alloy UTS (980 MPa) was sufficient to cause such severe deformation. Another important feature observed in this sample is the intense precipitation of fine particles all over the matrix as displayed in Figure 5.18(a). The associated EDS spectrum shown in Figure

5.18(b) indicates that these precipitates are mainly Mg_2Si particles. However, due to the fact that these particles are very fine and embedded in the aluminum matrix, the composition of these particles could not be identified with certainty.

The fracture surface of the aged B alloy (with UTS approximately 1GPa), Figure 5.19(a), exhibits several cracks (arrowed) along with fine dimples compared to those shown in Figure 5.15(a). High magnification images revealed the presence of α-Fe in its Chinese script form, Figure 5.19(b), and the cleavage fracture of undissolved AlFeCu phase particles, Figure 5.19(c). Figures 5.19(d) and (e) show the EDS spectra corresponding to these two phases, respectively.

The backscattered electron image of the fracture surface of the overaged B alloy, Figure 5.20(a), reveals the presence of incoherent phase particles as evident from their well-defined boundaries (arrowed). These particles were identified to be mainly Al_2Cu phase as confirmed from the associated EDS spectrum shown in Figure 5.20(b). These Al_2Cu precipitates are believed to be the reason for the observed high strength achieved in the B alloy.

The observations reported on the microstructure, mechanical properties and the fracture behavior of the conventional 7075 alloy (A alloy) are in satisfactory agreement with the findings of several researchers. [192-201] Among the more recent of these studies, Kaka *et al.* [201] have reported a UTS value of 774 MPa for the 7075-type Al-Si-Mg alloy investigated in their work. This value appears to be the closest (~ 80%) to the UTS value of 980 MPa (nearly 1 GPa) obtained in the present study for the new developed B alloy.

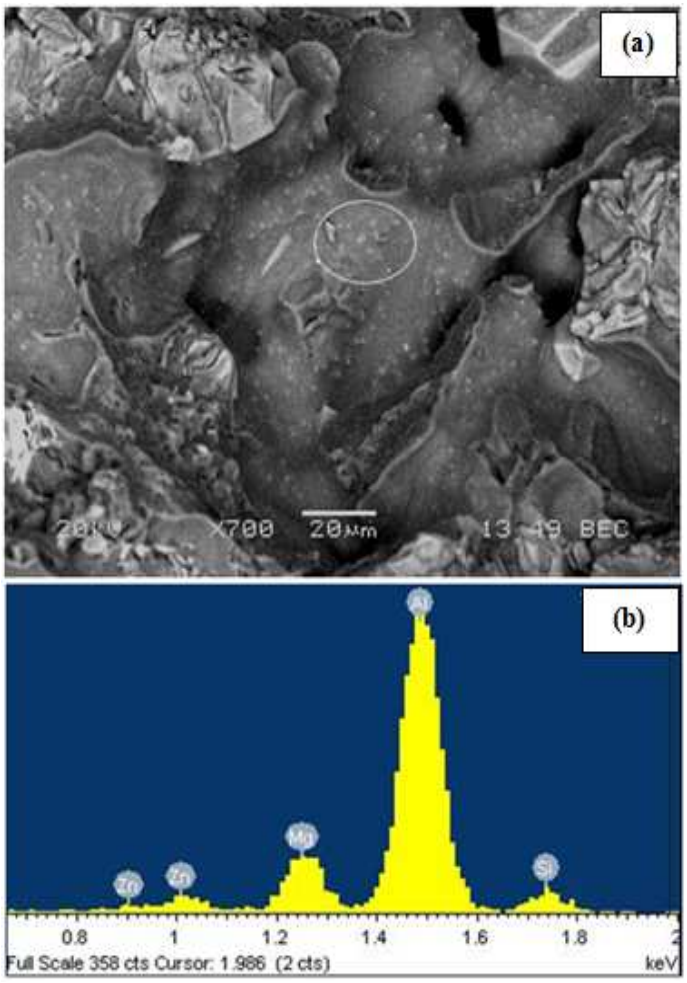

Figure 5.18 (a) Backscattered electron image of the newly developed B allo**y** after aging and (b) EDS spectrum taken from the circled area in (a), revealing Al, Si, Zn and Mg peaks.

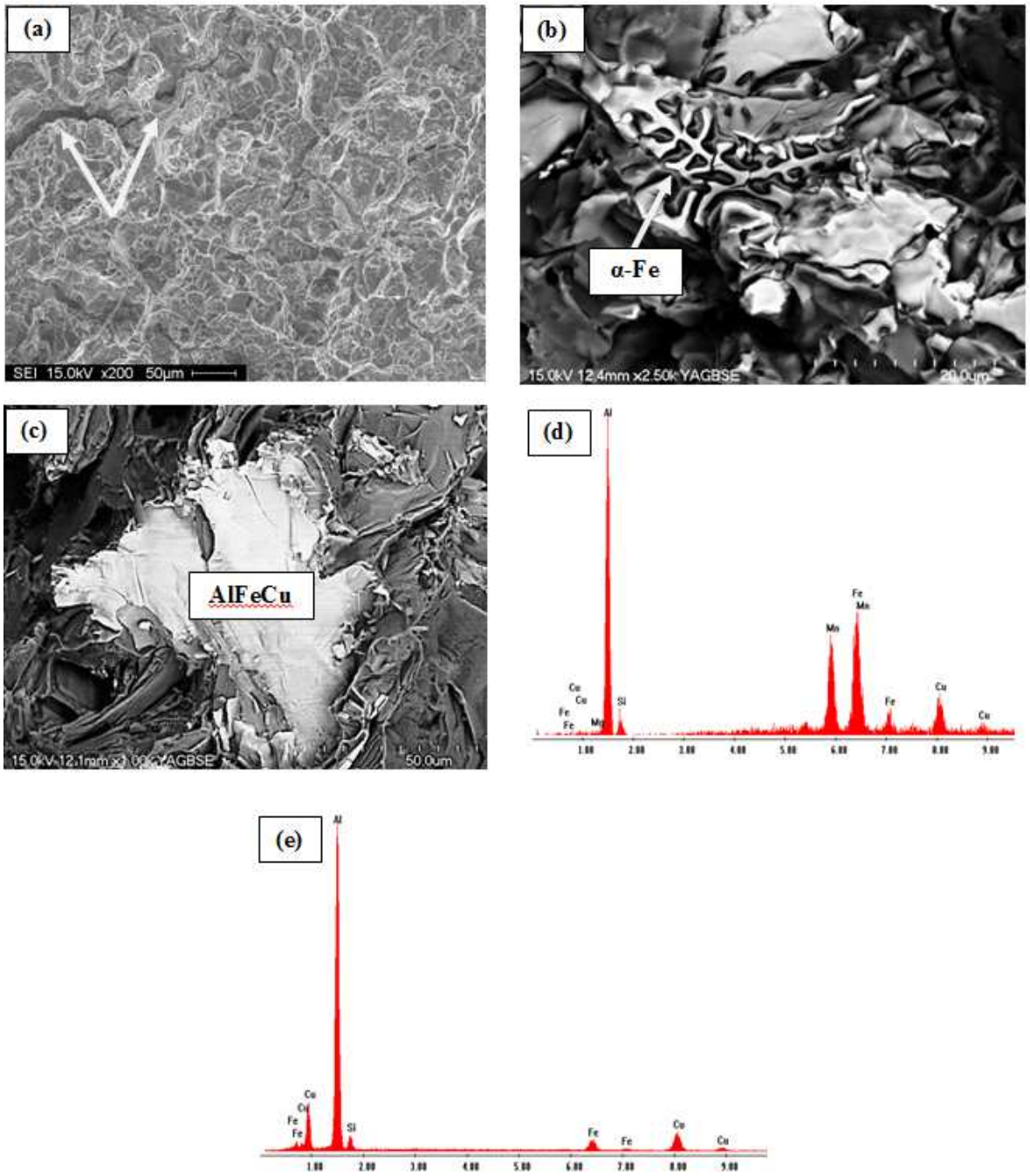

Figure 5.19 A series of secondary electron images and EDSs taken from B alloy following the new aging regime: (a) general view showing the presence of several cracks, (b) high magnification image revealing the presence of α-Fe phase, (c) high magnification image exhibiting the fracture of undissolved AlFeCu phase, (d) EDS spectrum corresponding to (b), and (e) EDS spectrum corresponding to (c).

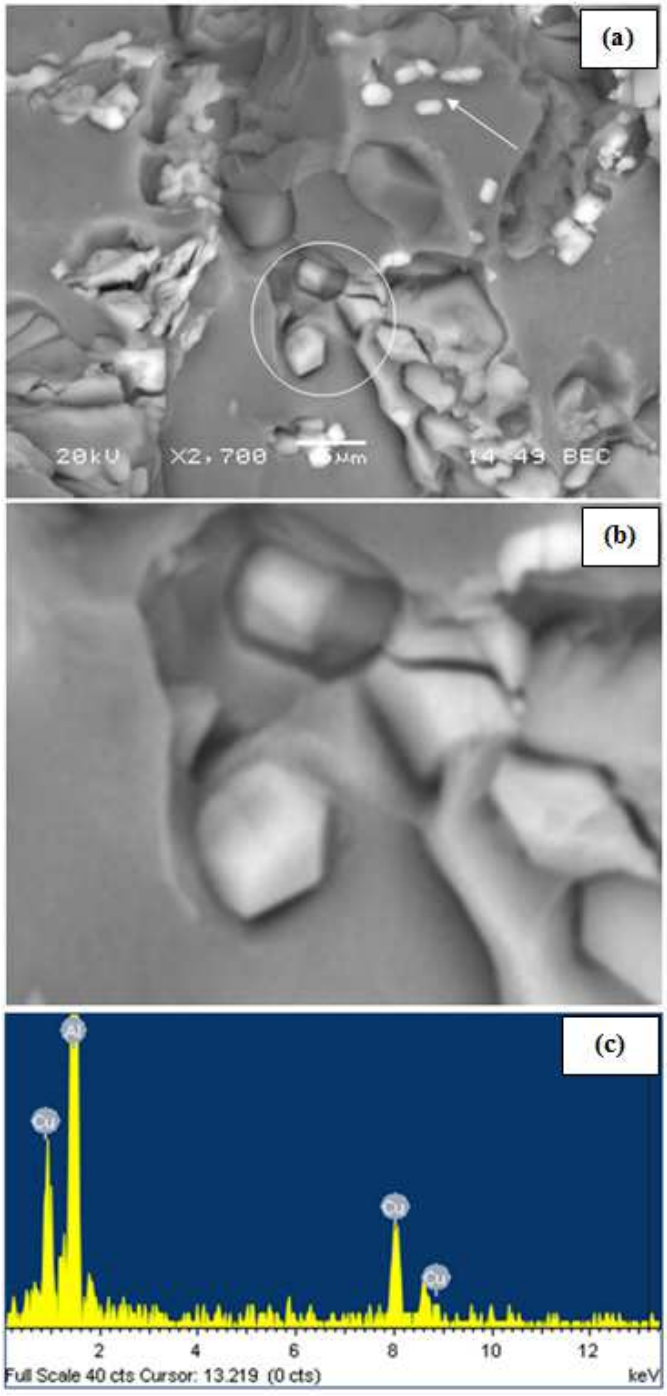

Figure 5.20 (a) Backscattered electron image of the fracture surface of overaged B alloy revealing the presence of incoherent phase particles (white arrows), (b) a high magnification micrograph of the circled area in (a) showing the morphology of the precipitates, and (c) EDS spectrum corresponding to (b) revealing reflections due to Al and Cu.

5.3 CONCLUSIONS

Based upon the results documented in this chapter, the following conclusions may be drawn:

1. Solution heat treatment for 48h at 460°C and 470°C results in dissolution of Mg- and Cu rich phases whereas as Fe-rich phases remain in the matrix.

2. Increasing the solutionizing temperature to 485°C causes incipient melting of the Cu-rich phases.

3. The use of proper additives, cold/hot deformation, homogenization and aging, as applied in this study, shows that 7075 alloys have the potential to reach UTS levels as high as 980 MPa, after aging.

4. Alloy ductility may be improved using proper casting technology. The results of this study indicate that modification of both alloy composition and casting technique would provide the means to achieve much higher percentage elongation values.

5. The EDS spectra taken from the fracture surfaces of solution heat-treated samples indicated dissolution of Zn, Mg, and Cu in the aluminum matrix. In contrast, the presence of fragments of Fe-based intermetallic particles were also observed on the fracture surfaces, due to their low solubility in the matrix.

6. The fracture surfaces of aged samples exhibited cleavage fracture due to poor alloy ductility. Ultra-fine dimples were also observed caused by the precipitation of a mixture of fine particles, mainly Al_2Cu, Mg_2Si and $MgZn_2$.

7. The observed marked increase in the alloy strength through adjusting the alloy chemistry and heat treatment may be attributed to the dense precipitation of ultrafine particles of Al_2Cu phase distributed uniformly throughout the matrix.

8. Adjusting the chemical composition of the 7075 alloy with proper casting and heat treatment techniques, the alloy could reach 1GPa with at least 5-8% elongation.

RECOMMENDATIONS FOR FUTURE WORK

In order to arrive at a complete understanding of the effects of Be, Sr, Fe and Mg interactions on the microstructure and mechanical properties of aluminum-based aeronautical alloys, the following may be suggested:

1- Determining the exact formation temperature of the new observed eutectic reaction in Be-containing alloys using Differential Scanning Calorimetric analysis.

2- More experimental work may be required to arrive at a clear understanding of Mg_2Si clustering and coarsening during the aging process.

3- Mathematical treatment of the obtained tensile results using Minitab, MATLAB and SigmaPlot softwares.

4- Elaborating on the new technology of the production of super strength aluminum alloys to make it applicable on an industrial scale through adjustment of the casting and deformation processes.

REFERENCES

[1] J.E. Gruzleski and B.M. Closset, "*The Treatment of Liquid Aluminum-Silicon Alloys*," American Foundrymen's Society, Inc., Des Plaines, IL, 1990.

[2] J.R. Davis, ASM Special Handbook, "*Aluminum and Aluminum Alloys*," ASM International, the Materials Information Society, Materials Park, OH, 1994, pp. 1-30.

[3] J.H. Sokolowski, M.B. Djurdjevic, C.A. Kierkus, and D.O. Northwood, "Improvement of 319 Aluminum Alloy Casting Durability by High Temperature Solution Treatment," *Journal of Materials Processing Technology*, 2001, Vol. 109, pp. 174-180.

[4] J.H. Sokolowski, X-C. Sun, G. Byczynski, D.E. Penord, R. Thomas, and A. Esseltine, "The Removal of Copper-Phase Segregation and the Subsequent Improvement in Mechanical Properties of Cast 319 Aluminum Alloys by a Two-Stage Solution Heat-Treatment," *Journal of Materials Processing Technology*, 1995, Vol. 53, pp. 385-392.

[5] S. Shivkumar, C. Keller, M. Trazzera and D. Apelian, "Precipitation Hardening in 356 Alloys," *Proceedings International Symposium on Production, Refining, Fabrication and Recycling of Light Metals*, Hamilton, Ontario, August 26-30, 1990, pp. 264-278.

[6] C.H. Cáceres, C.J. Davidson, J.R. Griffiths and Q.G. Wang, "The Effect of Mg on the Microstructure and Mechanical Behavior of Al-Si-Mg Casting Alloys," *Metallurgical and Materials Transactions A*, Vol. 30A, March1999, pp.1999-2611.

[7] J.E. Hatch (Ed.), "*Aluminum: Properties and Physical Metallurgy*," American Society for Metals, Metals Park, OH, 1984.

[8] S. Murali, K. S. Raman, K. S. S. Murthy, "The Formation of β-phase and Be-Fe phases in Al-7Si-0.3Mg Alloy Containing Be," *Materials Science and Engineering A*, Vol. 190, 1995, p. 165-172.

[9] C. Kammer, *Aluminum Handbook*, Vol. 1: Fundamentals and Materials, Aluminium-Verlag, Inc., 1999.

[10] F. Paray and J.E. Gruzleski, “Factors to Consider in Modification,” *AFS Transactions*, Vol. 102, 1994, pp. 833-842.

[11] J.L. Jorstad, “Hypereutectic Al-Si Casting Alloys: 25 Years, What’s Next?,” Silver Anniversary Paper, *AFS Transactions*, Vol. 104, 1996, pp. 669-671.

[12] D. Apelian, S. Shivkumar and G. Sigworth, “Fundamental Aspects of Heat Treatment of Cast Al-Si-Mg Alloys,” *AFS Transactions*, Vol. 97, 1989, pp. 727-742.

[13] E.L. Rooy, *ASM Handbook, Castings*, 9th Edition, ASM International, Materials Park, OH, 1992, Vol. 15, pp. 743-769.

[14] ASM, *Properties and Selection: Nonferrous Alloys and Special-Purpose Materials*, Metals Handbooks, 10th Edition, 1990, Vol. 2, pp. 52-53.

[15] A. Joenoes, J. Gruzleski, “Magnesium Effects on the Microstructure of Unmodified and Modified Al-Si Alloys,” *Cast Metals*, 1991, Vol. 4(2), pp. 62-71.

[16] R. Dunn, W. Dickert, “Magnesium Effect on the Strength of A380.0 and 383.0 Aluminum Die Casting Alloys,” *Die Casting Engineer*, 1975, Vol. 19, pp. 12-20.

[17] I.J. Polmear, “*Light Alloys Metallurgy of Light Metals*,” Edward Arnold Ltd and American Society for Metals, 1981, Vol. 58-63, pp. 82-83.

[18] F. King, “*Aluminum and its Alloys*,” Ellis Howood Limited, 1987, pp. 112-117.

[19] J.E. Hatch, “*Aluminum: Properties and Physical Metallurgy*,” American Society for Metals, Metals Park, OH, 1984, pp. 50-51.

[20] J. Gilbert and E. Leroy, “Aluminum Alloy Castings: Properties, Processes and Applications,” *AFS*, ASM International Materials Park, Dec. 2004.

[21] J. Barresi, M.J. Kerr, H. Wang and M. J. Couper, “Effect of Magnesium, Iron and Cooling Rate on Mechanical Properties of Al-7Si-Mg Alloys,” *AFS Transactions*, Vol. 108, 2000, pp. 563-570.

[22] J.A. Taylor, D. H. StJohn, J. Barresi, and M. J. Couper, “Influence of Mg Content on the Microstructure and Solid Solution Chemistry of Al-7Si-Mg Casting Alloys During Solution Treatment,” *Materials Science Forum*, Vol. 331-337, 2000, pp. 277-282.

[23] N. Tenekedjiev, H. Mulazimoglu, B. Closset and J. Gruzleski, “Microstructures and Thermal Analysis of Strontium Treated Aluminum Silicon Alloys,” *American Foundrymen’s Society Inc.*, Des Plaines, IL, USA, 1995.

[24] S.L. Bäckerud, G. Chai, J. Tamminen, “Solidification Characteristics of Aluminum Alloys, Vol.2: Foundry Alloys,” *AFS/Skanaluminium*, Oslo, Norway, 1990.

[25] G. Phragmén, “On The Phases Occurring in Alloys of Aluminum with Copper, Magnesium, Manganese, Iron, and Silicon,” *Journal of the Institute of Metals*, Vol. 77, 1950, pp. 498-553.

[26] S.K. Tang and T. Sritharan, “Morphology of β-AlFeSi Intermetallic in Al-7Si Alloy Castings,” *Materials Science and Technology*, Vol. 14(8), August 1998, pp.738-742.

[27] S. Foss, A. Olsen, C.J. Simensen and J. Tafto, “Determination of the Crystal Structure of The π-AlFeMgSi Phase Using Symmetry and Site-Sensitive Electron Microscope Techniques,” *Acta Crystallographica*, Section B, Vol. B59, 2003, pp. 36-42.

[28] G. Gustafsson, T. Thorvaldsson, and G.L. Dunlop, “The Influence of Fe and Cr on the Microstructure of Cast Al-Si-Mg Alloys,” *Metallurgical and Materials Transactions A*, Vol. 17A, January1986, pp. 45-52.

[29] L.F. Mondolfo, “Aluminum Alloys: Structure and Properties,” *Butterworths*, London, 1976.

[30] J.A. Taylor, “The Effect of Iron in Al-Si Casting Alloys,” *35th Australian Foundry Institute National Conference*, Adelaide, South Australia, 31 Oct. - 3 Nov. 2004, pp. 148-157.

[31] G.K. Sigworth, “The Modification of Al-Si Casting Alloys: Important Practical and Theoretical Aspects,” *International Journal of Metal casting*, Vol.2(2), 2008, pp. 19-40.

[32] J.E. Gruzleski, M. Pekguleryuz, and B. Closset, “Strontium Addition to Al-Si Alloy Melts,” *in Proceedings of the Third International Solidification Conference*, Institute of Metals, Sheffield, UK, September 1987, pp. 52-54.

[33] F.H. Samuel, P. Ouellet, A.M. Samuel and H.W. Doty, “Effect of Mg and Sr Additions on the Formation of Intermetallics in Al-6 Wt Pct Si-3.5 Wt Pct Cu-(0.45) to (0.8) Wt Pct Fe 319-Type Alloys,” *Metallurgical and Materials Transactions A*, 1998, Vol. 29A, pp. 2871-2884.

[34] P. Ashtari, H. Tezuka and T. Sato, "Influence of Sr and Mn Addition on Intermetallic Compound Morphologies in Al-Si-Cu-Fe Cast Alloys," *Materials Transactions*, Vol. 44(12), 2003, pp. 2611-2616.

[35] A.M. Samuel, F.H. Samuel, and H.W. Doty, "Observations on the Formation of β-AlFeSi Phase in 319 Type Al-Si Alloys," *Journal of Materials Science*, Vol. 31, 1996, pp. 5529-5539.

[36] A. Pennors, A.M. Samuel, F.H. Samuel and H.W. Doty, "Precipitation of β-Al_5FeSi Iron Intermetallic in Al-6Si-3.5Cu (319) Type Alloys: Role of Sr and P," *AFS Transactions*, Vol. 106, 1998, pp. 251-264.

[37] I. Huang, "*Nonferrous Cast Alloys and Their Melting*," National Industry Publishers, Beijing, P.R. China, 1980, pp. 9-29.

[38] B. Closset and J.E. Gruzleski, "Structure and Properties of Hypoeutectic Al-Si-Mg Alloys Modified with Pure Strontium," *Metallurgical Transactions A*, 1982, Vol. 13, pp. 945-951.

[39] M. Pekguleryuz, "*Strontium Dissolution in Liquid Aluminum and A356 Alloy*," Ph.D. Thesis, McGill University, 1987.

[40] B. Closset, M. Pekguleryuz and J.E. Gruzleski, "The Aluminum-Strontium Phase Diagram," *Metallurgical Transactions A*, 1986, Vol. 17A, pp. 1250-1253.

[41] J.A. Taylor, D.H. StJohn, L.H. Zheng, G.A. Edwards, J. Barresi and M.J. Couper, "Solution Treatment Effects in Al-Si-Mg Casting Alloys: Part 1 - Intermetallic Phases," *Aluminium Transactions*, 2001, Vol. 45, pp. 95-110.

[42] C.H. Caceres, C.J. Davidson, J.R. Griffiths and Q.G. Wang, "The Effect of Mg on the Microstructure and Mechanical Behavior of Al-Si-Mg Casting Alloys," *Metallurgical and Materials Transactions A*, 1999, Vol. 30A, pp. 2611-2618.

[43] Q.G. Wang, "Microstructural Effects on the Tensile and Fracture Behavior of Aluminum Casting Alloys A356/357," *Metallurgical and Materials Transactions A*, Vol. 34A, Dec. 2003, pp. 2887-2899.

[44] A. Granger and R.R. Sawtell, "Effect of Beryllium on the Properties of A357 Castings," *AFS Transactions*, Vol. 115, 1984, pp. 579-586.

[45] G.K. Sigworth, S. Shivkumar and D. Apelian, "The Influence of Molten Metal Processing on Mechanical Properties of Cast Al-Si-Mg Alloys," *AFS Transactions*, Vol. 97, 1989, pp.811-823.

[46] C.H. Cáceres, I.L. Svensson and J.A. Taylor, "Strength- Ductility Behavior of Al-Si-Cu-Mg Casting Alloys In T6 Temper," *International Journal of Cast Metals Research*, Vol. 15, 2003, pp. 531-543.

[47] H. Möller, G. Govender, W.E. Stumpf and P.C. Pistorius, "Comparison of Heat Treatment Response of Semisolid Metal Processes Alloys A356 and 357," *International Journal of Cast Metals Research*, Vol. 23(1), 2010, pp. 37-43.

[48] H.W. Phillips, "Annotated Equilibrium Diagrams of Some Aluminum Alloy Systems," *Institute of Metals*, London, 1959, pp. 8-10.

[49] O. Vorren, J.E. Evensen and T.B. Pederson, "Microstructure and Mechanical Properties of AlSi(Mg) Casting Alloys," *AFS Transactions*, 1984, Vol. 93, pp. 459-466.

[50] S. Yaneva, N. Stoichez, Z. Kamenova, S. Budurov, "Quaternary Iron-containing Phases in Al-Si Cast Alloys," *Zeitschrift für Metallkunde*, 1984, Vol. 75, pp. 395-398.

[51] S. Murali, K.S. Raman and K.S.S. Murthy, "Effect of the Trace Additions (Be, Cr, Mn and Co) on The Mechanical Properties and Fracture Toughness of Fe-Containing Al-7Si-0.3Mg Alloy," *Cast Metals*, Vol. 6(4), 1994, pp. 189-198.

[52] M. Hansen and K. Anderko, "*Construction of Binary Alloys*," 2nd Edition, Chicago, IL, 1958.

[53] Aluminum Beryllium Master Alloys, http://www.freedomalloyssusa.com/.

[54] Y. Wang and Y. Xiong, "Effects of Beryllium in Al-Si-Mg-Ti Alloy," *Materials Science and Engineering A*, Vol. 280(1), March 2000, pp. 124-127.

[55] S. Murali, A. Trivedi, K.S. Shamanna and K.S.S. Murthy, "Effect of Iron and Combined Iron and Beryllium Addition on the Fracture Toughness and Microstructures of Squeeze-Cast Al-7Si-0.3Mg Alloy," *Journal of Materials Engineering and Performance*, Vol. 5(4), 1996, pp. 462-468.

[56] E.A. Elsharkawi, "*Effect of Metallurgical Parameters on the Decomposition of the π-AlFeMgSi Phase in Al-Si-Mg Alloys and its Influence on the Mechanical Properties*," Ph.D. Thesis, Université du Québec à Chicoutimi, Chicoutimi, Quebec, Canada, 2011.

[57] S.S. Sreeja Kumari, R.M. Pillai, T.P.D. Rajan and B.C. Pai., “Effect of Individual and Combined Additions of Be, Mn, Ca and Sr on the Solidification Behavior, Structure and Mechanical Properties of Al-7Si-0.3Mg-0.8Fe Alloy,” *Materials Science and Engineering A*, Vol. 460-461, 2007, pp. 561-573.

[58] P.S. Mohanty, R.L. Guthrie and J.E. Gruzleski, “Studies on the Fading Behavior of Al-Ti-B Master Alloys and Grain Refinement Mechanism Using LiMCA,” *Light Metals*, 1995, pp. 859-868.

[59] Y. Wang and Y. Xiong, “Effects of Beryllium in Al–Si–Mg–Ti Cast Alloy,” *Materials Science and Engineering A*, Vol. 280, 2000, pp. 124-127.

[60] S. Yie, S. Lee, Y. Lin and J. Lin, “Mechanical Properties of Al-11%Si Casting Alloys Containing Trace Be and Sr,” *Materials Transactions*, JIM, Vol. 40(4), 1999, pp. 294-300.

[61] Z. Lin, Z. Wang, H. Yang, C. Chen and M. Lee, “Mechanism for linear and nonlinear optical effects in $SrBe_3O_4$ crystal,” *Journal of Chemical Physics*, Vol. 117(6), 2002, p. 2809.

[62] C. Zhongwei, Z. Haifang and Z, Ruijie, “Effects of Beryllium and Iron Additions on Iron-Bearing Phase in A357 Aluminum Alloys,” *China Foundry, Research & Development*, Vol. 7(3), 2010, pp. 275-277.

[63] Y. Tan, S. Lee and Y. Lin, “Effects of Be and Fe Additions on the Microstructure and Mechanical Properties of A357.0 Alloys,” *Metallurgical and Materials Transactions A*, Vol. 26A, May 1995, pp. 1195-1205.

[64] A.A. Nayeb-Hashemi and J.B. Clark, “The Be-Mg (Beryllium-Magnesium) System,” *Bulletin of Alloy Phase Diagrams*, Vol. 8(1), 1987, pp. 57-58.

[65] Z. Xiaoqin, W. Qudong, L. Yizhen, Z. Yanping, D. Wenjiang and Z. Yunhu, “Influence of Beryllium and Rare Earth Additions on Ignition-Proof Magnesium Alloys,” *Journal of Materials Processing Technology*, Vol. 112, 2001, pp. 17-23

[66] V.E. Ivanov, V.F. Zelenskii, S.I. Faifer, S.M. Zhdanov, V.I. Maksimenko and V.I. Savchenko, “Sintered Magnesium and Magnesium-Beryllium alloys,” *Physicotechnical Institute, Academy of Sciences*, UkrSSR, Khar’kov, translated from Poroshkovaya Metallurgiya, Vol. 5(29), 1965, pp. 46-53.

[67] FactSage Thermochemical Software and Databases, http://www.crct.polymtl.ca/fact/documentation/.

[68] M.F. Ibrahim, "*Effects of Magnesium Content and Aging Conditions on the Impact Toughness of 319-Type Al-Si-Cu-Mg Alloys*," M.Sc. Thesis, Université du Québec à Chicoutimi, Chicoutimi, Quebec, Canada, 2010.

[69] L. Heusler and W. Schneider, "Influence of Alloying Elements on the Thermal Analysis Results of Al–Si Cast Alloys," *Journal of Light Metals*, Vol. 2, 2002, pp. 17–26.

[70] F.H. Samuel, P. Ouellet, A.M. Samuel, and H.W. Doty, "Effect of Mg and Sr Additions on the Formation of Intermetallics in Al-6 Wt Pct Si–3.5 Wt Pct Cu-(0.45) to (0.8) Wt Pct Fe 319–Type Alloys," *Metallurgical and Materials Transactions A*, Vol. 29A, 1998, pp. 2871-2884.

[71] G.A. Edwards, K. Stiller, G.L. Dunlop and M.J. Couper, "The Precipitation Sequence in Al-Mg-Si Alloys," *Acta Materialia*, Vol. 46(11), 1998, pp. 3893-3904.

[72] S. Shivkumar, S. Ricci Jr., B. Steenhoff, D. Apelian and G. Sigworth, "An Experimental Study to Optimize the Heat Treatment of A356 Alloy," *AFS Transactions*, Vol. 97, 1989, pp. 791-810.

[73] K.A. Yoshida and R.M. Arrowood, "Microstructure and Mechanical Properties of A356 Aluminum Castings as Related to Various T6-Type Heat Treatments," *in Light Weight Alloys for Aerospace Applications III*, 1995, The Minerals, Metals, and Materials Society, Warrendale, PA, pp. 77-87.

[74] M.A. Moustafa, F.H. Samuel, and H.W. Doty, "Effect of Solution Heat Treatment and Additives on the Hardness, Tensile Properties and Fracture Behaviour of Al-Si (A413.1) Automotive Alloys," *Journal of Materials Science*, Vol. 38, 2003, pp. 4523-4534.

[75] M. Tsukuda and S. Koike, "The Heat Treatment of Al-7%Si-0.3%Mg Alloy," *Journal of Japan Institute of Light Metals*, Vol. 28(3), 1978, pp.109-115.

[76] O. Vorren, J.E. Evensen and T.B. Pederson, "Microstructure and Mechanical Properties of AlSi(Mg) Casting Alloys," *AFS Transactions*, Vol. 93, 1984, pp. 459-466.

[77] J. Espinoza-Cuadra, G. Garcia-Garcia and H. Mancha-Molinar, "Influence of Defects on Strength of Industrial Aluminum Alloy Al-Si-Cu 319," *Materials and Design*, Vol. 28, 2007, pp. 1038-1044.

[78] M. Hajkowski, L. Bernat and J. Hajkowski, "Mechanical Properties of Al-Si-Mg Alloy Castings as a Function of Structure Refinement and Porosity Fraction," *Archives of Foundry Engineering*, Vol. 12(4), 2012, pp. 57-64.

[79] B. Closset and J.E. Gruzleski, “A Study on the Use of Pure Metallic Strontium in the Modification of Al-Si Alloys,” *AFS Transactions*, Vol. 89, 1981, pp. 801-808.

[80] N. Roy, A.M. Samuel and F.H. Samuel, “Porosity Formation in Al-9%Si-3%Cu Alloy Systems: Metallographic Observations,” *Metallurgical and Material Transactions A*, Vol. 27, 1996, pp. 415-429.

[81] N. Roy, L. Zhang, P.R. Louchez and F.H. Samuel, “Porosity Formation in Al-9%Si-3%Cu-X Alloy systems: Measurements of Porosity,” *Journal of Materials Science*, Vol. 31, 1996, pp. 1243-1254.

[82] Y. Awano and Y. Shimizu, “Non-equilibrium Crystallization of AlFeSi Compound in Melt-Superheated Al-Si Alloy Castings,” *AFS Transactions*, Vol. 98, 1990, pp. 889-895.

[83] M.M. Haque, “Strontium Modification of Aluminum-Silicon Eutectic Alloy and the Factors Affecting It,” *Metal Forum*, Vol. 6(1), 1983, pp. 54-56.

[84] M. Garat and R. Scalliet, “A Review of Recent French Casting Alloy Developments,” *AFS Transactions*, Vol. 86, 1978, pp. 549-62.

[85] G. Kumar, S. Hegde and K.N. Prabhu, “Heat Transfer and Solidification Behaviour of Modified A357 Alloy,” *Journal of Materials Processing Technology*, Vol. 182, 2007,pp. 152-56

[86] S. Shivkumar, S. Ricci and D. Apelian, “Influence of Solution Parameters and Simplified Supersaturation Treatments on Tensile Properties of A356 Alloy,” *AFS Transactions*, Vol. 98, 1990, pp. 913-922.

[87] R.X. Li, R.D. Li, Y.H. Zhao, L.Z. He, Li, H. Guan and Z. Hu, “Age-Hardening Behavior of Cast Al-Si Base Alloy,” *Materials Letters*, Vol. 58, 2004, pp. 2096-2101.

[88] American Society of Testing and Materials, Standard Methods of Tension Testing of Metallic Materials, ASTM B557-84, ASTM, Philadelphia, 1986.

[89] H. Ammar, “*Quality of Aluminum-Silicon Casting Alloys*,” Lambert Academic Publishing, Saarbrücken, Germany, 2012.

[90] M. Drouzy, S. Jacob and M. Richard, “Interpretation of Tensile Results by Means of Quality Index and Probable Yield Strength,” *AFS International Cast Metals Journal*, Vol. 5, 1980, pp. 43-50.

[91] S. Jacob, "Quality Index in Predicting of Properties of Aluminum Castings-A Review," *AFS Transactions*, Vol. 108, 2000, pp. 811-818.

[92] ASM Handbook Vol. 2, "*Properties and Selection: Nonferrous Alloys and Special-Purpose Materials*," ASM International, Materials Information Society, U.S.A., 1990.

[93] C.H. Cáceres, "Microstructure Design and Heat Treatment Selection for Casting Alloys Using the Quality Index," *Journal of Materials Engineering and Performance*, Vol. 9(2), 2000, pp. 215-221.

[94] T. Din, A.K.M.B. Rashid and J. Campbell, "High Strength Aerospace Casting Alloys: Quality Factor Assessment," *Materials Science and Technology*, Vol. 12, 1996, pp. 269-273.

[95] C.H. Cáceres, "A Rationale for the Quality Index of Al-Si-Mg Casting Alloys," *International Journal of Cast Metals Research*, Vol. 10, 1998, pp. 293-299.

[96] C.H. Cáceres, "A Phenomenological Approach to the Quality Index of Al-Si-Mg Casting Alloys," *International Journal of Cast Metals Research*, Vol. 12, 2000, pp. 367-375.

[97] N.D. Alexopoulos and S.G. Pantelakis, "A New Quality Index for Characterizing Aluminum Cast Alloys with Regard to Aircraft Structure Design Requirements," *Metallurgical and Materials Transactions A*, Vol. 35A, 2004, pp. 301-308.

[98] N.D. Alexopoulos and S.G. Pantelakis, "Quality Assessment of Artificially Aged A357 Aluminum Alloy Cast Ingots by Introducing Approximate Expressions of the Quality Index Q_D," *Metallurgical and Materials Transactions A*, Vol. 35A, 2004, pp. 3079-3089.

[99] N.D. Alexopoulos and S.G. Pantelakis "Evaluation of the Effects of Variations in Chemical Composition on the Quality of Al-Si-Mg, Al-Cu, and Al-Zn-Mg Cast Aluminum Alloys," *Journal of Materials Engineering and Performance*, Vol. 12(2), 2003, pp. 196-205.

[100] N.D. Alexopoulos and S.G. Pantelakis, "Quality Evaluation of A357 Cast Aluminum Alloy Specimens Subjected to Different Artificial Aging Treatment," *Materials and Design*, Vol. 25, 2004, pp. 419-430.

[101] N.D. Alexopoulos, "Definition of Quality in Cast Aluminum Alloys and Its Characterization with Appropriate Indices," *Journal of Materials Engineering and Performance*, Vol. 15 (1), 2006, pp. 59-66.

[102] M. Tiryakioğlu, J.T. Staley and J. Campbell, "Evaluating Structural Integrity of Cast Al-7%Si-Mg Alloys Via Work Hardening Characteristics: II. A New Quality Index," *Materials Science and Engineering A*, Vol. 368, 2004, pp. 231-238.

[103] R.T. Holt, M.D. Raizenne and W. Wallace, "RRA Heat Treatment of Large Al 7075-T6 Components," *RTO MP-25*, Corfu, Greece, April 1999, pp. 1-11.

[104] F. Viana, A.M.P. Pinto, H.M.C. Santos and A.B. Lopes, "Retrogression and Re-aging of 7075 Aluminum Alloy: Microstructural Characterization," *Journal of Materials Processing Technology*, Vol. 92-93, 1999, pp. 54-59.

[105] J. Oñoro and C. Ranninger, "Stress-Corrosion-Cracking Behavior of Heat-Treated Al-Zn-Mg-Cu Alloy with Temperature," *Journal of Materials Science*, Vol. 35(4), 1999, pp. 509-514.

[106] M. Benachour, N. Benachour and M. Benguediab, "Fatigue Crack initiation of Al-Alloys "Effect of Heat Treatment Condition"," *International Journal of Mechanical, Aerospace, Industrial and Mechatronics Engineering*, Vol. 7(11), 2013, pp. 1195-1197.

[107] I.J. Polmear, "Recent Developments in Light Alloys," *Materials Transactions*, JIM, Vol. 37(1), 1996, pp. 12-31.

[108] S. K. Panigrahi and R. Jayaganthan, "Development of Ultrafine Grained High Strength age Hardenable Al 7075 Alloy by Cryorolling," *Materials & Design*, Vol. 32(6), 2011, pp. 3150–3160.

[109] J.T. Staley, "History of Wrought-Aluminium-Alloy Development," *Aluminum Alloys: Contemporary Research and Applications, Treaties on Materials Science and Technology*, Academic Press, Vol. 31, 1989, pp. 3-31.

[110] Patent No. EP0377779B2, "*Aluminum Alloy Product Having Improved Combinations of Strength, toughness and Corrosion Resistance*," New European Patent Specification, Bulletin 2001/36, 5 September 2001.

[111] J.K. Park, "Influence of Retrogression and Reaging Treatments on the Strength and Stress Corossion Resistance of Aluminum Alloy 7075-T6," *Materials Science and Engineering A*, Vol. 103(2), 1988, pp. 223-231.

[112] X.J. Wu, M.D. Raizenne, W.R. Chen, C. Poon, and W. Walllace, "Thirty Years of Retrogression and Re-aging," *ICAS Congress*, 2002, pp. 1-11.

[113] N.E. Paton and A.W. Sommer, “Influence of Thermomechanical Processing Treatments on Properties of Aluminum Alloys,” *Proceeding Third international Conference on Strength of Metals and Alloys*, Metals Society, London, 1, 1973, pp. 101-108.

[114] A. Yamamoto, K. Minami, U. Ishihara and H. Tsubakino, “Calorimetric and Resistivity Study of formation and Redissolution of Precipitates in 7050 Aluminum Alloy,” *Materials Transactions*, JIM, Vol. 39(1), 1998, pp. 69-74.

[115] S.K. Panigrahi and R. Jayaganthan, “Development of Ultrafine Grained High Strength Age Hardenable Al 7075 Alloy by Cryorolling,” *Materials and Design*, Vol. 32, 2011, pp. 3150-3160.

[116] A. Joshi, C.R. Shastry and M. Levy, “Effect of Heat Treatment on Solute Concentration at Grain Boundaries in 7075 Aluminum Alloy,” *Metallurgical Transactions A*, Vol. 12A, 1981, pp. 1081-1088.

[117] I.J. Polmear , “Aluminium Alloys – A Century of Age Hardening,” *Materials Forum*, Vol. 28, 2004, pp. 1-14, Edited by J.F. Nie, A.J. Morton and B.C. Muddle, *Institute of Materials Engineering*, Australasia Ltd.

[118] J.K. Park and A.J. Arndell, “Microstructures of the Commercial 7075 Al Alloy in the T651 and T7 Tempers,” *Metallurgical Transactions A*, 14A, 1983, pp. 1957-1965.

[119] A. Karaaslan, I. Kaya and H. Atapek, “Effect of Aging Temperature and of Retrogression Treatment Time on the Microstructure and Mechanical Properties of Alloy AA 7075,” *Metal Science and Heat Treatment*, Vol. 49(9-10), 2007, pp. 443-447.

[120] J.K. Park and A.J. Ardell, “Effect of Retrogression and Reaging treatments on the Microstructure of Al-7075-T651,” *Metallurgical Transactions A*, Vol. 15A, 1984, pp. 1531-1543.

[121] S.V. Emani et al., “Double Aging and Thermomechanical Heat Treatment of AA 7075 Aluminum Alloy Extrusions,” *Journal of Materials Science*, Vol. 44, 2009, pp. 6384-6391.

[122] R.N. Lumley, I.J. Polmear and A.J. Morton, “Temper Developments Using Secondary Aging,” *Materials Forum*, Vol. 28, 2004, pp. 85-95.

[123] J.T. Staley, R.H. Brown and R. Schmidt, “Heat treating Characteristics of High Strength Al-Zn-Mg-Cu Alloys With and Without Silver Additions,” *Metallurgical Transactions*, Vol. 3, 1972, pp. 191-199.

[124] H.Y. Hunsicker, J.T. Staley and R.H. Brown, "Stress Corrosion Resistance of High Strength Al-Zn-Mg-Cu Alloys With and Without Silver Additions," *Metallurgical Transactions*, Vol. 3, 1972, pp. 201-209.

[125] O.N. Senkov, R.B. Bhat, S.V. Senkova and J.D. Schloz, "Microstructure and Properties of Cast Ingots of Al-Zn-Mg-Cu Alloys Modified with Sc and Zr," *Metallurgical and materials Transactions A*, Vol. 36A, 2005, pp. 2115-2126.

[126] Y-L. Wu, C. Li, F.H.S. Froes and A. Alvarez, "Microalloying of Sc, Ni, and Ce in an Advanced Al-Zn-Mg-Cu Alloy," *Metallurgical and materials Transactions A*, Vol. 30A, 1999, pp. 1017-1024.

[127] M. Alipour and M. Emamy, "Effects of Al-5Ti-1B on the Structure and Hardness of a Super High Strength Aluminum Alloy Produced by Strain-Induced Melt Activation Process," *Materials and Design*, Vol. 32, 2011, pp. 4485-4492.

[128] A.D. Isadare, B. Aremo, M. O. Adeoye, O. J. Olawale and M.D. Shittu, "Effect of Heat Treatment on Some Mechanical Properties of 7075 Aluminum Alloy," *Journal of Materials Research*, Vol. 16(1), 2013, pp. 190-194.

[129] G. Silva, B. Rivolta, R. Gerosa and U. Derudi, "Study of SCC Behavoir of 7075 Aluminum Alloy after One-Step Aging at 163°C," *Journal of Materials Engineering and Performance*, Vol. 22(1), 2013, pp. 210-214.

[130] J.M. Salman, S.A.A. Alsada and K.F. Al-Sultani, "Improvement Properties of 7075-T6 Aluminum Alloy by Quenching in 30% Polyethylene Glycol and Addition 0.1%B," *Research Journal of Material Sciences*, Vol. 1(6), 2013, pp. 12-17.

[131] H.T. Naeem and K.S. Mohammed, "Microstructural Evaluation and Mechanical Properties of an Al-Zn-Mg-Cu-Alloy after Addition of Nickel under RRA conditions," *Materials Sciences and Applications*, Vol. 4, 2013, pp. 704-711.

[132] F. Wei, Z.K. Zhao, P.Y. Liu and T.T. Zhou, "Research and Development of Al-Zn-Mg-Cu-Li Alloys," *Materials Forum*, Vol. 28, 2004, pp. 75-84.

[133] A. Nabawy, A. Samuel, F. Samuel and H. Doty, "Influence of Additions of Zr, Ti–B, Sr and Si as well as of Mold Temperature on the Hot-Tearing Susceptibility of an Experimental Al–2% Cu–1% Si Alloy," *Journal of Materials Science*, Vol. 47, 2012, pp. 4146-4158.

[134] G.A. Farhadi, A.M. Samuel, F.H. Samuel, H.W. Doty and B. Kulunk, "Alloy Performance in Relation to Intermetallic Fragmentation Observed in 5XXX Aluminum Alloys in the Sr-Modified and Annealed Conditions," *International symposium, Light metals*, 2000, pp. 71-94.

[135] E.A. Elsharkawi and S. Alkahtani, "Role of Decomposition of AlMgFeSi Phase in Mechanical Properties and Fracture Behaviour of 357 Alloys," *International Journal of Cast Metals Research*, Vol. 26(5), 2013, pp. 262-272.

[136] E.A. Elsharkawi, E. Samuel, A.M. Samuel and F.H. Samuel, "Effects of Mg, Fe, Be additions and solution heat treatment on the pi-AlMgFeSi iron intermetallic phase in Al-7Si-Mg alloys," *Journal of Materials Science*, 45(6), 2010, pp. 1528-1539.

[137] L. Lu, A. K. Dahle, and M. J. Couper, "Formation of Iron Intermetallic Phases during Solidification of the Aluminum Casting Alloys," *Solidification of Aluminum Alloys*, TMS (The Minerals, Metals and Materials Society), 2004.

[138] L. Lu and A. K. Dahle, "Iron-Rich Intermetallic Phases and Their Role in Casting Defect Formation in Hypoeutectic Al-Si Alloys," *Metallurgical and Materials Transactions A*, Vol. 36(3), March 2005, pp. 819-835.

[139] A. T. Joenoes and J. E. Gruzleski, "Magnesium Effects on the Microstructure of Unmodified and Modified Al-Si Alloys," *Cast Metals*, Vol. 4(2), 1991, pp. 62-71.

[140] M. A. Moustafa, F. H. Samuel, H. W. Doty and S. Valtierra, "Effect of Mg and Cu Additions on the Microstructural Characteristics and Tensile Properties of Sr-Modified Al-Si Eutectic Alloys," *International Journal of Cast Metals Research*, 2003, Vol. 15, pp. 609-626.

[141] S. Murali, K.S. Raman and K.S.S. Murthy, "Morphological Studies on β-FeSiAl5 Phase in Al-7-Si-0.3Mg Alloy with Trace Additions of Be, Mn, Cr, and Co," *Materials Characterization*, Vol. 33(2), Sep. 1994, pp. 99-112.

[142] Y. H. Tan, S. L. Lee, and Y. Lin, "Effect of Be and Fe Additions on the Microstructure and Mechanical properties of A357 Alloys," *Metallurgical and Materials Transactions A*, Vol. 26A, May 1995, pp. 1195-1205.

[143] J. A. Taylor, D. H. StJohn, Barresi, and M. J. Couper, "Influence of Mg Content on The Microstructure and Solid Solution Chemistry of Al-7Si-Mg Casting alloys During Solution Treatment," *Materials Science Forum*, Vol. 331-337, 2000, pp. 277-282.

[144] Conservation of Mass in Chemical Changes, *Journal of the Chemical Society* (Great Britain), Vol. 64 (2).

[145] D. Apelian and S. K. Chaudhury, "Heat Treatment of Aluminum Cast Components: Recent Developments and Future Challenges," *WFO Technical Forum-St. Louis*, Missouri, USA, April 19, 2005.

[146] L.A. Narayanan, F.H. Samuel and J.E. Gruzleski, "Dissolution of Iron Intermetallics in Al-Si Alloys through Nonequilibrium Heat Treatment," *Metallurgical and Materials Transactions A*, Vol. 26A, 1995, pp. 2161-2174.

[147] E. Tillová and M. Panušková, "Effect of Solution Treatment on Intermetallic Phases Morphology in AlSi9Cu3 Cast Alloy," *Metalurgija*, Vol. 47 (3), 2008, pp. 207-210.

[148] S.M.M. Kashani, H. Rhodin and S.M.A. Boutorabi, "Effects of Hot Isostatic Pressing on the Tensile Properties of A356 Cast Alloy," *Iranian Journal of Materials Science & Engineering*, Vol. 10(3), 2013, pp. 54-64.

[149] B. Closset and J.E. Gruzleski, "Mechanical Properties of A356.0 Alloys Modified with Pure Strontium," *AFS Transactions*, Vol. 90, 1982, pp. 453-464.

[150] J.A. Taylor, D.H. StJohn and M.J. Couper, "Solution Treatment Effects in Al-Si-Mg Casting Alloys: Part II: Solid Solution Chemistry," *Aluminum Transactions*, Vol. 4-5, 2001, pp. 111-124.

[151] Q.G. Wang and C.J. Davidson, "Solidification and Precipitation Behaviour of Al-Si-Mg Casting Alloys," *Journal of Materials Science*, Vol. 36, 2001, pp. 739-750.

[152] G. Gustafsson, T. Thorvaldsson and G.L. Dunlop, "The Influence of Fe and Cr on the Microstructure of Cast Al-Si-Mg Alloys," *Metallurgical Transactions A*, Vol. 17A, 1986, pp. 45-52.

[153] H. Ammar, "*Influence of Metallurgical Parameters on the Mechanical Properties and Quality Indices of Al-Si-Cu-Mg and Al-Si-Mg Casting Alloys*," Ph.D. Thesis, Université du Québec à Chicoutimi, Chicoutimi, Quebec, Canada, 2010.

[154] J. Campbell, "*Complete Casting Handbook: Metal Casting Processes, Metallurgy, Techniques and design*," Butterworth-Heinemann, MA, USA, 2011.

[155] M. Hajkowski, L. Bernat, J. Hajkowski, "Mechanical Properties of Al-Si-Mg Alloy Castings as a function of Structure Refinement and Porosity Fraction," *Archives of Fundry engineering*, Vol. 12(4), 2012, pp. 57-64.

[156] E. Ogris, "*Development of Al-Si-Mg Alloys for Semi-solid Processing and Silicon Spheroidization Treatment (SST) for Al-Si Cast Alloys*," Ph.D. Thesis, Swiss Fedral Institute of Technology, Zurich, Switzerland , 2002.

[157] S.E. Maube, D.N. Wangombe, S.M. Maranga and J.M. Kihiu, "Effect of Cooling Rate and Heat Treatment on the Microstructure and Impact resistance of recycled Aluminum Sand Cast Alloy," *Proceeding of the Mechanical Engineering Conference*, Vol. 4, May 2012, pp. 214-218.

[158] S.H. Juang and S.M. Wu, "Study on Mechanical Properties of A356 Alloys Enhanced with Preformed Thixotropic Structure," *Journal of Marine Science and Technology*, Vol. 16(4), 2008, pp. 271-274.

[159] J.H. Peng, X.L. Tang, J.T. He and D.Y. Xu, "Effect of Heat Treatment on Microstructure and tensile Properties of A356 Alloys," *Transactions of Nonferrous Metals Society of China*, Vol. 21, 2011, pp. 1950-1956.

[160] D.A. Lados and D. Apelian, "Solution Heat Treatment Effects on Microstructure and Mechanical Properties of Al-(1 to 13Pct)Si-Mg Cast Alloys," *Metallurgical and Materials Transactions B*, Vol. 42B, 2011, pp. 171-180.

[161] J.H. Yao, K.R. Elder, H. Guo and M. Grant, "Theory and Simulation of Ostwald Ripening," *Physical Review B*, Vol. 4(21), 1993-I, pp. 110-125.

[162] P.W. Voorhees, G.B. McFadden and R.F. Boisvert, "Numerical Simulation of Morphological Development during Ostwald Ripening," *Acta Metallurgica*, Vol. 36(1), 1988, pp. 207-222.

[163] H. Möller, G. Govender, W.E. Stumpf and R.D. Knutsen, "Influence of Temper Condition on Microstructure and Mechanical Properties of Semisolid Metal Processed Al-Si-Mg Alloy A356," *International Journal of Cast Metals Research*, Vol. 22(6), 2009, pp. 417-421.

[164] M. Abdulwahab, I.A. Madugu, S.A. Yaro, S.B. Hassan and A.P.I. Popoola, "Effects of Multiple-Step Thermal Aging Treatment on the Hardness Characteristics of A356.0-Type Al–Si–Mg Alloy," *Materials and Design*, Vol. 32, 2011, pp.1160-1165.

[165] N.D. Alexopoulos and M. Tiryakioglu, "The Relationship between fracture Toughness and Tensile Properties of A357 Cast Aluminum Alloy," *Metallurgical and Materials Transactions A*, Vol. 40A, 2009, pp. 702-716.

[166] A. Morri, “Empirical Models of Mechanical Behaviour of Al-Si-Mg Cast Alloys for High Performance Engine Applications,” *Metallurgical Science and Technology*, Vol. 28(2), 2010, pp. 2-8.

[167] J. Rajabi, E. Alibeiki, M. Rajabi, J. Rajabi, M. Nekoei and M.R. Meschian, “Modeling the T6 Heat Treatment of Al-Mg-Si Alloy by Artificial Neural Network,” *Academic Research International*, Vol. 2(3), 2012, pp. 114-119.

[168] S. Kuntongkum, S. Wisutmethangoon, T. Plookphol and J. Wannasin, “Influence of Heat Treatment Processing Parameters on the Hardness and the Microstructure of Semi-Solid Aluminum Alooy A356,” *Journal of Metals, Materials and Minerals*, Vol. 18(2), 2008, pp. 93-97.

[169] E. Alibeiki, J. Rajabi and J. Rajabi, “Prediction of Mechanical Properties of the Heat Treatment by Artificial Neural Networks,” *Journal of Asian Scientific Research*, Vol. 2(11), 2012, pp. 742-746.

[170] H.R. Ammar, A.M. Samuel, F.H. Samuel, E. Simielli, G.K. Sigworth and J. C. Lin, “Influence of Aging Parameters on the Tensile Properties and Quality Index of Al-9 Pct Si-1.8 Pct Cu-0.5 Pct Mg 354-Type Casting Alloys,” *Metallurgical and Materials Transactions A*, Vol. 43(1), 2012, pp. 61-73.

[171] A. Morri, “Correlations among Microstructure, effect of Thermal Exposure and Mechanical Properties, in Heat Treated Al-Si-Mg and Al-Cu Aluminium Alloys,” *Doctoral School on Engineering Sciences*, UNIVPM, Italy, 2012, pp.1-11.

[172] B.N. Sarada, P.L. Srinivasamurthy and Swetha, “Microstructural Characteristics of Sr and Na Modified Al-Mg-Si Alloy,” *International Journal of Innovative Research in Science, Engineering and Technology*, Vol. 2(8), 2013, pp. 3975-3983.

[173] G.K. Sigworth, “Understanding Quality in Aluminum Castings,” *American Foundry Transactions*, 2011, pp. 1-17.

[174] J.F.H. Paz, “*Heat Treatment and Precipitation in A356 Aluminum Alloy*,” Ph.D. Thesis, McGill University, Montreal, Quebec, Canada, 2003.

[175] F. Ernst, “Precipitation Hardening of Al-Si-Mg Alloys,” *Materials Laboratory III*, EMSE-290, Sep. 2004, pp. 1-29.

[176] A. Hossain and A.S.W. Kurny, “Effect of Aging Temperature on the Mechanical Properties of Al-6Si-0.5Mg Cast Alloys with Cu Additions Treated by T6 Heat Treatment,” *Universal Journal of Materials Science*, Vol. 1(1), 2013, pp. 1-5.

[177] M. Abdulwahab, I.A. Madugu, F. Asuke, O.S.I. Fayomi and F.A. Ayeni, " Effect of Thermal Aging treatment on the Mechanical Properties of Antimony-Modified A356.0-Type Al-Si-Mg Alloy," *Journal of Materials and Environmental Science*, Vol. 4(1), 2013, pp. 87-92.

[178] R.S. Rana, R. purohit and S. Das, "Reviews on the Influences of Alloying Elements on the Microstructure and Mechanical Properties of Aluminum Alloys and Aluminum Alloy Composites," *International Journal of Scientific and Research Publications*, Vol. 2(6), 2012, pp. 1-6.

[179] L.A. Dobrzañski, R. Maniara and J.H. Sokolowski, "The Effect of Coolin Rate on Microstructure and mechanical properties of AC AlSi9Cu Alloy," *Archives of Materials Science and Engineering*, Vol. 28(2), 2007, pp. 105-112.

[180] S. Sato, Y. Harada, N. Ishibashi and M. Adachi, "Effect of Strontium, Magnesium and Iron Content on Mechanical Properties of Rheocast Al-7 mass%Si-Mg Alloys," *Materials Transactions*, Vol. 50(2), 2009, pp. 354-360.

[181] J. Petrik and M. Horvath, "The Iron Correctors in Al-Si Alloys," *ANNALS of Faculty Engineering Hunedoara - International Journal of Engineering*, ISSN 1584-2673, Vol. 3, 2011, pp. 401-405.

[182] W. Kasprzak, B.S. Amirkhiz and M. Niewczas, "Structure and Properties of Cast Al-Si Based Alloy with Zr–V–Ti Additions and its Evaluation of High Temperature Performance," *Journal of Alloys and Compounds*, Vol. 595, 2014, pp. 67-79.

[183] L. Ceschini, A. Morri, A. Morri, F. Rotundo and S. Toschi, "Heat Treatment Response and Influence of Overaging on Mechanical Properties of C355 Cast Aluminum Alloy," *La Metallurgia Italiana*, Vol. 5, 2014, pp. 11-17.

[184] S. Kavin, C. Bhagyanathan and M. Ravi, "Microstructural Modifications in Squeeze Cast Al-7.0 wt% Si-0.3 wt%Mg alloy," *International Journal of Current Engineering and Technology*, Special Issue-2, Feb. 2014, pp. 152-155.

[185] G.A. Farhadi, A.M. Samuel, F.H. Samuel and B. Kulunk, "Parameters Controlling the Performance of Al-Si-Mg Automotive Alloys Containing Fe-Intermetallics: Part II-Work Hardening Behavior," *in International Symposium on light metals as held at the 40th Annual Conference of Metallurgists of CIM (COM 2001)*, Toronto, ON, Canada, 2001, pp. 323-338.

[186] G.A. Farhadi, A.M. Samuel, F.H. Samuel and B. Kulunk, "Effect of Trace Elements and Heat Treatment on the Microstructure and Performance of 6XXX Aluminum Automotive Skin: Part II - Alloy Formability," *Aluminum Transactions*, Vol. 4, 2001, pp. 71-94.

[187] M.F. Ibrahim, E. Samuel, A.M. Samuel, A.M.A. Al-Ahmari and F.H. Samuel, "Impact Toughness and Fractography of Al-Si-Cu-Mg Base Alloys," *Materials and Design*, Vol. 32(7), 2011, pp. 3900-3910.

[188] Z. Ma, E. Samuel, A.M.A. Mohamed, A.M. Samuel, F.H. Samuel and W.H. Doty, "Influence of Aging Treatments and Alloying Additives on the Hardness of Al-11Si-2.5Cu-Mg Alloys," *Materials and Design*, Vol. 31(8), 2010, pp. 3791-3803.

[189] O. Elsebaie, A.M.A. Mohamed, A.M. Samuel, F.H. Samuel and A.M.A. Al-Ahmari, "The Role of Alloying Additives and Aging Treatment on the Impact Behavior of 319 Cast Alloy," *Materials and Design*, Vol. 32(6), 2011, pp. 3205-3220.

[190] E.A. Elsharkawi, A.M. Samuel, F.H. Samuel, E. Simielli and G.K. Sigworth, "Influence of Solutionizing Time, Modification, and Cooling Rate on the Decomposition of Mg-Containing Iron Intermetallic Phase in 357 Alloys," *Transactions of the American Foundry Society*, 2012, pp.1-9.

[191] H.R. Ammar, C. Moreau, A.M. Samuel, F.H. Samuel and H.W. Doty, "Effects of Aging Parameters on the Quality of 413-Type Commercial Alloys," *Materials and Design*, Vol. 30(4), 2009, pp. 1014-1025.

[192] A.E. Hughes, N. Birbilis, J.M.C. Mol, S.J. Garcia, X. Zhou and G.E. Thompson, "High Strength Al-Alloys: Microstructure, Corrosion and Principles of Protection," Chapter 10, *INTECH*, 2011, pp. 223-262.

[193] K. Pieła, L. Błaz, Z. Sierpinski and T. Forys, "Non-Isothermal Annealing of AA7075 Aluminum Alloy – Structural and Mechanical Effects," *Archives of Metallurgy and Materials*, Vol. 57(3), 2012, pp. 703-709.

[194] J.F. Chinella and Z. Guo, "Computational Thermodynamics Characterization of 7075, 7039, and 7020 Aluminum Alloys Using JMatPro," *Army Research Laboratory*, ARL-TR-5660, Sep. 2011, pp. 13-47.

[195] S. Bourzam, N. Bouzroura and M.K. Hanifi, "Etude de la précipitation dans le système Al-20%Zn-1%Mg," *SENAMAP'9*, Dec. 2009, pp. 77-79.

[196] H. Ji, L. Yuan and D. Shan, "Effect of Microstructure on Thermal Expansion Coefficient of 7A09 Aluminum Alloy," *Journal of Materials Science & Technology*, Vol. 27(9), 2011, pp. 797-801.

[197] K.S. Ghosh and N. Gao, "Determination of Kinetic Parameters from Calorimetric Study of Solid State Reactions in 7150 Al-Zn-Mg Alloy," *Transactions of Nonferrous Metals Society of China*, Vol. 21, 2011, pp. 1199-1209.

[198] K. Rajan, W. Wallace and J.C. Beddoes, “Microstructural Study of a High-Strength Stress-Corrosion resistant 7075 Aluminum Alloy,” *Journal of Materials Science*, Vol. 17, 1982, pp. 2817-2824.

[199] N.C. Danh, K. Rajan and W. Wallace, “A TEM Study of Microstructural Changes during Retrogression and Reaging in 7075 Aluminum,” *Metallurgical Transactions A*, Vol. 14A, 1983, pp. 1843-1850.

[200] P.L. Srinivasamurthy, B.N.Sarada, B.S. Karthik and S.S. Holla, “Effect of Retrogression and Reaging Heat Treatment on Microstructure and Corrosion Properties of Al-7075,” *International Journal of Innovative Research in Science*, Engineering and Technology, Vol. 2(11), 2013, pp. 6434-6441.

[201] K. Ma, H. Wen, T. Hu, T.D. Topping, D. Isheim, D.N. Seidman, EJ. Lavernia and J.M. Schoenung, “Mechanical Behavior and Strengthening Mechanisms in Ultrafine Grain Precipitation-Strengthened Aluminum Alloy,” *Acta Materialia*, Vol. 62, 2014, pp. 141-155.